## INFORMATION TO USERS

This material was produced from a microfilm copy of the original document. While the most advanced technological means to photograph and reproduce this document have been used, the quality is heavily dependent upon the quality of the original submitted.

The following explanation of techniques is provided to help you understand markings or patterns which may appear on this reproduction.

1. The sign or "target" for pages apparently lacking from the document photographed is "Missing Page(s)". If it was possible to obtain the missing page(s) or section, they are spliced into the film along with adjacent pages. This may have necessitated cutting thru an image and duplicating adjacent pages to insure you complete continuity.

2. When an image on the film is obliterated with a large round black mark, it is an indication that the photographer suspected that the copy may have moved during exposure and thus cause a blurred image. You will find a good image of the page in the adjacent frame.

3. When a map, drawing or chart, etc., was part of the material being photographed the photographer followed a definite method in "sectioning" the material. It is customary to begin photoing at the upper left hand corner of a large sheet and to continue photoing from left to right in equal sections with a small overlap. If necessary, sectioning is continued again — beginning below the first row and continuing on until complete.

4. The majority of users indicate that the textual content is of greatest value, however, a somewhat higher quality reproduction could be made from "photographs" if essential to the understanding of the dissertation. Silver prints of "photographs" may be ordered at additional charge by writing the Order Department, giving the catalog number, title, author and specific pages you wish reproduced.

5. PLEASE NOTE: Some pages may have indistinct print. Filmed as received.

University Microfilms International
300 North Zeeb Road
Ann Arbor, Michigan 48106 USA
St. John's Road, Tyler's Green
High Wycombe, Bucks, England HP10 8HR

77-19,268

KALE, Billy Michael, 1950-
MAGNETOELASTIC CONTRIBUTIONS TO THE ELASTIC CONSTANTS OF DYSPROSIUM.

Rice University, Ph.D., 1977
Physics, solid state

**Xerox University Microfilms,** Ann Arbor, Michigan 48106

RICE UNIVERSITY

# MAGNETOELASTIC CONTRIBUTIONS TO THE ELASTIC CONSTANTS OF DYSPROSIUM

by

Billy Michael Kale

A THESIS SUBMITTED
IN PARTIAL FULFILLMENT OF THE
REQUIREMENTS FOR THE DEGREE OF

Doctor of Philosophy

Thesis Director's Signature:

Houston, Texas

August, 1976

To Jonita

Acknowledgements

My first acknowledgement goes to Dr. P. L. Donoho who suggested the topic of the research, and who provided invaluable assistance and ancouragement throughout the course of the research.

I wish also to thank the Universidade Estadual de Campinas for support during the work, Fundacao Amparo de Pesquisa do Estado de Sao Paulo (FAPESP) for the purchase of the equipment used in the experiment, and Dr. Daltro Pinatti for maintainance of the infrastructure necessary for the experiment. Technicians, Carlos and Antonio Pinelli, I thank for their machine work and maintainance of the helium liquifier.

I acknowledge my colleagues in the Low Temperature Laboratory, Milton Torikachivili, Manuel Arrellano, Sergio Gama, and Juan Fernandez , for the many hours spent taking data and assembliing the apparatus.

The help and concern of Daltro and Ondina Pinatti made the adjustment to life in Brazil much easier. I sincerely appreciate the support and encouragement that Les and Dee Hulett provided during the final frantic weeks of the work.

I wish to acknowledge my parents support during my earlier education and their continuing encouragement.

Finally, I want to thank my wife, Jonita, who had to accomodate herself to many different and some difficult

situations during the course of my research. Without her presence and encouragement, my work would have been substantially more difficult and less enjoyable.

Table of Contents

List of Figures

I. Introduction..... 1.

A. Motivation..... 1.

B. History..... 3.

C. The Ordered Phases of the Heavy Rare Earths..... 4.

D. The Indirect Exchange Interaction..... 8.

E. Magnetic Anisotropy..... 8.

F. The Callen and Callen Theory of Magnetic Anisotropy..... 10.

G. The Callen and Callen Theory of Magnetostriction..... 11.

H. Magnetoelastic Contributions to the Elastic Constants..... 14.

I. Southern and Goodings' Theory of the Magnetoelastic Contributions to the Longitudinal Elastic Constants in the Paramagnetic Phase of the Heavy Rare Earths..... 27.

J. Freyne's Method and Its Extension to the Highly Anisotropic Rare Earth Metals.... 34.

II. Experimental Apparatus and Procedure..... 40.

A. Magnet and Power Supply..... 41.

B. Cryostats..... 42.

C. Vacuum and Cryogenic Procedures..... 45.

D. Diodes and Heaters..... 47.

E. Temperature Controller..... 50.

F. Sample Holders..... 54.

G. Samples..... 61.

H. Magnetometer..... 62.

I. Calibration of the Magnetometer and Measurement of the Magnetization..... 69.

J. Transducers and Bonding Materials..... 73.

K. Ultrasonic Equipment and the Echo-Overlap Method..... 77.

L. Measurement of the Elastic Wave Velocities..... 88.

III. Theory..... 92.

A. Discussion of the Model Hamiltonian..... 94.

1. Exchange Interaction and the Molecular Field Approximation..... 94.

2. Anisotropic Exchange..... 97.

3. Zeeman Interaction..... 98.

4. Crystal Field Interaction..... 99.

5. One-Ion Magnetoelastic Interaction... 102.

6. Two-Ion Magnetoelastic Interaction... 109.

B. Applications of the Model Hamiltonian... 110.

1. Phase Transitions and Magnetic Ordering..... 110.

2. Magnetization and Susceptibility..... 115.

3. Anisotropy..... 116.

4. Magnetostriction..... 124.

C. Dependence of the Elastic Constants on the Magnetization..... 127.

1. Southern and Goodings' Theory of the Magnetic Field Dependence of the Longitudinal Elastic Constants..... 130.

2. Freyne's Thermodynamic Approach..... 137.

3. The General Thermodynamic Approach Applied to the Heavy Rare Earths..... 140.

IV. Numerical Calculations..... 153.

A. Preliminary Data Analysis..... 158.

B. Determination of the Parameters that Enter the Zero-Order Hamiltonian..... 161.

C. Self-Consistent Calculation of the Magnetization..... 172.

D. Self-Consistent Calculation of the Static Magnetostriction..... 176.

E. Calculation of the Second Derivatives of the Internal Energy..... 178.

F. Nonlinear Least Squares Fit of the Ultrasonic Data..... 180.

V. Experimental Data and Data Analysis..... 184.

A. Magnetization Data..... 184.

B. Elastic Constant Data..... 188.

VI. Conclusion..... 212.

Bibliography..... 215.

Appendix A

Appendix B

Appendix C

Appendix D

Appendix E

List of Figures


| Figure | Caption | Page |
|---|---|---|
| I-1 | Schematic representation of the ordered phases of the heavy rare earths. | 5. |
| I-2 | Comparison of the theoretical and experimental temperature dependences of the magnetostriction in Dy. | 15. |
| I-3 | Velocities and polarizations of the elastic waves used to measure the elastic constants in materials with hcp structures. | 17. |
| I-4,5 | Temperature dependence of the elastic constants of Er. | 18. |
| I-6,7 | Temperature dependence of the longitudinal elastic constants of Tb. | 19. |
| I-8 | Temperature dependence of the shear elastic constants of Tb. | 20. |
| I-9,10 | Temperature dependence of the longitudinal elastic constants of Ho. | 22. |
| I-11,12 | Temperature dependence of the shear elastic constants of Ho. | 23. |
| I-13 | Temperature dependence of the longitudinal elastic constants of Dy. | 24. |
| I-14 | Temperature dependence of the shear elastic constants of Dy. | 25. |
| I-15 | Temperature dependence of the mixed elastic constants of Dy. | 26. |
| I-16 | Temperature dependence of the attenuation of longitudinal elastic waves propagating along the c-axis in Er. | 28. |
| I-17 | Temperature dependence of the ultrasonic echo height in Tb single crystals at various applied magnetic fields. | 29. |
| I-18 | Comparison of the experimentally measured magnetostriction with the magnetostriction predicted by the theory of Southern and Goodings. | 33. |

| Figure | Caption | Page |
|---|---|---|
| II-1 | Variable temperature cryostat and the cryostat for the superconducting magnet. | 43. |
| II-2 | Sample holder for the vibrating sample magnetometer. | 55. |
| II-3 | Longitudinal sample holder for measurements of the ultrasonic velocity. | 57. |
| II-4 | Transverse sample holder for measurements of the ultrasonic velocity. | 59. |
| II-5 | Model of the PAR Model 155 vibrating sample magnetometer as an operational amplifier with feedback. | 66. |
| II-6 | Block diagram of the electronics used in the simultaneous measurement of ultrasonic velocity and attenuation. | 81. |
| III-1 | Model of the hcp lattice showing the three interplanar exchange constants. | 112. |
| IV-1 | Flow chart of the calculation of the second derivatives of the internal energy that are necessary to fit the observed dependence of the elastic constants on the magnetization | 155. |
| IV-2 | Flow chart of the FORTRAN and APL programs that were used in the fitting of the elastic constant data. | 159. |
| IV-3,4,5 | Comparison of the measured isothermal magnetostriction in Dy with the magnetostriction calculated munerically. | 164.<br>165.<br>166. |
| IV-6 | Comparison of the measured isofield magnetostriction with the magnetostriction calculated numerically. | 167. |
| IV-7 | Comparison of the experimentally measured susceptibilities in Dy with the calculated susceptibilities. | 169. |
| V-1 | Magnetization of DyB at 4.2K with the field applied along the a-axis. | 186. |

| Figure | Caption | Page |
|---|---|---|
| V-2 | Magnetization of DyB at various temperatures. | 187. |
| V-3 | Magnetization of DyB in the HAF phase, with the field applied along the a-axis. | 189. |
| V-4 | Experimental data and calculated fit to the elastic constant $C_{22}$ with the field along the a-axis. | 196. |
| V-5 | Experimental data and calculated fit to the elastic constant $C_{22}$ with the field along the b-axis. | 197. |
| V-6 | Experimental data and calculated fit to the elastic constant $C_{22}$ with the field along the c-axis. | 198. |
| V-7 | Experimental data and calculated fit to the elastic constant $C_{33}$ with the field along the a-axis. | 200. |
| V-8 | Experimental data and calculated fit to the elastic constant $C_{33}$ with the field along the c-axis. | 201. |
| V-9 | Experimental data and calculated fit to the elastic constant $C_{66}$ with the field along the a-axis. | 202. |
| V-10 | Field dependence of the attenuation of longitudinal waves propagating along the c-axis of the sample DyB. | 210. |
| V-11 | Field dependence of the attenuation of longitudinal waves propagating along the b-axis of the sample DyB. | 211. |

# I. Introduction

## A. Motivation

The techonological importance of the rare earths has increased greatly in scope in recent years. Although the uses of the pure elements are still limited, compounds of the rare earths, especially with the iron-group elements, are now finding technological applications. Permanent magnet materials such as $SmCo_5$ have very high energy products, which means that they have large remanent magnetizations and large coercive forces. Their large remanent magnetizations make them suitable for permanent magnet materials, and because of their high coercive forces, these materials resist demagnetization and can be fabricated in shapes that would be impossible with normal permanent magnet materials.

The rare earth garnets are, presently[71], the most promising magnetic bubble materials. Magnetic bubble domain devices require materials that are ferromagnets (or ferrimagnets) with fairly high uniaxial anisotropies and low remanent magnetizations. Other considerations are the sizes of the bubble domains and the width, mobility and structure of the domain walls.

The rare earth-iron compounds, $TbFe_2$ in particular, exhibit very large room temperature magnetostriction[72]. It has been shown in the laboratory that thin films of $TbFe_2$ can function as microwave frequency ultrasonic transducers

when deposited on quartz or ruby substrates[73]. In some cases, the films were found to have a remanent magnetization at room temperature, which allowed them to function even in the absence of a bias field.

The purpose of this thesis is to explore the magneto-elastic interactions in single-crystals through the dependence of the adiabatic elastic constants on the sample magnetization. The research reported in this thesis is a part of a larger program being carried out in Brazil at Universidade Estadual de Campinas (UNICAMP) and at Rice University. The goal of the program is to explain the magnetoelastic contributions to the elastic constants of the elements gadolinium through erbium using the theoretical model presented in this thesis. Work is now in progress at UNICAMP on the elements Tb, Ho, and Er. It is clear that an understanding of the magnetoelastic behavior of the pure elements will greatly facilitate the treatment of the more technologically important compounds.

The theoretical model that was used to account for the dependence of the elastic constants treated the exchange interaction in the molecular field approximation and defined the elastic constants in terms of thermodynamic quantities which are easily calculable in the theoretical model. Because of the complexity of the calculations, they were all done numerically on a high-speed digital computer. This approach was adopted because it is simpler and more

appropriate for high temperatures than a fully quantum mechanical treatment of the interaction of the quantized phonon and magnon fields.

It should be pointed out that the model also allows other properties such as the magnetization, magnetic anisotropy, and the static magnetostriction to be calculated (numerically, of course). The experimentally obtained quantities are compared with numerically calculated quantities in Chapter IV.

Because of the success of this model in the pure Dy metal, it is hoped that the model proposed in this thesis will, with some changes, of course, find use in more applied problems. For example, the role of the magnetostriction in the permanent magnet materials is not fully understood, and could be a mechanism responsible for the fact that the energy products that are experimentally realized are less than the theoretical maxima. In bubble materials, the magnetostriction plays a part in the formation and behavior of the domain walls, and a better understanding of its role might indicate which materials will support smaller, more mobile bubble domains.

## B. History

The early work on the bulk magnetic properties of the rare earth elements was carried out at Ames Laboratory at Iowa State by Spedding and his coworkers. Rhyne[1] has given a good review of the bulk properties of the rare earth metals which includes many of the results of these early

investigations. Until ion-exchange techniques for separating the rare earths were developed at Ames Laboratory, the difficulty of obtaining samples of sufficient purity had made studies of the fundamental properties of the rare earth elements almost impossible. As reasonable quantities of the pure metals started to become available, measurements of the bulk properties of the heavy rare earths began at Ames Laboratory. The magnetization, specific heat, and resistivity measurements that were made on polycrystalline and later on single-crystal samples clearly indicated that the magnetic behavior of the metals below room temperature was fairly complicated.

C. The Ordered Magnetic Phases of the Heavy Rare Earths

The exact nature of the magnetic ordering in the heavy rare earth metals remained a mystery, however, until single-crystals of sufficient size became available for neutron diffraction studies. The neutron diffraction experiments of Koehler and his coworkers at Oak Ridge National Laboratories revealed the complex magnetic orderings of the heavy rare earth metals. The article by Koehler[2] gives a good review of the experimentally determined ordered phases. Figure I-1 shows, schematically, the magnetic orderings that are found in the elements Gd-Tm. In all ordered phases of the heavy rare earths, all the moments in a given plane perpendicular to the c-axis are ferromagnetically aligned, but in the periodically ordered phases, the direction and magnitude of

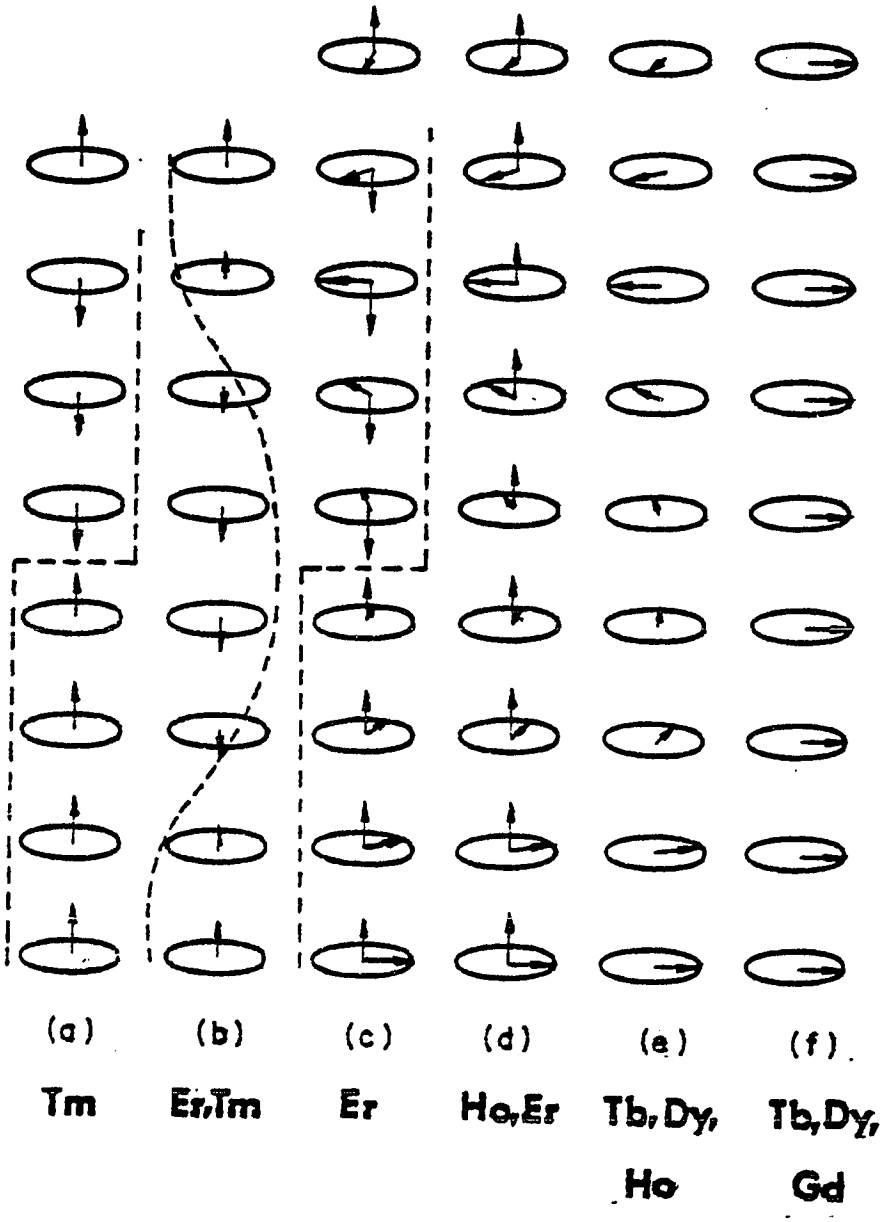


Figure I-1 Schematic representation of the ordered phases of the heavy rare earths. After Ref. 2.

the ordered moments are functions of displacement along the c-axis.

The wide variety of magnetic orderings is probably the most spectacular property of the rare earths. Each element exhibits a paramagnetic phase (PM) at high temperatures, but the orderings at lower temperatures are widely varied. All the heavy rare earths (Gd-Tm) have an antiferromagnetic phase, except for Gd, which is ferromagnetic below its Curie temperature ($T_C$), 293K. However, none of the heavy rare earths exhibit the simple Neel antiferromagnetic ordering. Their observed behavior in their antiferromagnetic phases varies from a simple helical order in Dy, Tb, and Ho, to a combination, in Er, of helical order of the basal plane components of the moments and square-wave modulation of the c-axis components.

Dy and Tb are the simplest of the heavy rare earth metals. They are simple helical antiferromagnets (HAF) between their Neel temperatures ($T_N$), 197K and 229 K, respectively, and their Curie temperatures. Below their Curie temperatures, 85K and 221K, respectively, they are simple ferromagnets.

Ho has the same structure as Dy and Tb in its HAF phase, but below its Curie temperature, 20K, it is a conical ferromagnet with the c-axis as the axis of the cone. The cone angle is large because the anisotropy tends to hold the moments in the basal plane.

In Er, the sign of the second order anisotropy has changed[3], so the c-axis is the easy axis of magnetization. Er has two distinct antiferromagnetic phases. In the phase just below the Neel temperature, 85K, there is no spontaneous moment in the basal plane, and the magnitude of the spontaneous moment parallel to the c-axis varies sinusoidally with displacemant along the c-axis. This phase is generally referred to as having the c-axis modulated (CAM) structure. As the temperature is lowered from the Neel temperature, the modulation of the c-axis moment becomes less sinusoidal and more like a square-wave. At the second transition temperature, 53K, Er enters the quasi-antiphase domain structure (QAD). The components of the moments along the c-axis become square-wave modulated and the basal plane components order into a spiral. At its Curie temperature, 20K, Er becomes a conical ferromagnet with the c-axis as the axis of the cone. The cone angle is smaller than the one found for Ho.

Tm has not been studied as extensively as the other heavy rare earth metals, because it is relatively rare. Its magnetic orderings are known, however. Below its Neel temperature, Tm has the CAM structure. At its Curie temperature, the sinusoidal modulation squares up and becomes an asymmetric square-wave modulation of the c-axis component of the moment. The structure has three layers with moments parallel to the c-axis and four layers anti-parallel to the

c-axis, so there is a net spontaneous moment.

D. The Indirect Exchange Interaction

Since the 4f electrons are in an inner shell, the direct exchange between the 4f electrons on different ions is negligible. The actual mechanism for the exchange interaction is the indirect (RKKY) exchange interaction[4-6], which couples the moments on different ions through their mutual interactions with the conduction electrons.

The long-range oscillatory nature of the indirect exchange interaction is responsible for the periodic orderings that occur in the rare earths, but the wide range of orderings that has been observed is due to the interplay of the exchange interaction with the anisotropy and magnetostriction. The ordered phases of Dy and the phase transitions that occur are discussed in more detail in Chapter III.

E. Magnetic Anisotropy

All the heavy rare earth metals except for Gd are highly anisotropic, magnetically, and the single-ion anisotropy dominates the two-ion anisotropy. The single-ion anisotropy is due to the interaction of the quadrupole moments of the 4f electron cloud with the crystalline electric field. Since $Gd^{3+}$ is an S-state ion, the quadrupole moment of its electron cloud is zero and its single-ion anisotropy vanishes.

Experiments investigating the anisotropy are generally

only done on Dy or Tb, since all the other highly anisotropic rare earths are periodically ordered in their ferromagnetic phases, and theoretical interpretation of the experiments is difficult. Dy and Tb are very similar, but Dy will be chosen as an example, since it is the element under investigation in this thesis.

At low temperatures, the c-axis of Dy is a very hard magnetic axis[7], and fields of 60kOe can only lift the magnetization out of the basal plane by an angle of 5°-6° [8]. The anisotropy energy, which is discussed more fully in Chapter III, can be calculated from a measurement of the magnetic field dependence of the angle that the magnetization makes with the basal plane at low temperatures. Equivalently, the anisotropy energy can be calculated from a measurement of the torque that is necessary to hold the sample stationary when a field is applied along the hard magnetic axis. Accounting for the temperature dependence of this anisotropy energy is a long standing problem that still has not been completely explored. Experimentally, difficulties are encountered because of the large magnetic fields which must be applied to the sample. Theoretically, it is hard to separate the magnetostrictive contribution to the effective anisotropy from the part due strictly to the anisotropy. The Callen and Callen[9,10] theory accounts quite well for the observed temperature dependence of the anisotropy energy, but the problem of the magnetostrictive

contribution to the energy remains.

F. The Callen and Callen Theory of Magnetic Anisotropy

The Callen and Callen theory takes the Zeeman and exchange interactions as the zero-order Hamiltonian. The exchange interaction is considered in the molecular field approximation, and the single-ion anisotropy is treated in first-order perturbation theory, an approximation which should be valid in the ordered phases where the anisotropy measurements were carried out. The form of the crystal field Hamiltonian, which is derived in Chapter III, is:

$$\mathcal{H}_a(i) = P_2^0 Q_2^0(\vec{J}_i) + P_4^0 Q_4^0(\vec{J}_i) + P_6^0 Q_6^0(\vec{J}_i) + P_6^6 Q_{66}^+(\vec{J}_i) \quad \text{I-1}$$

where the $Q_\ell^m$'s are the angular momentum tensor operators which are discussed and defined in Appendix A.

Since the anisotropy energy is calculated from quantities measured under static conditions, the free energy must be a minimum. In order to calculate the free energy, it is necessary to calculate the thermodynamic average of the tensor operators in the representation in which the zero-order Hamiltonian is diagonal. The zero-order Hamiltonian is diagonal in the coordinate system in which the magnetization lies along the z-axis. Since the rotational properties of the tensor operators are well known, the problem reduces to the problem of finding the thermodynamic average of the operator $Q_\ell^0$. This is the central problem in the Callen and Callen theory of magnetic anisotropy. By

making the approximation that J= ∞, Callen and Callen[9] find a closed form expression for the thermodynamic average:

$$< Q_\ell^0 > = \hat{I}_{\ell+1/2}(L^{-1}(\sigma)) = \frac{I_{\ell+1/2}(L^{-1}(\sigma))}{I_{1/2}(L^{-1}(\sigma))} \qquad \text{I-2}$$

where $I_{\ell+1/2}$ is the modified Bessel function of half-integral order, L(x) is the Langevin function, and σ is the reduced magnetization, $M/M_0$. The temperature dependence of the second and fourth order anisotropy constants of Dy has been measured and fit to the Callen and Callen theory. The fit, shown in the article by Rhyne[1], is very good.

G. The Callen and Callen Theory of Magnetostriction

The static magnetostriction has been studied in Gd, Tb, and Dy, and less thoroughly in Ho and Er. The experimental magnetostriction at a fixed temperature in the paramagnetic phase varies as the square of the magnetization[11,12]. The magnetostriction is also anisotropic; it depends on the orientation of the magnetization relative to the crystallographic axes.

Theoretically, the single-ion magnetostriction arises from the strain dependence of the crystalline electric field, and from the rearrangement of the conduction electrons in response to the strains[13]. The two-ion magnetostriction arises from the strain dependence of the exchange interaction.

Following the treatment of Callen and Callen[14], the

lowest order terms in the single-ion magnetoelastic Hamiltonian (linear in the strain and bilinear in the angular momentum operators) are, for hcp symmetry:

$$\mathcal{H}^{I}_{me}(i) = -(B_1^{\alpha,2}\, e^{\alpha,1} + B_2^{\alpha,2}\, e^{\alpha,2}) Q_2^0(\vec{J}_i) - B^{\gamma,2}(e_1^{\gamma}\, Q_{22}^{+}(\vec{J}_i) + e_2^{\gamma}\, Q_{22}^{-}(\vec{J}_i)) - B^{\varepsilon,2}(e_2^{\varepsilon}\, Q_{21}^{+}(\vec{J}_i) + e_1^{\varepsilon}\, Q_{21}^{-}(\vec{J}_i)) \qquad \text{I-3}$$

This Hamiltonian is derived from group theoretical considerations that are presented in more detail in Chapter III. Basically, the symmetry strains $e^{\alpha,1}$, $e^{\alpha,2}$, $e_1^{\gamma}$, $e_2^{\gamma}$, $e_1^{\varepsilon}$, and $e_2^{\varepsilon}$ are combinations of the Cartesian strains that transform according to the irreducible representation with which they are labeled, and the tensor operators transform according to the same row of the same irreducible representation as the symmetry strains that they multiply.

The Callen and Callen[14] theory of magnetostriction is concerned with the prediction of the dependence of the single-ion magnetostriction on the temperature and the magnitude and orientation of the magnetization. The two-ion magnetostriction depends on the two-ion correlation functions such as $< J_i \cdot J_j >$ which are not reliably handled in the molecular field approximation, especially at low temperatures. The problem of the single-ion magnetostriction is very similar to the one encountered in the treatment of the single-ion anisotropy. The magnetoelastic interaction is

treated in first-order perturbation theory, so the thermodynamic averages of the tensor operators that were derived in the treatment of the anisotropy can be used directly in the magnetostriction problem.

The dependence of the magnetostriction on the magnetic field and temperature is contained in the thermodynamic average of $Q_2^0(\vec{J})$. For small magnetizations, such as those at moderate fields in the paramagnetic phase[13]:

$$< Q_2^0 > = < Q_2^0 >_{T=0K} \hat{I}_{5/2}(L^{-1}(\sigma))$$

$$= \frac{3}{5}\sigma^2 \quad ((\sqrt{2/3}\ J(2J-1)) \qquad \text{I-5}$$

so the Callen and Callen theory correctly predicts the dependence of the magnetostriction on the magnetization in the paramagnetic phase.

The magnetostriction can be characterized at all temperatures by the six magnetostriction constants[11,14]: $\lambda_1^{\alpha,0}$, $\lambda_2^{\alpha,0}$, $\lambda_1^{\alpha,2}$, $\lambda_2^{\alpha,2}$, $\lambda^{\gamma,2}$, $\lambda^{\varepsilon,2}$ and the direction of the magnetization. The two constants $\lambda_1^{\alpha,0}$ and $\lambda_2^{\alpha,0}$ are strictly of two-ion origin, whereas, formally, the other four are of mixed origin. Assuming that the single-ion magnetostriction dominates the two-ion magnetostriction, the Callen and Callen theory predicts the dependence of these four mixed constants on temperature and magnetization:

$$\lambda_i^{\Gamma,j}(\sigma,T) = \lambda_i^{\Gamma,j}(T=0)\ \hat{I}_{5/2}(L^{-1}(\sigma(H,T))) \qquad \text{I-6}$$

Experimentally, these constants are determined at a constant temperature from the change in a given strain as the (constant) magnetization is rotated from one specific direction relative to the crystalline axes to another. (See Clark et al[11] for the definitions of the $\lambda_i^{\Gamma,j}$'s and for the details of their measurement.)

The magnetostriction constants that require the magnetization to be rotated from a hard to an easy axis can only be measured in the paramagnetic phase, since the magnetization can not be completely aligned along a hard axis in an ordered phase, because of the large magnetic anisotropy. Thus, the only constant that can be measured over the entire temperature range, 4.2K to room temperature, is $\lambda^{\gamma,2}$, which is measured by rotating the magnetization from the a-axis to the b-axis.

As Figure I-2 shows, the Callen and Callen theory accounts well for the observed temperature dependence of $\lambda^{\gamma,2}$ in Dy. Rhyne et al[12] found that, to fit the measured basal plane magnetostriction in Tb, however, it was necessary to include a term of fourth-order in the angular momentum operators, $\lambda^{\gamma,4}$. The temperature dependences of the two constants $\lambda^{\gamma,2}$ and $\lambda^{\gamma,4}$ of Tb fit the predicted temperature dependences $\hat{I}_{5/2}$ and $\hat{I}_{9/2}$, respectively, fairly well. (See Rhyne[1].)

## H. Magnetoelastic Contributions to the Elastic Constants

The magnetoelastic interaction manifests itself in

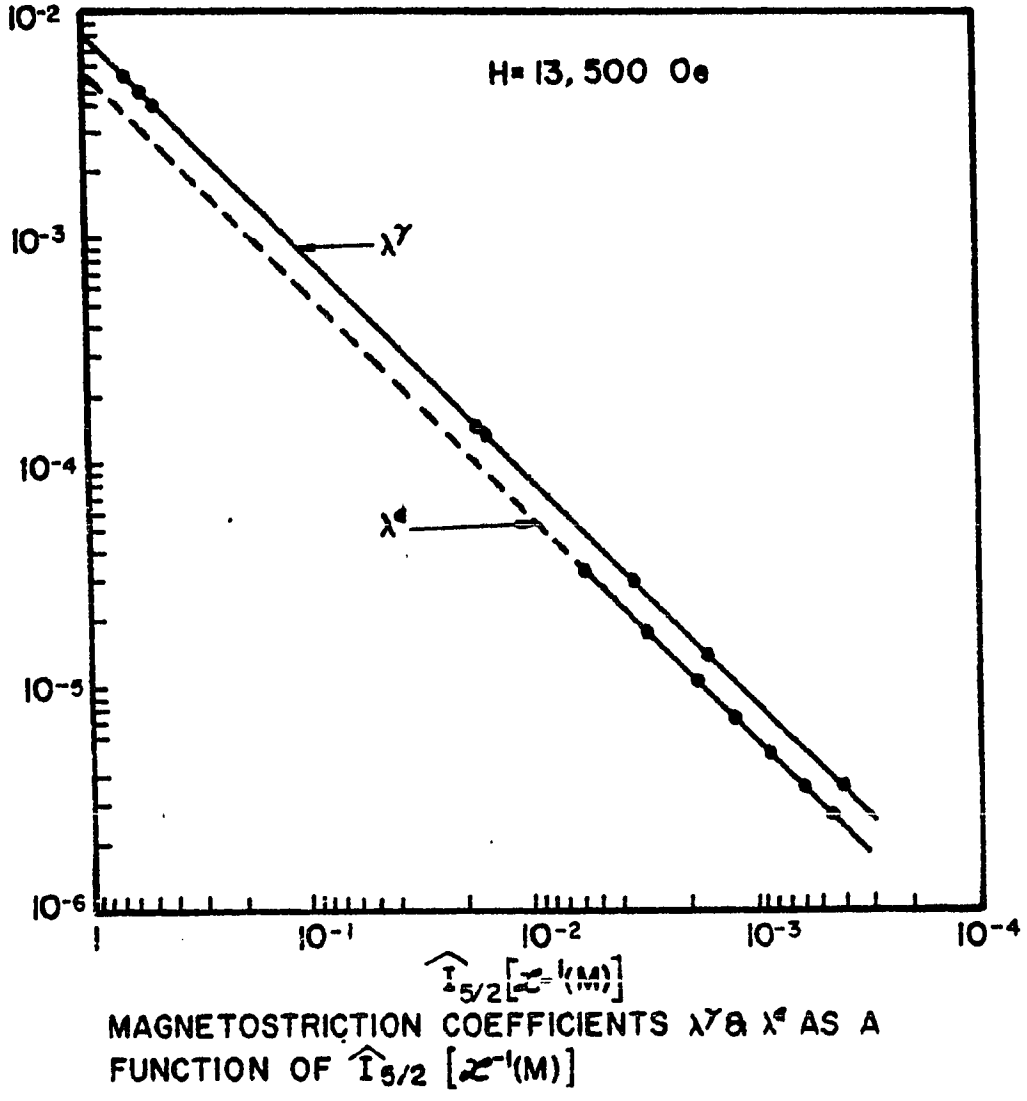


Figure I-2 Comparison of the theoretical and experimental temperature dependences of the magnetostriction in Dy.

ways other than the static magnetostriction just discussed. The elastic constants exhibit anomalies at the magnetic phase transitions that are of magnetoelastic origin, for example.

There are five independent elastic constants in the rare earths that have hcp structures[15], but there are more than five independent ways to measure the elastic constants, so it is possible to check the consistency of the measurements. Figure I-3 shows some of the combinations of propagation directions and polarizations that are possible, and how the velocities that are measured in these situations are related to the five elastic constants.

The behavior of the elastic constants of Er[16], whose magnetic phases were discussed in a previous section of this chapter, is particularly striking. The typical behavior of the longitudinal elastic constants, shown in Figure I-4, is a discontinuous change at the transition temperature. The velocities that are shown in the figures are the same as those defined in Figure I-3. The behavior of the shear elastic constants, shown in Figure I-5, is also quite pronounced. The behavior of $C_{44}$ is particularly anomalous since the normal behavior at a phase transition is either a change in slope or a small dip. The mixed constants, $C_{12}$ and $C_{13}$, are not shown because their anomalies at the transitions were small.

The elastic constants of Tb[17] as a function of

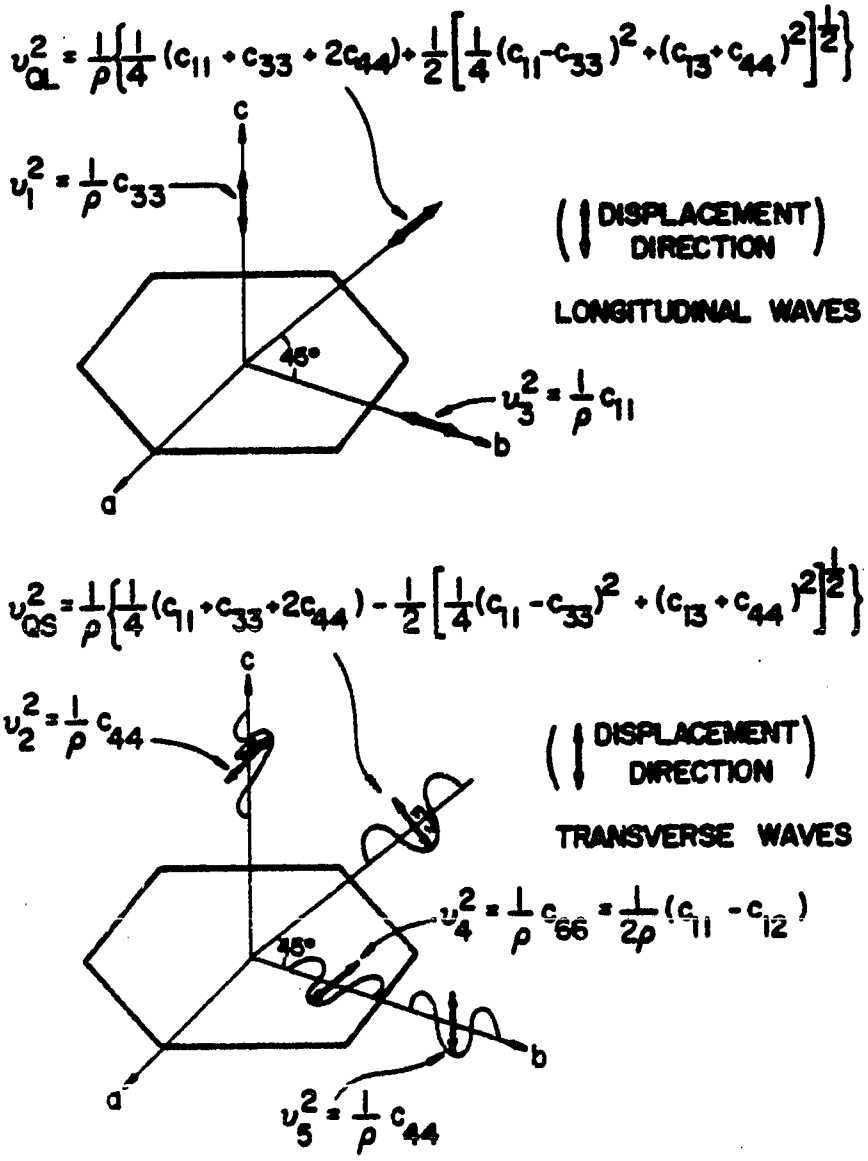


Figure I-3 Velocities and polarizations of the elastic waves used to measure the elastic constants in materials with hcp structure.

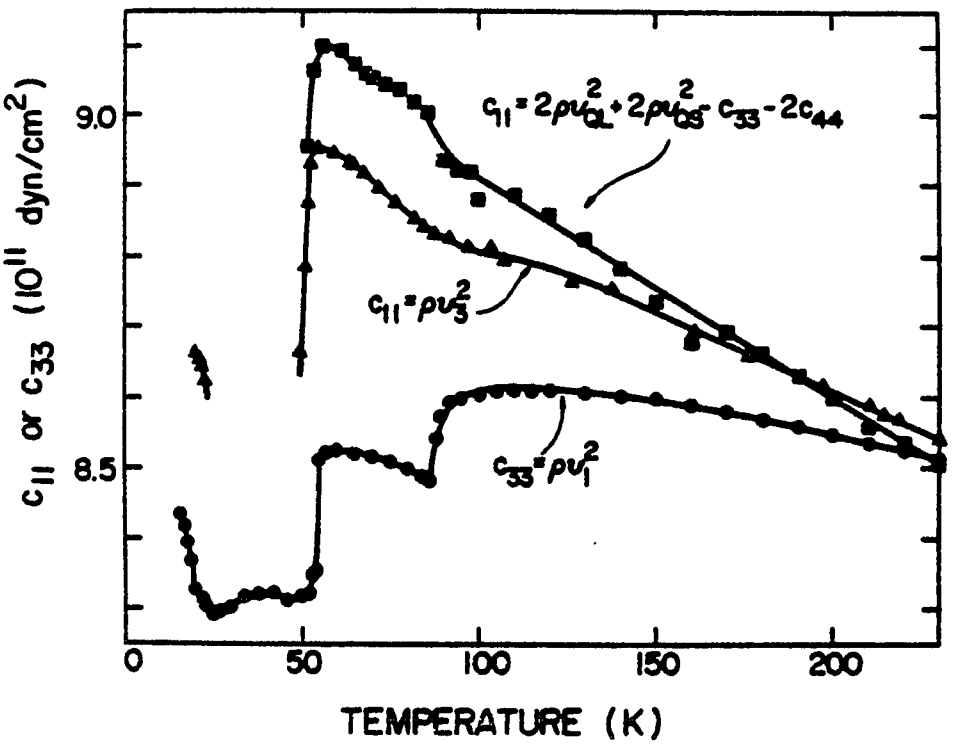


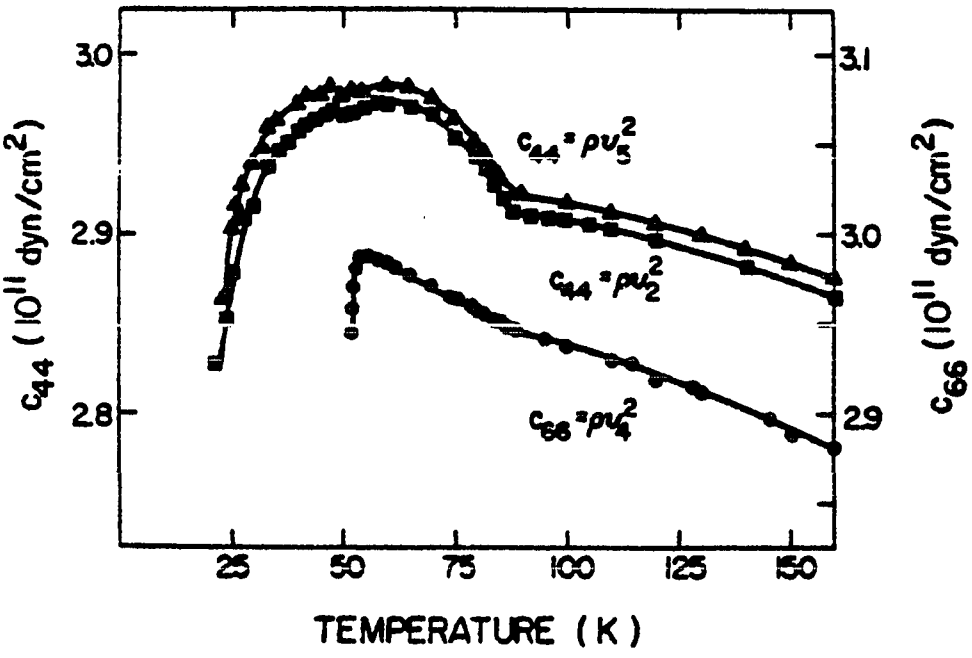


Figures I-4 and I-5 Temperature dependence of the elastic constants of Er. After Ref. 16.

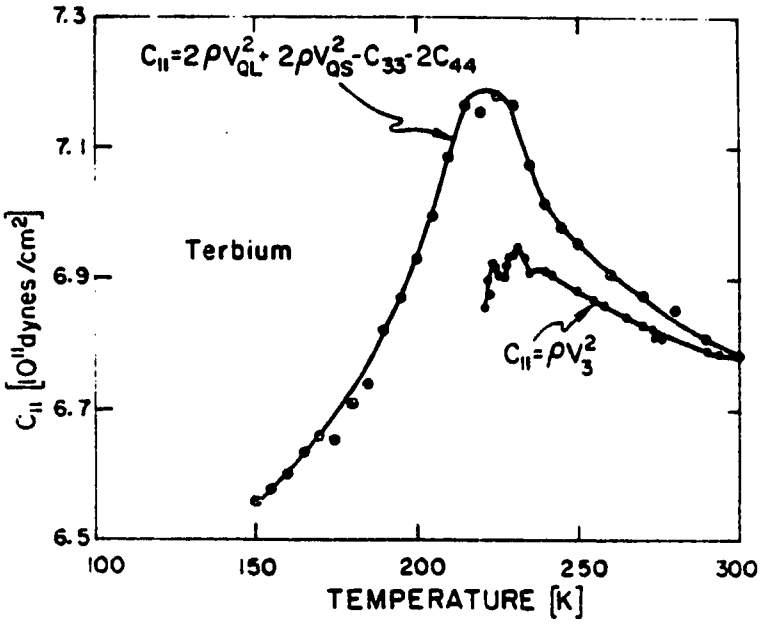


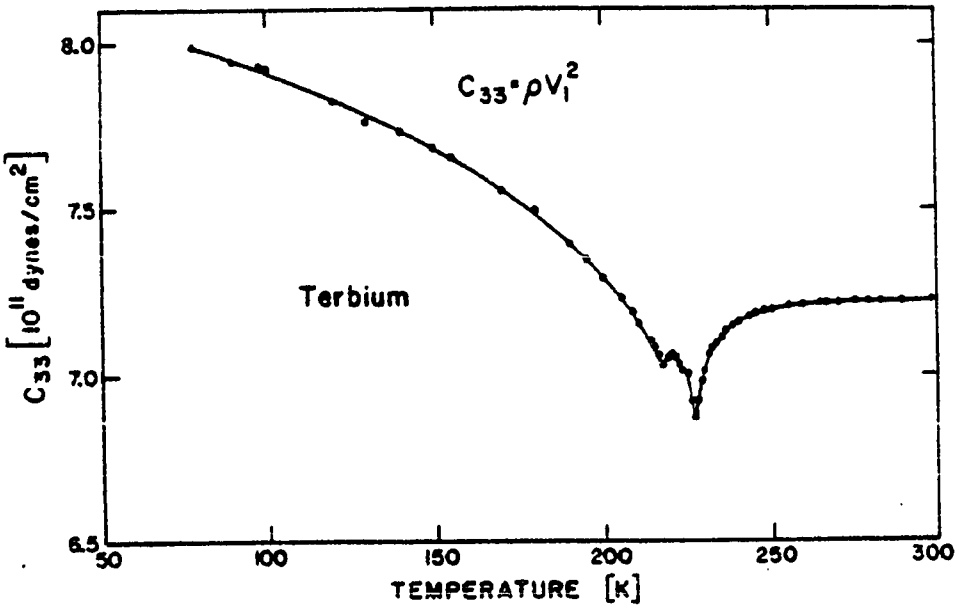


Figures I-6 and I-7 Temperature dependence of the longitudinal elastic constants of Tb. After Ref. 17.

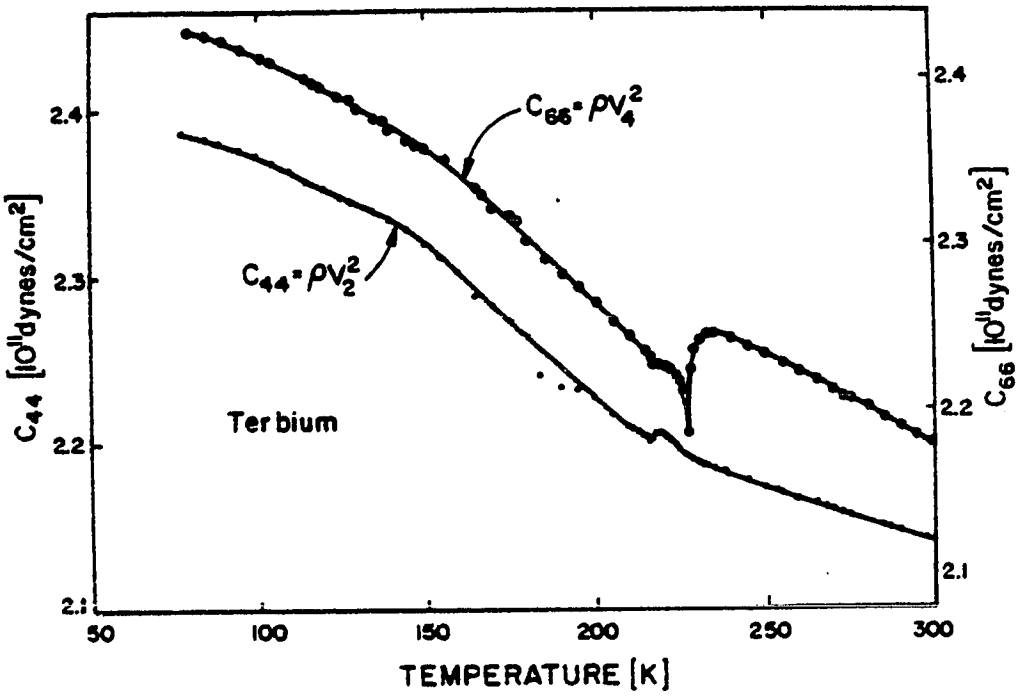


Figure I-8 Temperature dependence of the shear elastic constants of Tb. After Ref. 17.

temperature are shown in Figures I-6, 7, and 8. The behavior of the elastic constants of Tb is considerable different from that of Er. There is a dip in $C_{33}$ at each of the transitions, but at higher and lower temperatures, $C_{33}$ depends more or less normally on the temperature. $C_{11}$, on the other hand, has small peaks at the transition temperatures, and at lower temperatures, $C_{11}$decreases with temperature , in contrast to the normal increase as the temperature is lowered. The shear elastic constants have small anomalies superimposed on the normal temperature dependence.

The measurements of the elastic constants of Ho[18] were only made between 77K and room temperature, so only the transition from the paramagnetic phase to the HAF phase is included in the figures. $C_{33}$, shown in Figure I-9, has such a large dip at $T_N$ that even at 77K, it still has not reached its peak value, which occurred at about 170K. $C_{11}$, shown in Figure I-10 is affected relatively little, showing only a change of slope at $T_N$. The shear constants, shown in Figures I-11 and I-12, show larger changes in slope but little else.

The elastic constants of Dy, shown in Figures I-13, 14, and 15 , were measured by Rosen and Klimker at temperatures between 4.2K and 300K. The behavior of the longitudinal elastic constants of Dy at the PM-HAF phase transition is similar to the behavior in Tb. This fact is not unexpected since the HAF phases of the two elements are so

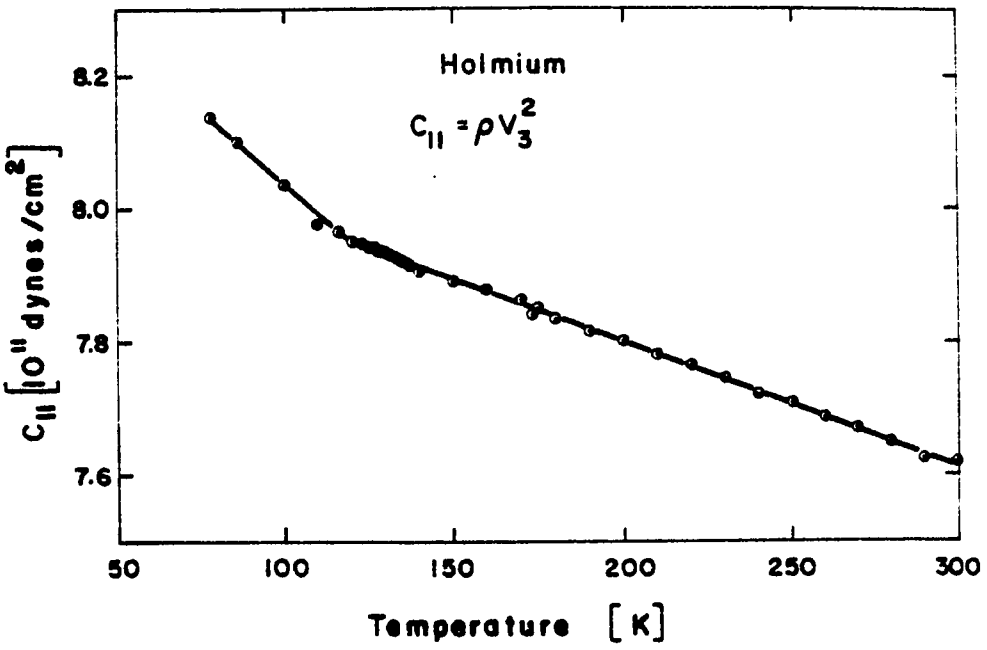


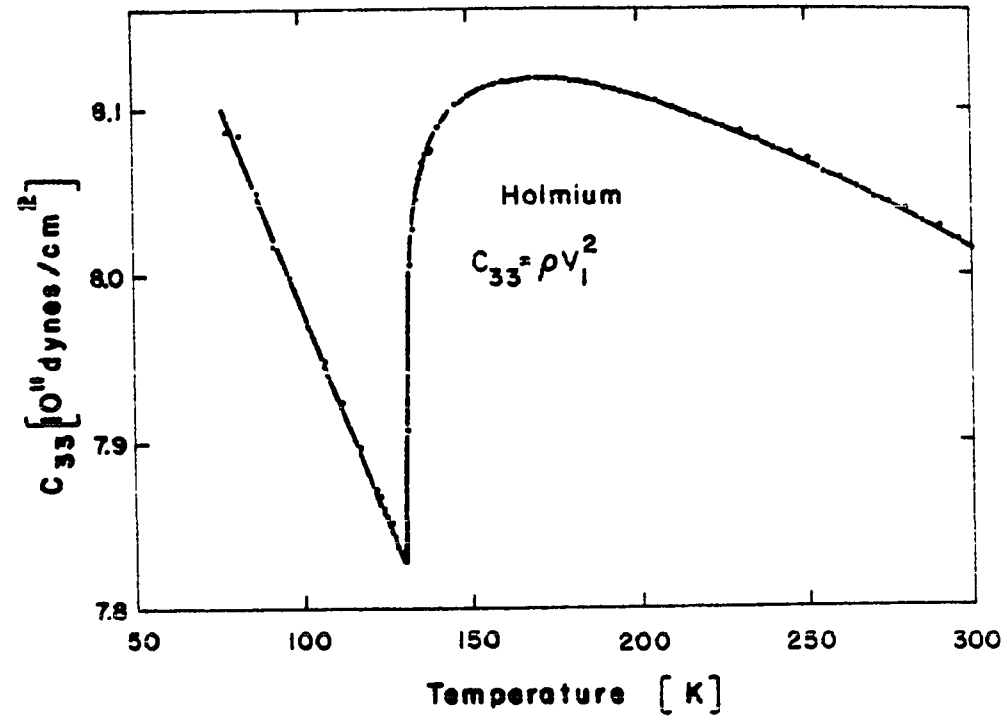


Figures I-9 and I-10 Temperature dependence of the longitudinal elastic constants of Ho. After Ref. 18.

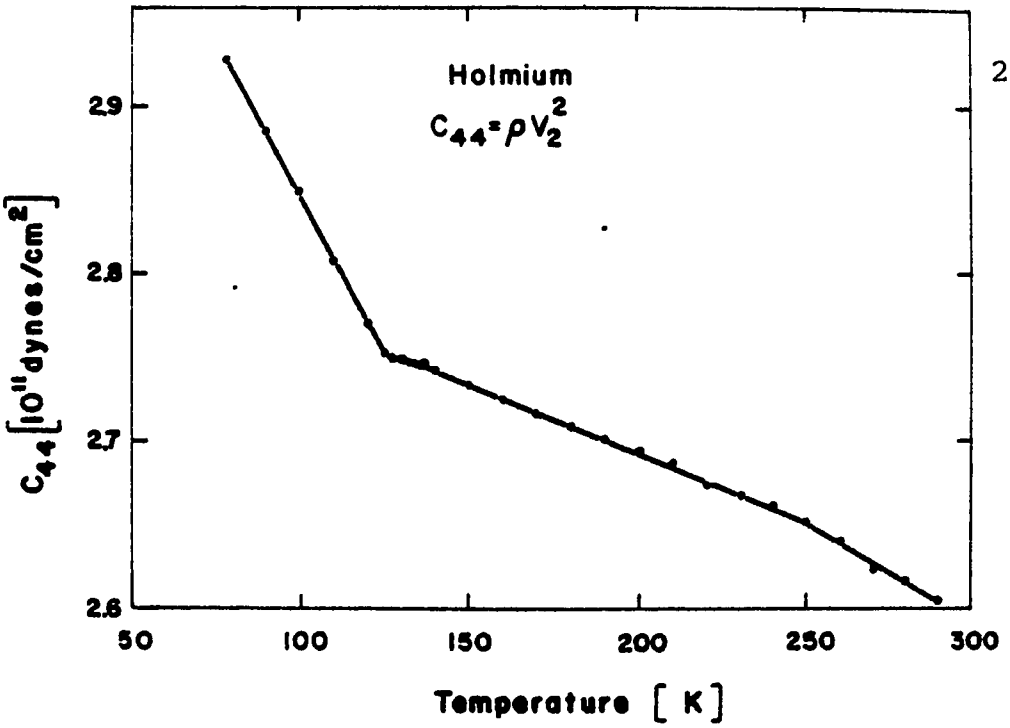


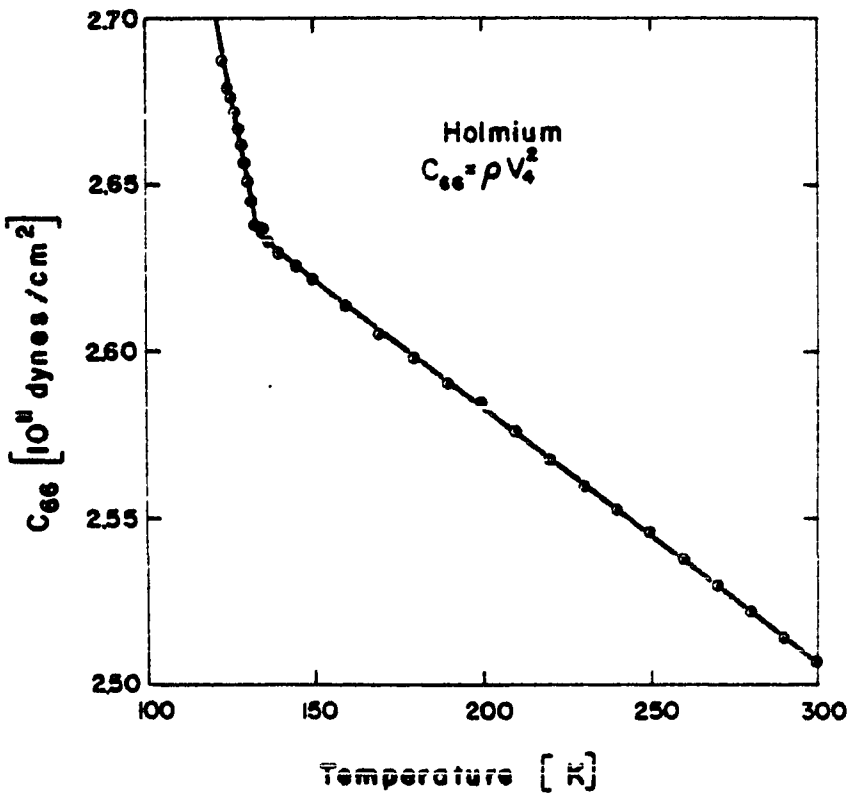


Figures I-11 and I-12 Temperature dependence of the shear elastic constants of Ho. After Ref. 18.

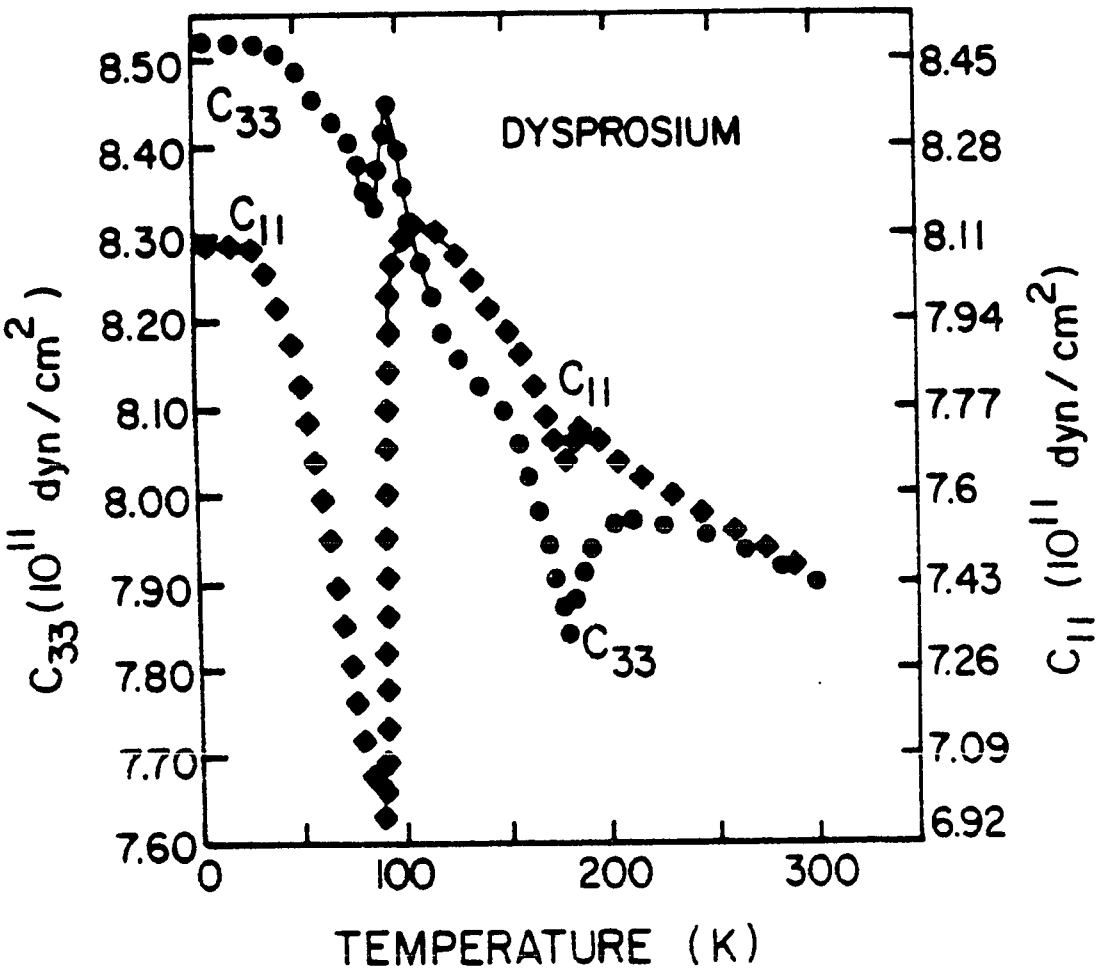


Figure I-13 Temperature dependence of the longitudinal elastic constants of Dy. After Ref. 19.

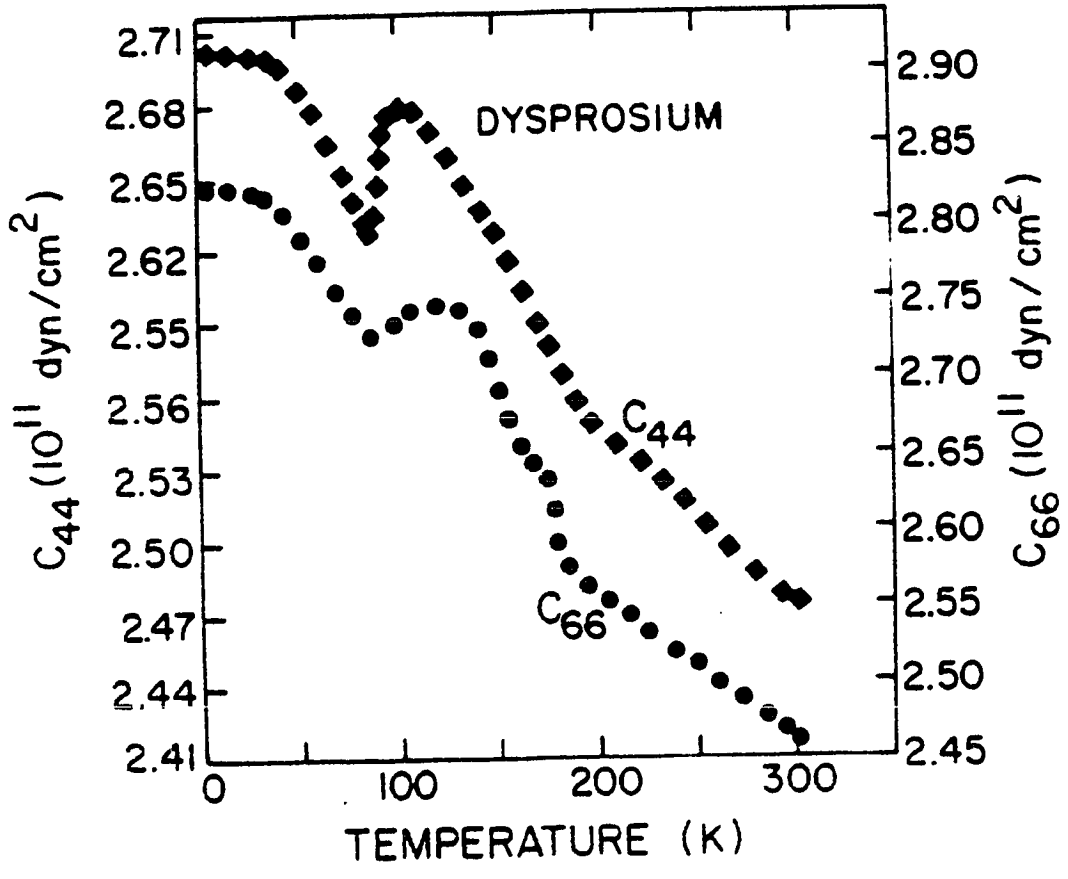


Figure I-14 Temperature dependence of the shear elastic constants of Dy. After Ref. 19.

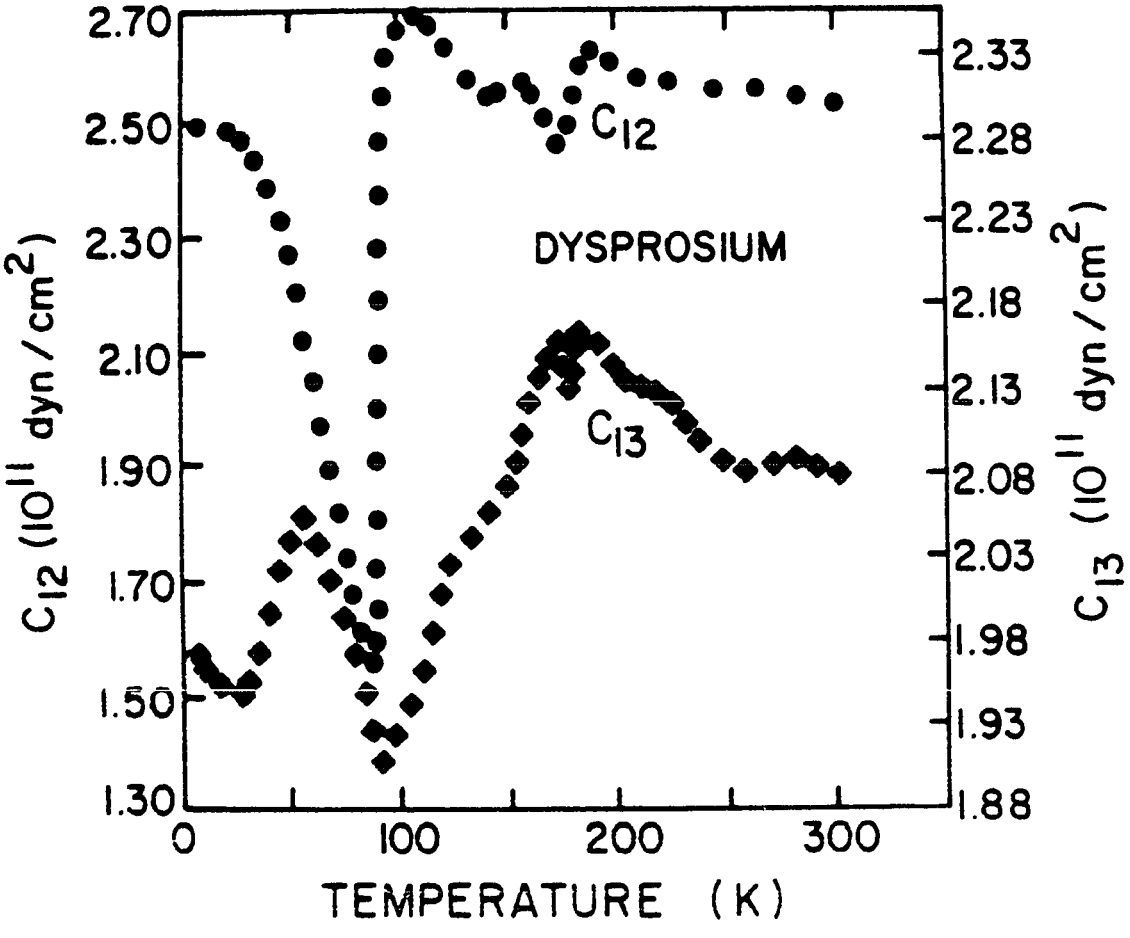


Figure I-15 Temperature dependence of the mixed elastic constants of Dy. After Ref. 19.

similar. The anomalies in the elastic constants of Dy at $T_C$ are more pronounced than the anomalies in Tb, as might be expected since the HAF phase of Dy is much more energetically stable than the HAF phase of Tb. The anomalously large changes in the elastic constants at $T_C$ are undoubtedly due in part to the magnetostrictive strains that change the symmetry of the crystal at the transition[53].

The anomalous behavior of the elastic constants at the transitions is accompanied by anomalous peaks in the attenuation[16]. Figure I-16 shows the measured attenuation of longitudinal elastic waves propagating along the c-axis of Er. Similar results have been found for the other rare earths elements[20,21]. The attenuation also exhibits an intriguing dependence on the magnetic field, as is shown in Figure I-17. It shows the echo height in Tb[22], as a function of temperature, measured with a constant applied field. Since the HAF phase of Tb is suppressed by fields larger than 1kOe, only one peak in the attenuation is seen for fields greater than 1kOe, and the temperature at which the peak occurs moves to higher temperatures as the field is increased.

## I. Southern and Goodings' Theory of the Magnetoelastic Contributions to the Longitudinal Elastic Constants in the Paramagnetic Phase of the Heavy Rare Earths

The anomalies in the elastic constants that were discussed in the last section are all due to the

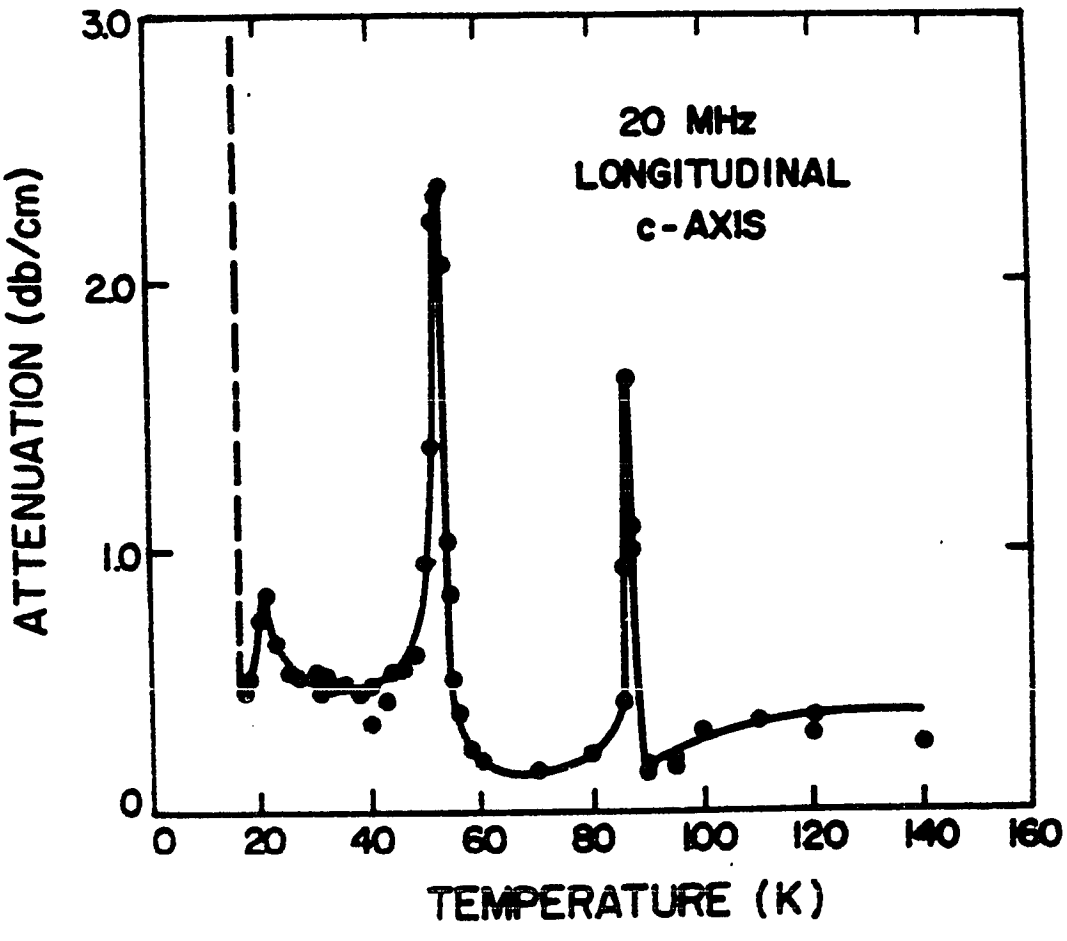


Figure I-16 Temperature dependence of the attenuation of longitudinal elastic waves propagating along the c-axis in Er. After Ref. 16.

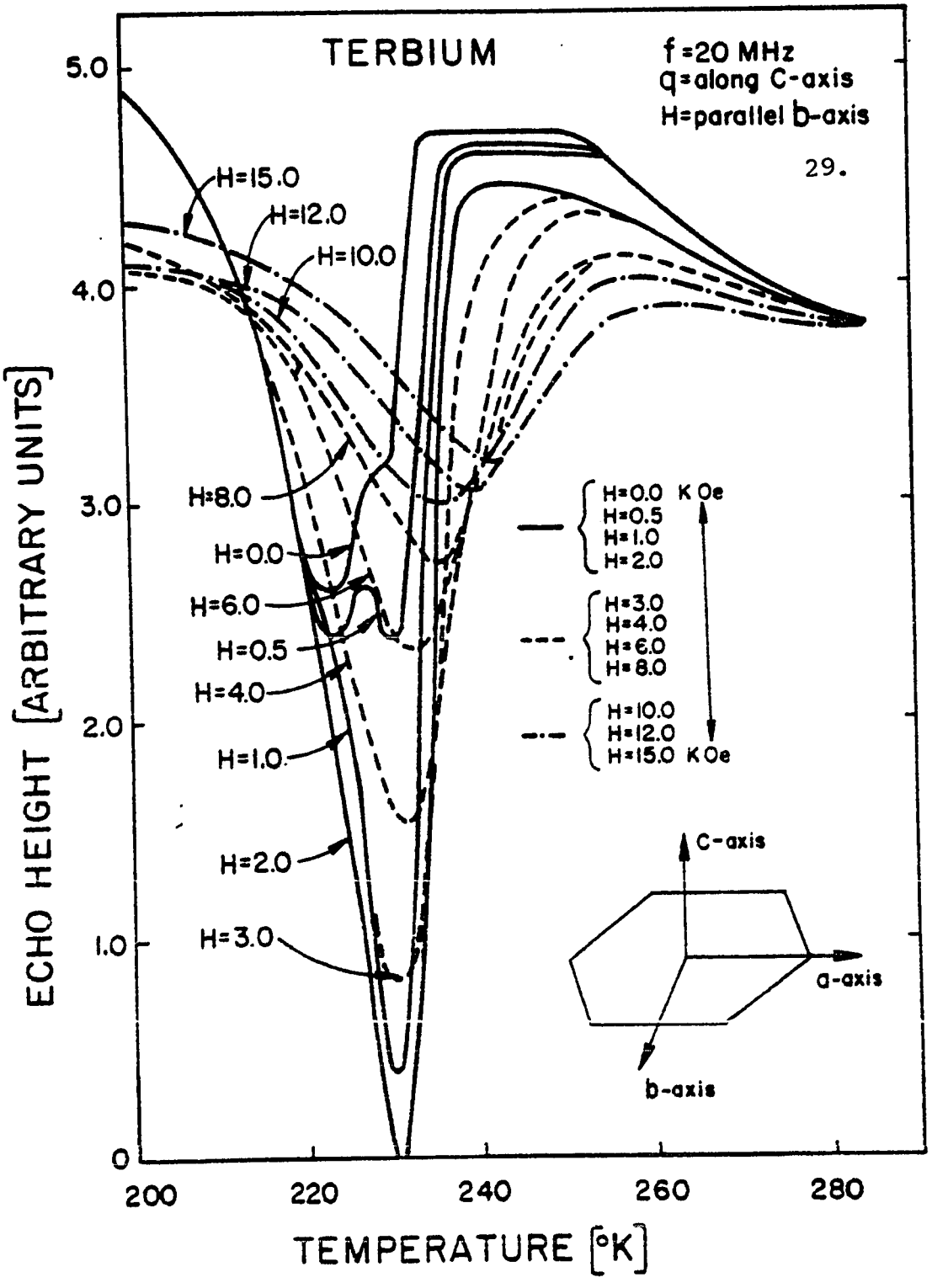


Figure I-17 Temperature dependence of ultrasonic echo height in terbium single crystals at various applied magnetic fields. Longitudinal waves propagating along the c-axis, and magnetic fields applied parallel to the b-axis.

magnetoelastic contributions to the elastic constants with zero applied field. The main interest of this thesis is the contribution of the magnetoelastic interaction to the elastic constants in the paramagnetic phase, as a function of the sample magnetization. The treatment of this problem requires an extension of the usual Callen and Callen theory of magnetostriction since the definition of the elastic constants that is appropriate for this problem is:

$$C_{ijkl} = \frac{\partial^2 U}{\partial \varepsilon_{ij} \partial \varepsilon_{kl}} \qquad \text{I-7}$$

where $\varepsilon_{ij} = \partial u_i / \partial x_j$ is the unsymmetrized strain tensor. One consequence of this definition of the elastic constant is that the internal energy U must have terms in it that depend on the magnetization and that are bilinear in the strains, if the magnetoelastic contribution to the elastic constants is to be nonzero. Callen and Callen[14] were concerned with the static magnetostriction which only depends on terms in the free energy that are linear in the strains and that depend on the magnetization. Thus, their treatment predicts a vanishing magnetoelastic contribution to the elastic constants.

Southern and Goodings[23] gave the first comprehensive treatment of the magnetoelastic contributions to the elastic constants of the heavy rare earths. Their approach, discussed in more detail in Chapter III, involved the application of finite strain theory[24-26] to the heavy rare earths.

Finite strain theory, also discussed in Chapter III, requires that the total energy be expressed in terms of a certain set of quantities. The application of finite strain theory by Southern and Goodings entailed the replacement of the usual (symmetric) part of the infinitesimal strain tensor:

$$e_{ij} = \frac{1}{2}\left( \frac{\partial u_i}{\partial x_j} + \frac{\partial u_j}{\partial x_i} \right) \qquad \text{I-8}$$

with the finite strain tensor:

$$E_{ij} = \frac{1}{2}\left(\frac{\partial u_i}{\partial x_j} + \frac{\partial u_j}{\partial x_i}\right) + \frac{1}{2} \sum_k \frac{\partial u_k}{\partial x_i} \frac{\partial u_k}{\partial x_j} \qquad \text{I-9}$$

and the replacement of the usual angular momentum operators, $\vec{J}$, with:

$$J_i^* = \sum_j (\delta_{ij} - \omega_{ij}) J_j \qquad \text{I-10}$$

where $\omega_{ij}$ is the anisymmetric part of the infinitesimal strain tensor, which is usually neglected in classical elasticity theory. The majority of Southern and Goodings' paper is concerned with the effect of the inclusion of the antisymmetric part of the strain tensor, $\omega_{ij}$, on shear waves whose velocities are degenerate in the usual elasticity theory, but which are not degenerate when the rotational (or antisymmetric) strain terms are included. In one section of the paper, however, they consider the effect of the inclusion of the finite strains themselves on the longitudinal elastic constants in the paramagnetic phase. Since

$$E_{ii} \simeq e_{ii} + \frac{1}{2} e_{ii}^2 \qquad \text{I-11}$$

the straightforward substitution of the finite strains for the infinitesimal strains is sufficient to give a nonzero magnetoelastic contribution to the longitudinal elastic constants.

Several investigations[27-31] of the longitudinal elastic constants in the paramagnetic phase were motivated by the theory of Southern and Goodings. The theory of Southern and Goodings allows certain combinations of the magnetoelastic constants to be determined from the experimentally measured contributions to the elastic constants $C_{11}$ and $C_{33}$. The static magnetostrictive strains can then be calculated from these constants and compared to those obtained experimentally. Figure I-18 shows the results of this calculation for the strain $\bar{e}_1^{\gamma}$ in Ho[30,31]. The calculated strain is more than an order of magnitude larger than the measured strain. On the basis of this result and other similar results for Dy[29] and for Tb[27], the Southern and Goodings theory of the field dependence of the longitudinal elastic constants was judged to be inadequate. Later investigations[30], including experimental measurements reported in this thesis, have now shown other inadequacies. In particular, in the theory of Southern and Goodings, the entire dependence of the elastic constant on the magnetization is included in the function: $\hat{I}_{5/2}(L^{-1}(\sigma))$ (see III.B.3 for its

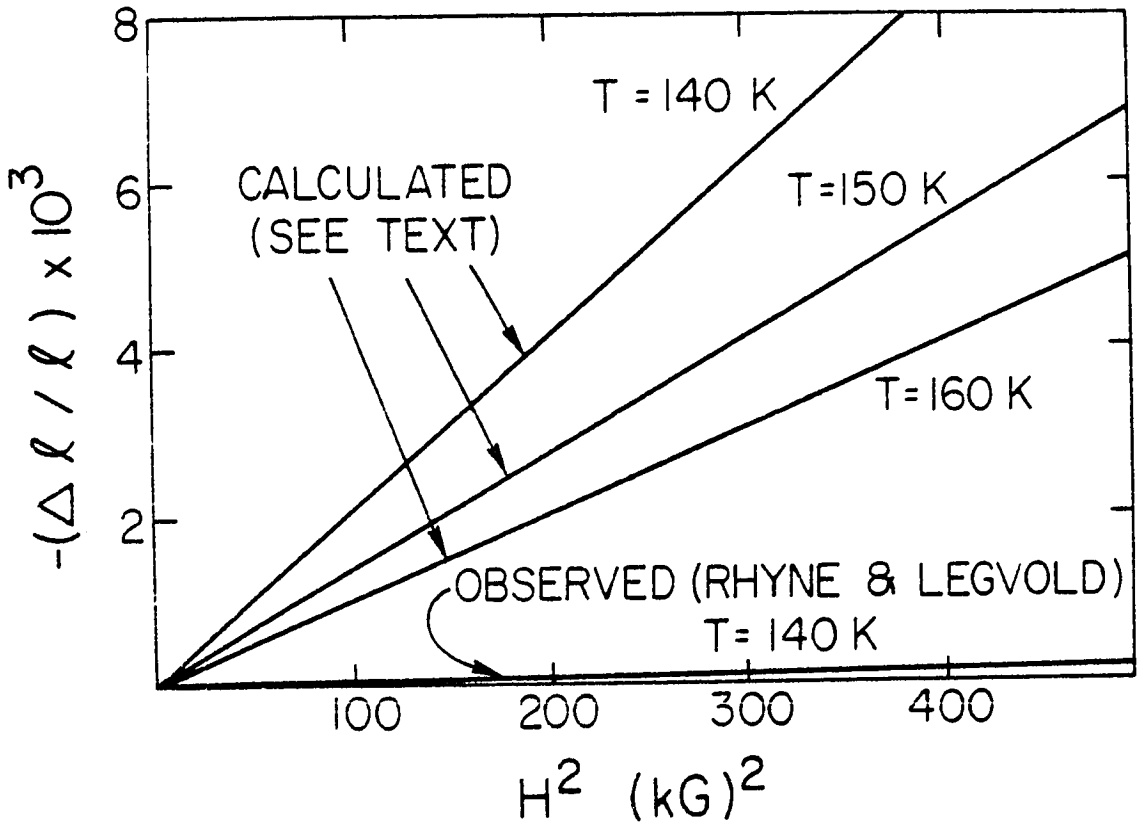


Figure I-18 Comparison of the experimentally measured magnetostriction in Ho and the magnetostriction predicted from the theory of Southern and Goodings.

definition), which is a monotonic function of the magnetization. Experimental measurements of $C_{33}$ in Dy and Tb have shown, however, that the dependence of some of elastic constants on the magnetization is far from monotonic. In some cases, the magnetoelastic contribution to the elastic constant even changes its sign at high fields. This behavior is completely unaccounted for in the theory of Southern and Goodings.

## J. Freyne's Method and Its Extension to the Highly Anisotropic Rare Earth Metals

In this thesis, the thermodynamic method, inspired by the work of Freyne[32], is used to explain the experimentally measured magnetoelastic contributions to the elastic constants of Dy. The elastic constants $C_{22}$, $C_{33}$, $C_{44}$, and $C_{66}$ were measured by the ultrasonic echo-overlap technique developed by May[33] and Papadakis[34]. The elastic constants were measured as a function of magnetic field , for fields up to 75kOe, at temperatures in the paramagnetic phase. In some cases the elastic constants were measured over the temperature range 4.2K to 300K, but no analysis was done of the low temperature data. The magnetic fields were were applied only along:

1. the a-axis in the measurement of the shear constants $C_{44}$ and $C_{66}$
2. the a and c-axes in the measurement of $C_{33}$
3. all three axes in the measurement of $C_{22}$.

The magnetizations of the same samples that were used for the ultrasonic work were also measured as a function of the magnetic field, so the ultrasonic properties could be related to the state of the magnetization in the sample.

The theoretical model that was used in the calculation presented in this thesis is similar to the method of Freyne[32] with which he was able to explain an experimental zero field anomaly in the elastic constant $C_{33}$ of Gd, as well as the effect on the anomaly of magnetic fields applied either parallel or perpendicular to the c-axis.

Using the elastic wave dispersion relation derived from the equations of motion, Freyne calculated the elastic wave velocity as a function of the second derivative, $\partial^2 U/\partial e_{33}\partial z$, of the internal energy. He used the Callen and Callen Hamiltonian, but truncated the terms that were not necessary for his problem. Freyne calculated the internal energy from the truncated Callen and Callen[14] Hamiltonian by treating the exchange interaction in the molecular field approximation and the anisotropy and magnetostriction in first-order perturbation theory. Having calculated the energy levels, $E_m$, the calculation of the internal energy:

$$U = \frac{\sum_m E_m \, e^{-E_m/kT}}{\sum_m e^{-E_m/kT}} \qquad \text{I-12}$$

was straightforward. His expression for the second derivative of the internal energy is rather complicated, but

Freyne was using a computer for the numerical computations, so there was no problem in calculating the derivative.

The agreement of Freyne's calculations with the experiment were good in zero field and fair in an applied field. In all cases, his results agreed qualitatively with the observed behavior.

Although Freyne's method was successful in Gd, it can not be applied directly to the other heavy rare earths because of approximations which Freyne made that are justified for Gd, but not for the other heavy rare earths. His method was extended somewhat in the work of Hubbell et al[35] on a similar anomaly in $C_{33}$ at the PM-CAM transition in Er. However, Freyne's method had to be extended still more to handle the class of problems that are considered in this thesis.

The zero-order Hamiltonian adopted for the calculations presented in this thesis included the isotropic and anisotropic exchange interactions, the Zeeman interaction, the crystal field interaction, and the static magnetoelastic interaction. The isotropic and anisotropic exchange interactions and the two-ion magnetoelastic interaction were treated in the molecular field approximation. The 16 by 16 Hamiltonian matrix is nondiagonal in general, so its eigenvalues and eigenvectors were calculated numerically using a high speed digital computer.

The perturbing Hamiltonian, $\mathcal{H}_{me}^{rf}$, is the part of the magnetoelastic interaction that is a function of the small dynamic strains that are applied to the sample by the transducer. Written in abbreviated notation, $\mathcal{H}_{me}^{rf}$ is:

$$\mathcal{H}_{me}^{rf} = \sum_{i=1}^{7} X_i Q_i \qquad \text{I-13}$$

where the $Q_i$'s are the seven angular momentum and tensor operators that appear in the Hamiltonian and the $X_i$'s are their coefficients, which depend on the strains and on the magnetoelastic constants. The contribution of the dynamic magnetoelastic interaction ($\mathcal{H}_{me}^{rf}$) to the energies was calculated in second-order perturbation theory, so if:

$$\mathcal{H}_0 |m> = E_m^0 |m> \qquad \text{I-14}$$

then

$$E_m = E_m^0 + E_m^1 + E_m^2 \qquad \text{I-15}$$

or more explicitly:

$$E_m = E_m^0 + < m |\mathcal{H}_{me}^{rf}| m > + \sum_{n \neq m} \frac{< m |\mathcal{H}_{me}^{rf}| n >< n |\mathcal{H}_{me}^{rf}| m >}{E_m^0 - E_n^0} \qquad \text{I-16}$$

The magnetoelastic contribution to the elastic constant is defined theoretically as:

$$\Delta C_{ijkl}(\sigma) = \frac{\partial^2 U}{\partial \varepsilon_{ij} \partial \varepsilon_{kl}}(\sigma) - \frac{\partial^2 U}{\partial \varepsilon_{ij} \partial \varepsilon_{kl}}(\sigma=0) \qquad \text{I-18}$$

where the internal energy is defined in equation I-12. The second derivative of the internal energy with respect to the strains must eventually be expressed in terms of the derivatives of $E_m^1$ and $E_m^2$ since only they depend on the strain. This presents a problem, since the magnetoelastic constants are initially unknown. Inspection of equations I-13 and I-16 shows, however, that the derivatives of $E_m^1$ and $E_m^2$ with respect to the $X_i$'s depend only on the matrix elements of the operators, $Q_i$. As a result, the second derivatives of the internal energy with respect to the strains must be expressed in terms of the second derivatives of the internal energy with respect to the $X_i$'s:

$$\frac{\partial^2 U}{\partial \varepsilon_{ij} \partial \varepsilon_{kl}} = \sum_{m,n} \frac{\partial X_m}{\partial \varepsilon_{ij}} \frac{\partial X_n}{\partial \varepsilon_{kl}} \frac{\partial^2 U}{\partial X_m \partial X_n} \qquad \text{I-19}$$

The derivatives, $\partial^2 U / \partial X_m \partial X_n$, can be calculated numerically, and the derivatives, $\partial X_m / \partial \varepsilon_{ij}$, are just linear combinations of the magnetoelastic constants, so the coefficients of the calculated derivatives are bilinear in the magnetoelastic constants. Thus, given the experimental values of the $\Delta C_{ijkl}$, and the calculated derivatives of the internal energy with respect to the $X_i$'s, the magnetoelastic constants can be determined by using a nonlinear least squares procedure.

The theoretical model used in this thesis still has defects and omissions which should be made clear. Its most glaring defect is that the helically ordered phase is not

included. In the model, Dy becomes ferromagnetic at 170K ($\theta_\perp$) and below this temperature has a spontaneous moment that is described approximately by the Brillouin function with J = 15/2. The use of the molecular field approximation is not desirable, but is almost inevitable because of the complexity of other methods of treating the exchange interaction. Also, for simplicity, only terms linear in the strains and bilinear in the angular momentum operators were included in the magnetoelastic Hamiltonian.

## II. Experimental Apparatus and Techniques

The primary goal of the experiment was to measure the elastic constants as a function of the magnetization. In practice, the elastic constants and magnetization were measured as a function of the applied field, and the elastic constants were then expressed as a function of the magnetization. By expressing the elastic constants as a function of the magnetization, it was possible to avoid having to account for the nonuniform demagnetizing fields that appear in the nonellipsoidally shaped samples, and by making measurements of the magnetization on the same samples that were used in the measurement of the elastic constants, it was possible to avoid small differences in the magnetization due to differences in the impurities found in different samples. Thus, it was possible to do a more reliable interpretation of the elastic constant data when it was expressed as a function of the sample magnetization.

A large part of the equipment discussed in this section was used in both experiments, even though they were carried out separately. In particular, the magnet and power supply, the dewar and temperature controller and the diodes were the same. The sample holders were different, as was the actual apparatus used in making the measurements: the magnetometer in one case, and the MATEC ultrasonic equipment in the other case.

A. Magnet and Power Supply

Both experiments were done using an Oxford Equipment 75kOe superconducting magnet, which was constructed from NbTi wire potted in an epoxy resin. The solenoid had a clear bore of 5cm and the inhomogeneity of the applied field was less than 1 part in $10^5$ inside a sphere of 1cm diameter. This inhomogeneity in the field was negligible compared with the inhomogeneous demagnetizing fields inside the nonellipsoidally shaped samples. Since no gaussmeter was available to measure the magnitude of the applied magnetic field directly, the current in the coil, as indicated by the current monitor output of the power supply, and the calibration of the coil provided by Oxford, 1.714kOe/A, were used to calculate the value of the applied field when it was of some interest. In most cases, however, the exact value of the field was of no importance, since both the magnetization and the elastic constants were measured as a function of the applied current, and the elastic constants were eventually expressed as functions of the magnetization. The current or field was, therefore, only an intermediate parameter which was later eliminated and any error in the calibration, if it was constant with time, had no effect on the final results.

The magnet current was supplied by an Oxford Instruments 60A power supply. A potentiometer mounted on the front panel of the power supply allowed the maximum magnet

current to be chosen before the start of the experiment so the magnet would never be quenched by exceding the critical field. The power supply also provided a current monitor voltage which was proportional to the current, with a constant of proportionality of 1.25mV/A. In all cases, the current monitor voltage was measured with a Systron-Donner 7004 digital multimeter (4 1/2 digits) and, when the magnetization was being recorded, the current monitor voltage was used to drive the X-axis of a Hewlett-Packard 7004B X-Y recorder.

The power supply current was externally controllable, by the application of 0-5Vdc to the external sweep input, from 0A to the maximum set by the front panel potentiometer. The 0-5 V was provided by an Oxford Instruments electronic sweep generator as a linear function of time, with the total duration of the sweep being variable from 1 to 100 minutes. Most of the data in this thesis were taken at the 10 minute sweep rate to conserve liquid helium (LHe) but, in temperature or field regions where the magnetization was changing more rapidly, the sweep time was raised to 20 or 50 minutes.

B. Cryostats

The main cryostat shown in Figure II-1 was supplied by Oxford Instruments specially for the 75kOe coil that was used in this experiment. The cryostat consisted of a liquid nitrogen shield surrounded by a continuously pumped isolation vacuum. The LHe reservoir was located inside the cylindrical nitrogen shield, but was separated from it by

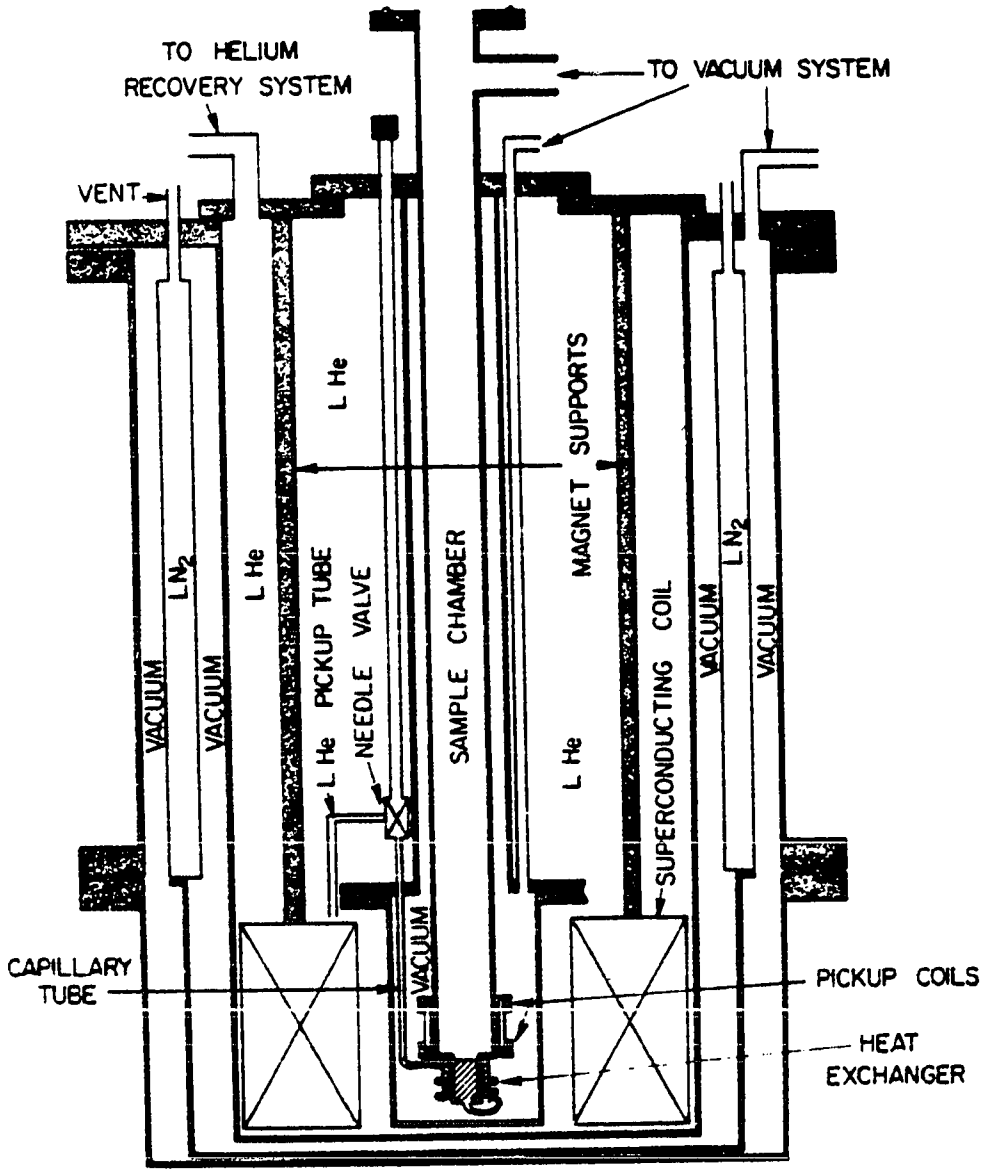


Figure II-1 Cryostat for the superconducting magnet and the variable temperature cryostat.

the isolation vacuum. The superconducting coil itself was suspended at the bottom of the LHe reservoir by three rods which connected to a plate which was screwed to the top of the cryostat. The plate contained feedthroughs for the leads to the magnet as well as ports for the transfer of the LHe, and other assorted feedthroughs. Two copper radiation shields were attached to the three rods to minimize the radiation into the LHe.

The variable temperature cryostat shown in Figure II-1 was constructed specially for the type of experiment reported here. The variable temperature cryostat was of the conventional flowing-gas type, with the rate of flow of the exchange gas controlled by a needle valve. The sample chamber had three accesses, one at the top for placing the sample holder inside, one at the side for the recovery of the flowing helium and for pumping the sample chamber, and one at the bottom where the liquid or gaseous helium entered from the LHe reservoir after passing through the capillary tube and the heat exchanger. The sample chamber was surrounded by a continuously pumped vacuum space which separated it from the LHe reservoir and which prevented large losses of LHe while operating at temperatures near room temperature in the sample chamber. The vacuum space also included the capillary tube which connected the heat exchanger and the LHe reservoir, the leads to the heater on the heat exchanger, and the magnetometer detection coils and leads.

The pumpout port for the vacuum space of the variable temperature cryostat, the knob that opened and closed the needle valve, and the feedthrough for the heater and detection coil leads were located on the support plate of the variable temperature cryostat that screwed to the plate that supported the magnet.

C. Vacuum and Cryogenic Procedures

When starting the cool-down of the cryogenic system after it had been warmed to room temperature and the vacuum had been broken, it was first necessary to get a good diffusion pump vacuum in the main isolation space. Generally, the vacuum space in the variable temperature cryostat was also evacuated at this time. The vacuum systems of the two were separate, each consisting of a mechanical pump, a diffusion pump, and the necessary valves and connections to allow both rough pumping and pumping with the diffusion pump backed by the mechanical pump. After achieving a good vacuum in the isolation space, the rough pumping and flushing of the reservoir was started. Because of the presence of the superconducting coil and many feedthroughs in the reservoir, it was usually necessary to allow several hours for the cleaning of the reservoir. After the cleaning had been completed, the $LN_2$ shield was filled and cooling began. The magnet and reservoir were rarely precooled with $LN_2$ because of the difficulty of removing all the liquid and the danger of contaminating the LHe if any liquid remained when the LHe

was transferred. However, a thermocouple had been mounted in contact with the body of the magnet, so it was possible to avoid large losses of LHe by delaying the transfer of LHe until the magnet temperature was in the neighborhood of the temperature of the liquid nitrogen.

The LHe was transferred from 100 liter storage dewars into the reservoir through a vacuum insulated transfer line. The LHe was transferred by maintaining an overpressure in the storage dewar after the line had been inserted into the dewar and reservoir.

All the helium used in this experiment was recovered, purified and reliquified, so the cryogenic equipment was designed with this fact in mind. The evaporated gas from the LHe reservoir went directly into the recovery system through a flexible brass tube that connected to the exhaust port of the reservoir.

The reservoir was kept at an overpressure when controlling the temperature so that the LHe would be forced through the capillary tube into the bottom of the sample chamber. This liquid became the exchange gas when vaporized in the heat exchanger, so it was necessary to keep its flux constant to avoid perturbing the temperature. The gas passing out of the sample chamber passed through a fluxmeter before entering the recovery system, so the flux could be monitored and kept constant by either changing the pressure in the reservoir or by opening or closing the needle valve.

D. Diodes and Heaters

GaAs diodes supplied by Lakeshore Cryogenics were used as temperature sensors and, since large magnetic fields were being used, diodes designed to reduce errors in the temperature when placed in a magnetic field were used. With a constant 10μA of current through the diode, the voltage across the diode was almost linear with temperature above 50K, with a sensitivity of approximately 3mV/K, about 100 times larger than the sensitivity of thermocouples normally used at low temperatures. The data sheet supplied by Lakeshore showed that at a temperature of 4.2K, in a field of 75kOe, with the junction of the diode parallel to the field, the error in temperature was 1.5K, whereas at 77K, the error was not shown, but was presumed to be zero. Temperature errors of this magnitude should not have affected, appreciably, the data reported in this thesis. Most of the the data were taken at temperatures in the paramagnetic phase of Dy, 179K and above, where the temperature error was small. In addition, since the ordering temperature of Dy is relatively high, most quantities of interest are slowly varying functions of temperature in the region where the errors are the greatest, i.e. at temperatures below 77K and at magnetic fields greater than 20kOe.

The diodes were received uncalibrated, so it was necessary to calibrate them versus some temperature standard. Although its sensitivity drops off rapidly below 20K, a

copper vs. constantan thermocouple was chosen as the temperature standard. At 20K and below, the interesting physical quantities vary so slowly that a very precise calibration was not necessary, at least for Dy. The copper vs. constantan thermocouple had the advantage that its properties were well known and that it had good sensitivity between 20K and 300K. Another important point that should be mentioned with respect to the calibration of the diodes, is that, although there may be some systematic error in the calibration of the diodes versus absolute temperature, any two diodes should measure the same relative temperature. This is an important point because in order to do a good analysis of the ultrasonic data, it was necessary to measure the magnetization fairly accurately at the same temperature at which the ultrasonic data had been taken. Thus, it was more important that all the diodes measure the same relative temperature, than that they all measure the correct absolute temperature. The calibration of the diodes was done accordingly. The three diodes were calibrated together, and as they began to fail, the new diodes were calibrated versus one of the remaining original diodes.

The three original diodes were calibrated by gluing them all to the top of a copper cylinder with GE-7031 varnish. A heater made of constantan wire was wound on the outside of the cylinder, and one junction of the thermocouple was glued, with GE-7031 varnish, in a hole that was in the

center of the three diodes. The reference junction of the thermocouple was placed in a covered bath in a vacuum insulated dewar-like container containing distilled water, ice made from distilled water, and, hopefully, saturated water vapor. The temperature of the ice bath was presumed to be the triple point of water, 273.2K. The emf of the thermocouple was measured using a Leeds and Northrup K-1 potentiometer, an Eppley unsaturated standard cell, a Hewlett-Packard 6111A power supply as the battery, and a Sullivan Type 3333 null detector. The National Bureau of Standards calibration of the absolute emf of a copper vs. constantan thermocouple as a function of temperature was used to calculate the temperature.

Using the temperature controller described in the next paragraphs, one of the uncalibrated diodes was used to control the temperature. After allowing a few minutes for the temperature to stabilize, the thermocouple voltage was measured with the Leeds and Northrup potentiometer, and the voltage across each of the two free diodes was measured with the Systron-Donner multimeter while a constant 10μA current was flowing through the diode from a separate current source. The set point of the temperature controller provided the voltage across the diode being used to control the temperature. The temperature was varied between 4.2K and 300K with smaller increments at lower temperatures.

In later calibrations, when one of the diodes had

already been calibrated, the diodes were glued to the same copper cylinder and the calibrated diode was used to control at known temperatures. The Systron-Donner multimeter was then used to measure the voltage across the new diodes.

All the heaters were constantan wire wound on copper forms; the intended use of the heater determined the shape of the form. The wire was wound directly onto the sample holders for ultrasonic measurements. For use with the magnetometer, a small heat exchanger was made by filling a copper sleeve with braid from coaxial cable, and soldering copper screens over the ends of the sleeve. The heater was wound directly onto the outside of the sleeve, and the heat exchanger was mounted a few inches below the sample. The heat exchanger at the bottom of the sample chamber was more complicated, and consisted of two concentric sleeves. The inner sleeve was filled with a fine copper powder. The tube from the reservoir entered its bottom, and the heater was wound around its outside. The capillary tube came from the reservoir, and entered a small copper tube which wound around the outer copper sleeve in a helix. The copper tube then entered the bottom of the inner sleeve. The heater was sandwiched between the two sleeves, so little of its heat was radiated into the reservoir, and the heat exchanger was more efficient.

E. Temperature Controller

The temperature controller was a proportional

controller with an integrator and differentiator added. Its design was based on the design of the Princeton Applied Research (PAR) Model 152 temperature controller, but was considerably simplified by the replacement of many discrete circuit components, mainly the voltage regulators and operational amplifiers, with integrated circuits. The controller was designed and built by Prof. P. L. Donoho in the laboratory at UNICAMP.

A calibrated current source in the controller supplied a constant 10μA current to the GaAs diode, the positive terminal of which was connected to the direct input of a differential amplifier. A known voltage, controllable from the front panel, and usually referred to as the set point, was applied to the inverting input of the differential amplifier. The difference voltage was amplified by a factor of 1000, and a portion of it was applied to the integrator-differentiator, an RC differentiator followed by an operational amplifier used as an integrator. The portion of the amplified difference voltage that was applied to the integrator-differentiator was controlled by the GAIN potentiometer, and the time constants of the differentiator and integrator were set by the DIFF and INTEG potentiometers, respectively.

The current to the heater was proportional to the output of the differentiator-intgrator, and the output depended on the settings of the GAIN, DIFF, and INTEG

potentiometers. A more detailed description of the functioning of the controller follows in the next paragraph.

Assuming that the integrating capcitor was initially uncharged, and that the difference voltage was not zero, one of two things happened. If the difference voltage was changing too fast (according to the conditions set by the front panel potentiometers) the differentiator overcame the integrator and changed the heater current in such a way as to slow the change of the difference voltage. If, on the other hand, the rate of change of the difference voltage was small enough and the error voltage itself was small enough, the integrator dominated.

In order to allow the temperature to be changed faster, the integrator became inactive when the difference voltage became too large, about 1mV. When the error voltage was too large, a solid state switch closed which shorted the integrating capacitor,and the integrator began to act like a fixed gain amplifier. The temperature controller was then in the proportional mode, and the heater current was proportional to the difference voltage up to the point where the power amplifier saturated.

In normal operation, the integrator is active and its output determines the current to the heater. Small fluctuations in the temperature cause positive or negative error voltages which are integrated and change the output in the sense necessary to correct the error.

Through experience, it was learned that using the temperature controller to control the current in the heater at the bottom of the sample chamber led to long thermal time constants and made the temperature very difficult to control. The problem was that the heater was several inches from the sample and diode, so the portion of the sample chamber between the heater and sample had to be warmed (or cooled) before the temperature of the sample changed. To avoid this problem, secondary heaters were placed nearer the sample. The heater at the bottom was then supplied with a constant current from a Phillips PE-1512 power supply that supplied a maximum of 35V at 3A. The heater at the bottom of the sample chamber preheated the gas entering the sample chamber from the LHe reservoir and left the secondary heaters to be controlled by the temperature controller. The current in the bottom heater was set to keep the current in the secondary heater near 250mA, thus allowing ample reserve power for controlling. The maximum current applied to the bottom heater was about 700mA, when controlling near room temperature, and the minimum, applied at low temperatures, was about 150mA, which was enough to prevent LHe from collecting in the bottom of the sample chamber.

The stability of the temperature depended greatly on the sample holder and the settings of the controller. In general, the oscillations in the temperature of the diode were less than .1K, so the oscillations of the temperature

of the sample, which had greater thermal inertia, were even smaller. Finally, the reproducibility of the temperature using this temperature controller should be on the order of .1K, the specification that PAR claims for their controller.

F. Sample Holders

Three different sample holders were used in the work reported in this thesis: One to hold the sample when making magnetization measurements, and two to hold the sample when making ultrasonic measurements: one for propagation parallel to the field and one for propagation with velocities perpendicular to the field.

The sample holder, shown in Figure II-2, that was used in making magnetization measurements, was the simplest. It consisted, essentially, of a removable extension of the vibrating rod that was driven by the magnetometer. The extensions provided by PAR were constructed from a solid rod of quartz approximately 25cm long, with a male threaded plastic cup glued to one end and a female threaded plastic cup glued to the other end. A teflon spacer, to prevent the lateral motion of the rod in the support tube, was screwed onto the plastic cup with the male threads which then screwed into the bottom of the vibrating rod. After all the quartz rods supplied by PAR had broken, it was necessary to replace the quartz rods with thin walled stainless steel tubing.

The sample was actually glued to a plastic cylinder with male threads on one end, and a flat platform

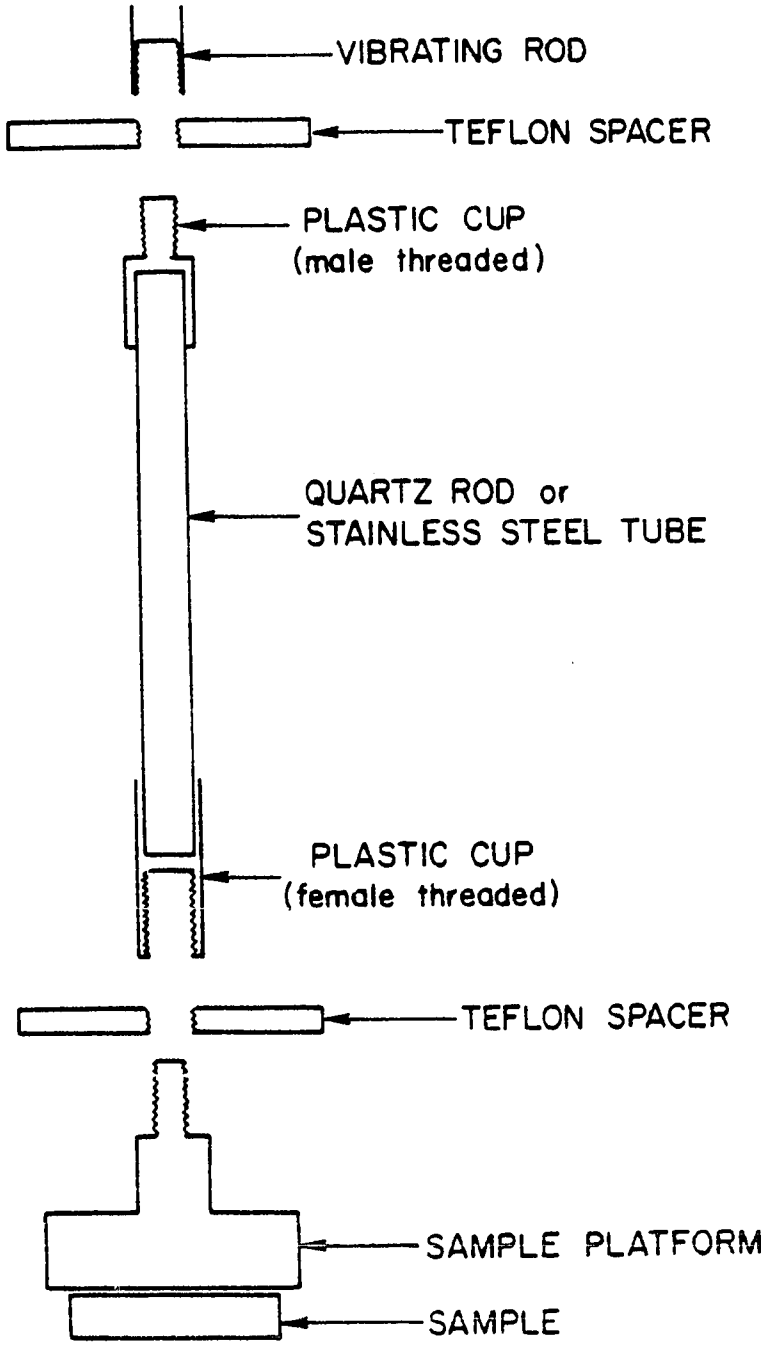


Figure II-2 Sample holder for the vibrating sample magnetometer.

perpendicular tothe axis of the cylinder on the other end. After the sample had been glued to the platform, a second teflon spacer was screwed onto the male threads, and the whole piece was screwed to the bottom of the quartz or stainless steel rod. The diode was not in direct contact with the sample during the magnetization measurements, so it was necessary to take great precautions to avoid temperature gradients between the sample and the diode, and the only effective way that was found, was to avoid shielding the sample from the gas flow. The sample was glued to the platform to allow the flux of He to pass directly over it.

The simpler of the two ultrasonic holders was the longitudinal sample holder, the one that was used for holding the sample with the direction of the propagation of the ultrasonic waves parallel to the applied field. The sample holder, shown in Figure II-3, is similar to the one used in previous work, but was modified to allow better control of the temperature, and to decrease its size to allow it to be used in the superconducting magnet .

The bottom part of the holder was a solid block of copper that had been turned down to a cylinder. A hole was drilled to the center of the block a few millimeters below the platform on which the sample rested, so the temperature gradient between the sample and diode was negligible. The diode was glued into the hole with GE-7031 varnish to insure good thermal contact between the mass of copper and the

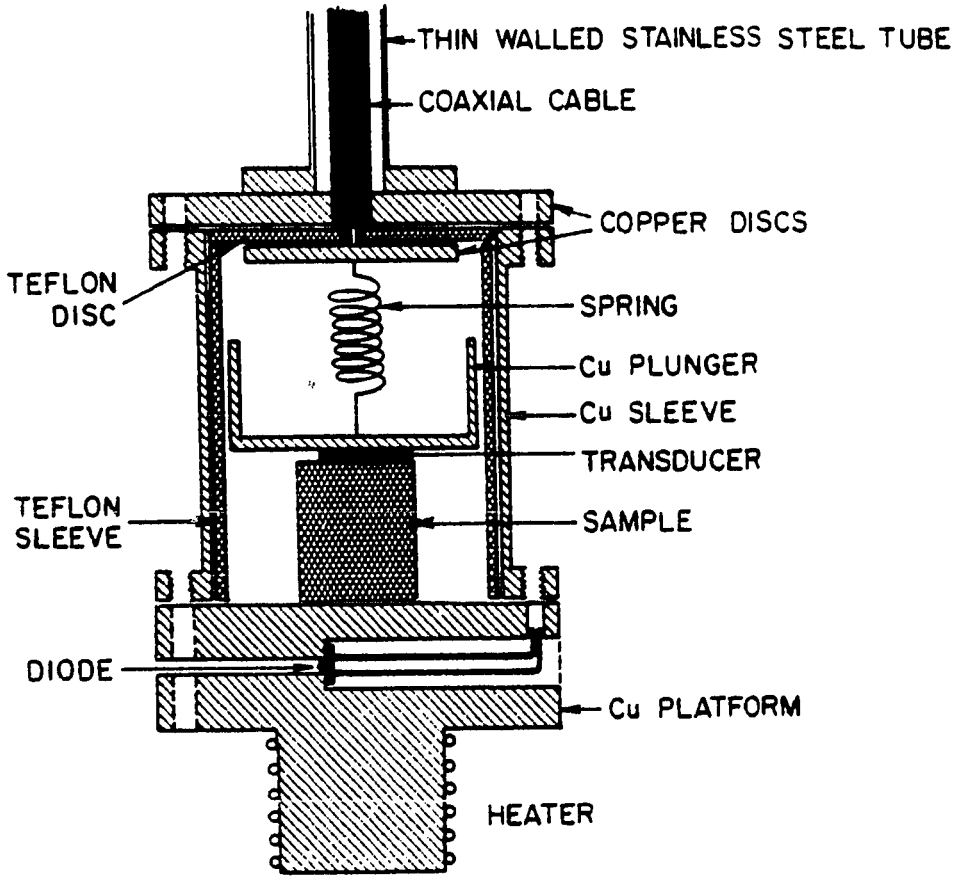


Figure II-3 Longitudinal sample holder for measurements of the ultrasonic velocity.

diode, and the heater was wound on the bottom of the cylinder. The sample was glued to the platform, and silver paste was used to provide the electrical contact between the copper platform and the sample that was necessary for efficient operation of the ultrasonic generator-receiver.

The top of the support consisted of a brass plug which fit into the same support tube as the magnetometer and vibrating rod. The BNC connector for the cable that transmitted the rf pulses from the generator, as well as a feedthrough for the diode and heater connections was located on the brass plug. A coaxial cable which passed through the stainless steel support tube carried the rf pulses from the BNC connector to the sample holder. The shield of the coaxial cable was connected to the mass of the sample holder, and the metal sample was electrically connected to the copper mass by the silver paste. The center conductor of the coaxial cable was connected to a spring and plunger which were electrically insulated from the mass of the sample holder, and which provided the second electrode necessary for efficient excitation of the piezoelectric transducer. The sample itself was the first electrode, so, essentially, the transducer was in the electric field of a capacitor whose plates were formed by the sample and the plunger.

The transverse sample holder, shown in Figure II-4, required a more sophisticated design. Because of the limited space available inside the tube which supported the vibrating

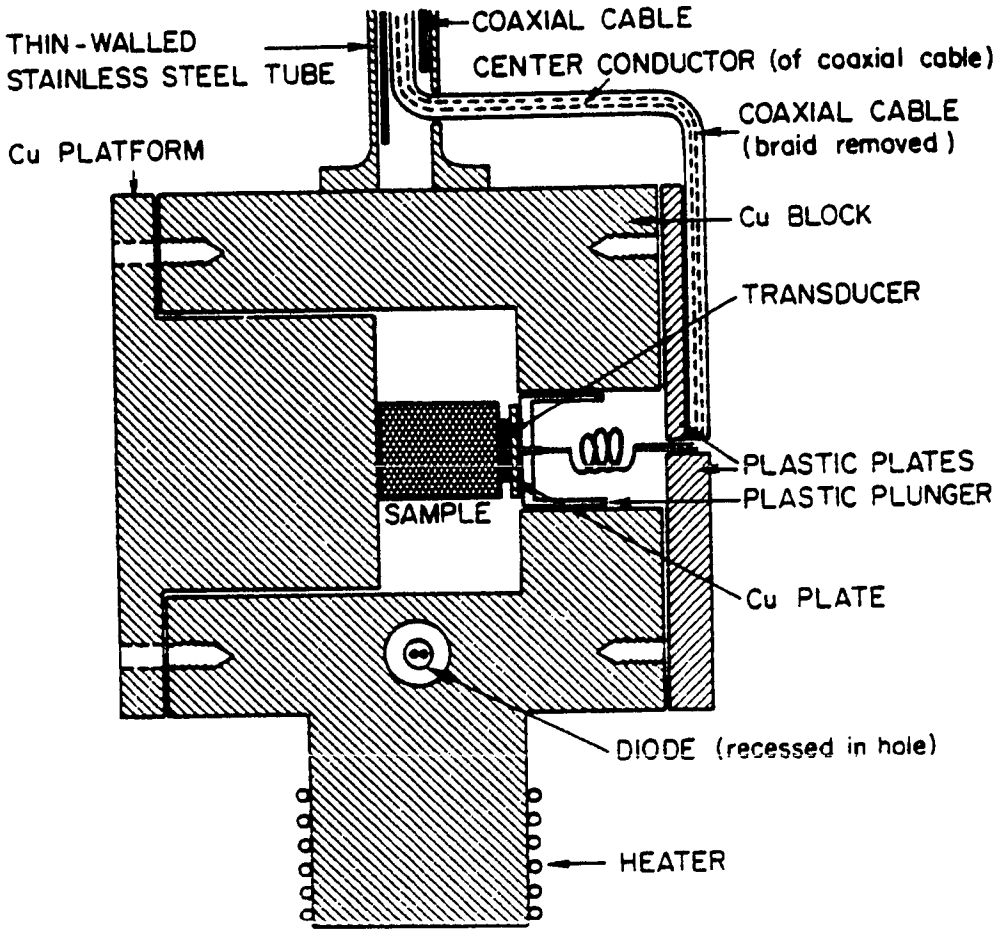


Figure II-4 Transverse sample holder for measurements of the ultrasonic velocity.

rod, the tube was removed, and the transverse holder was placed directly into the sample chamber. The main body of the holder was a block of copper, rectangular in shape, with a small cylindrical extension on the bottom for the heater. A hole approximately 14mm in diameter was bored through one side of the block for the plastic plunger to move in, and a larger hole with the same center as the smaller hole was bored from the other side for the entrance of the copper platform and sample. The samples were small enough to pass through the smaller of the two holes when the copper platform was secured to the main copper block, so the distance that the plunger moved into the hole depended on the length of the sample and the height of the platform. Different sized platforms were made for different sized samples, since the plunger could only move about 4mm.

The top plate of the transverse holder was essentially the same as the top of the longitudianl holder, and the support was a thin walled stainless steel tube with the coaxial cable passing through it. The diode was glued in a hole drilled between the sample and the heater, so it is clear that, because of the position of the diode, the thermal coupling between the sample and diode was not as good in this sample holder as in the other. However, measurements of the temperature gradient, made by putting one junction of a thermocouple at the position of the diode and the other junction at the position of the sample showed

that for heater currents of 200mA or less, the temperature gradient was less than 1K.

G. Samples

Both samples that were used in the work reported here were cut from a single crystal purchased from Metals Research. The original crystal was grown from 99.9% pure stock by the strain anneal method. The two samples were cut from the original crystal using a Metals Research Servomet spark-cutter, and were oriented using Laue back scattering of X-rays. After being oriented, two surfaces, parallel to within 1° and perpendicular to the c-axis to within 2° , were spark-planed, again using the Servomet spark-cutter. Surfaces were also planed perpendicular to the b-axis of both samples. The samples were shaped approximately like flattened cylinders, with the axis of the cylinder approximately along the c-axis.

Sample A was 7.33mm in length, and had a mass of 1.636g. Sample B was somewhat shorter, 5.69mm, and had a mass of 1.0234g. Sample A was found to give good results for waves along the c-axis, but poor patterns for waves along the b-axis. The echo patterns obtained for waves along the c-axis of sample B were somewhat inferior to those of sample A, but for waves along the b-axis, the patterns were far superior to those of sample A. As a result, sample B was used in most of the measurements.

H. Magnetometer

Although various types of vibrating sample magnetometers had been in use before Foner[36], his name is generally associated with the vibrating sample magnetometer. The reason that the vibrating sample magnetometer carries his name becomes more apparent when the difficulties with the earlier magnetometers are considered. In particular, earlier magnetometers required that the direction of the vibration of the sample be parallel to the direction of the applied magnetic field. The use of a conventional magnet with these magnetometers required that one pole piece have a hole in it for the driving rod to pass through, and the hole, of course, introduced inhomogeneities into the magnetic field. Foner's design eliminated this problem by allowing the vibration of the sample to be perpendicular to the magnetic field.

The basic principles of the vibrating sample magnetometer are simple. The output of a low frequency sinusoidal oscillator is amplified and used to drive an electro-mechanical transducer (essentially a loud-speaker driver) which converts the alternating current into reciprocating, one-dimensional motion. The transducer is in turn connected to the magnetized sample which oscillates in the magnetic field. Because of the spatial dependence of the dipole magnetic field of the magnetized sample, the movement of the sample induces a voltage in the detection coils which have been mounted near the sample. The induced voltage is generally

of the order of 1μV, and has a constant phase relation with the oscillator, so the magnitude of the induced signal can be measured accurately using phase-sensitive detection. The value of the magnetic moment itself can be determined after the magnetometer has been calibrated with a sample of known moment.

The magnet used in this investigation was a superconducting solenoid, so the direction of vibration was parallel to the field. The principle of operation is the same as the magnetometer used with a conventional magnet, but the location of the pickup coils is different.

The magnetometer used in this work was a PAR Model 155 vibrating sample magnetometer. The transducer and all electronics were included with the magnetometer, but the detection coils were designed specially for the superconducting solenoid that was used. The coils constructed for these measurements were wound with copper wire on a plastic form. The form was machined to a size large enough to fit around the outside of the sample chamber, but small enough to fit in the vacuum space. Two coils of 100 turns each were wound, in the same direction, on opposite ends of the cylindrical form and were connected in opposition. The coil form was securely attached to the outside of the sample chamber. Normally, the coils would have been mounted on the magnet itself to prevent the coherent pickup of any signal from the motion of the coils in the static magnetic field, but

space limitations, as well as concern about the sheilding effects of the intervening metal walls dictated that the coils be attached to the sample chamber. The coils were intentionally wound with less turns than the PAR coils, so their sensitivity was about 10 times smaller, and the actual moment, after calibration, was 10 times the indicated moment. It was, thus, no longer necessary to use the 1:100 attenuator to measure large magnetizations (100emu or more).

The Model 155 magnetometer was designed to be used at room temperature with conventional magnets, so extensive mechanical work was necessary to adapt it for use at low temperatures with the superconducting solenoid. The main problem was to find a way to couple the magnetometer to the variable temperature cryostat in a way that allowed the head of the magnetometer to be moved. The final solution was to mechanically center the sample laterally, and to allow the head to move only vertically.

The description of the PAR magnetometer will begin with the transducer, usually called the head. The driving mechanism of the PAR magnetoemter was essentially the same as a loud-speaker driver. The alternating current passed through a coil that was held, by copper-beryllium springs, in the static field of a permanent magnet. The interaction of the static field with the alternating current caused the coil to oscillate vertically. The top of the vibrating rod was screwed into the top of the coil, so the rod moved along

with the coil, as did the sample, which was mounted on the rod. Problems could arise if the oscillatory motion of the head were able to mechanically couple to the detection coils. The coils would then be moving in the applied field at the same frequency as the sample, and small inhomogeneities in the field would induce voltages in the detection coils that would be indistinguishable from the signals due to the motion of the magnetized sample. In order to avoid these problems, PAR included vibration damping in the head of the magnetometer. Mechanical resonators, tuned to the vibration frequency of the coil, were connected to the coil support, the parts of the magnetometer that supported the coil were isolated from the rest of the magnetometer by rubber shock absorbers, and the head itself was supported by vibration absorbing rubber. The design of the magnetometer head effectively prevented coupling of the vibration of the driving coil to the detection coils. The head also included a vibrating capacitor which was used in a feedback loop to eliminate the effect of variations of the vibration amplitude on the measured moment. The operation of the vibrating capacitor will be discussed later in this section.

The operation of the electronics associated with the magnetometer can best be understood by analogy with the operation of an operational amplifier with feedback; the model is shown in Figure II-5. The non-inverting input of the amplifier is the ac voltage from the detection coils,

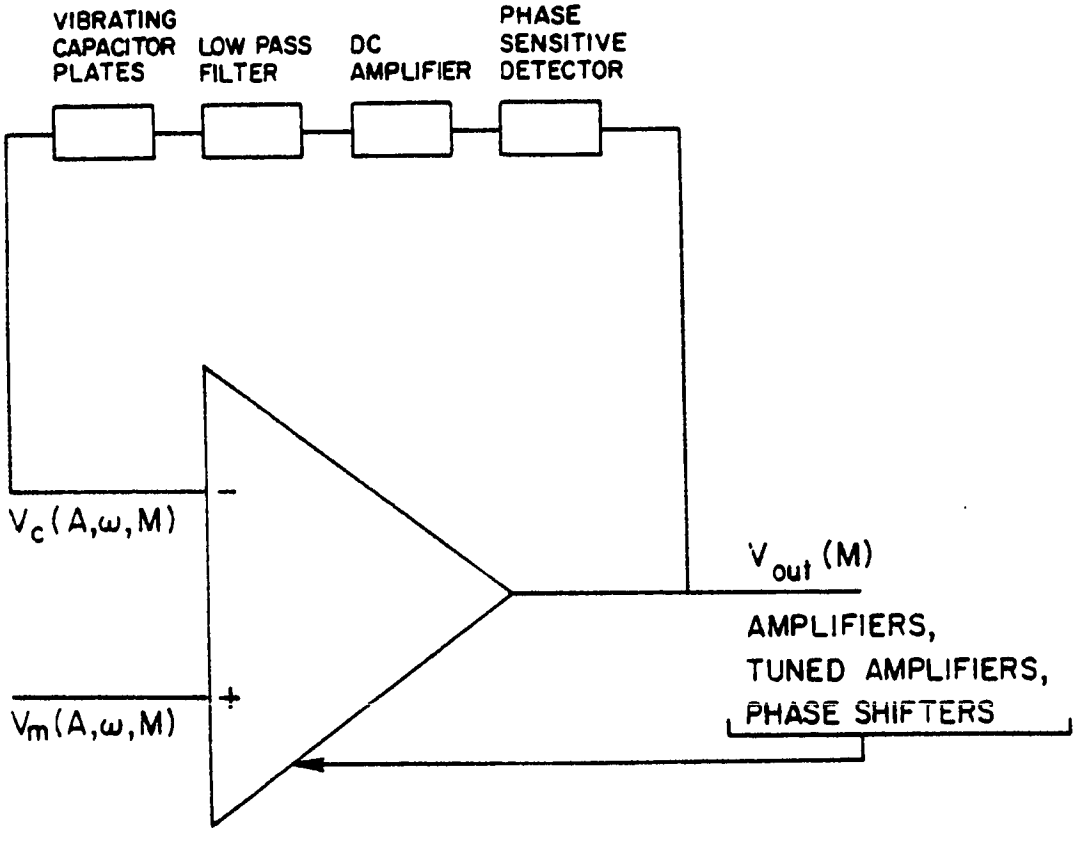


Figure II-5 Model of the PAR Model 155 vibrating sample magnetometer as an operational amplifier with feedback.

which is proportional to the amplitude of the vibration of the sample and the magnitude of the magnetic moment, and the the inverting input of the operational amplifier is the voltage from the vibrating capacitor plate which is proportional to the amplitude of the vibration.

An ideal operational amplifier with feedback operates by keeping its inputs at the same voltage. Since there is feedback, the output of the amplifier will seek the level that gives just enough feedback to keep the inputs equal. In this model of the magnetometer as an operational amplifier, the feedback comes about because the dc voltage across the oscillating capacitor plates is proportional to the output of the operational amplifier. The output of the amplifier will seek the value that gives a dc voltage across the capacitor plates that is just sufficient to cause the ac voltage from the capacitor plates to be equal to the instantaneous value of the voltage from the detection coils. Since the sample and capacitor plates are rigidly connected, the signals from them are affected equally by small changes in the vibration amplitude and frequency, and the output depends only on the magnetization.

In reality, of course, the operational amplifier consists of many amplifiers, tuned amplifiers, and other components, and the feedback loop contains a phase sensitive detector, dc amplifiers, filters, and voltage dividers.

Before discussing the calibration procedure for the

magnetometer, the functions of the front panel controls will be explained. There was an on-off switch for the main power as well as the Signal switch which allowed the input from the detection coils to be shorted while zeroing the panel meter. The panel meter had 3 1/2 digits (20% over-range) with the polarity indicated, and there was also an auxiliary D'Arsonval type meter. The digital meter always indicated the value of the measured moment, but there was a switch which set the function of the auxiliary meter. The functions were: Standby, which interrupted the driving signal to the transducer; Drive Amplitude, which allowed the magnitude of the driving voltage to be set; Vibration Amplitude, which monitored the amplitude of vibration of the coil and indicated when there was some problem with the transducer or rod; Moment, which indicated the same as the panel meter; and Offset, which allowed the moment to be measured with greater precision by the nulling of the dc voltage proportional to the moment.

A full scale sensitivity of 100, 10, 1, .1, or .01emu was selectable with a front panel switch. An overload light indicated when one or more of the amplifiers was overloaded by either too large a signal, or by noise on the incoming signal. Another switch allowed either the in-phase or quadrature component of the signal to be measured. Potentiometers were available on the front panel to adjust the amplitude of the driving signal, the zero of the panel meter,

the calibration of the magnetometer, and to allow fine adjustment of the phase of the signal from the detection coils relative to the phase of the signal from the vibrating capacitor. The time constant of the low-pass filter following the phase sensitive detector could be selected from the possibilities: 1, 3, 10, 30, 100, or 300sec, or an external capacitor could be added in the back of the unit if longer or shorter time constants were desired. A recorder output was also available with an output of $\pm$10V, where 10V corresponded to positive full scale on the panel meter. In addition, four decades of calibrated offset were available to null the signal, as well as a switch to choose the polarity of the offset, and a switch that allowed the full scale sensitivity of the D'Arsonval meter to be set at 100, 10, or 1% of full scale, as indicated by the Sensitivity switch. The rear panel had toggle switches that allowed the polarity of the magnetization to be changed, and that enabled the input from the detection coils to be attenuated by a factor of 100 if the signal to be measured was greater than 100emu. A test switch used in trouble-shooting and electrical alignment of the magnetometer was also located on the back panel.

## I. Calibration of the Magnetometer and Measurement of the Magnetization

To begin the calibration procedure, the nickel sample was glued to a sample holder and placed in the dewar. The

calibration sample was machined from high purity nickel to approximately the same size as the Dy samples to minimize the form effect. The form effect is the fact that the shape of the sample may affect its measured magnetization because the sample occupies a finite volume of space and can not be treated as a point dipole. The magnetic flux passing through the detection coils depends on an integral over the volume of the sample, thus on its shape. After the sample was in the cryostat, the temperature was stabilized, usually at 4.2K. The field was increased until the magnetization was saturated, usually at about 10-15kOe, and the sample was positioned vertically to maximize the indicated moment. The magnetometer was then calibrated to indicate the correct saturation magnetization of the nickel sample. The saturation magnetization was calculated from the mass and temperature of the sample.

The next few paragraphs will describe the procedure for measurement of the magnetization. After the magnetometer had been calibrated, the sample and its holder were put into place in the cryostat. At some constant temperature, the field was increased to a value high enough to give an appreciable magnetization relative to the expected maximum magnetization, and the sample was vertically positioned to maximize the measured moment. The head of the magnetometer was rotated 360°, in increments of 45°, to check the variation in the measured moment as a function of angle.

Ideally, of course, the moment should not have changed with angle, but normally, the variation was 1 or 2% peak to peak. The magnetic field in the solenoid was fairly constant in the radial direction, so the difference in magnetization could not be attributed to the variation in magnetic field in the region through which the sample moved. The more likely explanation is that the axis of the sample was not exactly parallel to the magnetic field, so there was some change in the magnetization because the orientation of the hard axis of the sample was changed slightly as the head was turned. If the angular variation of the magnetization exceded a few percent, the head of the magnetometer was repositioned over the cryostat so that the axis of the sample was closer to the direction of the field. In addition, the error was minimized by rotating the sample to the position consistent with the expected behavior of the magnetization. The position of maximum magnetization was chosen if the field was along an easy axis, and the position of minimum magnetization was chosen if the field was along a hard axis. The head was then kept stationary for the remainder of the measurements along that axis. This procedure having been completed, the temperature was chosen and allowed to stabilize.

While awaiting the stabilization of the temperature, the rest of the equipment was calibrated. The X-axis of the X-Y recorder was calibrated by, first, removing the magnet leads from the power supply and replacing them with a short

circuit across the terminals. The current was then raised until the current monitor voltage (as indicated by the digital multimeter) was a convenient multiple of the desired sensitivity in mV/cm, and the X-axis was calibrated using the vernier control for the X-axis sensitivity. In order to calibrate the Y-axis of the recorder, it was necessary to have a good idea of the maximum that the magnetization could reach. Having estimated this quantity, the input signal from the detection coils to the magnetometer was shorted, and the Offset controls on the magnetometer were used to produce an offset voltage corresponding to some multiple of the desired sensitivity in emu/cm. The calibration having been completed, the Offset was returned to zero, and the magnet was reconnected to the power supply. By this time, the temperature had stabilized and the measurement could begin. A sweep speed was chosen that was appropriate for the magnetization to be measured, and the sweep was started. The magnetization was then recorded on millimeter graph paper and stored. In addition, if the temperature was in the paramagnetic range, the sweep was stopped at approximately ten points, and the current monitor voltage and magnetization were noted. This procedure was convenient because the magnetization curves in the paramagnetic range are smooth curves that can be approximated well by low order polynomials. The ten points that were recorded were later entered into the computer and used to find coefficients that

characterized the magnetization completely, within experimental error. It was thus possible to avoid having to go back to the original plots each time new magnetization data were required, and many potential errors were avoided. The magnetization curves in the antiferromagnetic and ferromagnetic phases were too irregular to be parameterized easily, so the plots themselves were used when data was required.

Magnetization curves were recorded only when increasing the field, so when the field reached its maximum, the temperature was changed while the field was reversed and swept to zero. This procedure saved both time and LHe, since the field could be swept down faster than the magnetometer could follow the changing magnetization.

## J. Transducers and Bonding Materials

Plates of quartz that oscillate in either pure shear or pure longitudinal modes when placed in fields parallel to the normals to the plates can be obtained by cutting the plates with their normals parallel to certain well known crystallographic directions. The thickness of the plate determines its resonant frequency. Plates (transducers) whose faces have been sufficiently well polished can also be excited at odd harmonics of their fundamental frequency.

The transducers used in the work reported in this thesis were all piezoelectric quartz transducers supplied by Valpey-Fischer Corporation. All measurements that were made on sample A were made using 20MHz, X-cut, 1/8"

diameter transducers with a fine ground finish. Shear wave measurements were made on sample B using 20MHz, AC-cut, 1/8" diameter transducers with a fine ground finish. During the time that the longitudinal wave measurements were being made on sample B, the original supply of 20MHz X-cut transducers was exhausted. Some 3/4" diameter, X-cut transducers that were already available were cut into smaller transducers. Consequently, the transducers that were used to finish the measurements on sample B were 10MHz, X-cut, nomimally 1/8" diameter transducers with overtone polish. Some measurements were attempted at the first odd harmonic, 30MHz, but the overall quality of the results was judged to be superior at 10MHz, so all measurements using the 10MHz transducers were made at 10MHz.

The first measurements, on sample A, were made using Nonaq, a water soluble stopcock grease widely used for ultrasonic bonds, as the bonding material. Nonaq's primary advantage is that it is easy to apply and to remove, and that bonds made with it can be tested immediately. It does have the disadvantages of solidifying and becoming brittle at temperatures not too far below room temperature, and of being useless for shear waves. The large magnetostrictive strains generated at the phase transitions in Dy and the other heavy rare earths tend to either break the Nonaq bonds completely, or to introduce such distortion into the echo pattern that they become impossible to use. As a result,

the measurements made on sample A were not made below the Neel temperature, and in the measurement of $\Delta C_{22}^{b}$ ($\Delta C_{22}^{b}$ is the change in $C_{22}$ when the field is applied along the b-axis), the bond was impossible to use below 195K. The ultrasonic data are therefore, incomplete below 195K. Time did not permit the measurements to be extended to lower temperatures using stronger bonding materials.

Various other materials were substituted for Nonaq in an attempt to avoid the problems caused by the magnetostriction. Initially, materials such as the silicone greases were tried because they do not crystallize at low temperatures, and should be able to adjust to the changing strain. The bonds that were made with the silicone greases had better low temperature properties, but were less efficient than Nonaq at temperatures near room temperature. Perhaps, had more time been spent in the attempt to use the silicone greases, the problems could have been overcome, but no measurements are reported in this thesis that were made with bonds of silicone grease.

It was known that epoxy is a good bonding material for low temperature ultrasonic work because it is so strong that it doesn't usually break at the phase transitions. Epoxy is harder to use than Nonaq, however, because the echo pattern must be watched continually while the epoxy is curing, so, if the bond is not satisfactory, the transducer can be removed before the epoxy becomes too hard. A more serious

problem with the use of epoxy is the removal of the transducer from the sample without damaging the sample, or, hopefully, the transducer. The solution of this problem was found by accident. GE-7031 varnish was used to glue the samples to prevent their moving when a magnetic field was applied. After the varnish had been applied, it was baked for several hours to speed the hardening process. It was observed that after several such treatments, a transducer that had been epoxied to a holmium sample fell off intact. Further experiments showed that a transducer that been epoxied could be removed in 3-4 days. When a transducer was to be removed, the transducer and sample were covered with a layer of varnish and baked for a few hours under an infrared lamp. The varnish was then removed with acetone and the process was repeated several times over the period of a few days. Damage of the bond could generally be detected visually by this time. The sample and transducer were then placed in a mixture of equal parts of acetone, toluene, xylene, and ethyl alcohol and placed in an ultrasonic cleaner for a few hours. Sometimes it was necessary to leave the sample in the mixture for a few days, but in all cases, when this procedure was followed, the transducer was removed without being broken. The xylene, present in the varnish and in the mixture of solvents, was probably responsible for attacking the epoxy since xylene is known to attack epoxy.

The one sample that has been subjected to this procedure several times appears to have suffered a small amount of surface damage. Since, however, the procedure has only been used a relatively short time, it is impossible to say whether the damage is real, and if it is real, whether it resulted from the epoxy, the combination of epoxy and heat, or possibly, the mixture of organic solvents. It is clear, at least, that, in cases where epoxy bonds are the only solution to the bonding problems, the process described here is preferable to breaking the transducer (and probably damaging the surface of the sample as well) to remove an epoxy bond.

## K. Ultrasonic Equipment and the Echo-Overlap Method

The purpose of the ultrasonic equipment is to produce high power pulses of constant frequency rf energy at well defined, controllable repetion rates, and to detect the relatively weak rf signals that are the response of the matter (generally solid or liquid) to which the pulses were applied. Ordinarily, the rf energy is coupled to the matter through a piezoelectric transducer that converts the electo-magnetic waves to elastic waves. The ultrasonic waves interact with the matter, and after each traversal of the sample, the elastic wave echo is piezoelectrically detected by the transducer and converted to electromagnetic waves. The ultrasonic equipment detects this, relatively weak, electromagnetic radiation, amplifies it, and displays it so

that useful information can be gained from it. Generally, the quantities of interest are the delay of the elastic waves in passing through the matter and the attenuation of the elastic wave in passing through the matter. The time delay is related to the velocity of the elastic wave, and the attenuation is related to the strength of the interaction of the elastic waves with the matter and the excitations and impurities that are present in the matter.

The functioning of the ultrasonic system, shown in Figure II-5, can best be understood after a discussion of the method used for determining the velocity of the ultrasonic wave in the sample. The MATEC equipment was designed to be used with the echo-overlap method developed by May[33] and Papadakis[34]. The echo-overlap method relates the velocity of the elastic waves to the frequency, f, of a cw oscillator. This frequency is the frequency at which the trace of the oscilloscope is triggered, and it is also divided down and used to trigger the pulse generator. When the pulse generator is triggered, it produces a pulse of rf energy that interacts with the piezoelectric transducer which produces elastic waves in the sample to which it is bonded. Since the sample has parallel faces, the wave reflects between the two faces until it has been dissipated. Each time that it reflects from the face to which the transducer is bonded, the echo induces an rf electric field in the transducer that propagates back to the receiver. All the echoes are

amplified by the receiver, but only two are displayed on the oscilloscope. After the pulse generator has been triggered, the decade divider-dual delay generator produces two strobe pulses which enter the Z-axis of the oscilloscope and intensify the trace at the times when the two echoes to be overlapped are being displayed on the oscilloscope. By adjusting the delays of the strobe pulses, any two echoes can be displayed. The oscilloscope is triggered at the frequency, f, so if, for instance, echoes m and n are being strobed, and if f has been adjusted to the lowest frequency for which the two echoes overlap cycle for cycle, then the delay between the two echoes is just 1/f. The time delay is just the transit time for traversing the sample in both directions n-m times, so $1/f = 2\ell(m-n)/v$ , where v is the elastic wave velocity, and $\ell$ is the distance between the faces of the sample. The elastic constant can then be determined from the velocity using the relations in Figure I-3.

The echo-overlap method is preferable to the pulse superposition method for several reasons. First, the pulse superposition method requires that the repetition rate of the pulses be equal to the frequency, f, whereas the echo-overlap method requires only that the repetition rate, f', of the pulses be related to the frequency by the relation: $f' = f/n$, where n is some integer, usually a power of 2 or 10. Higher power pulses are thus possible when using the echo-overlap method because the duty cycle of the pulsed rf oscillator is

smaller. Higher power pulses mean that it may be possible to make measurements in regions of high attenuation with the echo-overlap method that would be impossible with the pulse superposition method. Second, the echo-overlap method requires only two good echoes, whereas the pulse superposition method requires at least 5 to 10. This fact is important because the rare earths are rather soft, and are naturally somewhat ultrasonically opaque, so it is difficult to get echo patterns with more that 10 or 20 good echoes under the best conditions. The application of magnetic fields aggravates the problem because the attenuation usually increases as the field is increased, and because the rare earths exhibit large magnetostriction which subjects the transducer-sample bond to stresses which change the behavior of the bond and sometimes distort the echoes. Using the pulse superposition method when the attenuation is large leads to decreased accuracy because of the smaller number of usable echoes, and when the echoes are distorted, use of the pulse superposition method may lead to situations where the results of the measurements are ambiguous. In either of the two situations just discussed, use of the echo-overlap method is preferable to the use of the pulse superposition method.

The necessary background having been presented, the block diagram of Figure II-6 will now be discussed component by component. The logical place to begin is with the cw oscillator, which operates at a frequency of several hundred

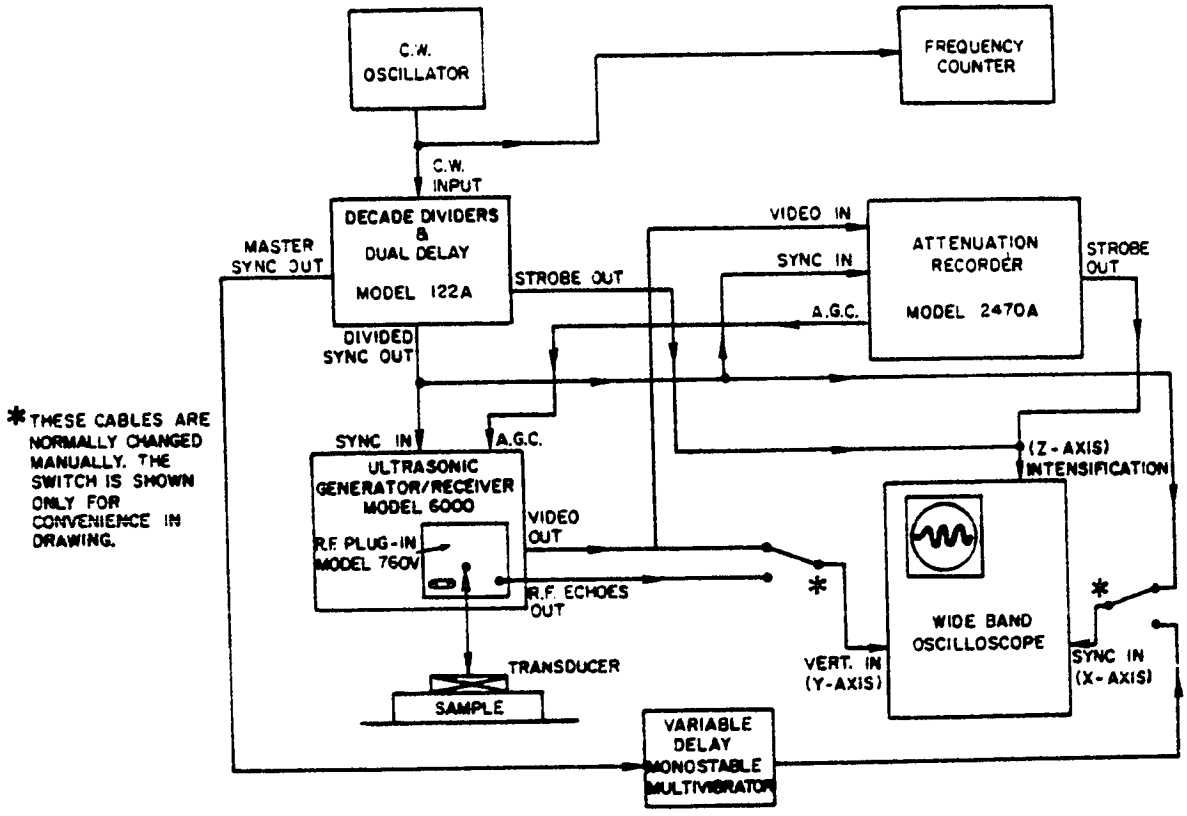


Figure II-6 Block diagram of the elecronics used in the simultaneous measurement of ultrasonic velocity and attenuation.

kHz. In the echo-overlap method, the frequency of the oscillator at overlap determines the elastic wave velocity, so it is necessary to have a stable oscillator and a way of accurately measuring its frequency. The oscillator provided as a part of the MATEC equipment was a Tektronix Model FG-501 function generator. The long term stability of the function generator was not good, but over the short period of time necessary to make the average ultrasonic measurement, it was stable to a few parts in $10^5$. The function generator had a variety of possible waveforms, including: sinusoidal, square-wave, sawtooth, and ramps. The frequency counter was a DC-501-OP1 110MHz frequency counter with variable attenuation, variable trigger level, and variable gate time. The counter was used almost exclusively with no attenuation, triggering at the level crossing, and a gate time of 1sec, which allowed the frequency to be measured to $\pm$ 1Hz.

Since the goal of the experiment was to measure small changes in the elastic constants as a function of the applied field, it was necessary to be able to set the frequency of the oscillator with a resolution of a few Hz. The adjustments of the function generator were much too coarse, so they were used to set the base frequency, and a variable dc voltage was applied to the Voltage Controlled Oscillator input of the function generator to fine-tune the frequency to give the best overlap. A 100kΩ resistor in series with a 10kΩ wire-wound potentiometer was connected across the

output of a Tektronix PS-501 power supply which provided a dc voltage that was variable from 0 to 20V. The voltage across the free end of the 100kΩ resistor and the wiper of the potentiometer was applied to the Voltage Controlled Oscillator input of the function generator. The coarse adjustment of the frequency was the vernier of the function generator itself, the medium adjustment was the output voltage of the power supply, and the fine adjustment was the 10kΩ potentiometer.

The MATEC Model 122A decade divider and dual delay generator is exactly what its name implies. Its only input is the output of the function generator, but it has three outputs: a Master Sync output which is a square-wave at the same frequency as the input, both positive and negative strobe outputs with independently variable delays, and a Divided Sync output which is a square wave at the frequency of the input divided by $10^n$, n = 1, 2, or 3, where the factor by which the input frequency is divided is selectable from the front panel. The strobe outputs are square waves with pulse widths independently variable from 1 to 8μsec.

The trigger from the Divided Sync triggers a variable-delay monostable multivibrator which triggers the first strobe pulse and another variable delay monostable multivibrator when it returns to its stable state. The second multivibrator triggers the second strobe pulse. The maximum delay time for the two multivibrators can be either 100μsec

or 1000μsec, and there is a ten-turn potentiometer that sets the delay as a percentage of the maximum.

The MATEC Model 6000 ultrasonic generator-receiver can be used with different plug-in units for producing pulsed rf in the 1-700MHz frequency range. Only the Model 760V plug-in, which operates between 10 and 90MHz, was utilized in the work reported here, so the generator receiver and plug-in will be discussed as one unit.

The pulsed rf oscillator is two ceramic tetrodes, connected in a push-pull configuration, which drive a tunable LC resonant circuit. The oscillator is turned on when a positive voltage is applied to the control grids of the tetrodes. The amplitude and width of the output pulse are determined by the amplitude and width of the positive square-wave that is applied to the tetrodes. The amplitude and width of the square-wave are controlled by the front panel Pulse Amplitude and Pulse Width potentiometers, respectively.

The returning signals, induced by the echoes of the applied pulse, are split into two parts and proceed to two different amplifiers. One part is amplified by a wide-band integrated circuit rf amplifier (20dB gain) and this signal is directed to the Receiver Monitor output where it is accessible for the velocity measurements. The second part of the signal from the echo is first amplified by a tuned rf preamplifier (12dB gain), and then passed to a double-

balanced mixer where it is mixed with the tunable local oscillator frequency to produce a 60MHz i.f. signal. The i.f.signal is then amplified by an i.f. preamplifier and passed to the final 5-stage i.f. amplifier. After being amplitude detected, the video signal passes through an impedance lowering circut and out to the Video Out BNC connector ($Z_{out}$ = 50Ω). The detected video output is linear within ± .5dB over a range of 26dB with a maximum video output of 8V.

In normal operation, the generator-receiver was triggered by the Divided Sync output of the decade divider-dual delay unit. The video output was normally not used unless the attenuation recorder was being used.

When checking the bond or setting the velocity strobes, the amplified rf (from the Receiver Monitor output of the receiver) was displayed on the Y-axis of the oscilloscope, a Tektronix Model 465 (100MHz bandwidth). The trigger of the oscilloscope was from the Divided Sync, so the whole echo pattern could be displayed on the screen of the oscilloscope. If the bond was acceptable, and the velocity strobes had been set on the desired echoes, the trigger signal was manually changed to the Master Sync signal from the decade divider-dual delay generator. By increasing the sweep speed of the oscilloscope, the two echoes that had been selected with the strobes could be displayed and overlapped, cycle for cycle, on the screen. In some cases, difficulties, due to

delays inherent in the system, were encountered in getting the echoes overlapped on the screen of the oscilloscope. In order to overcome this problem, an integrated circuit variable-delay monostable multivibrator was introduced into the line carrying the Master Sync signal to the oscilloscope. The oscilloscope was triggered when the multivibrator returned, after a time which could be varied to move the echoes onto the screen of the oscilloscope, to its stable state.

The MATEC Model 2470 attenuation recorder allows attenuation data to be continuously recorded during dynamic experiments. The measurements of the attenuation and velocity are independent and can be carried on simultaneously without interference. The basic mode of operation of the attenuation recorder involves the selection and peak detection of any two echoes in an ultrasonic echo train. The resultant dc voltages are then differentially compared in a logarithmic voltmeter. The attenuation is displayed on a front panel meter with a full scale sensitivity variable from 1dB to 20dB, and a recorder output is also available. A calibrated offset control allows the measurement of small dynamic changes superimposed on a large static background. Very little use was made of the attenuation recorder, so no detailed explanation of its functioning will be given.

The ultrasonic pulse generator had a 50Ω output impedance, so to get maximum transfer of power, the impedance

of the load had to be 50Ω also. The transducer presents a high impedance,capacitive load to the generator, so impedance matching is necessary. Two impedance matching units were available, the MATEC Model 60 and the MATEC Model 70. Impedance matching is accomplished with the Model 60 by placing a fixed inductor and a variable capacitor in parallel with the capacitive load of the transducer. The capacitor is then varied until the resonant frequency of the circuit is the same as the frequency of the driving signal. Seven different fixed inductors were available, and the Model 60 could be used between 1 and 50 MHz. The Model 70 contained a variable inductor which was put into series with the capacitive load of the transducer, and adjusted to resonate the capacitance of the transducer at the driving frequency. The Model 70 was designed to operate between 10 and 50MHz.

The Model 60 was used in most measurements, but, occasionally, the Model 70 was used. Even though the cables connecting the transducer and the pulse generator were quite long, with an impedance matching unit, no problems were experienced with small echo amplitudes except in regions of high attenuation. However, the impedance matching unit increased the Q of the circuit and caused the width of the echoes to be greater than the width of the driving pulse. The width of the pulses caused problems in thin samples because it became impossible to resolve an echo from the one following it or the one preceding it. The problem was

partially alleviated by placing resistors across the output terminals of the impedance matching unit to dampen the ringing in the circuit.

L. Measurement of the Elastic Wave Velocities

The ultrasonic measurement procedure began with the installation of the sample in the sample holder after the sample had been glued and a bond had been made. The cables were connected and the equipment was turned on. The frequency of the pulsed rf oscillator was roughly adjusted by using the tuning data chart provided with the plug-in, and the preamplifier and receiver tuning were also set to the correct value for the desired frequency of operation. The oscilloscope was adjusted to display the entire echo train, so the integrity of the bond could be checked. The impedance matching unit, the receiver tuning and the preamplifier tuning were then adjusted for maximum echo height. Now, in order to fine tune the rf oscillator frequency, it was necessary to use the attenuation recorder. The two strobes of the attenuation recorder were set on the first two video echoes, and the frequency was adjusted for minimum attenuation. The oscilloscope was set to display the video echoes, and the preamplifier and receiver were again tuned to give the largest video pulse echo heights. The quality of the bond then had to be assessed, and a new bond made if necessary.

Assuming that the bond was good enough, the next step

was to set up the equipment for the velocity measurements. Generally, a bond with ten or more echoes that decayed more or less exponentially was considered suitable for data taking. Experience showed, however, that some samples produced better echoes than others, so decisions concerning the quality of the bond had also to take into consideration the best possible bond that could be expected from a given sample.

After obtaining a sufficiently good bond, the strobes from the decade divider-dual delay generator were then set on the echoes that were to be overlapped for the velocity measurements, and the time delay between these echoes was measured roughly and recorded. Greater sensitivity in overlapping the echoes was obtained by taking echoes that were separated in time as far as possible, but often, because of the increasing attenuation, the echoes far out in the train would disappear when a field was applied. As a compromise, the first echo and the third or fourth were overlapped, unless the temperature was near a phase transition, in which case, the first and second echoes were overlapped. The sample holder was then put into the sample chamber, the operating temperature was chosen, and the temperature controller was set accordingly.

Using the previously measured value of the time delay, $\Delta t$, between the strobed echoes, the frequency, $f=1/\Delta t$, was calculated and the function generator was set to approximately

this frequency. The strobed echoes were then nearly overlapped. All subsequent adjustments of the frequency were made by varying the input voltage to the Voltage Controlled Oscillator input of the function generator.

The sweep speed of the oscilloscope was increased until the two echoes extended across most of the oscilloscope screen. The intensity of the trace was increased until the baseline was barely visible and the frequency was set to cause the zero-crossings of the two strobed echoes to intersect each other at the baseline and to cause the envelopes of the two echoes to be aligned. Alignment of the echoes meant that the maxima of the echoes were aligned on the oscilloscope screen. Sometimes, because of distortion of the shape of the echoes, there were two frequencies that caused the zero crossings of the two echoes to intersect with the baseline, and at both of which, the envelopes appeared to be equally well overlapped. However, since measurements of the change in velocity from its zero field value as a field was applied were being made and not absolute measurements of the velocity, the error resulting from taking the wrong zero-crossing was negligible.

The sweep speed was increased further,after choosing the zero-crossing of best overlap, by using the 10X sweep expander. It was necessary to use a hood on the oscilloscope for measurements made with the expanded sweep, because the trace was very dim. Measurements began at zero

field by adjusting the frequency of the function generator until the zero-crossings of the echoes intersected the baseline, and then recording the frequency. Since the lines that were overlapped had some breadth, there was some uncertainty about the exact frequency of overlap. To eliminate errors caused by the breadth of the line, the frequency was measured several times, approaching the overlap from both higher and lower frequencies. The errors, due to the breadth of the lines, should then have tended to cancel one another in the average which was used in the data analysis.

The values of the field at which the measurements were taken depended on the expected behavior of the velocity as a function of the applied field. Measurements were taken at closer intervals in regions where the velocity was changing fastest, or in regions where the behavior was anomalous. The value of the current monitor voltage and several values of the frequency were recorded for each point.

## III. Theory

Dy (atomic number 66) is a metallic element that has an hexagonal close-packed structure at room temperature, with a c/a ratio of 1.574, which is slightly smaller than the theoretical value of 1.633 obtained for close-packing of spheres. The ground state configuration of the electrons of Dy is $[Xe]6s^2 4f^{10}$, but in a solid, the atom becomes triply ionized, and the two 6s electrons and one of the 4f electrons are lost to the conduction band.

Like the other rare earths, Dy has a partially filled 4f shell, and although the 4f electrons are higher in energy than the 5s and 5p electrons, their mean radii are smaller. Thus, the 5s and 5p electrons partially shield the 4f electrons from their environment. Since it is the 4f electrons that are responsible for the chemical properties of the rare earths, the fact that they are shielded means that the chemical properties of the rare earths are very similar. The shielding of the 4f electrons also means that they are only slightly affected by the crystalline electric fields in a solid, so the ions act very much like free ions. In particular, the orbital angular momentum is not quenched by the crystalline field, and the spin-orbit coupling remains strong. Because of the large number of electrons, the heavy

rare earths can have total angular momenta that are quite large. The ground state of the $Dy^{3+}$ ion has J = 15/2, for example.

Although weaker than the configuration interaction, the spin-orbit coupling is much stronger than any of the other magnetic interactions, such as the exchange interaction, the crystal field interaction, the Zeeman interaction, and the magnetoelastic interactions. Thus, if only the relatively weak magnetic interactions are present, and if the temperature is near room temperature, the behavior of Dy can be characterized by the spin-Hamiltonian which describes the lowest J- manifold. Since the energy separation between the two lowest J-manifolds is about 5000°K, the higher level is not populated at temperatures near room temperature, and none of the magnetic interactions will mix states of the two J-manifolds. The remainder of this chapter will only be concerned with the description of the lowest J- manifold.

The Model Hamiltonian (actually a Hamiltonian density) that describes this manifold is:

$$\mathcal{H} = \mathcal{H}_{ex}^{is} + \mathcal{H}_{ex}^{a} + \mathcal{H}_{z} + \mathcal{H}_{a} + \mathcal{H}_{me}^{I} + \mathcal{H}_{me}^{II} \qquad \text{III-1}$$

where $\mathcal{H}_{ex}^{is}$ and $\mathcal{H}_{ex}^{a}$ are the isotropic and anisotropic exchange interactions, respectively. $\mathcal{H}_{z}$ is the Zeeman interaction,

$\mathcal{H}_a$ is the crystal field interaction, and $\mathcal{H}_{me}^{I}$ and $\mathcal{H}_{me}^{II}$ are the one and two-ion magnetoelastic interactions, respectively. Each term in the Hamiltonian (density) will be discussed separately. (Note that the components of the angular momentum operator, $\vec{J}$, that are used in the Hamiltonian, are defined to be dimensionless. They are equal to the usual angular momentum operators divided by $\hbar$.)

## A. Discussion of the Model Hamiltonian

### 1. Exchange Interaction and the Molecular Field Approximation

Although the form of the isotropic exchange:

$$\mathcal{H}_{ex}^{is} = \sum_i \sum_{j \neq i} J_{ij} \vec{J}_i \cdot \vec{J}_j \qquad \text{III-2}$$

is the same as the form of the Heisenberg exchange, the actual mechanism of the exchange is much different, since the 4f electrons are very closely bound to the nucleus and the direct exchange is negligible. The exchange interaction in the rare earths is called the Ruderman-Kittel-Kasuya-Yosida (RKKY) interaction.[4-6] The RKKY interaction is an indirect interaction that couples the moments on different ions through their mutual interaction with the conduction electrons. A calculation of the RKKY interaction, assuming free electrons, yields the expression:[38]

$$J_{ij} = J(\vec{R}_{ij} = \vec{r}_i - \vec{r}_j) \qquad \text{III-3}$$

$$= \frac{3z\, J^2\, \pi}{2\, \epsilon_f} \; \Phi(2\, k_f\, R_{ij})$$

where:

$$\Phi(Y) = (Y \cos(Y) - \sin(Y))/Y^4 \qquad \text{III-4}$$

and $\epsilon_f$ is the Fermi energy, $k_f$ is the Fermi wavevector, and J is the s-f interaction, the interaction between a localized f electron and a conduction electron. The RKKY interaction is oscillatory with a period characteristic of the Fermi wavevector because the electrons responsible for the interaction must be able to change their polarizations to participate in the interaction, so they must have energies near the Fermi surface. In reality, of course, the Fermi surface is not spherical, but the results of the simpler calculation using the free electron approximation shows the long-range oscillatory nature of the interaction.

Using inelastic scattering of neutrons to determine the dispersion relation of magnons propagating along the c-axis in Dy, Nicklow *et al*[39] showed that the exchange interaction in Dy is, in fact, oscillatory and long-range. A realistic calculation of the exchange has not been done, since the

interaction depends on the shape of the Fermi surface which has not been measured in any of the heavy rare earths.

The exchange interaction, as it stands, is very difficult to treat, so the well known molecular field approximation[40] was employed in all calculations. The molecular field approximation assumes that the effect of all the other moments on a given moment can be described by a hypothetical magnetic field called the molecular field. The exchange interaction, in the molecular field approximation, is written in a form reminiscent of the Zeeman interaction:

$$\mathcal{H}_{ex}^{mf} = g\mu_B \vec{H}_{mf} \cdot \sum_i \vec{J}_i \qquad \text{III-5}$$

where:

$$\vec{H}_{mf} = \frac{\sum_j J_{ij} \langle \vec{J} \rangle}{g \mu_B} = \Gamma \vec{\sigma} \qquad \text{III-6}$$

and:

$$\Gamma = \frac{-J \sum_j J_{ij}}{g \mu_B} \qquad \text{III-7}$$

The form of the interaction is slightly nonstandard because it is written in terms of the reduced magnetization $\vec{\sigma} = \vec{M}/M_o$

rather than in terms of the volume magnetization $\vec{M}$. The molecular field approximation is, of course, not too reliable at low temperatures because it neglects correlations between the moments, and treats only their average interactions. Nevertheless, the moelcular field is the only approximation that allows easy computation of the exchange interaction, and it is used throughout the rest of this thesis.

2. Anisotropic Exchange

The calculations of Kaplan and Lyons[41] and Specht[41a], which treated the RKKY exchange interaction in second-order perturbation theory, showed that there can be an appreciable (10% or greater) anisotropic contribution to the exchange in the rare earths. There was no experimental manifestation of the presence of an anisotropic component in the exchange until Nicklow et al[42] found that they could not explain their inelastic scattering data on Er. They found that the spin-wave spectrum could be fitted to the theory only if the anisotropic contribution was allowed to be wavevector dependent. Since, in the usual treatment, the single-ion anisotropy is not wavevector dependent, Nicklow et al attributed the discrepancy to their failure to include the anisotropic exchange interaction, which is wavevector dependent. Later, Jensen et al[43] also found evidence that there was a small anisotropic contribution to the exchange in Tb, and Nicklow[43] was reported to have obtained preliminary results that indicated that the anisotropic exchange in Dy was intermediate between

that of Er and Tb. As a result, a small anisotropic exchange was included in the calculations reported here. Recently, however, Lindgard[44] has shown that the difficulty in fitting the spin-wave data was not due to the absence of the anisotropic exchange from the Hamiltonian, but was due to the fact that the usual treatment of the single-ion anisotropy was wrong to lowest order. By treating the one-ion anisotropy correctly, Lindgard was able to get good agreement between theory and experiment without invoking the anisotropic exchange. The effect of the inclusion of the anisotopic exchange on the calculations reported here is minimal, however, for reasons that will be explained later.

The form assumed for the anisotropic exchange was the simplest possible second-order axial anisotropy:

$$\mathcal{H}_{ex}^{a} = - \sum_{i} \sum_{j \neq i} K_{ij} \left(3J_{iz}J_{jz} - \vec{J}_i \cdot \vec{J}_j\right) \qquad \text{III-8}$$

The anisotropic exchange was also treated in the molecular field approximation. Equation III-8 becomes in the molecular field approximation:

$$\mathcal{H}_{ex}^{a,mf} = g \mu_B \Gamma_1 \sum_{i} \left(3\sigma_z J_z - \vec{\sigma} \cdot \vec{J}_i\right) \qquad \text{III-9}$$

3. Zeeman Interaction

The Zeeman interaction is the ordinary one:

$$\mathcal{H}_z = - \sum_i \vec{\mu}_i \cdot \vec{H}_{app} = g \mu_B \sum_i \vec{J}_i \cdot \vec{H}_{app} \qquad \text{III-10}$$

where g is the Lande g-factor calculated for the free tripositive ion.

4. Crystal Field Interaction

The one-ion anisotropy or crystal field interaction is due, in the heavy rare earths, to the non-sphericity of their 4f electron clouds (except for Gd which has no one-ion anisotropy). The electric fields set up by the neighboring ions in the crystal establish a preferential orientation for the electron cloud in the crystal. Since the 4f electrons are shielded by the outer electrons, the orbital angular momentum is not quenched, but its orientation depends on the orientation of the electron cloud in the crystal. The spin angular momentum is strongly coupled to the orbital moment, so the preferred direction of the total angular momentum, $\vec{J}$, and thus, the magnetic moment, is determined by the crystalline electric field. A simple calculation serves to illustrate the origin of the form of the interaction.

Let the nucleus of the ion, at which the calculation of the electric field is being done, be taken as the origin

of the coordinate system, and let the axes of the coordinate system be parallel to the crystallographic axes. The electrical potential due to the other ions can be expressed as a function of the coordinates of the ion, $\vec{x}_i$, the coordinates at which the potential is being calculated, $\vec{x}_i$, and the charges of the ions, $e_i$:

$$V(r,\theta,\varphi) = \sum_i \frac{e_i}{|\vec{x}-\vec{x}_i|} \qquad \text{III-11}$$

$(|\vec{x}-\vec{x}_i|)^{-1}$ can be expanded in spherical harmonics[45]:

$$V(r,\theta,\varphi) = 4\pi \sum_i e_i \sum_{\ell=0}^{\infty} \sum_{m=-\ell}^{\ell} (2\ell+1)^{-1} r_<^{\ell} r_>^{-\ell-1} \cdot$$

$$Y^*_{\ell m}(\theta_i,\varphi_i)\, Y_{\ell m}(\theta,\varphi) \qquad \text{III-12}$$

or, in a more phenomenological form, the potential at a point nearer the origin than any of the other ions is:

$$V(r,\theta,\varphi) = \sum_{\ell=0}^{\infty} \sum_{m=-\ell}^{\ell} B_\ell^m\, r^\ell\, Y_{\ell m}(\theta,\varphi) \qquad \text{III-13}$$

where:

$$B_\ell^m = 4\pi \sum_i e_i\, (2\ell+1)^{-1}\, r^{-\ell-1}\, Y^*_{\ell m}(\theta_i,\varphi_i) \qquad \text{III-14}$$

The result of the summations for a simple hcp lattice is that only $B_4^0$, $B_6^0$, and $B_6^{\pm 6}$ are nonzero. Because, however, the c/a ratio does not have its ideal value[37], $B_2^0$ is also nonzero. These parameters can be determined from this simple model, but they are not reliable because the effects of conduction electron screening on the electric fields of the ions has not been included. To calculate the anisotropy energy, the expectation value of the Hamiltonian must be found. The radial part of the wave function must be calculated numerically, and the straightforward method of calculating the angular part would be to calculate the eigenfunctions of the $|LSJM_J\rangle$ representation in terms of the single electron wave functions $|\ell m_\ell s m_s\rangle$. This a formidable task for the $4f^9$ configuration, but fortunately there is an alternative, due to Stevens[46]. Using the Wigner-Eckhart theorem within the ground state J-multiplet, the matrix elements of the spherical harmonics can be replaced by matrix elements of the irreducible tensor operators multiplied by a constant factor which is the ratio of their reduced matrix elements. The irreducible tensor operators are polynomials in the components of the angular momentum operator, $\vec{J}$, so their matrix elements are relatively easy to calculate in the $|LSJM_J\rangle$ representation. The final form of the crystal field is thus:

$$\mathcal{H}_a(i) = P_2^0\, Q_2^0(\vec{J}_i) + P_4^0\, Q_4^0(\vec{J}_i) + P_6^0\, Q_6^0(\vec{J}_i) + P_6^6\, Q_{66}^+(\vec{J}_i) \qquad \text{III-15}$$

where the $Q_\ell^m$'s are the angular momentum irreducible tensor operators defined in Appendix A. The $P_\ell^m$'s are phenomenological constants that are normally measured experimentally, because the theoretical calculations are liable to large errors due to the difficulty of including the conduction electron screening.

5. One-Ion Magnetoelastic Interaction

Before considering the magnetoelastic Hamiltonian, which is written in the group theoretical notation of Callen and Callen[14], it is instructive to consider their derivation of the form of the elastic energy. In general, the elastic energy is written:

$$\mathcal{H}_e = (1/2)\, C_{ijkl}\, e_{ij}\, e_{kl} \qquad \text{III-16}$$

where the $C_{ijkl}$'s are the elastic constants and the $e_{ij}$'s are the symmetric part of the infinitesimal strain tensor:

$$e_{ij} = (1/2)\,(\partial u_i/\partial x_j + \partial u_j/\partial x_i) \qquad \text{III-17}$$

The symmetry of the crystal reduces the number of independent elastic constants to five: $C_{11}$, $C_{33}$, $C_{44}$, $C_{12}$, and $C_{13}$.

It is fairly easy to find the number of independent elastic constants using group theory. The six Cartesian strains $e_{xx}$, $e_{yy}$, $e_{zz}$, $e_{xy}$, $e_{xz}$, and $e_{yz}$ form the basis of a reducible six-dimensional representation of the hexagonal group $D_{6h}$. This representation reduces into two one-dimensional and two two-dimensional representations whose basis functions are:

$$e^{\alpha,1} = e_{xx} + e_{yy} + e_{zz}$$

$$e^{\alpha,2} = 3e_{zz} - e^{\alpha,1} \qquad \text{III-17a}$$

$$e_1^{\gamma} = e_{xx} - e_{yy} \qquad e_2^{\gamma} = 2e_{xy}$$

$$e_1^{\varepsilon} = 2e_{yz} \qquad e_2^{\varepsilon} = 2e_{xz}$$

where some of the basis functions differ by a constant factor from those of Callen and Callen[14]. Coupling is allowed only between basis functions of the same representation and only between basis functions with the same index in multi-dimensional representations. The elastic energy can thus be written[14]:

$$\mathcal{H}_e = (1/2)\ c_1^{\alpha}(e^{\alpha,1})^2 + c_{12}^{\alpha}\ e^{\alpha,1}\ e^{\alpha,2} + (1/2)\ c_2^{\alpha}(e^{\alpha,2})^2$$

$$+ (1/2)\ c^{\gamma}((e_1^{\gamma})^2 + (e_2^{\gamma})^2) \qquad \text{III-18}$$

$$+ (1/2)\ c^{\varepsilon}((e_1^{\varepsilon})^2 + (e_2^{\varepsilon})^2)$$

where the $c_j^{\Gamma}$'s are expressed in terms of the Cartesian elastic constants in the following way:

$$c_1^{\alpha} = (2c_{11} + c_{33} + 2c_{12} + 4c_{13})/9$$

$$c_2^{\alpha} = (c_{11} + c_{12} + 2c_{33} - 4c_{13})/18$$

$$c_{12}^{\alpha} = (c_{33} - c_{11} + c_{13} - c_{12})/9 \qquad \text{III-19}$$

$$c^{\gamma} = c_{66} = (1/2)(c_{11} - c_{12})$$

$$c^{\varepsilon} = c_{44}$$

where some of the elastic constants are defined differently from those of Callen and Callen. The elastic contribution to the energy is a purely classical term that will not be explicitly included in most calculations.

The one-ion magnetoelastic interaction is due to the strain dependence of the crystal field anisotropy energy. The infinitesimal strain tensor is:

$$\epsilon_{ij} = \partial u_i / \partial x_j \qquad \text{III-20}$$

where $\vec{u}$ is the displacement a point $\vec{x}$ in the unstrained solid suffers when a strain characterized by $\epsilon_{ij}$ is applied to the solid, so $\vec{u} = \vec{x}' - \vec{x}$. Normally, in infinitesimal strain theory, only the symmetric part of the infinitesimal strain tensor:

$$e_{ij} = (1/2)(\epsilon_{ij} + \epsilon_{ji}) \qquad \text{III-21}$$

is considered. This is the only part of the strain that was considered by Callen and Callen for example. Southern and Goodings[23] first pointed out that, because of the large single-ion anisotropy of the heavy rare earths, the anti-symmetric (or rotational) part of the infinitesimal strain:

$$\omega_{ij} = (1/2)(\epsilon_{ij} - \epsilon_{ji}) \qquad \text{III-22}$$

can also lead to measurable effects. Appendix B discusses a general expansion[47] of the crystal field anisotropy energy in powers of the infinitesimal strain, including both the symmetric and antisymmetric parts of the infinitesimal strain tensor. The form of the contribution to the one-ion

magnetoelastic Hamiltonian that is linear in the $\omega_{ij}$'s is derived in Appendix B, and is written:

$$\mathcal{H}_{me}^{I,rot}(i) = \sqrt{6}\, P_2^0(\omega_{13}\, Q_{21}^+(\vec{J}_i) + \omega_{23}\, Q_{21}^-(\vec{J}_i)) \qquad \text{III-23}$$

where only terms bilinear in the angular momentum operators are shown. These terms are manifested experimentally when measuring the dependence of the elastic constant $C_{44}$ on the magnetic field. There are two independent measurements from which $C_{44}$ can be calculated in hexagonal materials, both of which are shown in Figure I-3. The two ways in which $C_{44}$ can be calculated are: $C_{44} = \rho v_2^2$ where $v_2$ is the velocity of a shear wave polarized along the a or b-axis and propagating along the c-axis; or $C_{44} = \rho v_5^2$ where $v_5$ is the velocity of a shear wave polarized along the c-axis and propagating along the a or b-axis. The strains which describe these shear waves are: $\partial u_x/\partial z$ or $\partial u_y/\partial z$ for $v_2$ and $\partial u_z/\partial x$ or $\partial u_z/\partial y$ for $v_5$. Since the antisymmetric strains are:

$$\omega_{13} = (1/2)(\partial u_x/\partial z - \partial u_z/\partial x) \qquad \text{III-24}$$

$$\omega_{23} = (1/2)(\partial u_y/\partial z - \partial u_z/\partial y)$$

the rotational contribution to the magnetoelastic interaction enters with opposite sign for $v_2$ and $v_5$. At zero field, $v_2 = v_5$, but in an applied field, $v_2 \neq v_5$, generally.

The symmetric part of the infinitesimal strain lowers the symmetry of the crystal, so, in general, the single-ion magnetoelastic Hamiltonian includes all irreducible tensor oeprators of orders $\ell = 2$, 4, or 6. In fact, Donoho's[47] numerical expansion of the crystal field anisotropy energy in powers of the strain shows that the tensor operators with $m = 3$ do not appear in the expansion. Group theory can be used to show rigorously that the operators with $m = 3$ do not enter the Hamiltonian. Following Callen and Callen[14], only terms with $\ell = 2$ will be kept in the single-ion magnetoelastic Hamiltonian. It is reasonable to believe that the $\ell = 2$ terms will be larger than the higher order terms because the second-order contribution to the anistropy dominates the higher order terms. It should be stated, however, that Rhyne and Legvold[12] found that it was necessary to include one $\ell = 4$ term in order to fit the temperature dependence of the basal plane magnetostriction of Tb. The possibility exists that a better fit to the experimental data could be obtained by the inclusion of higher order terms, but the ensuing increase in complexity makes their addition worthwhile only in extreme cases.

The six symmetrized bilinear products of the angular momentum operators are isomorphic to the six Cartesian strains, so basis functions can be formed from them in the same way that they were formed from the strains. The coupling of the strain basis functions and the angular momentum basis functions follows the same rules that were stated in the derivation of the form of the elastic energy. The complete one-ion magnetoelastic Hamiltonian, to first order in the infinitesimal strains and second order in the angular momentum operators is:

$$\begin{aligned}\mathcal{H}^{I}_{me}(i) = &-(B_1^{\alpha,2}\, e^{\alpha,1} + B_2^{\alpha,2}\, e^{\alpha,2})\, Q_2^0(\vec{J}_i) \\ &- B^{\gamma,2}(e_1^{\gamma}\, Q_{22}^{+}(\vec{J}_i) + e_2^{\gamma}\, Q_{22}^{-}(\vec{J}_i)) \\ &- B^{\epsilon,2}(e_2^{\epsilon}\, Q_{21}^{+}(\vec{J}_i) + e_1^{\epsilon}\, Q_{21}^{-}(\vec{J}_i)) \\ &+ \sqrt{6}\, P_2^0(\omega_{xz}\, Q_{21}^{+}(\vec{J}_i) + \omega_{yz}\, Q_{21}^{-}(\vec{J}_i)).\end{aligned} \qquad \text{III-25}$$

Note that terms in $Q_0^0$ (isomorphic to $e_1^{\alpha}$) do not appear in the Hamiltonian because $Q_0^0$ is just a constant and shifts all the energy levels equally. The relations between the coupling constants used here and those used by Callen and Callen[14] and Southern and Goodings[23] are given in Appendix C.

## 6. Two-Ion Magnetoelastic Interaction

The two-ion magnetoelastic interaction has its origins in the strain dependence of the exchange interaction. The form of the Hamiltonian is the same as for the one-ion interaction except for the fact that the angular momentum symmetry operators are formed from bilinear products of angular momentum operators associated with different ions. This change has the effect of increasing the number of coupling constants by two, because the operator, $\vec{J}_i \cdot \vec{J}_j$, which is the basis function for the fully symmetric representation, is no longer trivial. The two-ion magnetoelastic interaction has the form:

$$\mathcal{H}_{me}^{II}(i) = -\sum_j (D_{1ij}^{\alpha,0}\, e^{\alpha,1} + D_{2ij}^{\alpha,0}\, e^{\alpha,2})\, \vec{J}_i \cdot \vec{J}_j \qquad \text{III-26}$$

$$-\sum_j (D_{1ij}^{\alpha,2}\, e^{\alpha,1} + D_{2ij}^{\alpha,2}\, e^{\alpha,2})\,(3J_{iz}J_{jz} - \vec{J}_i \cdot \vec{J}_j)$$

$$-\sum_j D_{ij}^{\gamma,2}\,(e_1^{\gamma}(J_{ix}J_{jx} - J_{iy}J_{jy}) + e_2^{\gamma}(J_{ix}J_{jy} + J_{iy}J_{jx}))$$

$$-\sum D_{ij}^{\varepsilon,2}\,(e_1^{\varepsilon}(J_{iy}J_{jz} + J_{iz}J_{jy}) + e_2^{\varepsilon}(J_{ix}J_{jz} + J_{iz}J_{jx}))$$

The two-ion interaction, being closely related to the exchange, must also be treated in the molecular field approximation. The approximation is applied in exactly the same way as it was applied to the exchange interaction itself,

and the result is:

$$\mathcal{H}_{me}^{II,mf}(i) = J(G_1^{\alpha,0}\, e^{\alpha,1} + G_2^{\alpha,0}\, e^{\alpha,2})\, \vec{\sigma}\cdot\vec{J}_i \qquad \text{(III-27)}$$

$$+ J(G_1^{\alpha,2}\, e^{\alpha,1} + G_2^{\alpha,2}\, e^{\alpha,2})(3\sigma_z J_{iz} - \vec{\sigma}\cdot\vec{J}_i)$$

$$+ JG^{\gamma,2}(e_1^{\gamma}(\sigma_x J_{ix} - \sigma_y J_{iy}) + e_2^{\gamma}(\sigma_x J_{iy} + \sigma_y J_{ix}))$$

$$+ JG^{\varepsilon,2}(e_1^{\varepsilon}(\sigma_y J_{iz} + \sigma_z J_{iy}) + e_2^{\varepsilon}(\sigma_x J_{iz} + \sigma_z J_{ix}))$$

where in the molecular field approximation:

$$\sum_j D_{ij}^{\Gamma}\, \vec{J}_i\cdot\vec{J}_j = \vec{J}_i\cdot \sum_j D_{ij}^{\Gamma} \langle\vec{J}_j\rangle \qquad \text{III-28}$$

$$= -\vec{J}_i\cdot\vec{\sigma}\,(\sum_j D_{ij}^{\Gamma})/J$$

so

$$G_i^{\Gamma} = -(\sum_j D_{ij}^{\Gamma})/J^2 \qquad \text{III-29}$$

## B. Applications of the Model Hamiltonian

### 1. Phase Transitions and Magnetic Ordering

The existence of magnetic ordering in the heavy rare earths is, of course, due to the presence of the RKKY exchange interaction, but the diversity of types of magnetic ordering is due to the interplay of the exchange, crystal field and magnetoelastic interactions.

Although a prediction of the ordering temperature, which would require a detailed calculation of the exchange interaction, is difficult it is possible to make some predictions about transitions from one ordered state to another. As an example, Dy is appropriate, not only because it is the subject of this thesis, but also because it (and Tb) have the simplest ordered phases of the heavy rare earths.

At 179K, Dy has a phase transition from the paramagnetic phase to the helical antiferromagnetic (HAF) phase, in which the moments are ordered in a basal plane spiral.[2,7] The helical ordering is a consequence of the fact that the exchange is long-range and oscillatory. All that is theoretically necessary for the stability of the helical phase is that a given moment (all moments are considered equivalent) have a positive exchange interaction, $J_0$, with neighboring moments in the same plane, a positive exchange interaction, $J_1$ with its nearest neighbors in the adjacent planes, and a negative interaction, $J_2(<0)$, with the nearest moments in second-nearest planes. Figure III-1 shows the geometry of the interactions more clearly. Experimental measurements have shown that the exchange interaction in Dy is actually of longer range than this model assumes, but the simple model does illustrate the basic features of the helically ordered

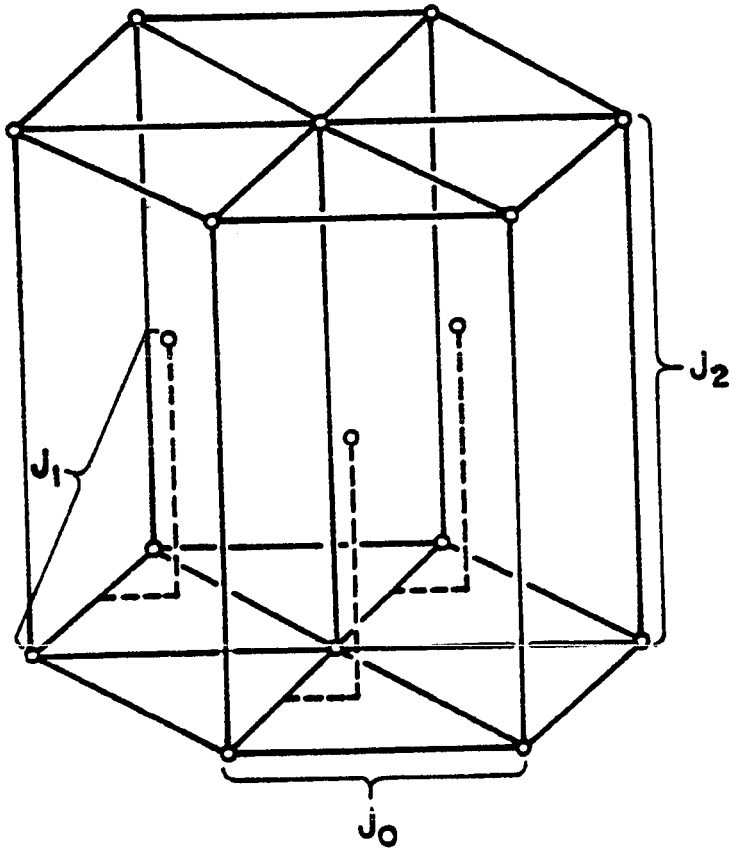


Figure III-1 Model of the hcp lattice showing the three interplanar exchange constants.

state. The details of the calculation can be found in Cooper's article[38]. The moments are confined to the basal plane because of the large axial anisotropy in Dy that makes the c-axis a hard magnetic axis.

In the ordered phases of all the rare earths, Dy in particular, all the moments in a given plane perpendicular to the c-axis are parallel[48]. The angle between the moments can vary from plane to plane, however. In the HAF phase of Dy, this angle varies from 43.2° at the Neel point to 26.5° at the Curie temperature.[48] The temperature dependence of the turn angle is not predicted by the simple model discussed in the previous paragraph, but it can be included phenomenologically by letting the exchange constants be functions of the temperature.

The theory of Elliott and Wedgewood[49] is generally accepted as the physical explanation of the temperature dependence of the turn angle. They argue that, since the symmetry of the exchange interaction in the HAF phase is not commensurate with the symmetry of the lattice, the Fermi surface will be distorted by the energy gaps that are introduced at the superzone boundaries. The magnitude of these gaps is[50]: $2VJ\sigma$, where V is the magnitude of the s-f interaction, J is the total angular momentum of the ion, and $\sigma$ is

the reduced magnetization. The predicted temperature dependence of the turn angle agrees with experiment fairly well for Ho, Er, and Tm, all of which have Neel temperatures less than 135K, but the agreement for Dy and Tb, which have Neel temperatures above 175K, is not so good. Elliott and Wedgewood attribute the disagreement to high temperature effects that were not included in their calculations.

The theory of Ellictt and Wedgewood predicts that the HAF phase of Dy is, in the absence of interactions other than the exchange, stable down to 0K, at which temperature the turn angle has decreased to 15°. Experimentally, a phase transition to the FM phase occurs spontaneously at 85K and can be induced at higher temperatures in the HAF phase by the application of a magnetic field in the basal plane. The critical field at which the transition occurs varies almost linearly with temperature from 0kOe at the Curie temperature to approximately 10kOe at 160K.[7] Cooper [51] has shown that the combination of the magnetoelastic and basal plane anisotropy energies has the correct magnitude and temperature dependence to account for the transition. Cooper used the three plane interaction model to account for the exchange. Although Cooper's explanation is widely accepted, it has recently been criticized by del Moral and Lee[50] because the

difference in the exchange interaction in the ferromagnetic and antiferromagnetic phases was neglected in Cooper's calculation. In addition, they show[52] that the temperature dependence that Cooper assumed for the exchange constants does not agree with their experimentally determined temperature dependences. They argue that the agreement of Cooper's theory with experiment is largely fortuitous, and that the real driving force behind the transition is the lowering of the exchange energy in the ferromagnetic phase relative to the antiferromagnetic phase. Del Moral and Lee[50] base their arguments on the spin wave dispersion relation measured by Nicklow et al[39] which clearly shows that the exchange interaction is different in the two phases. Del Moral and Lee's argument is also open to criticism, however, because, although the exchange interaction calculated from the spin-wave dispersion relation is different in the two phases, it is not clear whether the difference is primarily due to the additional periodicity of the antiferromagnetic ordering, as they suggest, or whether it is due to the magnetostrictive strains occuring at the transition that lower the crystalline symmetry from hcp to orthorhombic[53].

2. Magnetization and Susceptibility

The measured susceptibilities of Dy are well fitted at temperatures away from the Neel temperature by the Curie-

Weiss law modified for anisotropic ferromagnets:

$$\chi_{||} = C/(T-\theta_{||}) \qquad \chi_{\perp} = C/(T-\theta_{\perp}) \qquad \text{III-30}$$

$$C = Ng^2\mu_B^2 J(J+1)/3k$$

where C is the Curie constant and the $\theta$'s are the paramagnetic Curie temperatures obtained by extrapolation of the parallel and perpendicular susceptibilities measured at temperatures well above the Neel temperature. The paramagnetic Curie temperatures of Dy are: $\theta_{||} = 169K$ and $\theta_{\perp} = 121K$[7]. The saturation magnetization of Dy, 10.3 $\mu_B$/ion, which was measured by Behrendt *et al*[7], agrees well with the value, 10 $\mu_B$/ion, calculated for the free $Dy^{3+}$ ion. The excess magnetization is attributed to the polarization of the conduction electrons. A phase transition[8] has been observed at low temperatures when the field is applied along the c-axis. Near 80kOe, and at a temperature of 4.2K, the easy axis moves from the basal plane to the c-axis. This transition is accompanied by large non-reversible strains and is assumed to be of magnetostrictive origin.

3. Anisotropy

The Callen and Callen theory[9,10] is generally used to interpret experiments measuring the anisotropy in the heavy rare earths, and also to relate the measured quantities to the parameters that appear in the theory.

Callen and Callen were primarily interested in anisotropy in ferromagnetic materials, so they assumed that the exchange was the dominant interaction and that the crystal field and Zeeman interactions were small perturbations. It should be noted here that although the Callen and Callen theory has been applied in the paramagnetic phase, the assumption that the exchange is the dominant interaction is not always true in the paramagnetic phase. The magnetostriction is not included, although it does contribute to the measured anisotropy. The Hamiltonian that Callen and Callen adopt is:

$$\mathcal{H} = \mathcal{H}_{ex}^{is} + \mathcal{H}_{z} + \mathcal{H}_{a} \qquad \text{III-31}$$

The axis defined by the magnetization is taken as the axis of quantization. In general, this axis does not coincide with the symmetry axis of the crystal, so the irreducible tensor operators, that appear in $\mathcal{H}_a$, must be expressed in the new coordinate system. The irreducible tensor operators of order $\ell$ transform,by definition[54], like the basis functions of the $2\ell+1$ dimensional representation of the full rotation group (like spherical harmonics of order $\ell$), so:

$$Q_{\ell}^{m} = \sum_{n=-\ell}^{\ell} Q_{\ell}^{n}, \; D_{nm}^{\ell}(\omega) \qquad \text{III-32}$$

where $\omega = \alpha, \beta, \gamma$; the Euler angles of the rotation, $D_{nm}^{\ell}$ is the rotation matrix for the $2\ell+1$ dimensional representation,

and the primed operators are defined in the rotated coordinate system. Eventually, the thermodynamic averages of the operators will be calculated with the eigenfunctions of the zero-order Hamiltonian, and since the zero-order Hamiltonian has cylindrical symmetry about the axis defiined by the magnetization, the thermodynamic averages of the operators in the summation will be zero if $m \neq 0$. For the axial term ($m=0$), the only coefficient that appears is[54]:

$$D^{\ell}_{00}(\omega) = P_{\ell}(\cos\beta) \qquad \text{III-33}$$

and for the basal plane term ($m=6$), the only coefficient that appears is:

$$D^{\ell}_{0m} = (4\pi/2\ell+1)^{1/2}\, Y_{\ell m}(\beta,\gamma) \qquad \text{III-34}$$

so the crystal field Hamiltonian becomes, in the rotated coordinate system:

$$\mathcal{H}'_a = P^0_2\, P_2(\cos\theta)\, Q^{0\prime}_2 + P^0_4\, P_4(\cos\theta)\, Q^{0\prime}_4 + P^0_6\, P_6(\cos\theta) Q^{0\prime}_6$$
$$+ (1/180\sqrt{231})\, P^6_6\, P_{66}(\cos\theta)\, \cos 6\phi\, Q^{0\prime}_6.$$

The primes will be dropped in the remainder of the discussion.

The only remaining problem is now to find the thermodynamic average of $Q^0_{\ell}$. The thermodynamic average is, of

course, the sum of 2J+1 terms. However, since J is large for the heavy rare earths, Calen and Callen[9,10] replaced the summation with an integral over continuous orientations of the moment. This is the classical limit in which the irreducible tensor operators reduce to the spherical harmonics. In this limit, Callen and Callen obtained an integral over $\theta$ which they solved exactly for the result:

$$\langle Q_\ell^0 \rangle = N_\ell \frac{I_{\ell+1/2}(L^{-1}(\sigma))}{I_{1/2}(L^{-1}(\sigma))} \qquad \text{III-36}$$

$$= N_\ell \hat{I}_{\ell+1/2}(L^{-1}(\sigma))$$

where the normalization constant $N_\ell$ is the value of the thermodynamic average of the irreducible tensor operator at 0K, L is the Langevin function: $L(x) = \text{ctnh}(x) - 1/x$, $\sigma$ is the reduced magnetization: $M/M_0$, and $I_{\ell+1/2}$ is the modified Bessel function of half integral order.

This result implies that all the properties of the anisotropy are functions of the magnetization, and do not depend directly on the magnetic field or the temperature. Callen and Shtrikman[55] have shown that, although this result was derived in the molecular field approximation, only those properties of the molecular field that are common to all renormalized collective excitation theories (such as the molecular field approximation, spin-wave theory, and Green's

function theories) were invoked in its derivation, so it is of much wider validity than the molecular field approximation itself, at least in situations where the approximation that $J=\infty$ is a reasonable one.

The majority of the measurements of anisotropy involve the measurement of either magnetization or torque, so they are done at a constant temperature and the Helmholtz free energy is the proper thermodynamical potential to use. There are, however, two free energies that can be defined for use in magnetic problems. The first, called $F_a$ by Kittel[56], is:

$$F_a = -kT \ln(Z_0) \qquad \text{III-37}$$

where $Z_0$ is the partition function calculated with the eigenvalues of the zero-order Hamiltonian. $F_a$ includes the energy of interaction between the magnetized sample and the field as well as the energy that was necessary to magnetize the sample. The other free energy $F_a$:

$$F_b = F_a + \vec{H}\cdot\vec{M} \qquad \text{III-38}$$

is defined by subtracting the interaction energy, thus leaving only the energy that was added to the system that is necessary to keep the sample magnetized when the magnetization is rotated away from the easy axis of magnetization. Treating the crystal field interaction in first-order

perturbation theory the free energy is:

$$F_b = -kT \ln(Z_0) + \vec{H}\cdot\vec{M} + \langle \mathcal{H}_a \rangle \qquad \text{III-39}$$

Normally, the anisotropy energy $\langle \mathcal{H}_a \rangle$ is expressed in the form:

$$\langle \mathcal{H}_a \rangle = K_2^0(T,H)\ P_2(\cos\theta) + K_4^0(T,H)\ P_4(\cos\theta) \qquad \text{III-40}$$
$$+ K_6^0(T,H)\ P_6(\cos\theta) + K_6^6(T,H)\ \cos(6\phi)\ P_{66}(\cos\theta)$$

where:

$$K_\ell^m(T,H) = K_\ell^m(T=0K)\ \hat{I}_{\ell+1/2}(\ L^{-1}(\sigma(T,H))) \qquad \text{III-41}$$

At thermal equilibrium, the orientation of the magnetization is such as to minimize the free energy, so:

$$\partial F_a/\partial\theta = 0 = -HM\sin\theta + \partial\langle \mathcal{H}_a \rangle/\partial\theta \qquad \text{III-42}$$

The anisotropy constants $K_\ell^m(T)$ can be determined by measuring the magnetization and its orientation for several values of the field at a constant temperature. The field must have a component along the hard axis of the sample. A least squares fit of the experimental data then determines the anisotropy constants for that temperature. Note that, although the $K_\ell^m$'s are written, in general, as functions of the magnetic field, their dependence on the field is weak because the magnetization is almost independent of the field at

temperatures below $T_N$. The measured dependence of the anisotropy constants on temperature can then be compared to that predicted by the Callen and Callen theory. The comparison has been done for $K_2^0$, $K_4^0$, and $K_6^6$, for the elements Dy and Tb, and the results can be found in the review article by Rhyne[1]. The fit of the theory and experiment is very good considering the limited accuracies of the experiments.

The T = 0K values of the anisotropy constants can be calculated by a fit of the experimentally measured constants to the equation:

$$K_\ell^m(T) = K_\ell^m(T=0)\ I_{\ell+1/2}(\ L^{-1}(\sigma)) \qquad \text{III-43}$$

The T = 0K values of the anisotopy constants have been calculated using experimental data obtained by several methods. The agreement between methods is fairly good at least for the values of $K_2^0$. Analysis of the magnetization data of Feron and Pauthenet[57], in fields up to 70kOe, yielded the values: $K_2^0(T=0) = 126°K/ion$ and $K_4^0(T=0) = 12° K/ion$. The torque magnetometer data of Rhyne and Clark[58], taken in fields up to 150kOe, yielded the same value of $K_2^0$ as the data of Feron and Pauthenet, but the magnetization data of Rhyne et al[8], which was taken in fields up to 150kOe, yielded the value: $K_2^0(T=0) = 112°K/ion$. However, the value of $K_2^0$ that was obtained by analysis[59] of the paramagnetic data of Behrendt et al[7] was 57°K/ion , which is different by a factor of two. The difference may be due, at least in part, to the

fact that the data of Behrendt et al were taken at temperatures above 200K, whereas the other determinations of $K_2^0$ were made using data obtained at temperatures of 150K or below. The magnetostriction makes a relatively larger contribution to the effective anisotropy at lower temperatures, and may account for a good part of the discrepancy. Other measurements were discussed in the review article by Rhyne[1].

All the measurements discussed prevoiusly were made on single crystals of pure Dy metal. It was thus impossible to separate the one and two-ion contributions to the anisotropy. Recently, however, Touborg and Hog [60] measured all the crystal field constants of Tb, Dy, and Er, by analysis of the magnetization of single crystals of alloys consisting of scandium, yttrium, or lutetium, each with a few atomic percent of one of the heavy rare earths added. The three elements scandium, yttrium, and lutetium all have the same crystalline structure as the heavy rare earths (with the exception of a slightly different c/a ratio) and all three are either paramagnetic or diamagnetic, so the two-ion exchange interaction should be small or nonexistent. The crystal field parameters themselves can thus be measured in these alloys. Since, however, Touborg and Hog analyzed their data under the assumption that the anisotropic exchange interactions are of the same order of magnitude as the single-ion crystal field interaction, and since this

assumption has been shown to be unecessary[44], their results are suspect.

The basal plane anisotropy has been measured by several workers. Rhyne and Clark[58] obtained a value: $K_6^6(T=0) = -1.7°K/ion$, whereas Feron and Pauthenet[57] found that $K_6^6(T=0) = -2.5°K/ion$, and analysis[59] of the magnetization data of Behrendt et al yielded the value: $K_6^6(T=0) = -2.3°K/ion$.

It should be pointed out that, as in all least squares fits, the calculated $K_\ell^m$'s depend on the number of terms that were included in the fit. In particular, since Feron and Pauthenet included terms higher than second-order, whereas Rhyne et al[8] did not, their agreement on the value of $K_2^0$ should be interpreted accordingly.

4. Magnetostriction

The Callen and Callen theory[14] is generally used to interpret the magnetostriction data also. The isotropic exchange interaction and the Zeeman interaction are taken as the zero-order Hamiltonian, the single-ion anisotropy and the magnetoelastic interactions are treated in first-order perturbation theory, and the elastic energy is a classical term that is added. The static magnetostriction measurements are made under conditions of constant temperature, constant magnetic field and constant stress; so the proper thermodynamical potential to use is the Gibbs free energy that is derived from the Helmholtz free energy $F_a$, that has the magnetic field as an independent parameter, so:

$$G_a = F_a + \sum_{k,l} e_{kl} T_{kl} \qquad \text{III-44}$$

where the Helmholtz free energy is defined and discussed by Kittel[56]. In the standard treatment of magnetostriction, the Helmholtz free energy is used, so the small stress due to atmospheric pressure is neglected. If the anisotropy and magnetostriction are treated in first-order perturbation theory, the Gibbs free energy becomes:

$$G_a = F_a + \sum_{k,l} e_{kl} T_{kl} + \langle \mathcal{H}_a \rangle + \langle \mathcal{H}_{me}^{I} \rangle + \langle \mathcal{H}_{me}^{II} \rangle \qquad \text{III-45}$$

where $F_a$ does not depend on the strain. In equilibrium, the free energy must be a minimum, so the equilibrium strains can be found by solving the equations:

$$\partial G_a / \partial e_i^{\Gamma,j} = 0 \qquad \text{III-46}$$

where $e_i^{\Gamma,j}$ is the symmetry strain (defined in equation III-17a). The solutions of the equations are:

$$\begin{aligned} \bar{e}^{\alpha,1} = \Delta^{-1} [ & C_2^{\alpha} [B_1^{\alpha,2} P_2(\cos\theta) \langle Q_2^0 \rangle \\ & + J^2 (G_1^{\alpha,0} \sigma^2 + G_1^{\alpha,2} (3\sigma_z^2 - \sigma^2)) + T_{11}] \\ & - C_{12}^{\alpha} [B_2^{\alpha,2} P_2(\cos\theta) \langle Q_2^0 \rangle \\ & + J^2 (G_2^{\alpha,0} \sigma^2 + G_2^{\alpha,2} (3\sigma_z^2 - \sigma^2))]] \end{aligned} \qquad \text{III-47}$$

$$\bar{e}^{\alpha,2} = \Delta^{-1}[C_1^{\alpha}\ [B_2^{\alpha,2}\ P_2(\cos\theta)\ \langle Q_2^0\rangle + J^2(G_2^{\alpha,0}\sigma^2 + G_2^{\alpha,2}(3\sigma_z^2 - \sigma^2))]$$

$$-C_{12}^{\alpha}[B_1^{\alpha,2}\ P_2(\cos\theta)\ \langle Q_2^0\rangle + J^2(G_1^{\alpha,0}\sigma^2 + G_1^{\alpha,2}(3\sigma_z^2 - \sigma^2)) + T_{11}]]$$

$$\bar{e}_1^{\gamma} = 1/C^{\gamma}\ [B^{\gamma,2}\langle Q_{22}^+\rangle + J^2G^{\gamma,2}(\sigma_x^2 - \sigma_y^2)]$$

$$\bar{e}_2^{\varepsilon} = 1/C^{\varepsilon}\ [B^{\varepsilon,2}\langle Q_{21}^+\rangle + J^2G^{\varepsilon,2}(2\sigma_x\sigma_z)]$$

where:

$$\Delta = C_1^{\alpha}\ C_2^{\alpha} - (C_{12}^{\alpha})^2$$

Since the stress is just due to atmospheric pressure, $T_{11} = T_{22} = T_{33} \simeq 10^6 \text{ergs/cm}^3$, and the other stress components are zero, so the correction to $\bar{e}^{\alpha,1}$ is about 2μin/in. The correction to $\bar{e}^{\alpha,2}$ is even smaller, so both corrections are within experimental error. These expressions are more convenient for use in magnetostriction problems when recast in a slightly different form. In this form, the magnetostriction constants that appear can be measured experimentally (using standard strain gauge techniques) by measuring the change in strain along a particular crysallographic axis while rotating the magnetization. Clark *et al*[11] discuss this method in more detail. For example,

$\lambda^{\gamma,2}$ is the change in the strain $e_{xx}$ when the magnetization is rotated from the a-axis to the b-axis. In general, however, the magnetization must be rotated from a hard axis to an easy axis, and because of the large magnetic anisotropy of Dy, the magnetization can not be fully aligned along the c-axis except in the paramagnetic phase. Thus, only the magnetostriction constant $\lambda^{\gamma,2}$ can be measured over the full temperature range from room temperature to LHe temperature. The acceptance of the Callen and Callen[14] theory of magnetostriction is due mainly to its prediction of the temperature dependence of this magnetostriction constant in Tb[12] and Dy[11], and the prediction of the temperature dependence of one $\ell = 4$ magnetostriction constant in Tb[12]. Figure I-2 shows the measured value of $\lambda^{\gamma,2}$ for Dy plotted as a function of the predicted dependence: $\hat{I}_{5/2}(L^{-1}(\sigma))$.

C. Dependence of the Elastic Constants on the Magnetization

The Callen and Callen[14] theory of magnetostriction did not predict any dependence of the elastic constants on the magnetization because it only included magnetization dependent terms that were linear in the strains. Terms bilinear in the strains are necessary, however, for a nonzero magnetoelastic contribution to the elastic constants, since the elastic constant is defined as the second derivative of the internal energy with respect to the strain.

Under the assumption of small strains, the elastic energy can be expanded in a Taylor series and only the first

few terms kept. The first derivatives of the elastic energy are zero since the energy is assumed to be an extremum. The second derivatives of the elastic energy with respect to the strains are just the usual elastic constants. Normally, only terms in the elastic energy that are bilinear in the strains are necessary, but if the strains become large enough to cause the atomic restoring forces to become nonlinear, then the third-order elastic constants, the third derivatives of the elastic energy with respect to the strain, must be kept if the elastic energy is to be calculated correctly. These anharmonic terms in the elastic energy are responsible for the thermal expansion of a solid as its temperature is raised.

The elastic constants can be defined either as the second derivatives of the free energy with respect to the strain (isothermal elastic constant) or as the second derivatives of the internal energy with respect to the strains (adiabatic or isentropic elastic constant). The isothermal elastic constants are appropriate for experimental situations where the strains are changing slowly enough to allow the temperature to remain constant throughout the sample. The adiabatic elastic constants are appropriate when the strain is changing so fast that there is no heat flow from one part of the sample to another, so the entropy is constant. The elastic constants are generally measured using dynamic strains, so the isentropic elastic constants

are used. In practice, at temperatures near or below room temperature, the difference between the isothermal and adiabatic elastic constants is not significant[59a].

It is important, at this point, to state the exact definition of the elastic constant. In the usual elasticity theory, the elastic constants can be defined in three equivalent ways, which differ only in the notation. Take $C_{66}$ as an example. If the elastic energy $U_e$ is:

$$U_e = 1/2 \sum_{\substack{i,j=1 \\ i \geq j}}^{6} C_{ij} e_i e_j = \sum_{i,j,k,l=1}^{3} C_{ijkl} e_{ij} e_{kl} \qquad \text{III-48a}$$

then:

$$C_{66} = C_{1212} = C_{2121} = C_{1221} = C_{2112}$$

where:

$$C_{66} = \partial^2 U_e / \partial e_6^2$$

$$C_{1212} = \partial^2 U_e / \partial e_{12}^2 = \partial^2 U_e / \partial \varepsilon_{12}^2 \qquad \text{III-48b}$$

$$\varepsilon_{ij} = \partial u_i / \partial x_j \qquad e_{ij} = 1/2 \, ( \varepsilon_{ij} + \varepsilon_{ji})$$

The presence of the rotational terms in the Hamiltonain (discussed in section III.A.5) means that in general,

$$\partial^2 U / \partial \varepsilon_{12}^2 \neq \partial^2 U / \partial \varepsilon_{21}^2$$

where U is the total internal energy including magnetic terms. Thus, the appropriate definition of the elastic constant is:

$$C_{ijkl} = \partial^2 U/\partial\varepsilon_{ij}\partial\varepsilon_{kl} \qquad \text{III-48c}$$

Note, however, that in all problems considered in this thesis, the definition:

$$C_{ijkl} = \partial^2 U/\partial e_{ij}\partial e_{kl}$$

gives the same answer as the definition in equation III-48c, but the notation there is not as convenient.

Since the Callen and Callen[14] Hamiltonian is linear in the strains, and since, in the Callen and Callen treatment, the magnetoelastic correction to the energy is just the first-order perturbation theory correction, either the Callen and Callen Hamiltonian must be treated in higher order perturbation theory, or the Hamiltonian must be fundamentally modified. Southern and Goodings adopted the latter approach, and their application of finite strain theory[24-26] to the heavy rare earths resulted in their prediction of the field dependence of the longitudinal elastic constants in the paramagnetic phase.

1. Southern and Goodings' Theory of the Magnetic Field Dependence of the Longitudinal Elastic Constants

Finite strain theory, as developed by Toupin[24], Tiersten[25], and Brown[26], requires that the energy of a magnetoelastically coupled solid be expressed in terms of a certain set of quantities, which are chosen to make the energy rotationally invariant. As it was developed, finite strain

theory was more general than it had to be for the problem that Southern and Goodings were considering, so several simplifying assumptions were made and somequantities which appear in the general theory do not appear in Southern and Goodings treatment. One of the invariant quantities that is relevant to the rare earth problem[23] is the finite strain:

$$E_{ij} = \frac{1}{2}\left(\frac{\partial u_i}{\partial x_j} + \frac{\partial u_j}{\partial x_i}\right) + \frac{1}{2}\sum_k \frac{\partial u_k}{\partial x_i}\frac{\partial u_k}{\partial x_j} \qquad \text{III-49}$$

which replaces the infinitesimal strain in the Hamiltonian of Callen and Callen. The other quantity is the, so called, angular momentum invariant:

$$J_i^* = \sum_j (\delta_{ij} + \omega_{ij})\, J_j \qquad \text{III-50}$$

where $\vec{J}$ is the angular momentum operator, and $\omega_{ij}$ is the antisymmetric part of the infinitesimal strain tensor. $\vec{J}^*$ replaces the usual angular momentum operator in the Callen and Callen Hamiltonian. The application[23] of finite strain theory to the rare earths is just the substitution of these invariant quantities for the usual ones. The consequences of the substitution will be discussed later.

The experimental verification of finite strain theory rests on the workof Eastman[61] on ferrimagnetic YIG and the work of Melcher[62] on antiferromagnetic $MnF_2$. Both authors present experimentally measured effects that are unaccounted

for in infinitesimal strain theory, but that are predicted by finite strain theory. Upon examination, it is apparent that in both papers, the theoretical explanations rely upon the presence of the $\omega_{ij}$'s and not upon the presence of the $E_{ij}$'s. It is not necessary to invoke finite strain theory to include these effects, however, because the general expansion[47] of the crystal field interaction in terms of the infinitesimal strains, which was discussed in section III.A.5, includes these terms.

Apparently, the only test of the substitution of the finite strains themselves is found in the work of Salama et al[27], Kale et al[28,29], and Gama et al[30,31], who applied Southern and Goodings theory of the magnetic field dependence of the longitudinal elastic constants of the heavy rare earths in the paramagnetic phase. As was discussed in Chapter I, they found that the magnetoelastic constants calculated from the theory of Southern and Goodings were at least an order of magnitude too large to account for the static magnetostriction results.

Although the bulk of the paper by Southern and Goodings is concerned with the effect of the rotational terms, only the part of their paper that treats the behavior of the longitudinal elastic constants in the paramagnetic phase will be discussed here. The rotational terms have no effect on longitudinal waves, so only the substitution of the finite strains for the infinitesimal strains is important. After making the

substitution, the magnetoelastic contribution to the internal energy is:

$$\begin{aligned} U_{me} = &-(B_1^{\alpha,2}\, E^{\alpha,1} + B_2^{\alpha,2}\, E^{\alpha,2})\, P_2(\cos\theta)\langle Q_2^0\rangle \\ &-B^{\gamma,2}\, E_1^{\gamma}\langle Q_{22}^{+}\rangle - J^2(G_1^{\alpha,0}\, E^{\alpha,1} + G_2^{\alpha,0}\, E^{\alpha,2})\sigma^2 \\ &- J^2(G_1^{\alpha,2}\, E^{\alpha,1} + G_2^{\alpha,2}\, E^{\alpha,2})(3\sigma_z^2 - \sigma^2) \qquad \text{III-51} \\ &- J^2\, G^{\gamma,2}\, E_1^{\gamma}\,(\sigma_x^2 - \sigma_y^2) \end{aligned}$$

where the magnetoelastic interaction is treated in first-order perturbation theory and the two-ion interaction is treated in the molecular field approximation. The shear strains have been dropped from the Hamiltonian. In the paramagnetic phase, where the magnetization is small, the Langevin function can be approximated as:

$$L(\sigma) = (1/3)\sigma \qquad (\sigma<<1) \qquad \text{III-52}$$

so:

$$L^{-1}(\sigma) = 3\sigma$$

Callen and Callen give the approximation:

$$\hat{I}_{\ell+1/2}(x) = x^{\ell}/(2\ell+1)!! \qquad \text{III-53}$$

where $x<<1$, so:

$$\hat{I}_{\ell+1/2}(L^{-1}(\sigma)) = (3\sigma)^{\ell}/(2\ell+1)!! \qquad \text{III-54}$$

and:

$$\langle Q_2^0 \rangle = \sqrt{2/3}\ (2J^2-J)(3\sigma^2/5) \qquad \text{III-55}$$

$$\langle Q_{22}^+ \rangle = \sqrt{3/8}\ \sin^2\theta\ \cos 2\phi\ \langle Q_2^0 \rangle$$

Since:

$$\Delta C_{ijkl} = \partial^2 U_{me} / \partial \varepsilon_{ij} \partial \varepsilon_{kl} \qquad \text{III-56}$$

and:

$$E_{ii} \simeq e_{ii} + (1/2) e_{ii}^2 \qquad \text{III-57}$$

in voight notation, the changes in the elastic constants are:

$$\Delta C_{1111} = \Delta C_{11} = -(B_1^{\alpha,2} - B_2^{\alpha,2})\ P_2(\cos\theta)\ \langle Q_2^0 \rangle - B^{\gamma,2} \langle Q_{22}^+ \rangle$$
$$- J^2 (G_1^{\alpha,0} - G_2^{\alpha,0}) \sigma^2 - J^2\ G^{\gamma,2} (\sigma_x^2 - \sigma_y^2)$$
$$- J^2 (G_1^{\alpha,2} - G_2^{\alpha,2}) (3\sigma_z^2 - \sigma^2) \qquad \text{III-58}$$

$$\Delta C_{3333} = \Delta C_{33} = -(B_1^{\alpha,2} + 2B_2^{\alpha,2})\ P_2(\cos\theta)\ \langle Q_2^0 \rangle$$
$$- J^2 (G_1^{\alpha,0} + 2G_2^{\alpha,0}) \sigma^2 - J^2 (G_1^{\alpha,2} + 2G_2^{\alpha,2}) (3\sigma_z^2 - \sigma^2)$$

Now, if $\Delta C_{ii}^x$ is the change in the elastic constant $C_{ii}$ when the field is applied along the x-axis, the five equations that appear in the theory of Southern and Goodings are:

$$\Delta C_{11}^a / \sigma^2 = -A/2 + B/2 + C - D + E$$

$$\Delta C_{11}^b / \sigma^2 = -A/2 + B/2 + C - D - E \qquad \text{III-59}$$

$$\Delta C_{11}^c / \sigma^2 = A - B + C - D$$

$$\Delta C_{33}^{a}/\sigma^2 = -A/2 - B + C + 2D$$

$$\Delta C_{33}^{c}/\sigma^2 = A + 2B + C + 2D$$

where:

$$A = -(3/5)\sqrt{2/3}\ (2J^2-J)\ B_1^{\alpha,2} - 2J^2\ G_1^{\alpha,2}$$

$$B = -(3/5)\sqrt{2/3}\ (2J^2-J)\ B_2^{\alpha,2} - 2J^2 G_2^{\alpha,2}$$

$$C = -G_1^{\alpha,0} \qquad \text{III-60}$$

$$D = -G_2^{\alpha,0}$$

$$E = -(3/5)\sqrt{2/3}\ (2J^2-J)\ B^{\gamma,2} - J^2\ G^{\gamma,2}$$

Although the notation is different from that of Southern and Goodings, it is easy to see that, at a given temperature, if the five experimental values on the left sides of equations III-59 are known, then the five combinations of magnetoelastic constants in equations III-60 can be determined. These five combinations are the same ones that appear in the expressions for the static magnetostriction, so the magnetoelastic constants that were determined from the static magnetostriction can be used to predict the behavior of the elastic constants as a function of the magnetization. (Equivalently, the magnetoelastic constants determined from the elastic constant experiment can be used to predict the static magnetostriction, as was done in Chapter I.) In particular, the theory of Southern and Goodings predicts that:

PLEASE NOTE:

This page not included in material received from the Graduate School. Filmed as received.

UNIVERSITY MICROFILMS

$$\Delta C_{22}^{me}(\sigma)/C_{22}(0) = (\Delta C_{22}^{b}(\sigma) - \Delta C_{22}^{a}(\sigma))/C_{22}(0) \qquad \text{III-61}$$

$$= 2C^{\gamma}\ \lambda^{\gamma,2}(T=0)\,(3\sigma^2/5)$$

where $\lambda^{\gamma,2}(T=0)$ is the value obtained from the magnetostriction measurements of Clark et al[11]. The predicted value, with the dependence on the magnetization factored out is:

$$\Delta C_{22}^{me}(\sigma)/(C_{22}\sigma^2) = .0033 \qquad \text{III-62}$$

which is independent of the temperature. The measured value of $\Delta C_{22}^{me}(\sigma)/(C_{22}\sigma^2)$ varies from approximately .33 at 180K to .08 at 300K. The discrepancy is obvious. Since the predictions of Southern and Goodings are seen to be in qualitative error, the application of finite strain theory appears to be an inappropriate way to treat the problem of the magnetic field dependence of the elastic constants.

2. Freyne's Thermodynamic Approach

Another approach to the problem of finding the magnetoelastic contribution to the elastic constants is that of Freyne[32]. By adopting a thermodynamic approach, in which the partition function is calculated with the energies that include the corrections from the crystal field and magnetoelastic interactions, Freyne was successful in explaining an anomaly in the temperature dependence of the elastic constant $C_{33}$ in the ferromagnetic phase of Gd, and the corresponding lack of an anomaly in the elastic constant $C_{44}$.

Experimentally, the anomalous dip in $C_{33}$, measured by Long et al[63] and by Fischer and Dever[64], occurs at 240K. The dip was observed to move to lower temperatures when magnetic fields were applied in the basal plane. Fields of approximately 80kOe applied in either the basal plane or perpendicular to it were sufficient to suppress the dip. No anomaly was seen in the elastic constant $C_{44}$.

Freyne related this anomaly to the change in the direction of the easy axis of the magnetization that had been observed in Gd using neutron diffraction[65]. The change in the magnetoelastic energy that accompanied the change in the direction of the magnetization was responsible for the anomaly.

The magnetoelastic contribution to the elastic constants was calculated by using the dispersion relation for longitudinal elastic waves propagating along the c-axis[32]:

$$-\rho\omega^2 u_z(z,t) = \partial^2 U / \partial z \partial e_{zz} \qquad \text{III-63}$$

(where U is the internal energy) to calculate the magnetoelastic contribution to the ultrasonic velocity, which was then related to the elastic constant by the formula: $v = \sqrt{\rho C_{33}}$.

Freyne's important contribution was in the calculation of the internal energy. Whereas, Callen and Callen[14] used the eigenvalues of the zero-order Hamiltonian to calculate their thermodynamic quantities, Freyne used energies that included the first-order perturbation theory corrections to

the energy. The corrections came from the crystal field interaction and the magnetoelastic interaction.

Freyne used the molecular field approximation for the exchange interaction. He took experimentally derived values for the crystal field and magnetoelastic constants and he calculated the temperature dependence of the magnetization and the angle of the easy axis, to show that the parameters that he was using in his Hamiltonian were consistent with experiment.

His predictions of the anomaly in the elastic constant $C_{33}$ agreed fairly well with experiment. In zero applied field, the calculated dip appeared at the correct temperature, although it had a different shape. His calculations showed that the dip moved to lower temperatures when a field was applied, and that fields of approximately 8kOe in either the basal plane or perpendicular to it were sufficient to suppress the dip in $C_{33}$. The qualitative agreement between Freyne's theory and experiment was good. When Freyne calculated the change in the elastic constant $C_{44}$, he found an anomaly that was much smaller than the anomaly in $C_{33}$, and that was consistent with experimental observations.

Although Freyne's approach gave good results for Gd, his method is not directly applicable to the other heavy rare earths because of the approximations that he was justified in making for Gd which are not true for the highly anisotropic rare earths. In particular, he neglected all operators

giving off-diagonal terms in the zero-order Hamiltonian, such as the basal plane anisotropy and magnetostriction. He also assumed that the exchange interaction dominated the other interactions, which is true for Gd since it is an S-state ion and has no single-ion anisotropy, but which is not true for the other rare earths, especially in their paramagnetic phases. It is possible, however, to generalize Freyne's method the other rare earths at the expense of some added complications.

### 3. The General Thermodynamic Method Applied to the Heavy Rare Earths

In this thesis, the thermodynamic method has been extended to allow it to be applied to any of the heavy rare earths. Whereas Freyne used the magnetoelastic constants deduced from the magnetostricion measurements in his calculation of the anomalous dip in $C_{33}$, the thermodynamic method is applied in this thesis with the purpose of finding the set of magnetoelastic constants that best describe the dependence of the elastic constants on the magnetization. The helically ordered phase was not included in the calculations, but the method can be applied to elements in the temperature range over which they are normally antiferromagnetic, if a magnetic field is applied that is large enough to induce a transition to the ferromagnetic phase. As in the other methods that have been discussed, the exchange interaction and the two-ion magnetoelastic interaction were treated in the molecular field approximation.

In the paramagnetic phase, the exchange interaction does not always dominate the crystal field interaction and the static magnetostriction, so it was necessary to include the crystal field interaction and the static magnetostriction in the zero-order Hamiltonian. The anisotropic exchange interaction was included in the zero-order Hamiltonian also, for reasons that were discussed in the section on the Model Hamiltonian.

The total strain is divided into two parts, the static magnetostrictive strain, $\bar{e}_i^{\Gamma,j}$ and the externally applied dynamic strain , $e_i^{\Gamma,j,rf}$:

$$e_i^{\Gamma,j} = \bar{e}_i^{\Gamma,j} + e_i^{\Gamma,j,rf} \qquad \text{III-64}$$

so the magnetoelastic interaction can be divided into two parts also:

$$\mathcal{H}_{me} = \bar{\mathcal{H}}_{me} + \mathcal{H}_{me}^{rf} \qquad \text{III-65}$$

where $\bar{\mathcal{H}}_{me}$ contains only the static strains and $\mathcal{H}_{me}^{rf}$ contains only the dynamic strains. Although the strains $e_i^{\Gamma,j,rf}$ are actually functions of time and position, they are treated as uniform, static strains. Since the wavelengths of the elastic waves used in this investigation were on the order of $10^5$-$10^6$ interatomic spacings, the assumption of uniform strains is a good one, since an ion and all of its neighbors experience essentially the same strain. The assumption of static strain is justified because at the frequencies (10-20MHz) which were used in this investigation, the time during which the strain changes is $\sim 10^{-7}$ sec, which is much longer than

the spin-spin relaxation time, $\sim 10^{-10}$sec. The spin system is thus always in its internal equilibriun state with respect to the dynamic strain. However, the spin-lattice relaxation time is longer than the time over which the strain changes, so there is no flow of energy from the spin system to the lattice, and the use of the internal energy in the calculation of the dependences of the elastic constants is justified. Stated in more general terms, the spin system, because of its strong spin-spin interactions, is characterized by a spin temperature, which is different from the temperature of the lattice because of the weaker spin-lattice coupling.

In the calculations of the internal energy, all terms bilinear in the strains were retained. The energies used in the calculation of the internal energy included the first and second-order corrections to the energy resulting from $\mathcal{H}_{me}^{rf}$.

The parameters that enter the calculation, the molecular field constants, the crystal field constants, and the magnetoelastic constants that appear in $\bar{\mathcal{H}}_{me}$ were chosen to give the best calculated fit to the experimental magnetization, anisotropy and magnetostriction data. This procedure is discussed in more detail in the next chapter, where the numerical calculations themselves are explained. It was necessary to make numerical calculations of the thermodynamic quantities that appear in the theory, because the 16 by 16

Hamiltonian (J=15/2 for $Dy^{3+}$) had to be digonalized before the thermodynamic quantities could be calculated. In order to avoid having to diagonalize imaginary Hamiltonians, only fields applied along the x or z-axes were considered. The only loss of generality in making this restriction was that the magnetic field could not have components along both the a and b-axes of the sample. Fields in either the a-c or b-c planes could be simulated by changing the sign of the basal plane anisotropy constant so that tha x-axis of the model corresponded to either the a or b-axis of the sample.

The magnitude and orientation of the magnetization, the free energy, and the internal energy were calculated from their thermodynamic definitions. The static magnetostrictive strains were calculated by minimizing the free energy with respect to the strains. Theoretical expressions for the non-vanishing derivatives of the internal energy with respect to certain functions of the strain were also evaluated. These expressions for the second derivatives will be derived in the following section.

The Hamiltonian is written:

$$\mathcal{H} = \mathcal{H}_0 + \mathcal{H}_{me}^{rf} \qquad \text{III-66}$$

and the perturbing term is due to the small oscillating strains that are imposed on the sample. Since the static strain will not appear explicitly in this section, the dynamic strain will simply be referred to as $e_i^{\Gamma,j}$.

An abbreviated notation is used for the perturbing Hamiltonian, which is, in the abbreviated notation:

$$\mathcal{H}^{rf}_{me}(i) = AQ^0_2(\vec{J}_i) + BQ^+_{22}(\vec{J}_i) + CQ^-_{22}(\vec{J}_i) + DQ^+_{21}(\vec{J}_i)$$
$$+ EQ^-_{21}(\vec{J}_i) + J\sigma_x PJ_x + J\sigma_z QJ_z \qquad \text{III-67}$$

where:

$$A = -B^{\alpha,2}_1 e^{\alpha,1} - B^{\alpha,2}_2 e^{\alpha,2} \qquad B = -B^{\gamma,2} e^{\gamma}_1$$

$$D = -B^{\varepsilon,2} e^{\varepsilon}_2 + \sqrt{6}\, P^0_2 \omega_{13} \qquad C = -B^{\gamma,2} e^{\gamma}_2$$

$$E = -B^{\varepsilon,2} e^{\varepsilon}_1 + \sqrt{6}\, P^{\theta}_2 \omega_{23} \qquad \text{III-68}$$

$$P = (G^{\alpha,0}_1 - G^{\alpha,2}_1) e^{\alpha,1} + (G^{\alpha,0}_2 - G^{\alpha,2}_2) e^{\alpha,2} + G^{\gamma,2} e^{\gamma}_1$$

$$Q = (G^{\alpha,0}_1 + 2G^{\alpha,2}_1) e^{\alpha,1} + (G^{\alpha,0}_2 + 2G^{\alpha,2}_2) e^{\alpha,2}$$

In this investigation, $G^{\varepsilon,2}$ was assumed to be zero, so it does not appear in the Hamiltonian. Terms in $G^{\gamma,2}$ were included in the calculations, but not in the analysis of the experimental data. The eigenvalues and eigenvectors of the zero-order Hamiltonian are assumed to be known, and:

$$\mathcal{H}_0 |m> = E^0_m |m> \qquad \text{III-69}$$

Now let $X_i$ (i=1,7) denote any one of the coefficients: A, B, C, D, E, P, or Q. The internal energy is:

$$U = \frac{\sum_{m=-\ell}^{\ell} E_m e^{-\beta E_m}}{\sum_{m=-\ell}^{\ell} e^{-\beta E_m}} \qquad \text{III-70}$$

where $\beta=1/kT$, and the classical elastic energy is not included. The energies that appear in equation III-70 include both the first and second-order perturbation theory corrections due to the magnetoelastic interaction. It is necessary to find the magnetoelastic contribution to the elastic constant ($\Delta C_{ijkl}$) in a form that will allow the magnetoelastic constants to be determined from the experimental measurements of the elastic constants as functions of the magnetization. The magnetoelastic contribution can be written:

$$\Delta C_{ijkl}(\sigma) = C_{ijkl}(\sigma) - C_{ijkl}(\sigma=0) \qquad \text{III-71}$$

$$= \left[ \frac{\partial^2 U}{\partial \varepsilon_{ij} \partial \varepsilon_{kl}}(\sigma) - \frac{\partial^2 U}{\partial \varepsilon_{ij} \partial \varepsilon_{kl}}(\sigma=0) \right] \Bigg|_{\varepsilon_{\mu\nu}=0}$$

Since derivatives are taken with respect to the small dynamic strains, the derivatives are evaluated with the strain equal to zero. It is assumed in the remainder of this section that all derivatives are taken with respect to the small dynamic strains, and that all derivatives are evaluated with the strains equal to zero ( which implies that all the $X_i$ are also equal to zero). Since:

$$\frac{\partial}{\partial \varepsilon_{ij}} = \sum_l \frac{\partial X_l}{\partial \varepsilon_{ij}} \frac{\partial}{\partial X_l} \qquad \text{III-72}$$

the derivatives of the internal energy can be expressed in terms of derivatives with respect to the coefficients $X_i$:

$$\frac{\partial^2 U}{\partial \varepsilon_{ij} \partial \varepsilon_{kl}} = \sum_{m,n} \frac{\partial X_m}{\partial \varepsilon_{ij}} \frac{\partial X_n}{\partial \varepsilon_{kl}} \frac{\partial^2 U}{\partial X_m \partial X_n} \qquad \text{III-73}$$

Inspection of equations III-68 shows that the coefficients that multiply the second derivatives are bilinear functions of the magnetoelastic constants, so by numerically calculating the second derivatives of the internal energy with respect to the coefficients $X_i$, the magnetoelastic constants can be determined by fitting experimental measurements of $\Delta C_{ijkl}$ to the calculated derivatives that enter the expression for $\Delta C_{ijkl}$.

Now consider equation III-70, where

$$E_m = E_m^0 + E_m^1 + E_m^2 \qquad \text{III-74}$$

and;

$$E_m^1 = \langle m | \mathcal{H}_{me}^{rf} | m \rangle \qquad \text{III-75}$$

$$E_m^2 = \sum_{n \neq m} \frac{\langle m | \mathcal{H}_{me}^{rf} | n \rangle \langle n | \mathcal{H}_{me}^{rf} | m \rangle}{E_m^0 - E_n^0}$$

The second derivative of the internal energy with respect to the $X_i$'s is:

$$\frac{\partial^2 U}{\partial X_i \partial X_j} = \frac{1}{Z} \sum_m \frac{\partial^2 E_m}{\partial X_i \partial X_j} e^{-\beta E_m} - \frac{2\beta}{Z} \sum_m \frac{\partial E_m}{\partial X_i} \frac{\partial E_m}{\partial X_j} e^{-\beta E_m}$$

$$+ \frac{2\beta}{Z^2} \sum_m \frac{\partial E_m}{\partial X_i} e^{-\beta E_m} \sum_m \frac{\partial E_m}{\partial X_j} e^{-\beta E_m}$$

$$- \frac{\beta}{Z} \sum_m E_m \frac{\partial^2 E_m}{\partial X_i \partial X_j} e^{-\beta E_m}$$

$$+ \frac{\beta^2}{Z} \sum_m E_m \frac{\partial E_m}{\partial X_i} \frac{\partial E_m}{\partial X_j} e^{-\beta E_m}$$

$$- \frac{\beta^2}{Z^2} \sum_m E_m \frac{\partial E_m}{\partial X_j} e^{-\beta E_m} \sum_m \frac{\partial E_m}{\partial X_j} e^{-\beta E_m}$$

$$- \frac{\beta^2}{Z^2} \sum_m E_m \frac{\partial E_m}{\partial X_j} e^{-\beta E_m} \sum_m \frac{\partial E_m}{\partial X_i} e^{-\beta E_m}$$

$$+ \frac{\beta^2}{Z^2} \sum_m E_m e^{-\beta E_m} \sum_m \frac{\partial^2 E_m}{\partial X_i \partial X_j} e^{-\beta E_m}$$

$$- \frac{\beta^2}{Z^2} \sum_m E_m e^{-\beta E_m} \sum_m \frac{\partial E_m}{\partial X_i} \frac{\partial E_m}{\partial X_j} e^{-\beta E_m}$$

$$+ \frac{2\beta^2}{Z^3} \sum_m E_m e^{-\beta E_m} \sum_m \frac{\partial E_m}{\partial X_i} e^{-\beta E_m} \sum_m \frac{\partial E_m}{\partial X_j} e^{-\beta E_m}$$

where the derivatives must still be evaluated with $\epsilon_{kl}=0$ $(k,l=1,3)$. Now the perturbing Hamiltonian is:

$$\mathcal{H}_{me}^{rf}(i) = AQ_2^0(\vec{J}_i) + BQ_{22}^{+}(\vec{J}_i) + CQ_{22}^{-}(\vec{J}_i) + DQ_{21}^{+}(\vec{J}_i)$$

$$+ EQ_{21}^{-}(\vec{J}_i) + J\sigma_x PJ_x + J\sigma_z QJ_z \qquad \text{III-77}$$

so if $Q_i$ is defined as the angular momentum operator or tensor operator that is multiplied by $X_i$, then:

$$\mathcal{H}_{me}^{rf} = \sum_j X_j Q_j \qquad \text{III-78}$$

so:

$$\partial E_m / \partial X_i = \partial E_m^1 / \partial X_i = \langle m | Q_i | m \rangle \qquad \text{III-79}$$

and:

$$\partial^2 E_m / \partial X_i \partial X_j = \partial^2 E_m^2 / \partial X_i \partial X_j \qquad \text{III-80}$$

$$= 2 \sum_{n \neq m} \frac{\langle m | Q_i | n \rangle \langle n | Q_j | m \rangle}{E_m^0 - E_n^0}$$

where the derivatives are evaluated with $e_{ij} = X_k = 0$.

There are ten types of summations that appear in equation III-76, and to avoid confusion later, they will be labeled in the way in which they were labeled in the computer program:

$$Z = \sum_m e^{-\beta E_m^0}$$

$$U_o = \frac{1}{Z} \sum_m E_m^0 e^{-\beta E_m^0}$$

$$c_{1i} = \frac{1}{Z} \sum_m \frac{\partial E_m^1}{\partial X_i} e^{-\beta E_m^0}$$

$$c_{2i} = \frac{1}{Z} \sum_m \left[ \frac{\partial E_m^1}{\partial X_i} \right]^2 e^{-\beta E_m^0}$$

$$c_{3i} = \frac{1}{Z} \sum_m E_m^0 \frac{\partial E_m^1}{\partial X_i} e^{-\beta E_m^0}$$

$$c_{4i} = \frac{1}{Z} \sum_m E_m^0 \left[ \frac{\partial E_m^1}{\partial X_i} \right]^2 e^{-\beta E_m^0}$$

$$d_{1ij} = \frac{1}{Z} \sum_m \frac{\partial^2 E_m^2}{\partial X_i \partial X_j} e^{-\beta E_m^0} \qquad \text{III-81}$$

$$d_{2ij} = \frac{1}{Z} \sum_m E_m^0 \frac{\partial^2 E_m^2}{\partial X_i \partial X_j} e^{-\beta E_m^0}$$

$$e_{1ij} = \frac{1}{Z} \sum_m \frac{\partial E_m^1}{\partial X_i} \frac{\partial E_m^1}{\partial X_j} e^{-\beta E_m^0}$$

$$e_{2ij} = \frac{1}{Z} \sum_m E_m^0 \frac{\partial E_m^1}{\partial X_i} \frac{\partial E_m^1}{\partial X_j} e^{-\beta E_m^0}$$

In terms of these definitions, the derivatives are written:

$$\frac{\partial^2 U}{\partial X_i \partial X_j} = 2c_{1i}c_{1j}\beta(1+\beta U_0) - \beta^2(c_{1i}c_{3j} + c_{1j}c_{3i}) + d_{1ij}(1+\beta U_0) - \beta d_{2ij} - \beta e_{1ij}(2+\beta U_0) + \beta^2 e_{2ij}$$

and:

$$\frac{\partial^2 U}{\partial X_i^2} = 2c_{1i}^2\beta(1+\beta U_0) - 2\beta^2 c_{1i}c_{3j} + d_{1ij}(1+\beta U_0)$$

$$- \beta d_{2ij} - \beta c_{2i}(2+\beta U_0) + \beta^2 c_{4i} \qquad \text{III-83}$$

The second derivatives of the internal energy with respect to the $X_i$'s have now been defined in terms of the matrix elements of the seven angular momentum tensor operators, $Q_i$, that appear in the perturbing Hamiltonian. The matrix elements are calculated in the representation in which the zero-order Hamiltonian is diagonal. The derivatives are, of course, calculated numerically. The details of the numerical calculations will be presented in the chapter on the numerical computation.

It is necessary to relate the calculated derivatives of the internal energy to the experimentally measured magnetoelastic contributions to the elastic constants. Equations III-73 and III-71 define this relationship, but the derivatives of the $X_i$'s with respect to the strains have still not been evaluated explicitly. Using equation III-73, the dependence of $C_{11}$ on the derivatives of the internal energy is:

$$\Delta C_{11}^{a,b}(\sigma) = (B_1^{\alpha,2} - B_2^{\alpha,2})^2 D_{aa} \pm 2B^{\gamma,2}(B_1^{\alpha,2} - B_2^{\alpha,2}) D_{ab}$$

$$- 2(B_1^{\alpha,2} - B_2^{\alpha,2})[(G_1^{\alpha,0} - G_1^{\alpha,2}) - (G_2^{\alpha,0} - G_2^{\alpha,2}) \pm G^{\gamma,2}]D_{ap}$$

$$+ (B^{\gamma,2})^2 D_{bb} \mp 2B^{\gamma,2}[(G_1^{\alpha,0}-G_1^{\alpha,2})-(G_2^{\alpha,0}-G_2^{\alpha,2})\pm G^{\gamma,2}] D_{bp}$$

$$+ [(G_1^{\alpha,0}-G_1^{\alpha,2})-(G_2^{\alpha,0}-G_2^{\alpha,2}) \pm G^{\gamma,2}]^2 D_{pp} \qquad \text{III-84}$$

$$\Delta C_{11}^{c}(\sigma) = (B_1^{\alpha,2}-B_2^{\alpha,2})^2 D_{aa} + 2B^{\gamma,2}(B_1^{\alpha,2}-B_2^{\alpha,2}) D_{ab}$$

$$- 2(B_1^{\alpha,2}-B_2^{\alpha,2})[(G_1^{\alpha,0}+2G_1^{\alpha,2}) - (G_2^{\alpha,0}+2G_2^{\alpha,2})] D_{aq}$$

$$+ (B^{\gamma,2})^2 D_{bb} - 2B^{\gamma,2}[(G_1^{\alpha,0}+2G_1^{\alpha,2}) - (G_2^{\alpha,0}+2G_2^{\alpha,2})]D_{bq}$$

$$+ [(G_1^{\alpha,0}+2G_1^{\alpha,2}) - (G_2^{\alpha,0}+2G_2^{\alpha,2})]^2 D_{qq}$$

where the upper sign is for fields along the a-axis and the lower sign is for fields along the b-axis, and:

$$D_{xy} = \frac{\partial^2 U}{\partial X \partial Y}(\sigma) - \frac{\partial^2 U}{\partial X \partial Y}(\sigma = 0)$$

The equations for $C_{22}$ are obtained from equation III-84 by replacing $B^{\gamma,2}$ with $-B^{\gamma,2}$, and $G^{\gamma,2}$ with $-G^{\gamma,2}$.

The results for $C_{33}$ are somewhat different since only three derivatives enter each equation:

$$\Delta C_{33}^{a}(\sigma) = \Delta C_{33}^{b} = (B_1^{\alpha,2}+2B_2^{\alpha,2}) D_{aa}$$

$$- 2(B_1^{\alpha,2}+2B_2^{\alpha,2})[(G_1^{\alpha,0}-G_1^{\alpha,2})+2(G_2^{\alpha,0}-G_2^{\alpha,2})] D_{ap}$$

$$+ [(G_1^{\alpha,0}-G_1^{\alpha,2})+2(G_2^{\alpha,0}-G_2^{\alpha,2})]^2 D_{pp}$$

$$C_{33}^{c}(\sigma) = (B_1^{\alpha,2}+2B_2^{\alpha,2})^2 D_{aa} \qquad \text{III-85}$$
$$- 2(B_1^{\alpha,2}+2B_2^{\alpha,2})[(G_1^{\alpha,0}+2G_1^{\alpha,2})+2(G_2^{\alpha,0}+2G_2^{\alpha,2})]D_{aq}$$
$$+ [(G_1^{\alpha,0}+2G_1^{\alpha,2})+2(G_2^{\alpha,0}+2G_2^{\alpha,2})]^2 D_{qq}$$

In ordinary elasticity theory, there are several ways of measuring the shear elastic constants, for example:

$$C_{44} = C_{1313} = C_{3131} = C_{55} = C_{2323} = C_{3232} \qquad \text{III-86}$$

However, using the definition of the elastic constants given in equation III-48c, and including the rotational terms, the elastic constants in III-86 are not necessarily equal. In fact, the magnetoelastic contributions to the four elastic constants derived from $C_{44}$ are:

$$\Delta C_{1313}(\sigma) = (B^{\varepsilon,2} - \sqrt{3/2}\, P_2^0)^2 D_{dd}$$
$$\Delta C_{3131}(\sigma) = (B^{\varepsilon,2} + \sqrt{3/2}\, P_2^0)^2 D_{dd} \qquad \text{III-87}$$
$$\Delta C_{2323}(\sigma) = (B^{\varepsilon,2} - \sqrt{3/2}\, P_2^0)^2 D_{ee}$$
$$\Delta C_{3232}(\sigma) = (B^{\varepsilon,2} + \sqrt{3/2}\, P_2^0)^2 D_{ee}$$

Since to second-order in the angular momentum operators, there are no rotational terms that contribute to $C_{66}$, its calculation is easy, and:

$$\Delta C_{66}(\sigma) = (B^{\gamma,2})^2 D_{cc} \qquad \text{III-88}$$

# IV. Numerical Calculations

This chapter describes the FORTRAN programs and subroutines that were developed, primarily by Dr. P. L. Donoho, to do the calculations of the thermodynamic quantities that were described in the last section of the preceding chapter. The programs were used on the DEC-10 computer at UNICAMP, so the programs, copies of which are in Appendix D, are written in the version of FORTRAN that is implemented on the DEC-10. Minor modifications would be necessary before the programs could be used on other machines.

Since many approximations were made and many conventions were adopted in the writing of the program, it is important that they be brought together in one place.

1. The isotropic and anisotropic exchange interaction and the two-ion magnetoelastic interaction are treated in the molecular field approximation.

2. The HAF phase is not included in the calculation, so in the temperature range over which Dy is normally antiferromagnetic, the calculations can only be compared to experimental data obtained at fields high enough to suppress the helical antiferromagnetism. In the model, the Curie temperature is:

$$T_c = \theta_\perp = 170K \qquad \text{IV-1}$$

3. The contribution of the dynamic magnetoelastic interaction to the energy levels is calculated in second-order perturbation theory.

4. $C_{12}^{\alpha}$ is set equal to zero. Zero is within the experimental error, and $C_{12}^{\alpha}=0$ simplifies the equations for the static magnetostriction.

5. The magnetization can only have a component along either the a-axis or the b-axis, but not along both.

6. The magnetization and the static magnetostriction are calculated self-consistently.

7. Since the tensor operators for m=0 were defined in the programs without the irrational factor that appears in their definition, some of the constants that appear in the theoretical expressions are different from those that appear in the program. See Appendix C for the difference. Whenever one of the constants appears in an equation or in an expression , it is consistent with the standard definition of the tensor operators unless otherwise specified.

8. All energies are expressed in °K, all energy densities are in °K/ion, and all magnetic fields are in kOe in the programs.

9. $G^{\varepsilon,2} = 0$

10. The magnetoelastic constants that appear in the zero-order Hamiltonian are not necessarily equal to those that appear in the perturbing Hamiltonian.

The program actually consists of a main program, MAIN02, that determines the flow of the calculations, and many subroutines in which most of the calculations themselves are done. A flow chart is shown in Figure IV-1.

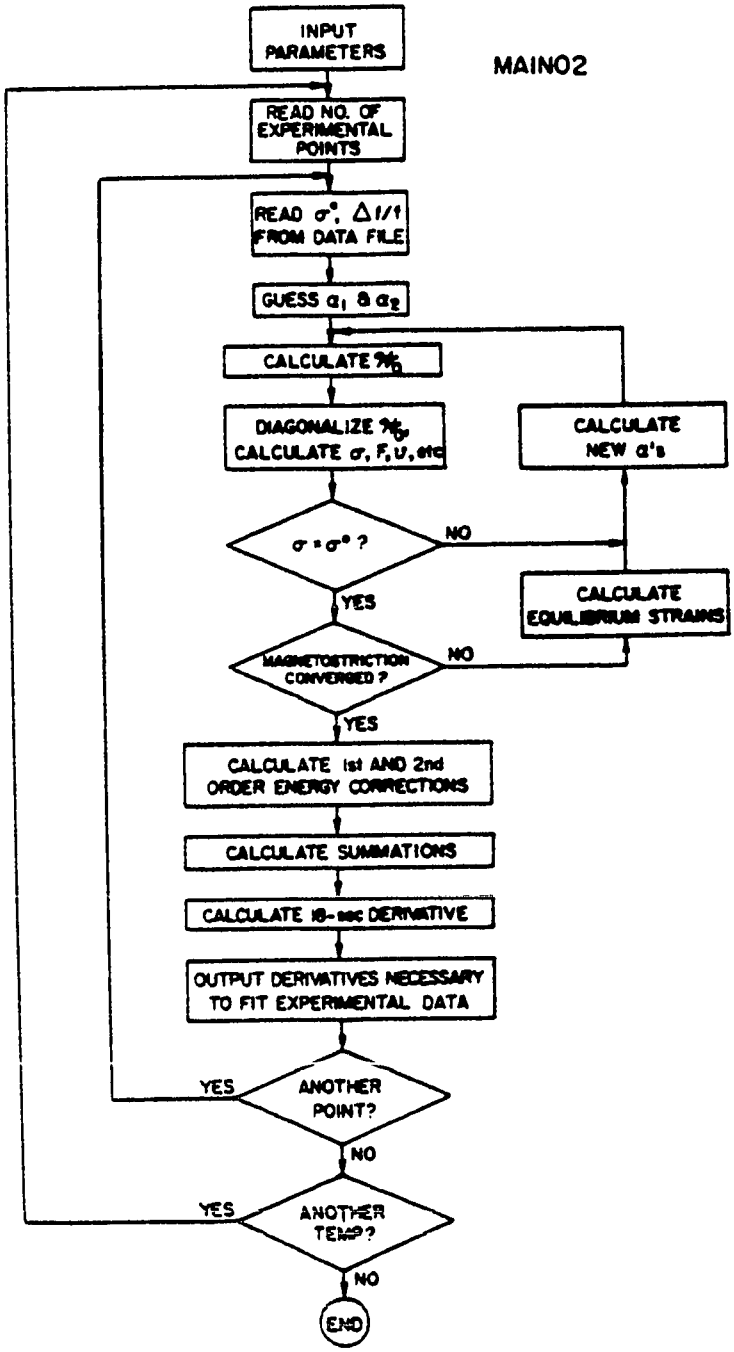


Figure IV-1 Flow chart of the calculation of the second derivatives of the internal energy that are necessary to fit the observed dependence of the elastic constants on the magnetization.

Slightly different notation was used in the program than was used in the theoretical calculations, so the Hamiltonian, as it was used in the numerical calculations, is developed. It is convenient in the numerical calculations to group all the terms which multiply a given angular momentum or irreducible tensor operator.

Since $\sigma_y = 0$, and $G^{\varepsilon,2} = 0$, $J_y$ does not appear in the Hamiltonian. The coefficients of $J_x$ and $J_z$ include contributions from the isotropic and anisotropic exchange, the Zeeman interaction, and the two-ion magnetoelastic interaction. The sum of these terms is:

$$\mathcal{H}_{ex}^{is} + \mathcal{H}_{ex}^{an} + \mathcal{H}_z + \mathcal{H}_{me}^{II} = \alpha_x J_x + \alpha_z J_z \qquad \text{IV-2}$$

where:

$$\alpha_x = Q\,H_x + \sigma_x \Gamma_x$$

$$\alpha_z = Q\,H_z + \sigma_z \Gamma_z \qquad \text{IV-3}$$

$$\Gamma_x = \frac{g\mu_B}{k}(\Gamma - \Gamma_1) + J(G_1^{\alpha,-}\,\bar{e}^{\alpha,1} + G_2^{\alpha,-}\,\bar{e}^{\alpha,2} + G^{\gamma,2}\,\bar{e}_1^{\gamma})$$

$$\Gamma_z = \frac{g\mu_B}{k}(\Gamma + 2\Gamma_1) + J(G_1^{\alpha,+}\,\bar{e}^{\alpha,1} + G_2^{\alpha,+}\,\bar{e}^{\alpha,2})$$

and:

$$Q = 1000(g\mu_B/k) \qquad \text{IV-4}$$

$$G_1^{\alpha,-} = G_1^{\alpha,0} - G_1^{\alpha,2} \qquad G_1^{\alpha,+} = G_1^{\alpha,0} + 2G_1^{\alpha,2}$$

$$G_2^{\alpha,-} = G_2^{\alpha,0} - G_2^{\alpha,2} \qquad G_2^{\alpha,+} = G_2^{\alpha,0} + 2G_2^{\alpha,2}$$

The entire zero-order Hamiltonian is:

$$\mathcal{H}_0(i) = \alpha_x J_x + \alpha_z J_z + P_2^+ Q_2^0(\vec{J}_i) + P_4^0 Q_4^0(\vec{J}_i) + P_6^0 Q(\vec{J}_i) + P_{66} Q_{66}^+(\vec{J}_i) \qquad \text{IV-5}$$

where:

$$P_2^+ = P_2^0 - B_1^{\alpha,2}\,\bar{e}^{\alpha,1} - B_2^{\alpha,2}\,\bar{e}^{\alpha,2} \qquad \text{IV-6}$$

The form of the perturbing Hamiltonian is not changed from equation III-67:

$$\mathcal{H}_{me}^{rf}(i) = AQ_2^0(\vec{J}_i) + BQ_{22}^+(\vec{J}_i) + CQ_{22}^-(\vec{J}_i) + DQ_{21}^+(\vec{J}_i) + EQ_{21}^-(\vec{J}_i) + J\sigma_x P J_x + J\sigma_z Q J_z \qquad \text{IV-7}$$

It is important to realize that there are two sets of magnetoelastic constants that appear in the Hamiltonian: the ones in the zero-order Hamiltonian that characterize the static magnetostriction and the ones in the perturbing Hamiltonian that are determined from the ultrasonic data. Ideally, the two sets should be the same, but in practice, they were not. There is a good reason for the difference, however. The magnetoelastic constants that were used in the zero-order Hamiltonian were chosen to give the best fit to the published data on the static magnetostriction, but it was found that there were several sets of magnetoelastic constants that gave approximately the same fit to the

magnetostriction. The magnetoelastic constants in the perturbing Hamiltonian are initially unknown, and are determined from the ultrasonic data. Optimally, an interative procedure would be used in which the magnetoelastic constants determined from the fit to the ultrasonic data would be substituted into the zero-order Hamiltonian, the calculation of the second derivatives of the internal energy would be repeated, and a new set of magnetoelastic constants would be calculated with the new second derivatives. The procedure would continue until the magnetoelastic constants that were calculated from the fit to the ultrasonic data were negligibly different from those that were used in the zero-order Hamiltonian. Each step in this procedure would require that all the second derivatives of the internal energy with respect to the coefficients, $X_i$, be recalculated and would invlove the use of a considerable amount of computer time.

A. Preliminary Data Analysis

Before the main program was used to calculate the derivatives needed to fit the ultrasonic data, the raw experimental data had to be put into a form that could be utilized by the main program. A flow chart of the programs, including those that operate on the raw data, is shown in Figure IV-2.

The raw data that resulted from the magnetization measurements were, for each orientation and temperature in

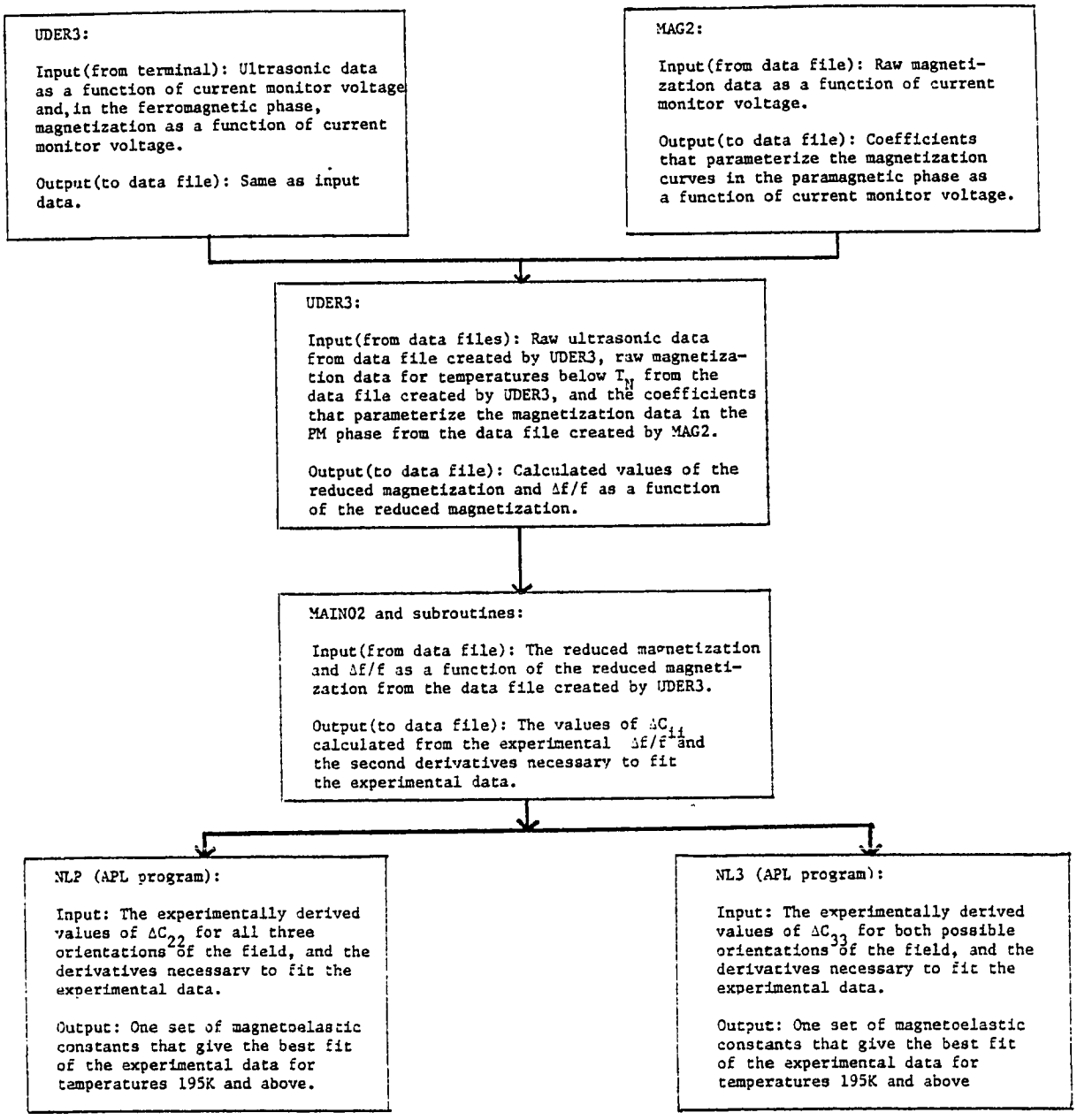


Figure IV-2 Flow chart of the FORTRAN and APL programs that were used in the fitting of the elastic constant data.

the paramagnetic phase, a list of the current monitor voltages and the magnetization measured at each voltage. A data file was created for each orientation and the raw data was entered into the file. The program MAG2 read this file and for fields in the basal plane, the magnetization was fit to the equation:

$$\sigma = A(T)v + B(T)v^2 + C(T)v^3 + D(T)v^4 \qquad \text{IV-8}$$

where $\sigma$ was calculated from the measured value of the magnetization and v is the current monitor voltage that appears in $\mathcal{H}_{me}^{rf}$. The magnetization with the field along the c-axis was fit to the equation:

$$\sigma = A(T)v \qquad \text{IV-9}$$

since it was assumed that the small amount of curvature that was observed in the plot of the magnetization versus current was due to sample misalignment. The temperature and the calculated coefficients were stored by MAG2 in another data file.

The raw data from the ultrasonic measurements were, for each temperature and orientation, a list of current monitor voltages and the frequency of best overlap at each voltage. Using the program UDER3, this data was entered into a data file, and after the errors had been corrected, the same program created another data file that had, for each temperature and orientation, a list of the quantities:

$$\sigma \text{ and } \Delta f(\sigma)/f = (f(\sigma)-f(\sigma=0))/f(\sigma=0) \qquad \text{IV-10}$$

where $\sigma$ was calculated from the current monitor voltage using either equation IV-8 or IV-9. The reduced magnetization at temperatures in the paramagnetic phase was calculated from the coefficients that were read from the data file that had been previously created by MAG2. For temperatures in the ferromagnetic phase, the reduced magnetization was calculated from the magnetization data that had been entered with the ultrasonic data using the program UDER3. This file was accessed by MAIN02 and the values of the reduced magnetization were the values at which the second derivatives of the internal energy were calculated.

## B. Determination of the Parameters That Enter the Zero-Order Hamiltonian

The magnetoelastic constants that appear in the zero-order Hamiltonian were calculated from the experimentally measured magnetostriction by assuming that the static strain is a linear function of the magnetoelastic constants. A given Cartesian strain would, in general, be a function of all eight magnetoelastic constants, but the symmetry strains are only functions of the magnetoelastic constants that are labeled with the same irreducible representation as the strain itself. If the strains are linear functions of the magnetoelastic constants, then, for example, the strains $\bar{e}_1^{\gamma}$ ans $\bar{e}^{\alpha,1}$ can be expressed in the following way:

$$\bar{e}_1^{\gamma} = \frac{\partial \bar{e}_1^{\gamma}}{\partial B^{\gamma,2}} B^{\gamma,2} + \frac{\partial \bar{e}_1^{\gamma}}{\partial G^{\gamma,2}} G^{\gamma,2} \qquad \text{IV-11}$$

and:

$$\bar{e}^{\alpha,1} = \frac{\partial \bar{e}^{\alpha,1}}{\partial B_1^{\alpha,2}} B_1^{\alpha,2} + \frac{\partial \bar{e}^{\alpha,1}}{\partial G_1^{\alpha,0}} G_1^{\alpha,0} + \frac{\partial \bar{e}^{\alpha,1}}{\partial G_1^{\alpha,2}} G_1^{\alpha,2}$$

The partial derivatives of the strains with respect to the magnetoelastic constants were calculated numerically by a slightly modified version of the main program.

The isothermal magnetostriction data that were used were taken from the data of Clark et al[11] for temperatures in the paramagnetic phase. Isofield data[1] (with a field of 30kOe along the a-axis) for the three strains $e_1$, $e_2$, and $e_3$ were also used. Since the equations that determine the magnetoelastic constants were overdetermined, a linear least squares program was used to calculate the coefficients that gave the best fit to the experimental data. The constants obtained from the least squares fit are:

$$B_1^{\alpha,2} = -15°K/ion \qquad B_2^{\alpha,2} = -8.17°K/ion \qquad \text{IV-12}$$

$$B^{\gamma,2} = 30.2°K/ion \qquad G^{\gamma,2} = -14.5°k/ion$$

$$G_1^{\alpha,0} = -1.02°K/ion \qquad G_2^{\alpha,0} = 10.6°K/ion$$

$$G_1^{\alpha,2} = 6.24°K/ion \qquad G_2^{\alpha,2} = 6.24°K/ion$$

The experimental data and the best fit are shown in Figures IV-3, 4, 5, and 6. Note that in Figure IV-6, the calculated strains do not include the thermal contraction. The calculated curves at a temperature T should be shifted in a negative direction by the amount of the thermal contraction from 300K to T. This correction would improve the fit of the c-axis strain relatively more because the c-axis thermal contraction is larger.

$B^{\varepsilon,2}$ did not appear in the calculation because it only enters when the magnetization has components along the c-axis and in the basal plane, simultaneously, and this situation was never experimentally realized in the ultrasonic measurements.

The assumption that the strains are linear in the magnetoelastic constants is, of course, only an approximation, so errors arose from the fact that higher order terms were neglected. Also, the partial derivatives in the Taylor series expansion were evaluated with all the magnetoelastic constants equal to zero except for the one with respect to which the derivative was being taken, so higher order cross terms that were neglected gave rise to errors. A solution could have been obtained even with the nonlinear dependence of the strains on the magnetoelastic constants by using an iterative procedure such as the Newton-Raphson method. The improvement in the solution would have been at the expense of a considerable amount of computer time, so only the

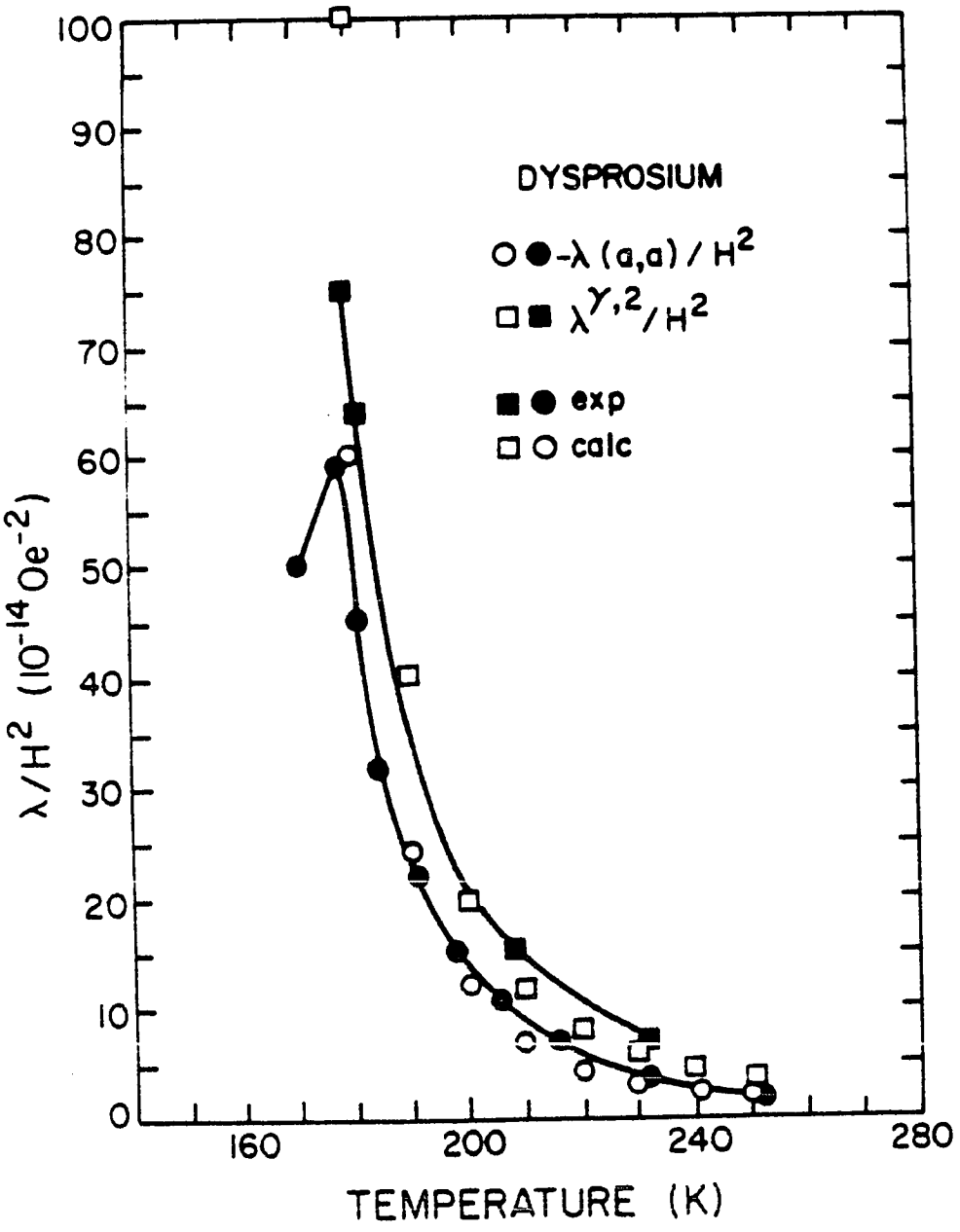


Figure IV-3 Comparison of the measured magnetostriction with the magnetostriction calculated numerically. The computer program was a modified version of MAIN02, and the magnetoelastic constants were those in equation IV-12. Experimental points after Ref. 11.

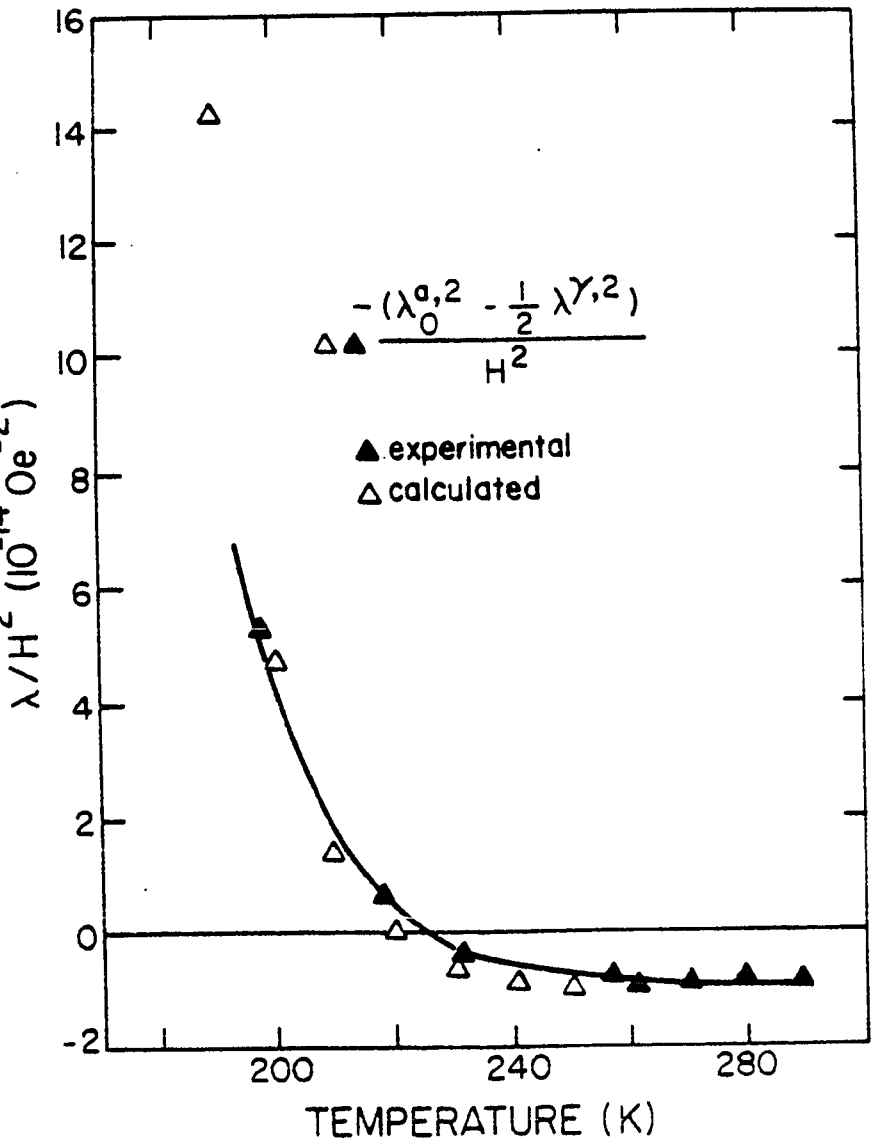


Figure IV-4 Comparison of the measured magnetostriction with the magnetostriction calculated numerically. The computer program was a modified version of MAIN02, and the magnetoelastic constants were those in equation IV-12. Experimental points after Ref. 11.

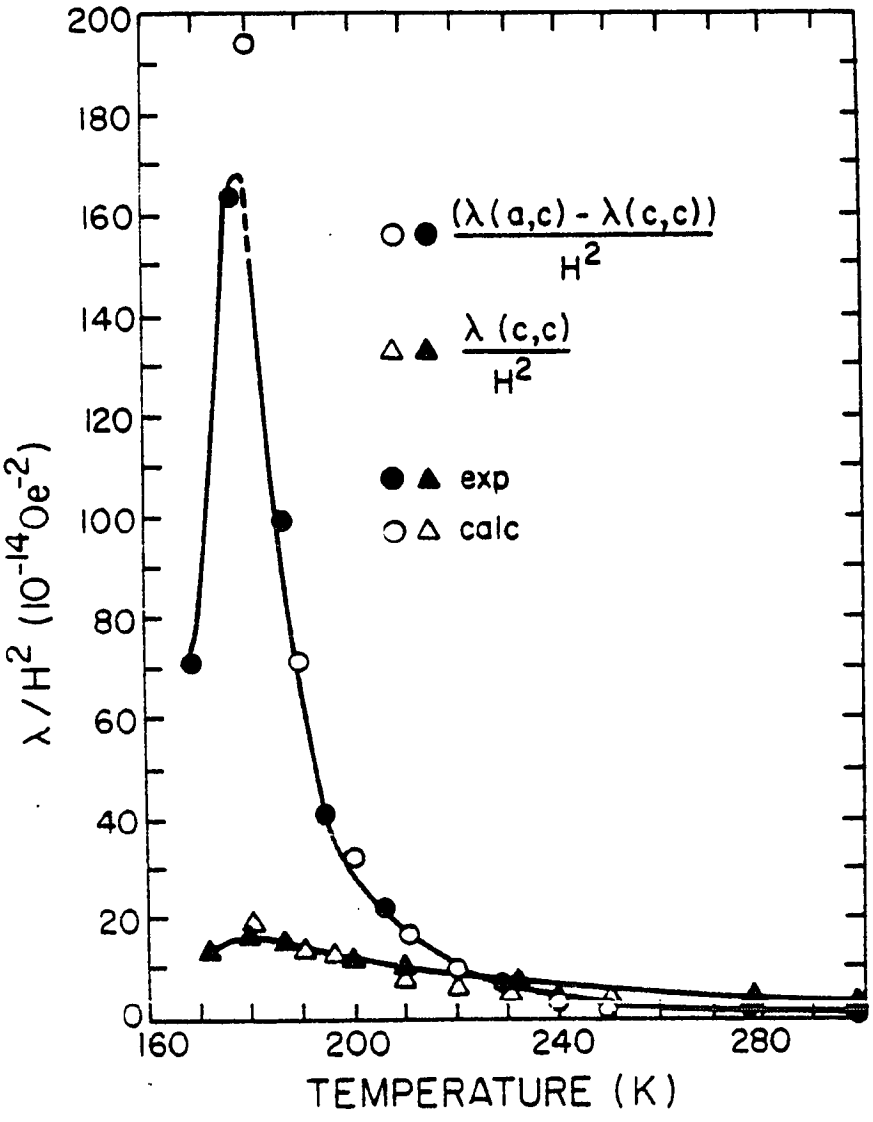


Figure IV-5 Comparison of the measured magnetostriction with the magnetostriction calculated numerically. The computer program was a modified version of MAIN02, and the magnetoelastic constants were those in equation IV-12. Experimental points after Ref. 11.

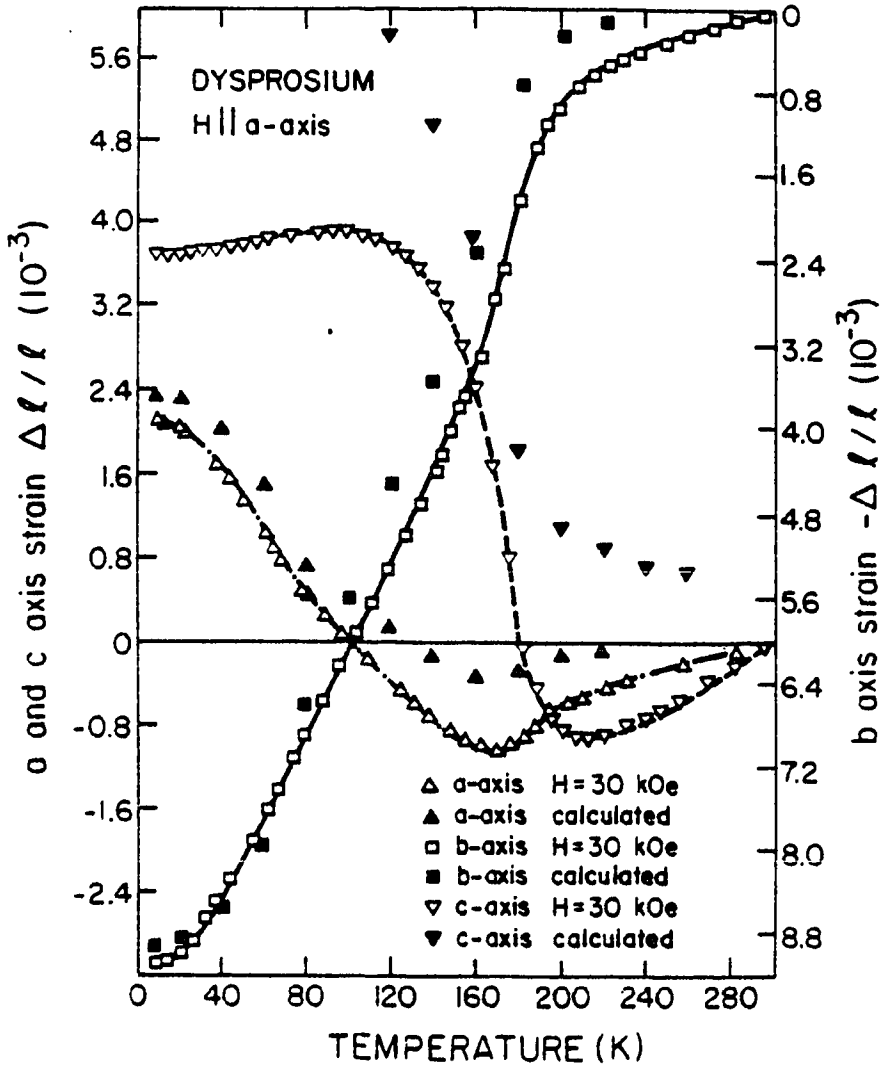


Figure IV-6 Comparison of the measured isofield magnetostriction with the magnetostriction calculated numerically. The computer program was a modified version of MAIN02 and the magnetoelastic constants that were used are given in equation IV-12. Experimental data after Ref. 1.

simple method was used to find the magnetoelastic constants that were used in the zero-order Hamiltonian for the calculations of the second derivatives of the internal energy.

A good approximation for the value of the isotropic molecular field constant, $\Gamma$, is its value for an isotropic ferromagnet without magnetostriction. The Curie temperature is proportional to the molecular field constant, $\gamma$:

$$T_C = \theta_\perp = 169K = \gamma C \qquad \text{IV-13}$$

where C is the Curie constant (equation III-30) and $\gamma = (g\mu_B/k)M_0\Gamma$. Small adjustments were, of course, necessary because of the presence of the anisotropy and magnetostriction. The value of the isotropic molecular field constant that was used in the calculations is: $\Gamma = 54.4°K/ion$. The paramagnetic magnetization data is shown in Figure IV-7. The fit is fairly good except for the fact that the slope of the reciprocal of the susceptibility, $1/\chi$, versus temperature is slightly too small. This slope is not readily adjustable, since it is the inverse of the Curie constant, C, which depends only on J and g.

The anisotropy constants were the most difficult to determine. The four crystal field constants, as well as the one anisotropic exchange constant, had to be chosen. The experimental data that were used to choose the constants were: the difference in the paramagnetic Curie temperatures,

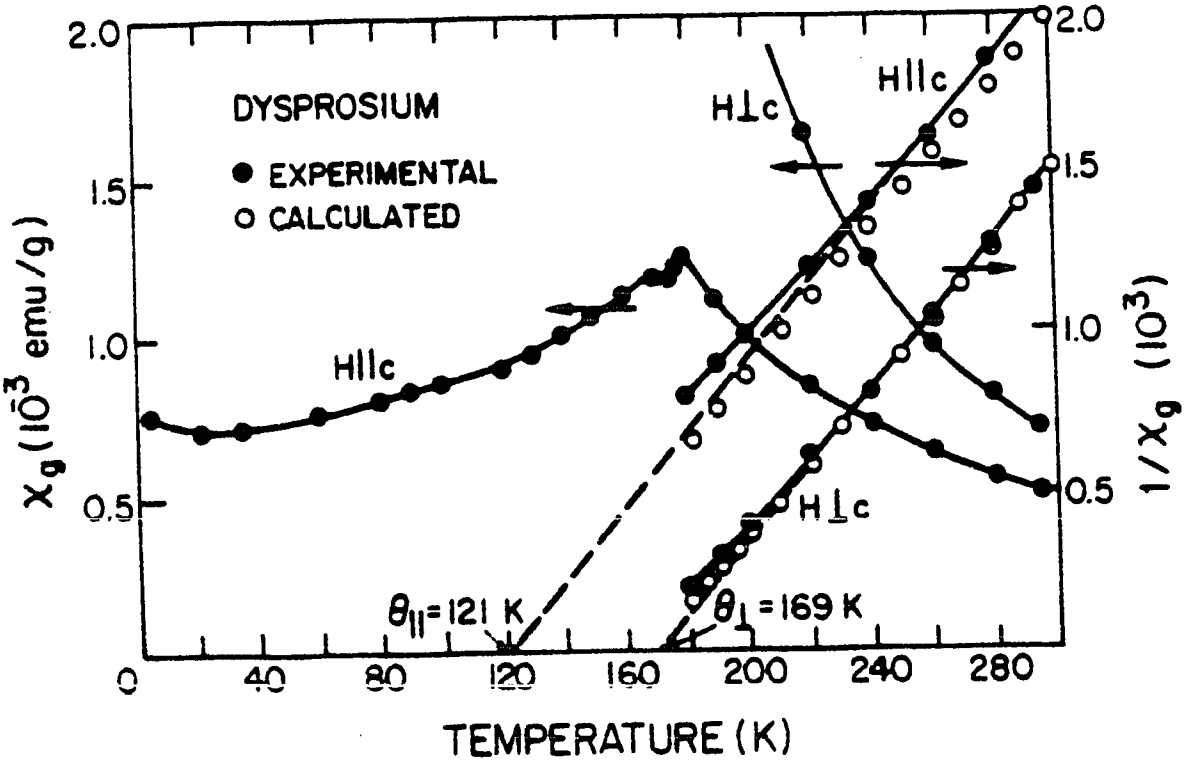


Figure IV-7 Comparison of the experimentally measured susceptibilities (after Ref. 7) with the susceptibilities calculated numerically.

$\theta_\perp - \theta_{||}$, taken from the magnetization data of Behrendt et al[7], and the low temperature magnetization data of Rhyne et al[8] that was taken at 4.2K with the field parallel to the c-axis. The low temperature magnetization[8], is almost a linear function of the field up to 60-70kOe, where there is a phase transition which makes the c-axis an easy axis. The phase transition occurred in the theoretical model too, but at higher fields, between 160 and 200kOe. The slope of the magnetization versus field along the c-axis depends primarily on the second-order anisotropy, as does the difference in the paramagnetic Curie temperatures. The anisotropic exchange constant, $\Gamma_1$, and $P_2^0$ were adjusted to give the best fit for both the low temperature data and the paramagnetic data. The higher order anisotropy constants, which are primarily responsible for the curvature of the plot of the c-axis magnetization versus field ( at low temperatures), were set to values small enough to introduce only a small amount of curvature (consistent with experiment) into the numerically calculated magnetization curve. The anisotropy constants that were used in the calculations are:

$$\Gamma_1 = -2.62°K/ion \quad P_2^0 = .39°K/ion \quad P_4^0 = -4.9\times10^{-3}°K/ion$$

$$P_6^0 = 4.72\times10^{-6}°K/ion \qquad P_{66} = -9.77\times10^{-9}°K/ion$$

The fitting of the low temperature c-axis

magnetization data and the data from the paramagnetic phase was made somewhat easier by the fact that the second-order anisotropy and the anisotropic exchange (in the molecular field approximation) have different temperature dependences. The second-order anisotropy depends on $< Q_2^0 >$ which goes approximately as $\sigma^2$ in the paramagnetic phase ($\sigma<<1$) and which goes as $\sigma^3$ in the ferromagnetic phase ($\sigma\simeq 1$). The anisotropic exchange, in the molecular field approximation, goes as $\sigma^2$ at all temperatures. The low temperature properties were thus dependent on the relative sizes of the crystal field anisotropy and the anisotropic exchange, whereas the paramagnetic properties, at least when the magnetization was not too large, were only dependent on the sum of the two. The susceptibility data from the paramagnetic phase and the calculated fit are shown in Figure IV-7. The calculated low temperature c-axis magnetization followed the experimental data up to about 60kOe, where the two began to differ because the experimental phase transition was at 70kOe, whereas the calculated phase transition occured at about 160kOe.

The explanation of why the, apparently, unecessary[44], anisotropic exchange had little effect on the paramagnetic properties, that were calculated with the computer program, is now easy. Since both the dominant crystal field term and the anisotropic exchange have the same dependence on the magnetization in the paramagnetic phase, only the sum of

the two is important, not their relative contributions. Thus, the thermodynamic properties are not appreciably affected in the paramagnetic phase by the presence of the anisotropic exchange.

C. Self-Consistent Calculation of the Magnetization

The calculation of the magnetization requires a self-consistent procedure because the magnetization is calculated from the formula:

$$\vec{\sigma} = \frac{1}{JZ} \sum_m \langle m | \vec{J} | m \rangle \, e^{-\beta E_m} \qquad \text{IV-14}$$

where the energies, $E_m$, depend on the magnetization because it appears in the zero-order Hamiltonian in the term:

$$(QH_x + \sigma_x \Gamma_x) J_x + (QH_z + \sigma_z \Gamma_z) J_z \qquad \text{IV-15}$$

For an anisotropic ferromagnet without magnetostriction, equation IV-14 becomes:

$$\sigma = B_J \left[ \frac{Jg\mu_B (H+\Gamma\sigma)}{kT} \right] \qquad \text{IV-16}$$

where:

$$B_J(x) = \frac{2J+1}{2J} \coth\left(\frac{2J+1}{2J} x\right) - \frac{1}{2J} \coth\left(\frac{x}{2J}\right) \qquad \text{IV-17}$$

Since the magnetostriction and the anisotropy are included in the zero-order Hamiltonian, a closed form expression for the magnetization can not be found, and a different approach had to be adopted for the numerical calculation of the magnetization.

The three quantities $\vec{\alpha}$, $\vec{H}$, and $\vec{\sigma}$ are related by two equations, so only one of the three is independent. The first relation is just the definition of $\vec{\alpha}$:

$$\alpha_x = QH_x + \Gamma_x\sigma_x \qquad \text{IV-18}$$

$$\alpha_z = QH_z + \Gamma_z\sigma_z$$

and the second relation is equation IV-14. The particular method employed in the calculation of $\vec{\sigma}$ depended on which of the three quantities $\vec{\alpha}$, $\vec{H}$, or $\vec{\sigma}$ was chosen as the independent variable.

The calculation of $\vec{\sigma}$ was simplest when $\vec{\alpha}$ was chosen as the independent variable. The desired value of $\vec{\alpha}$ was subsituted into the zero-order Hamiltonian which was diagonalized numerically. The eigenvalues and eigenvectors were then used to calculate $\vec{\sigma}$ using equation IV-14, and the magnetic field could be calculated from the definition of $\vec{\alpha}$ after $\vec{\sigma}$ had been calculated.

Taking the magnetic field as the independent variable was more complicated, and an iterative procedure was required. First, a value of $\vec{\alpha}$ was assumed, and the magnetization was calculated by the procedure described in the last paragraph. There are actually two magnetic fields that appear in this procedure, the desired value $\vec{H}$, and the actual value $\vec{H}'$, that is calculated from the definition of $\vec{\alpha}$ after the magnetization has been calculated with the

assumed value of $\vec{\alpha}$. The object of the procedure is to find the value of $\vec{\alpha}$ that, when used in the zero-order Hamiltonian to calculate $\vec{\alpha}$, yields the proper magnetic field:

$$H_x = H'_x = \frac{1}{Q}(\alpha_x - \Gamma_x\sigma_x) \qquad \text{IV-19}$$

$$H_z = H'_z = \frac{1}{Q}(\alpha_z - \Gamma_z\sigma_z)$$

A modified Newton-Raphson procedure was used to solve the equivalent equations:

$$F_x(\alpha_x,\alpha_z) = \frac{1}{\Gamma_x}(\alpha_x - QH_x) - \sigma_x = 0 \qquad \text{IV-20}$$

$$F_z(\alpha_x,\alpha_z) = \frac{1}{\Gamma_z}(\alpha_z - QH_z) - \sigma_z = 0$$

where the object is to find the value of $\vec{\alpha}$ that makes $\vec{F} = 0$, and where, as usual, $\sigma_y = 0$. The Newton-Raphson procedure requires an initial guess of the solution to start the iteration. The procedure then takes a Taylor series expansion of the function (keeping only the first derivatives) and finds the values of the arguments that make the linearized function zero. These arguments are used as the initial point for the next iteration. The procedure converges if the initial guess is sufficiently close to the root of the equation. In one-dimension, the Newton-Raphson procedure is summarized by the algorithm:

$$x_{i+1} = x_i - f(x_i)\frac{\partial f}{\partial x}\Big|_{x_i} \qquad \text{IV-21}$$

The generalization to n-variables is easy using the matrix of the Jacobian: $J_{ij} = \frac{\partial F_i}{\partial x_j}$; and the algorithm is:

$$x_j^{i+1} = x_j^i - \sum_{k=1} J_{jk}^{-1} F_k(\vec{x}^i) \qquad \text{IV-22}$$

The derivatives in the matrix of the Jacobian are evaluated numerically. The iteration continues until the following condition is met:

$$|F_x| , \ |F_z| \leq T_1 \qquad \text{IV-23}$$

where $T_1$ is on the order of $10^{-6}$-$10^{-10}$.

The procedure that is followed when the magnetization is chosen as the independent variable is similar to the one just described. When the magnetization is the independent variable, there are two magnetizations that are defined, the desired magnetization, $\vec{\sigma}_0$, and the calculated magnetization $\vec{\sigma}$, and the procedure iterates until a value of $\vec{\alpha}$ is found that, when substituted into the zero-order Hamiltonian makes:

$$|\sigma_x - \sigma_x^0| , \ |\sigma_z - \sigma_z^0| \leq T_1 \qquad \text{IV-24}$$

The equations that must be solved are then:

$$F_x(\alpha_x, \alpha_z) = \sigma_x - \sigma_x^0 = 0 \qquad \text{IV-25}$$

$$F_z(\alpha_x, \alpha_z) = \sigma_z - \sigma_z^0 = 0$$

The Newton-Raphson method proceeds in exactly the same way

as before, the only difference being in the definition of $\vec{F}$.

Generally, purely theoretical calculations were done as functions of the magnetic field, and the calculations of the second derivatives that were necessary to fit the ultrasonic data were done as functions of the magnetization. The programs that were used in the two cases had to be slightly different.

The full two-dimensional calculation of the magnetization was only necessary when there were nonzero components of the magnetization in both the x and z directions. This condition was only met in the low temperature calculations of the anisotropy. The fitting of the experimental ultrasonic data required that only one component of the magnetization be nonzero. With only one component nonzero, the procedure described above becomes the Newton method in one-dimension. The increased complexity of a program that allowed the magnetization to be either along the x-axis or along the z-axis or in the x-z plane was well worthwhile because the calculations were much faster when the magnetization was only along one axis. The three extra diagonalizations of the zero-order Hamiltonian, in each iteration, that were necessary to calculate the matrix of the Jacobian in two dimensions were not necessary in one dimension.

### D. Self-Consistent Calculation of the Static Magnetostriction

The problems involved in the calculation of the static

magnetostriction are similar to those encountered in the calculation of the magnetization, since the equilibrium strains are calculated from the derivatives of the free neergy. The free energy is, however, calculated from the eigenvalues of the zero-order Hamiltonian which is itself a function of the equilibrium strains. The procedure starts with the static strains equal to zero, so the values of $\Gamma_x$ and $\Gamma_z$ that enter the zero-order Hamiltonian are:

$$\Gamma_x = \frac{g\mu_B}{k} (\Gamma - \Gamma_1) \qquad \text{IV-26}$$

$$\Gamma_z = \frac{g\mu_B}{k} (\Gamma + 2\Gamma_1)$$

After the magnetization had been calculated, the static strains were calculated from the set of equations:

$$\frac{\partial F_e}{\partial e_i^{\Gamma,j}} = - \frac{\partial F_m}{\partial e_i^{\Gamma,j}} \qquad \text{IV-27}$$

where $F_e$ is the elastic energy, and $F_m$ is the free energy, not including the purely elastic part. The derivatives of $F_e$ are trivial, and the derivatives of $F_m$ were calculated numerically. The equation itself is derived from equation III-46, where the static stresses have not been included, and $C_{12}^{\alpha}$ has been set equal to zero. These equilibrium strains were then incorporated into the zero-order Hamiltonian through modifications of the coefficients of the operators: $Q_2^0$, $Q_{22}^+$, $Q_{21}^+$, and by modifying the values of $\Gamma_x$

and $\Gamma_z$, as shown in equations IV-3. Since the zero-order Hamiltonian had been modified at this stage, the magnetization that was calculated from it was also modified. The calculation of the magnetization thus had to be repeated for the new zero-order Hamiltonian. After reaching the correct value of the magnetization, the equilibrium strains were again calculated. The iteration continued until the new static strains were within a certain percentage of those calculated in the previous iteration.

After the static strains had converged, and the magnetization had been calculated for the zero-order Hamiltonian, the second derivatives of the internal energy were calculated using the eigenvalues and eigenvectors of the zero-order Hamiltonian and equations III-81, 82, and 83.

## E. Calculation of the Second Derivatives of the Internal Energy

The calculations of the second derivatives of the internal energy, using the second-order corrections to the energies, was discussed in the last chapter. These energy corrections were calculated in the subroutine ENCOR using the matrix elements of the operators, and were stored for use in the calculation of the summations that appear in the expressions for the second derivatives of the internal energy. The ten summations (equations III-81) that appear in the expressions were calculated in the subroutine SUMCAL and stored. The subroutine DERCAL used these values

of the summations and equations III-82 and 83 to calculate the second derivatives.

There are only eighteen nonzero second derivatives of the internal energy with respect to the seven coefficients ($X_i$) that appear in the perturbing Hamiltonian. The real and imaginary operators must be considered separately, since there can be no cross derivatives involving a real and an imaginary operator because that would lead to an imaginary energy correction. The real operators are: $J_x$, $J_z$, $Q_2^0$, $Q_{22}^+$, and $Q_{21}^+$. There are 25 possible second derivatives that can be taken with respect to the coefficients of these five operators, but since the derivatives are symmetric, only fifteen of the derivatives are distinct. Similarly, there are three distinct derivatives involving the coefficients of the imaginary operators: $Q_{22}^-$ and $Q_{21}^-$.

In an earlier computer program, the fifteen seocnd derivatives of the internal energy with respect to the coefficients of the real operators were calculated numerically, by incrementing the coefficients of the operators; for example:

$$\frac{\partial^2 U}{\partial A^2} = \frac{1}{\Delta^2}(2U(A) - U(A+\Delta) - U(A-\Delta)) \qquad \text{IV-28}$$

This is the simpler method, both conceptually and computationally, but it is very wasteful of cumputer time, since the evaluation of each derivative requires that the zero-

order Hamiltonian be diagonalized two or three additional times.

The numerically calculated derivatives were, however, compared with those that were calculated using the expressions derived in the last chapter, and were found to agree to within 1 part in $10^3$ or better. Since the derivatives calculated by the two methods agree so well, there is little doubt that the derivatives of the internal energy that were used to fit the ultrasonic data were calculated correctly.

After the derivatives had been calculated, the main program, MAIN02, created a data file with the values of the derivatives that were necessary to fit the experimental data. Also, the changes in the elastic constant, $\Delta C_{ii}$, had to be calculated from the experimentally measured $\Delta f/f$. If magnetostrictive effects are ignored, $\Delta C_{ii}$ is:

$$\Delta C_{ii}(\sigma) = 2C_{ii} \frac{\Delta f(\sigma)}{f}$$

The subroutine VEC multiplied the values of $\Delta f/f$, that were read from the data file, by the appropriate elastic constant, and calculated $\Delta C_{ii}$, which was then stored in the data file along with the calculated derivatives.

E. Nonlinear Least Squares Fit of the Ultrasonic Data

The coefficients that multiply the calculated derivatives in the expressions for the magnetoelastic

contributions to the elastic constants are bilinear in the magnetoelastic constants, so a nonlinear least squares fitting procedure had to be used to find the magnetoelastic constants.

There is no set method for solving nonlinear least squares problems[66]; each one must be approached separately. Three different methods were used in various stages of the data analysis. The grid-search method[66] was the first that was used, but it was either not implemented well, or was not appropriate for the problem. None of the data analysis that is reported here was done using this method.

The most straightforward method is the direct search of coefficient space. Assume that there are n coefficients to be determined. The direct search requires a starting point, which becomes the center of a grid of points that is set up in the n-dimensional coefficient space. The sum of the squares of the deviations:

$$\chi^2 = \sum_i (\Delta C^{exp} - \Delta C^{cal})^2 \qquad \text{IV-29}$$

is then calculated at each point of the grid, and the point at which $\chi^2$ is a minimum is chosen as the center of the next grid. By reducing the distance between the grid points, the procedure eventually converges.

The one advantage of the direct search is that it is easy to program. Its disadvantages are that it is very wasteful of computer time because the large number of

multiplications that must be done to evaluate $\chi^2$ is multiplied by the number of points in the grid, which is large when n is larger than 2 or 3. Also, there is no guarantee that the procedure will converge to the absolute minimum of $\chi^2$ rather than to one of the relative minima, so the whole calculation has to be repeated several times from different starting points to be sure that the absolute minimum has been found.

The method that was found to be the most useful in this problem was that of Levenberg[67], whose method is a modified version of the Newton-Raphson method. Essentially, the problem is to minimize:

$$\chi^2 = \sum_i h_i^2(\vec{a}) \qquad \text{IV-30}$$

with respect to the coefficients $\vec{a}$. Thus, the equations:

$$\partial_{\vec{a}}\chi^2 = 0 \qquad \text{IV-31}$$

must be solved. These equations are, in general, a set of coupled nonlinear equations. The function, $h_i$, is expanded in a Taylor series as a function of the coefficients, $\vec{a}$:

$$h_i(\vec{a}) = h_i(\vec{a}_0) + \vec{\nabla}_a h_i \cdot \Delta\vec{a} \qquad \text{IV-32}$$

where only the terms linear in the increments:

$$\Delta\vec{a} = \vec{a} - \vec{a}_0 \qquad \text{IV-33}$$

are retained. By substituting this approximation into equation IV-31, a set of coupled equations is obtained, the solutions of which are the increments of the coefficients.

The procedure operates iteratively, and requires a starting point for the coefficients. In general, it is found that if the initial guess is not close to the root of the equations, the increments of the coefficients that are calculated are very large, and the procedure diverges. to alleviate this problem, Levenberg changed the conditions somewhat, and required that the sum of $\chi^2$ and the square of the increments, $\Sigma_i \Delta a_i^2$, be minimized, and that the increments be such as to reduce $\chi^2$. This change has the effect of decreasing the increments, and of enlarging the radius of convergence, at the expense of some speed in the convergence. This procedure was implemented in APL and used to fit most of the experimental data shown in the next chapter.

# V. Experimental Data and Data Analysis

Two types of experiments were carried out in the course of the research reported in this thesis: measurements of the magnetization and measurements of the elastic constants as functions of the applied field. Limited measurements of the ultrasonic attenuation were also done.

## A. Magnetization Data

The magnetization data are fairly simple, but they do deserve a short discussion. In the paramagnetic phase, the magnetization as a function of the internal field is the same, within experimental error, for fields applied along any direction in the basal plane. The demagnetizing factors are different for different directions, however, so the magnetization was measured with fields applied along each crystallographic axis.

The magnetization of the sample, DyA, was measured in only the paramagnetic phase, and the data are not presented because the dependence of the magnetization on the applied field is quantitatively the same as for the DyB sample, for which there are more complete data. The magnetization of the sample DyB was measured at representative temperatures in the range, 4.2K to 300K, for fields in the basal plane. Because of the difficulty, at low temperatures, of holding the sample stationary in high fields when the field was being applied along the hard magnetic axis, the magnetization with fields parallel to the c-axis was measured only

at temperatures in the range 160K to 300K.

Figure V-1 is representative of the magnetization curves obtained in the ferromagnetic phase of Dy with the field along the a-axis. The saturation magnetization obtained at 4.2K, with a field of 48kOe along the a-axis of the sample DyB, was 351emu/g, which compares very well with the value of 350.5 emu/g obtained by Behrendt et al[7]. Figure V-2 shows the magnetization obtained at 180K with the magnetic field parallel to the c-axis. The c-axis magnetization was not measured at fields above about 35kOe because, at higher fields, deviations from the linear dependence of the magnetization on the field were observed. These deviations were attributed to movements of the sample or to lateral vibrational modes of the vibrating rod caused by the large torque on the sample. In situations where the magnetization at higher fields was needed, it was obtained from a linear extrapolation of the low field magnetization.

At temperatures in the HAF phase of Dy, the transition from the HAF phase to the FM phase was observed at the critical field. Because of the difficulty of calculating the demagnetizing factor of the oddly shaped samples, it was not possible to compare the measured critical fields with the values given in the literature. The nonzero demagnetizing factor caused the discontinuity in the magnetization, that appears at the critical (internal) field, to have a slope in the plot versus applied field.

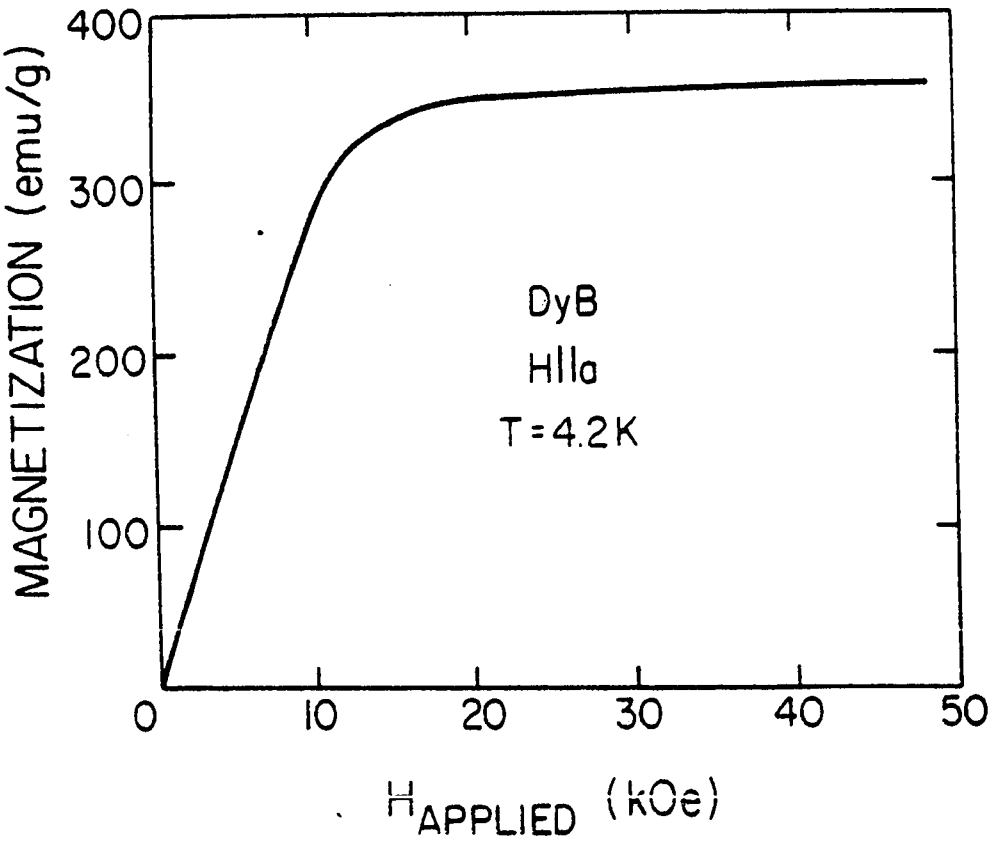


Figure V-1 Magnetization of DyB at 4.2K with the field applied along the a-axis.

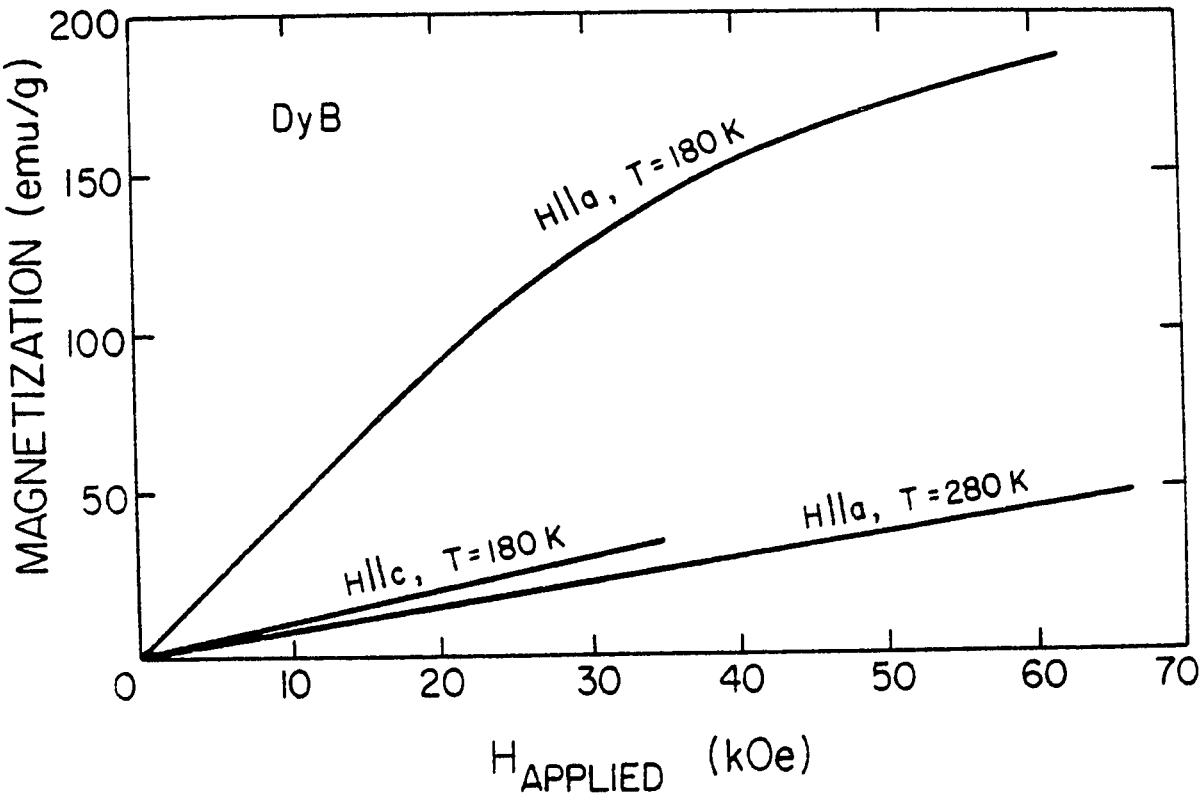


Figure V-2 Magnetization of DyB at various temperatures.

Approximate values of the demagnetizing factors along the a and b-axes were calculated from the slope (at the transition) of the magnetization as a function of the applied field, but no usewas made of them. Figure V-3 shows typical curves that were obtained in the HAF phase with fields in the basal plane.

Figure V-2 shows the magnetization that was obtained from the sample DyB at 180K, with the field parallel to the a-axis. The deviation of the magnetization from a linear dependence on the field is apparent. Some deviation from the linear dependence was observed up to 280K, for fields of 75kOe in the basal plane. Table V-1 gives the coefficients that parameterize the magnetization of the sample in the paramagnetic phase. Remember that the reduced magnetization is calculated from the formula:

$$\sigma = A(T)v + B(T)v^2 + C(T)v^3 + D(T)v^4 \qquad V\text{-}1$$

where the current monitor voltage, v, is in mV. Assuming that the calibration of the magnet is correct, the magnetization as a function of the applied field can be obtained by using the following conversion:

$$H = 1.372\ v \qquad V\text{-}2$$

where H is in kOe.

B. Elastic Constant Data

Only the magnetoelastic contributions to the longitudinal elastic constants, $C_{22}$ and $C_{33}$, and the contributions

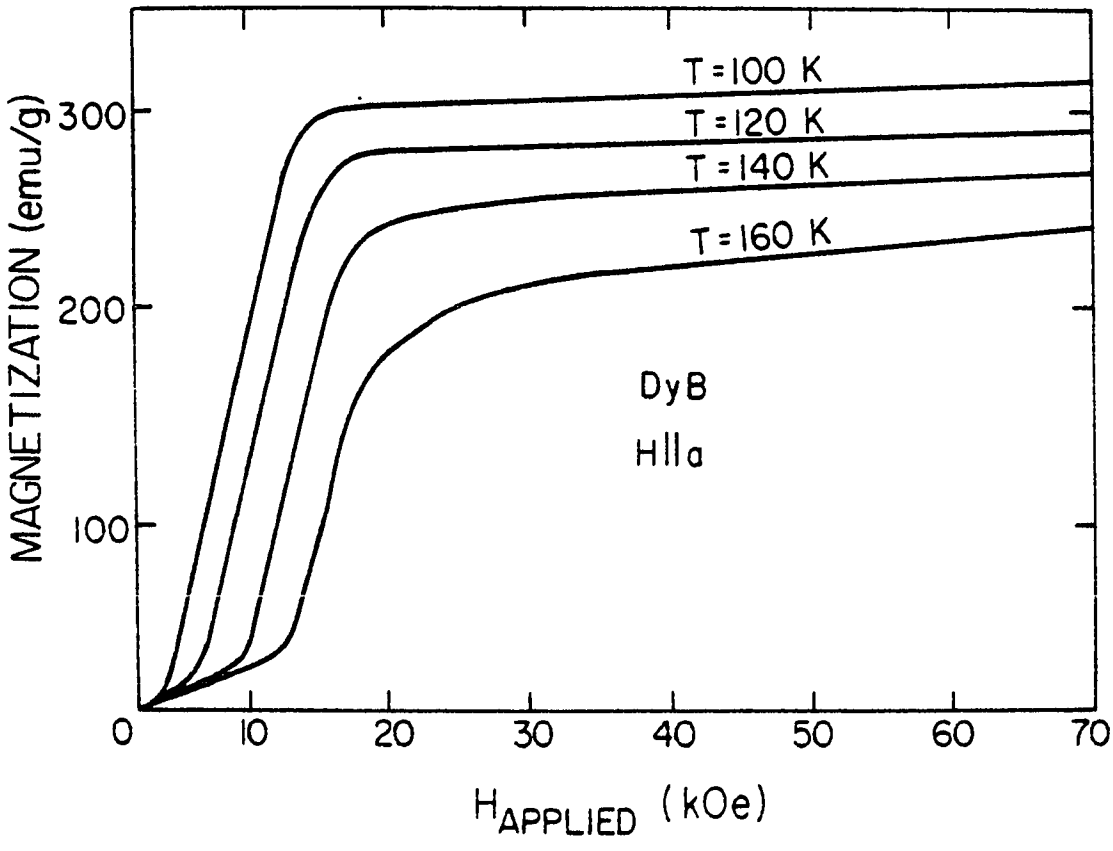


Figure V-3 Magnetization of DyB in the HAF phase, with the field applied along the a-axis.

Coefficients from which the magnetization in the paramagnetic phase can be calculated

| Temperature | $A(mV^{-1})$ | $B(mV^{-2})$ | $C(mV^{-3})$ | $D(mV^{-4})$ |
|---|---|---|---|---|
| 180.0000 | 0.1689297E-01 | 0.1583031E-03 | -0.1139931E-04 | 0.1163316E-06 |
| 185.0000 | 0.1375110E-01 | 0.1101918E-03 | -0.6813907E-05 | 0.6243816E-07 |
| 190.0000 | 0.1175782E-01 | 0.5640624E-04 | -0.3756866E-05 | 0.3239583E-07 |
| 195.0000 | 0.9986967E-02 | 0.6721975E-04 | -0.3367504E-05 | 0.2835816E-07 |
| 200.0000 | 0.8483296E-02 | 0.7029414E-04 | -0.3004686E-05 | 0.2551957E-07 |
| 210.0000 | 0.7069285E-02 | 0.1061911E-04 | -0.6418503E-06 | 0.3247899E-08 |
| 220.0000 | 0.5752187E-02 | 0.1044083E-04 | -0.4859678E-06 | 0.2998363E-08 |
| 230.0000 | 0.5034137E-02 | 0.4280568E-05 | -0.3080471E-06 | 0.2011750E-08 |
| 240.0000 | 0.4357312E-02 | 0.1001148E-04 | -0.4888860E-06 | 0.4285431E-08 |
| 250.0000 | 0.3883890E-02 | 0.6398902E-05 | -0.3952934E-06 | 0.3938495E-08 |
| 260.0000 | 0.3510365E-02 | 0.1220895E-05 | -0.1332698E-06 | 0.8237694E-09 |
| 270.0000 | 0.3129973E-02 | 0.4928992E-05 | -0.2467454E-06 | 0.2184461E-08 |
| 280.0000 | 0.2846639E-02 | 0.3775696E-05 | -0.1650114E-06 | 0.1317955E-08 |
| 290.0000 | 0.2712232E-02 | -0.4884747E-05 | 0.1324950E-06 | -0.1784389E-08 |
| 300.0000 | 0.2434618E-02 | 0.3414875E-05 | -0.1687620E-06 | 0.1529923E-08 |

Table V-1

Sample - DyB $\vec{H} \parallel a$

Coefficients from which the magnetization in the paramagnetic phase can be calculated.

| Temperature | $A(mV^{-1})$ |
|---|---|
| 160.0000 | 0.3975784E-02 |
| 170.0000 | 0.4386369E-02 |
| 175.0000 | 0.4151089E-02 |
| 180.0000 | 0.3885839E-02 |
| 185.0000 | 0.4001853E-02 |
| 190.0000 | 0.3512529E-02 |
| 195.0000 | 0.3432930E-02 |
| 200.0000 | 0.3318820E-02 |
| 210.0000 | 0.3021680E-02 |
| 220.0000 | 0.2728023E-02 |
| 230.0000 | 0.2584627E-02 |
| 240.0000 | 0.2470477E-02 |
| 250.0000 | 0.2228534E-02 |
| 260.0000 | 0.2131077E-02 |
| 270.0000 | 0.1983012E-02 |
| 280.0000 | 0.1913333E-02 |
| 290.0000 | 0.1816560E-02 |
| 300.0000 | 0.1696236E-02 |

Table V-1

Sample - DyB $\vec{H} \,||\, c$

to the pure shear constants $C_{44}$ and $C_{66}$ were measured. The shear constants were measured only with the field parallel to the a-axis, and $C_{33}$ was measured with the field parallel to either the a-axis or the c-axis, since by symmetry, there should be no difference in the dependence of $C_{33}$ on the orientation of the magnetization when it lies in the basal plane. $C_{22}$ was measured with the field parallel to all three crystallographic axes, since the axial symmetry that was present in the measurement of $C_{33}$ is not present in the measurement of $C_{22}$. Using the theory developed in Chapter III, and the measurements of the longitudinal elastic constants, the magnetoelastic constants: $B_1^{\alpha,2}$, $B_2^{\alpha,2}$, $B^{\gamma,2}$, $G_1^{\alpha,0}$, $G_2^{\alpha,0}$, $G_1^{\alpha,2}$, $G_2^{\alpha,2}$, and $G^{\gamma,2}$ can be determined from measurements of $\Delta C_{22}^{a,b,c}(\sigma)$ and $\Delta C_{33}^{a,c}(\sigma)$ and a separate determination of $B^{\gamma,2}$ can be made from measurements of $\Delta C_{66}^{a}(\sigma)$.

The measured magnetoelastic contributions to the longitudinal elastic constants were analyzed in several ways. Originally, a set of constants was determined from the data taken at each temperature and for each orientation of the field. However, some of the constants that can be determined from data taken with each of several orientations of the field were found to differ from orientation to orientation. For example, $B^{\gamma,2}$ appears in the expressions for $\Delta C_{22}^{a}$, $\Delta C_{22}^{b}$, and $\Delta C_{22}^{c}$. At a temperature of 195K, the

calculated values of $B^{\gamma,2}$ were: 24°K/ion, 21°K/ion, and 27°K/ion, respectively. To avoid such inconsistencies, the program used to calculate the magnetoelastic constants was modified to calculate the constants that gave the best fit to all the data at a given temperature, and for a given elastic constant. The magnetoelastic constants determined in this way were observed to have a small dependence on the temperature, and since the theory assumes no such temperature dependence, the program was changed to find the magnetoelastic constants that gave the best fit to all the data for a given elastic constant. At the same time, the program was modified to force $G^{\gamma,2}$ to be equal to zero, since it has been shown that the experimental measurements of the static strain, $\bar{e}_1^{\gamma}$, can be accounted for by a theory that includes only the single-ion magnetostriction. Because a considerable amount of experimental data is needed to do the fit at each temperature, only the data taken at the temperatures, 195K, 200K, 220K, 240K, and 260K were included in the calculation. Temperatures lower than 195K were not included in the calculation because they are too close to the phase transition at 179K, and at temperatures higher than 260K, the relative errors in the experimental data became larger, so the data taken at temperatures near room temperature were not included.

The equations that were used in the determination of the magnetoelastic constants are:, for $\Delta C_{22}(\sigma)$:

$$\Delta C_{22}^{a}(\sigma) = a^2 D_{aa} - 2abD_{ab} + 2acD_{ap} + b^2 D_{bb} - 2bcD_{bp} + c^2 D_{pp}$$

$$\Delta C_{22}^{b}(\sigma) = a^2 D_{aa} + 2abD_{ab} + 2acD_{ap} + b^2 D_{bb} + 2bcD_{bp} + c^2 D_{pp}$$

$$\Delta C_{22}^{c}(\sigma) = a^2 D_{aa} - 2abD_{ab} + 2adD_{aq} + b^2 D_{bb} - 2bdD_{bq} + d^2 D_{qq}$$

where:

$$a = -(B_1^{\alpha,2} - B_2^{\alpha 2}) \qquad b = -B^{\gamma,2}$$

$$c = G_1^{\alpha,-} - G_2^{\alpha,-} \qquad d = G_1^{\alpha,+} - G_2^{\alpha,+} \qquad \text{V-4}$$

$$D_{xy} = \frac{\partial^2 U}{\partial X \partial Y}(\sigma) - \frac{\partial^2 U}{\partial X \partial Y}(\sigma=0)$$

and $G^{\gamma,2}$ is assumed to be zero. $G_1^{\alpha,-}$, $G_1^{\alpha,+}$, $G_2^{\alpha,-}$, and $G_2^{\alpha,+}$ are defined in equation IV-4. There are, thus four constants to be determined from the approximately 200 experimental points that were used in the calculation. The magnetoelastic constants are:

$$B_1^{\alpha,2} - B_2^{\alpha,2} = 37°K/ion \qquad B^{\gamma,2} = 7°K/ion \qquad \text{V-5}$$

$$G_1^{\alpha,-} - G_2^{\alpha,-} = -17°K/ion \qquad G_1^{\alpha,+} - G_2^{\alpha,+} = -18°K/ion$$

( Note that the magnetoelastic constants that are used in this section are those that were defined in Chapter III, and in some cases they differ from those that were used in the computer programs. In particular, the constants $B_1^{\alpha,2}$ and $B_2^{\alpha,2}$ are equal to $\sqrt{3/2}$ times those that were used in the programs.)

The experimental data and the fit to the data,

calculated using the four magnetoelastic constants given in equation V-5, are shown in Figures V-4, 5, and 6. (Note that in Figures V-4 through V-9, the open symbols represent experimental points and the closed symbols of the same shape represent the corresponding calculated point. When only the open symbol is shown, the experimental and calculated points were too close together to be resolved.) The fit is not extremely good quantitatively, but qualitatively, the main features of the experimantal data are reproduced in the calculated functions. It should be noted that considerably better fits can be obtained by letting the magnetoelastic constants have a small temperature dependence, and by letting $G^{\gamma,2}$ be nonzero. Since only part of the experimental data is shown in the figures, all the data is reproduced in Appendix E.

The equations for $\Delta C_{33}$ are derived from equations III-85 and are written:

$$\Delta C_{33}^{a}(\sigma) = a^2 D_{aa} + 2abD_{ap} + b^2 D_{pp} \qquad \text{V-6}$$

$$\Delta C_{33}^{c}(\sigma) = a^2 D_{aa} + 2acD_{aq} + c^2 D_{qq}$$

where:

$$a = -(B_1^{\alpha,2} + 2B_2^{\alpha,2}) \qquad b = G_1^{\alpha,-} + 2G_2^{\alpha,-}$$

$$c = G_1^{\alpha,+} + 2G_2^{\alpha,+} \qquad \text{V-7}$$

The calculation of the magnetoelastic constants that appear

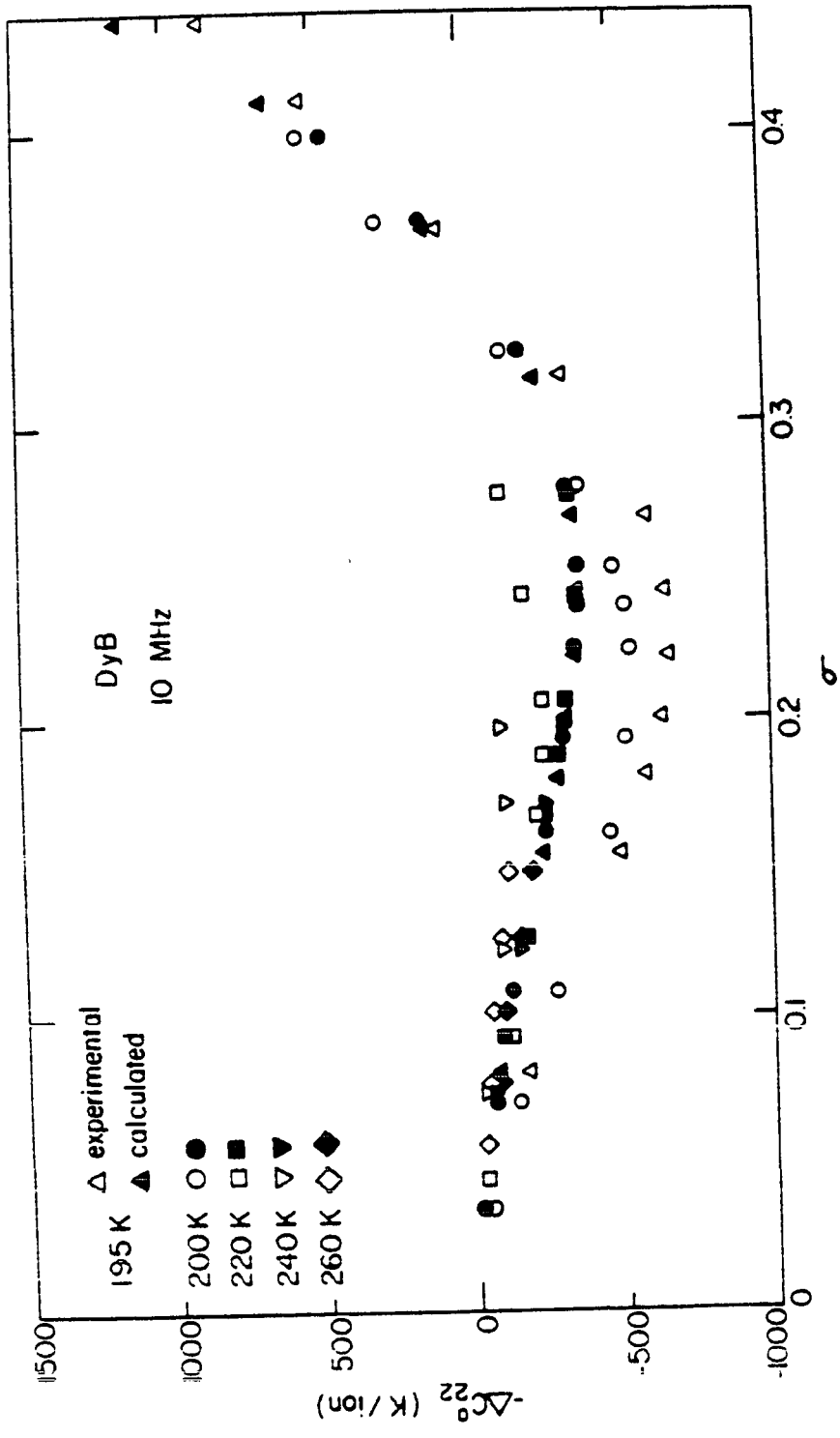


Figure V-4 Experimental data and calculated fit to the elastic constant $C_{22}$ with the field along the a-axis.

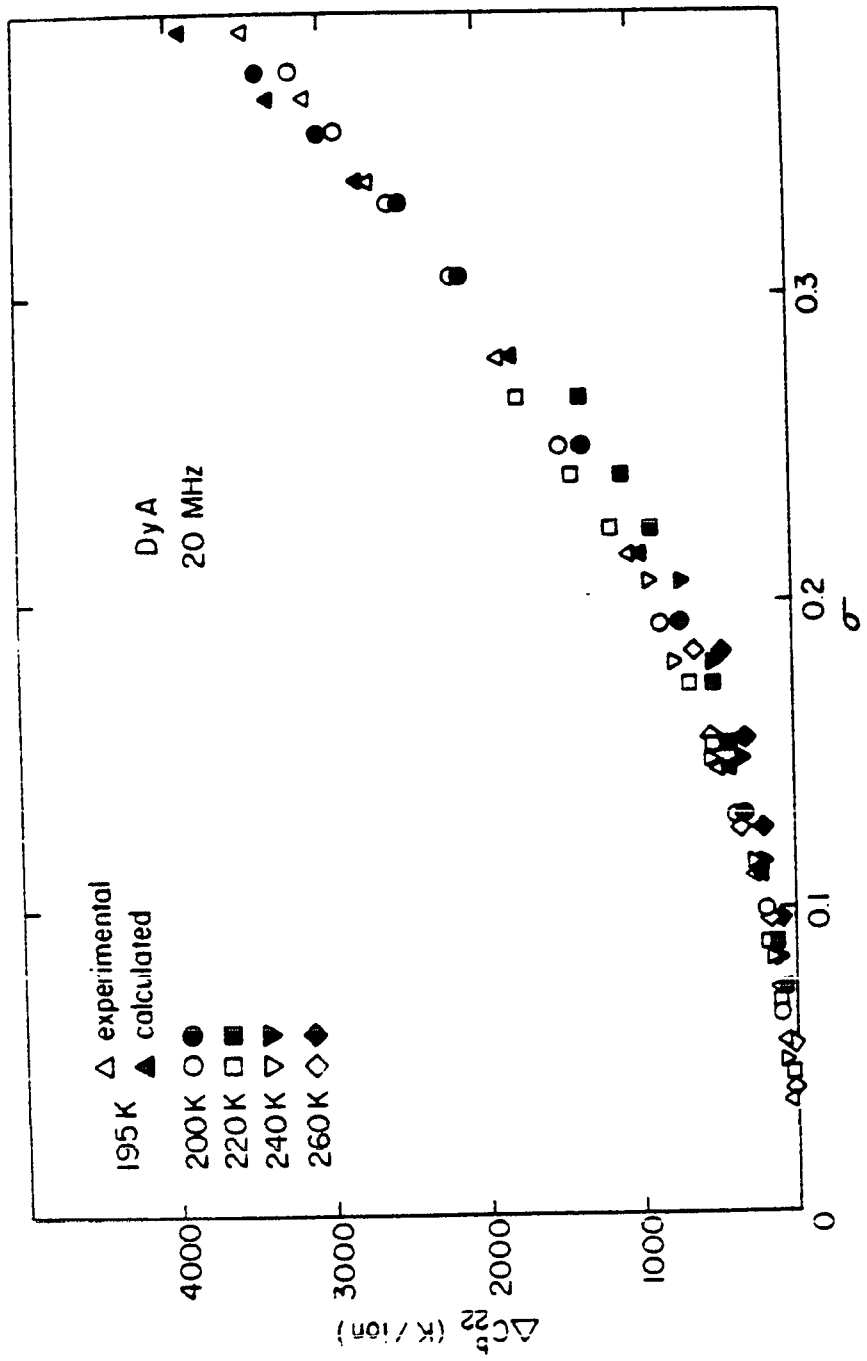


Figure V-5 Experimental data and calculated fit to the elastic constant $C_{22}$ with the field along the b-axis.

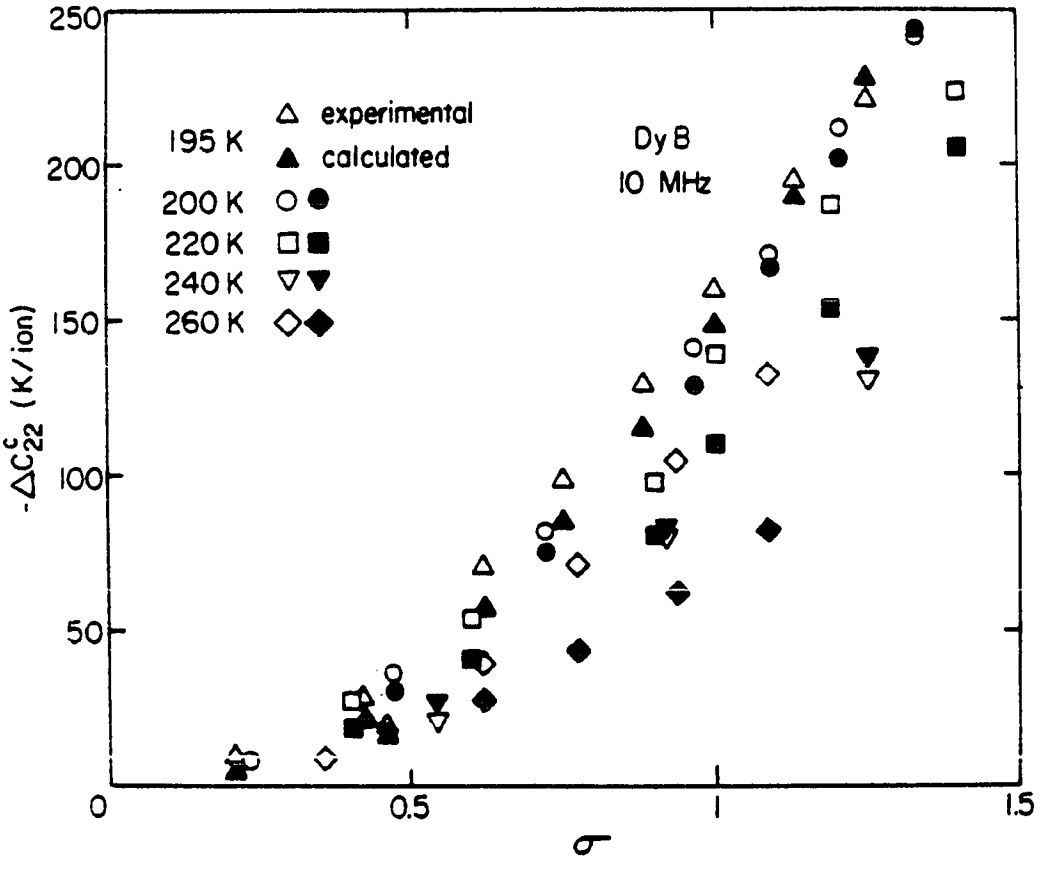


Figure V-6 Experimental data and calculated fit to the elastic constant $C_{22}$ with the field along the c-axis.

in the equations for $\Delta C_{33}(\sigma)$ were determined from approximately 105 experimental points. The calculated values of the constants are:

$$B_1^{\alpha,2} + 2B_2^{\alpha,2} = 28°K/ion \qquad G_1^{\alpha,-} + 2G_2^{\alpha,-} = 149°K/ion$$

$$G_1^{\alpha,+} + 2G_2^{\alpha,+} = 46°K/ion \qquad \text{V-8}$$

Figures V-7 and V-8 show the experimental and calculated values of $\Delta C_{33}(\sigma)$. The fit is somewhat better than for $\Delta C_{22}(\sigma)$, as might be expected since there is less data to be fit for $\Delta C_{33}$.

Since only one magnetoelastic constant, $B^{\gamma,2}$, was involved in the fit of $\Delta C_{66}^{a}(\sigma)$, it was only necessary to use the usual linear least squares method. The value of $B^{\gamma,2}$, that was determined from $\Delta C_{66}^{a}(\sigma)$, is:

$$B^{\gamma,2} = 25°K/ion \qquad \text{V-9}$$

and the fit to the experimental data is included in Figure V-9.

The $\Delta C_{44}^{a}(\sigma)$ data were taken with the field parallel to the a-axis and with the polarization of the shear wave in the basal plane at a angle of 45° between the a and b-axes. Thus, one component of the strain was parallel to the field and one component was perpendicular. Because of the magnetic field, the velocities of the two, normally degenerate,polarizations were different. Experimentally,

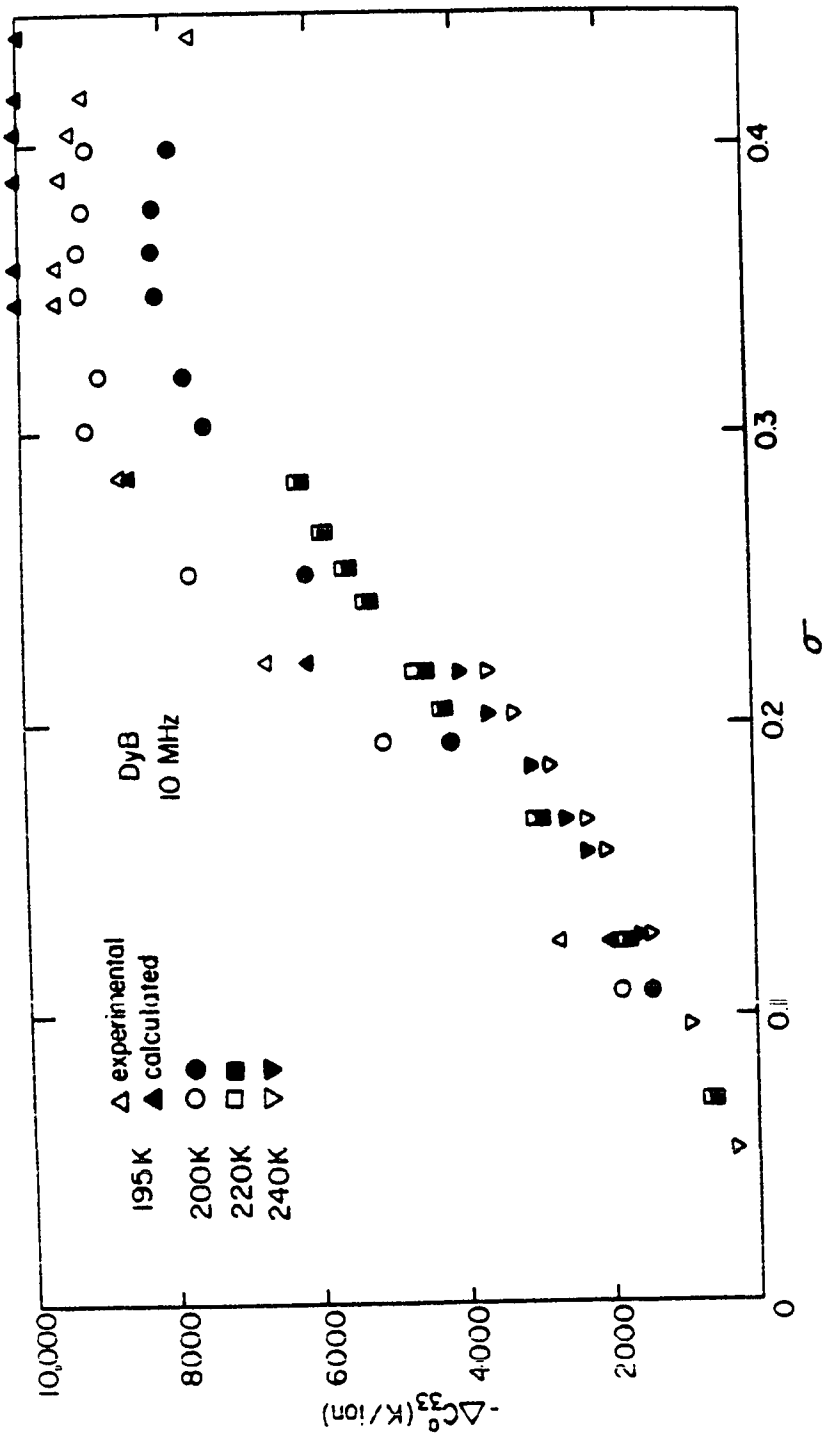


Figure V-7 Experimental data and calculated fit to the elastic constant $C_{33}$ with the field along the a-axis.

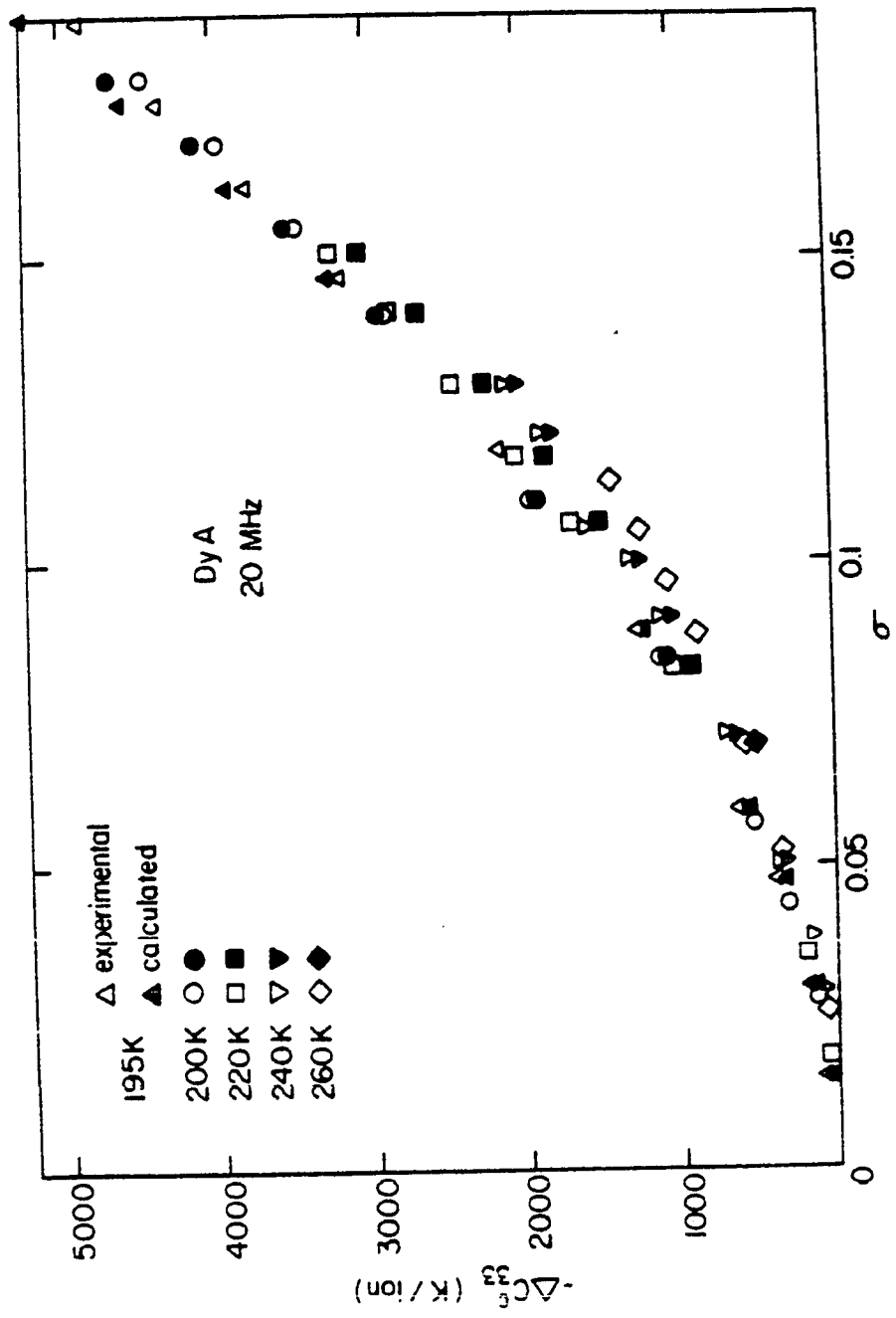


Figure V-8 Experimental data and calculated fit to the elastic constant $C_{33}$ with the field along the c-axis.

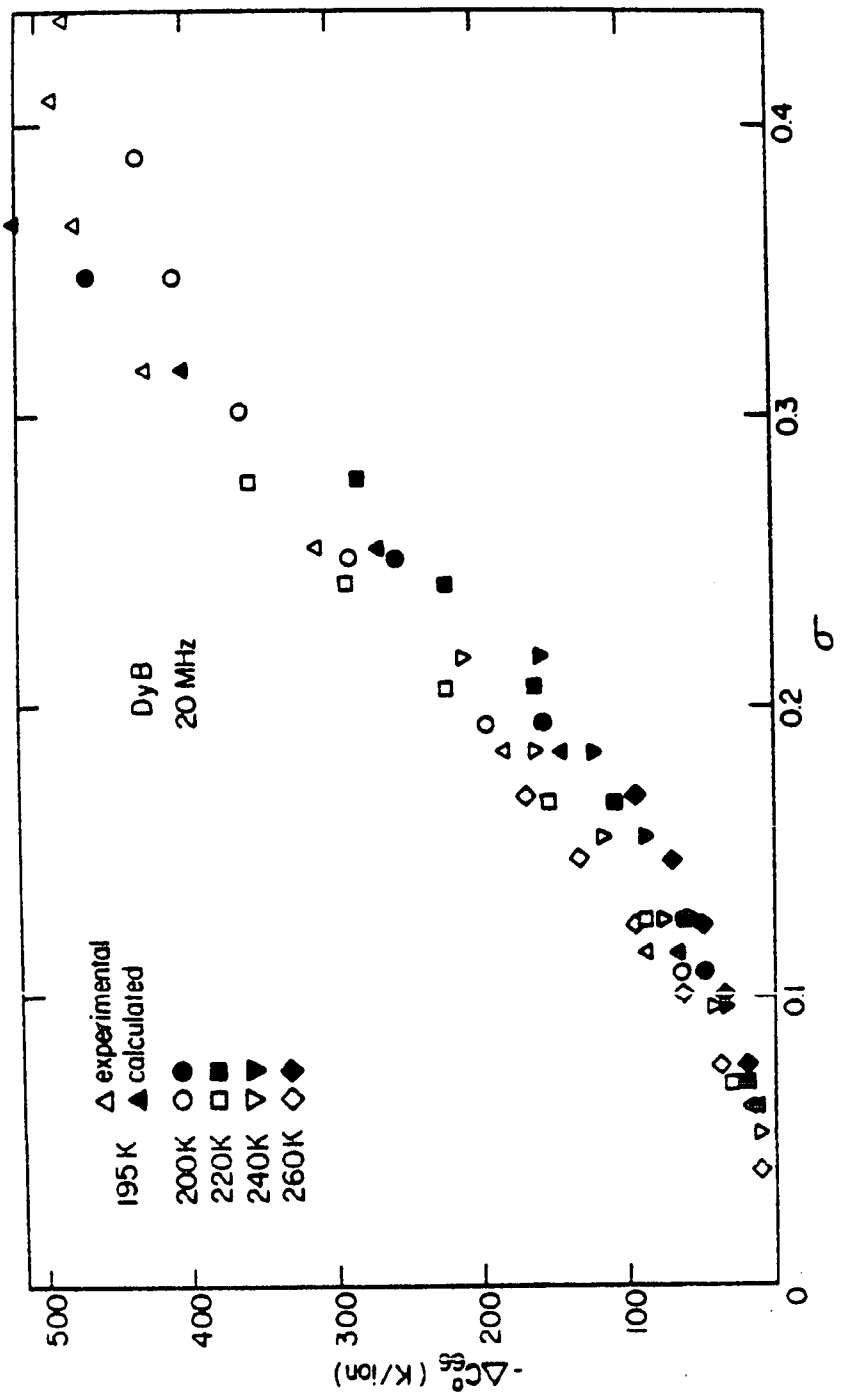


Figure V-9 Experimental data and calculated fit to the elastic constant $C_{66}$ with the field along the a-axis.

this difference in the velocities should have been manifested as an oscillatory variation of the attenuation as a function of the magnetic field, with the maximum attenuation occurring when the two waves reached the transducer 180° out of phase, and the minimum in the attenuation occurring when the two waves reached the transducer in phase. The experimental results were rather puzzling since the oscillations in the attenuation were not observed. Also, the numerical calculation predicts that the velocity of the shear wave polarized parallel to the a-axis will increase with field about three times as fast as the perpendicular shear wave decreases with field, so the average velocity should increase with field. Experimentally, however, the velocity was observed to decrease with field. Also, at temperatures near the Neel temperature, the ultrasonic velocity (as a function of the magnetization) was observed to reach a minimum and to begin increasing again, whereas theoretically, the dependence on the magnetization should monotonic. Probably, the discrepancies are due to a small longitudinal component in the strain that entered because of the error in the alignment of the face of the crystal. Since this component will have the velocity that characterizes $C_{33}$, which shows the largest dependence on field of any of the elastic constants and which does not depend monotonically on the field, it can account for the observed effects. No analysis of the $C_{44}$ data was attempted

because of the difficulty of accounting for the contribution of the longitudinal part of the strain. The raw data are presented in Appendix E, however.

The misalignment problem was not as severe for measurements of $\Delta C^{a}_{66}(\sigma)$, since the longitudinal constant that enters is $C_{22}$, which has a weak dependence on the field compared to $C_{33}$.

Probably the best test of the theory is the agreement of the calculated values of $B^{\gamma,2}$ with the value obtained from the static magnetostriction experiments. The fit of $\Delta C^{a}_{66}(\sigma)$ yielded a value of 25°K/ion, which is probably somewhat too large because of the error in the alignment of the face of the sample. Considering the complexity of the calculation, this value compares well with the value of 7°K/ion that was obtained from the fit of $\Delta C_{22}(\sigma)$. However, the important fact is that both values are in good agreement with the value of $B^{\gamma,2}$, 9.4°K/ion, that was obtained from the static magnetostriction[11]. The agreement of the three values of $B^{\gamma,2}$ is particularly good when compared with the results of the only other available theory, the theory of Southern and Goodings[23]. The value of $B^{\gamma,2}$ that is calculated from the ultrasonic data using the theory of Southern and Goodings is approximately 100 times larger than the one calculated from the static magnetostriction, so the error is an order of magnitude larger.

It is more difficult to compare the other magnetoelastic constants to those calculated from the static magnetostriction. The difficulty is that, whereas, $\bar{e}_1^{\gamma}$ depends only on $B^{\gamma,2}$, the strain $\bar{e}^{\alpha,1}$, for example, depends on $B_1^{\alpha,2}$, $G_1^{\alpha,0}$, and $G_1^{\alpha,2}$. It is thus more difficult to uniquely determine the other magnetoelastic constants. The best compromise is to use the magnetoelastic constants determined from the elastic constant measurements (equations V-5 and V-8) to calculate the static strains, and to compare these calculated strains with those measured experimentally[11].

Since the magnetoelastic constants used in the calculation of the magnetostriction were determined from ultrasonic data taken in the paramagnetic phase of Dy, only the magnetostriction in the PM phase will be calculated.

The calculation was a very rough one that was made under the assumption that the static strains depend linearly on the magnetoelastic constants. The derivatives used in the Taylor series expansion of the strains, as functions of the magnetoelastic constants, were those that were used in the determination of the magnetoelastic constants that were used in the zero-order Hamiltonian. (See Chapter IV for a better discussion.)

In all cases, the calculated strains reproduced the sign of the magnetostriction correctly. The calculated $\bar{e}_1^{\gamma}$

was very close to the measured strain, as expected. In addition to $\bar{e}_1^{\gamma}$ (and excluding $\bar{e}_2^{\varepsilon}$), Clark et al[11] measured the four strains (in their notation): $\lambda(c,c)$, $\lambda(a,a)$, $\lambda(a,c) - \lambda(c,c)$, and $\lambda_0^{\alpha,2} - \frac{1}{2}\lambda^{\gamma,2}$. The calculated $\lambda(c,c)$ was about a factor of two larger than the measured strains, $\lambda(a,c) - \lambda(c,c)$ was a factor of ten too large, $\lambda(a,a)$ was a factor of 6-8 too large. The worst agreement was for the strain $\lambda_0^{\alpha,2} - \frac{1}{2}\lambda^{\gamma,2}$ which was 20-100 times larger than the experimentally measured strain. It should be pointed out, however, the strain $\lambda_0^{\alpha,2} - \frac{1}{2}\lambda^{\gamma,2}$ was the smallest, experimentally, so the relative error was naturally larger. Clearly, the static magnetostriction is correctly predicted, qualitatively, if not quantitatively.

The thermodynamic approach used in this thesis also predicts the observed changes in the slopes of $\Delta C_{22}^a(\sigma)$ and $\Delta C_{33}^a(\sigma)$ that are unaccounted for in the theory of Southern and Goodings. In addition, Southern and Goodings predicted that the shear constants would not depend on the magnetization in the paramagnetic phase, whereas the thermodynamic method accounts for the observed dependences quite well, at least for the case of $\Delta C_{66}^a(\sigma)$.

There are , of course, ways in which the calculation could be improved. The inclusion of the helically ordered phase in the theoretical model would be interesting in itself, and would make comparisons of the theory with experiment possible in this phase. The properties of the

model in the paramagnetic phase would only be affected slightly, if at all, by the inclusion of the helical ordering, however.

There are contributions to the internal energy which are not included in the calculation, but which might have appreciable effects. One term that was neglected in the calculation of the internal energy is the elastic energy due to the third-order elastic constants. When the second derivatives of such terms are taken with respect to the dynamic strains, there will be acontribution due to the presence of the static strains. The third-order elastic constants have, apparently, not been measured for the rare earths, so no realistic analysis of their effect can be made. However, if, as is usual in other materials, the third-order elastic constants are comparable with the usual elastic constants, then their contributions to the relative changes in the elastic constants would be of the order of the static strains. Thus, in the paramagnetic phase,the contribution of the third-order elastic constants would be most important for elastic constants which have a relatively weak dependence on the magnetization. They could possibly explain why the fit to the $C_{22}$ data is not as good as the fit to the $C_{33}$ data, for instance. There are also terms in the expansion of the crystal field anisotropy energy that would lead to terms in the Hamiltonian that are bilinear in the strains and bilinear in the angular momentum

operators. These terms would contribute to the elastic constants in first-order perturbation theory. The inclusion of these terms is almost impossible, however, since the number of magnetoelastic constants that would then enter the theory and that would have to be determined would increase from 10 to 40 or 50. Presumably, since the strains are small, these terms are small also.

A more serious omission in the theory is that the magnetostrictive contributions to the changes in the elastic constants were neglected. The origin of these effects is easily seen by considering the definition of the elastic constants in terms of the measured frequency of best overlap, f:

$$C_{ii} = \rho v^2 = \rho \ell_{eff}^2 f^2 \qquad \text{V-10}$$

where $\rho$ is the mass density of the sample and $\ell_{eff}$ is the effective path length. $\ell_{eff}$ is equal to twice the number of round trips that the elastic wave makes in the sample during the time between the two strobe pulses, multiplied by the length of the sample, $\ell$, along the axis along which the elastic wave is propagating. Thus, the relative change in the elastic constant is:

$$\Delta C_{ii}/C_{ii} = 2\Delta f/f + \Delta \ell/\ell - \Delta V/V \qquad \text{V-11}$$

where the change in the path length and the change in the volume, V, are magnetostrictive effects, and the change in

the frequency is the quantity that is measured. The correction for these effects would be easy enough to make if magnetostriction data were available. However, the magnetostriction data that are available were taken with a maximum applied field of 30kOe[1], and even those data were almost impossible to use because they are isofield data, and isothermal data were needed.

Finally, some ultrasonic attenuation data are presented with out analysis. The data were obtained in the HAF phase, for the most part, and in all cases were ontained for longitudinal waves with the field applied along the a-axis. The attenuation as a function of the applied field is shown in Figures V-10 and V-11. The interesting feature of the attenuation data is that there are several peaks, some of which occur at fields above the critical field for the transition to ferromagnetic ordering.

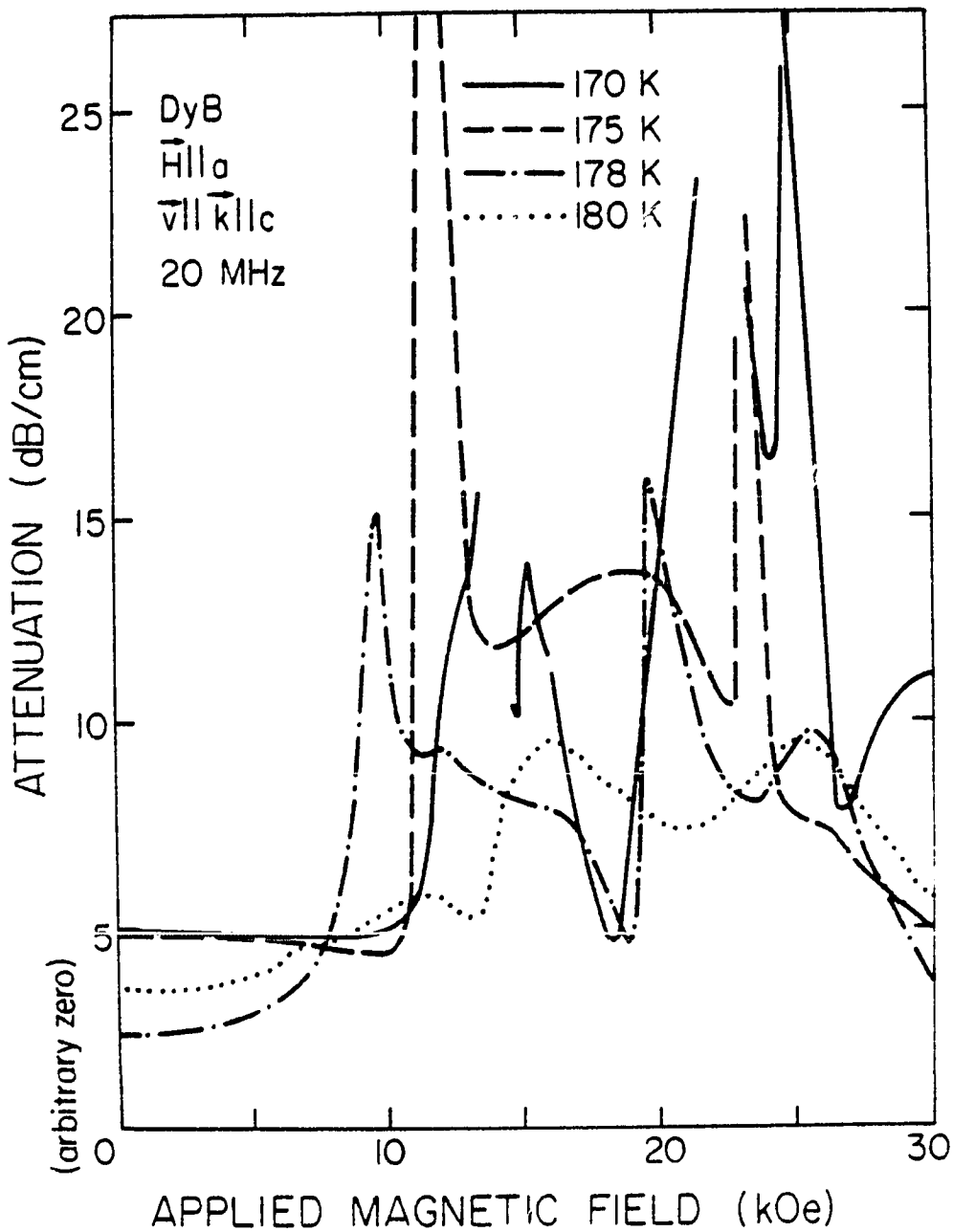


Figure V-10 Attenuation of longitudinal waves propagating along the c-axis of the sample DyB.

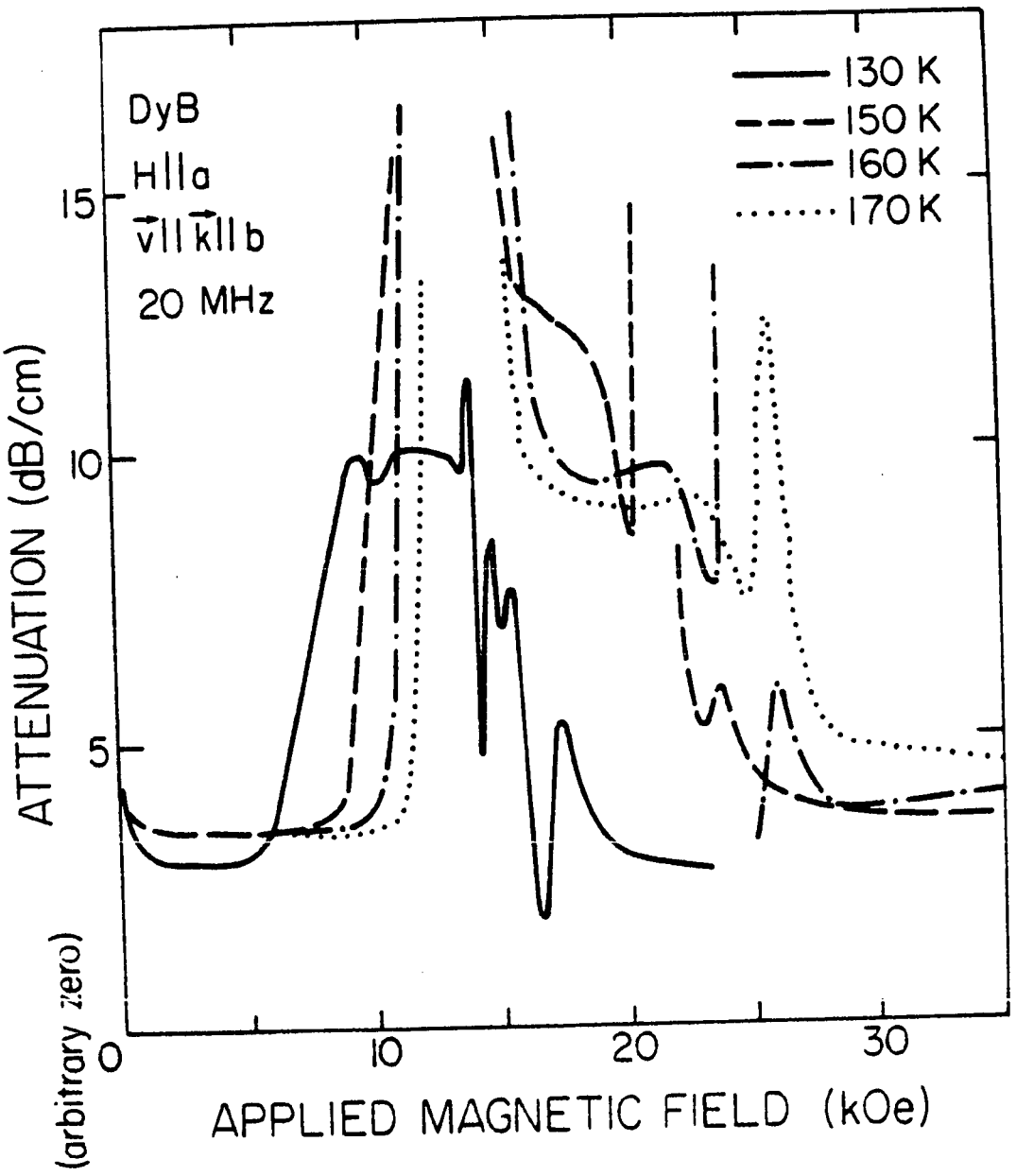


Figure V-11 Attenuation of longitudinal waves propagating along the b-axis of sample DyB.

## VI. Conclusion

In conclusion, it can be said that the thermodynamic method presented in this thesis represents a considerable improvement over the alternative method[23] of accounting for the magnetoelastic contributions to the elastic constants. In particular, the thermodynamic method accounts for the observed dependence of the shear constant $C_{66}$, and for the non-monotonic dependence of some of the longitudinal elastic constants on the magnetization. In spite of the detailed nature of the calculations, the agreement of the two experimentally independent determinations of $B^{\gamma,2}$ with the value obtained from the static magnetostriction is good. In addition, the Model Hamiltonian that was used accounts quite well for the single-ion anisotropy and the static magnetostriction. It is not clear at this time how well the model accounts for the low-temperature magnetoelastic properties, since they have not been studied in detail. Further work will be directed toward an exploration of the low temperature properties of the model. There is some reason to doubt that the results will be as satisfying at lower temperatures, since the accuracy of the molecular field approximation is suspect at low temperatures.

At low temperatures (in the ordered phases), the spontaneous magnetization depends relatively weakly on the applied field, so the experimental effects are more

difficult to measure accurately. The static magnetostriction will be more important, and more attention will have to be paid to the separation of the magnetostrictive effects from the intrinsic dependence of the elastic wave velocity on the magnetization. Since the static strains are so large in the ordered phases, the contributions of the third-order elastic constants to the internal energy will be more important.

The experimental contribution to the problem could be improved by the measurement of the static magnetostriction of the same samples that are used for the elastic constant measurements. The measurement of the magnetostriction using strain guage methods is relatively straightforward, but involves the expenditure of an amount of time and LHe that is comparable with the time necessary to measure the elastic constants themselves. There is no doubt, however, that a knowledge of the magnetostriction at high fields would improve the reliability of the results. The magneto-elastic constants that enter the zero-order Hamiltonian could be determined more accurately, as could the magneto-strictive contributions to the changes in the elastic constants.

Although there should be no frequency dependence of the ultrasonic properties in the frequency range of interest, the dependence should studied, since the presence of the magnetic field complicates the matter somewhat.

If there is, in fact, some dependence on the frequency, the dependence will have to be taken into account in the analysis of the experimental data.

Some theoretical properties of the model, such as the dependence of the second derivatives on the crystal field constants and the magnetoelastic constants, have not been investigated, but could lead to greater insight into the validity of the results.

Finally, further conclusions about the range of validity of the thermodynamic approach will be possible when the companion investigations of the magnetoelastic properties of Ho, Tb, and Er are completed at UNICAMP. The results for Tb are expected to be qualitatively the same as for Dy, since the two elements are so similar. However, the single-ion anisotropy in Ho and especially in Er is more complicated than in Dy or Tb, so the results may be qualitatively different for Ho and Er. The validity of the inclusion of the antisymmetric part of the strain in the model has not yet been tested experimentally, but experiments are now in progress at Rice to check the validity of this aspect of the theory.

# Bibliography


1. J. J. Rhyne, in Magnetic Properties of the Rare Earth Metals, R. J. Elliott ed., London: Plenum Press (1972)

2. W. C. Koehler, in Magnetic Properties of the Rare Earth Metals, R. J. Elliott ed., London: Plenum Press (1972)

3. R. J. Elliott and K. W. Stevens, Proc. Roy. Soc. 218, 553 (1953)

4. M. A. Ruderman and C. Kittel, Phys. Rev. 96, 99 (1954)

5. T. Kasuya, Progr. Theoret. Phys. (Japan), 16 45 (1956)

6. K. Yosida, Phys. Rev., 106, 893 (1957)

7. D. R. Behrendt, S. Legvold, and F. H. Spedding, Phys. Rev. 109, 1544 (1958)

8. J. J. Rhyne, S. Foner, E. J. McNiff, and R. Doclo, J. Appl. Phys. 39, 892 (1968)

9. E. Callen and H. B. Callen, J. Phys. Chem. Solids 16, 310 (1960)

10. H. B. Callen and E. Callen, J. Phys. Chem. Solids 27, 1271 (1966)

11. A. E. Clark, B. F. DeSavage, and R. Bozorth, Phys. Rev. 138, A216 (1965)

12. J. J. Rhyne and S. Legvold, Phys. Rev. 138, A507 (1965)

13. N. Tsuya, A. E. Clark, and R. M. Bozorth, Proc. Intl. Conf. on Magnetism, Institute of Physics and the Physical Society, London (1965) p. 250

14. E. Callen and H. B. Callen, Phys. Rev. 139, A455 (1965)

15. R. Truell, C. Elbaum, B. B. Chick, Ultrasonic Methods in Solid State Physics, New York: Academic Press, 1969 p. 7

16. W. C. Hubbell, P. L. Donoho, and F. R. Brotzen, unpublished

17. K. Salama, F. R. Brotzen, and P. L. Donoho, J. Appl. Phys. 43, 3254 (1972)

18. K. Salama, F. R. Brotzen, and P. L. Donoho, J. Appl. Phys. 44, 180 (1973)

19. M. Rosen and H. Klimker, Phys. Rev. B 1, 3748 (1970)

20. B. Luthi and R. J. Pollina, Phys. Rev. 167, 488 (1968)

21. R. J. Pollina and B. Luthi, Phys. Rev. 177, 841 (1969)

22. K. Salama. P. L. Donoho and F. R. Brotzen, unpublished

23. B. W. Southern and D. A. Goodings, Phys. Rev. B 7, 534 (1973)

24. R. A. Toupin, J. Ratl. Mach. Anal. 5, 849 (1956)

25. H. F. Tiersten, J. Math. Phys. 5, 1298 (1964)

26. W. F. Brown, J. Appl. Phys. 36, 994 (1965): Magneto-elastic Interactions, New York: Springer-Verlag,1966

27. K. Salama, C. L. Melcher, and P. L. Donoho, Proceedings of the IEEE Ultrasonics Symposium, 1973, p. 309

28. B. M. Kale, M. A. Thesis, Rice University; Houston, Texas (1972) unpublished

29. B. M. Kale, P. L. Donoho, D. G. Pinatti, and O. Ferreira, A.I.P. Conf. Proc. 24, 651 (1974)

30. S. Gama, M. A. Thesis, Universidade Estadual de Campinas; Campinas, Sao Paulo; Brazil (1975) unpublished

31. S. Gama, B. M. Kale, M. Torikachivili, O. Ferreira, M. Arrellano, D. G. Pinatti, and P. L. Donoho, A.I.P. Conf. Proc. 29, 596 (1975)

32. F. Freyne, Phys. Rev. B 5, 1327 (1972)

33. J. E. May Jr., IRE Nat. Conv. Rec. 6, Pt. 2, 134 (1958)

34. E. P. Papadakis, J. Acoust. Soc. Amer. 42, 1045 (1964); J. Appl. Phys. 35. 1474 (1964)

35. W. C. Hubbell, K. Salama, C. L. Melcher, and P. L. Donoho, A.I.P. Conf. Proc. 18, 1263 (1973)

36. S. Foner, Rev. Sci. Instr. 30, 548 (1959)

37. R. J. Elliott, in Magnetic Properties of the Rare Earth Metals, R. J. Elliott ed., London; Plenum Press (1972)

38. B. R. Cooper, in Solid State Physics, F. Seitz, D. Turnbull and H. Erenreich eds., New York: Academic Press (1968), Vol. 21, p. 393

39. R. M. Nicklow, N. Wakabayashi, M. K. Wilkinson, and R. E. Reed, Phys. Rev. Letters 26, 140 (1971)

40. A. H. Morrish, The Physical Principles of Magnetism, New York: John Wiley and Sons, 1965, p. 54

41. T. A. Kaplan and D. H. Lyons, Phys. Rev. 129, 2072 (1963)

41a. F. Specht, Phys. Rev. 162, 389 (1967)

42. R. M. Nicklow, N. Wakabayashi, M. K. Wilkinson, and R. E. Reed, Phys. Rev. Letters 27, 334 (1971)

43. J. Jensen, J. G. Houmann, and H. Bjerrum Moller, Phys. Rev. B 12, 303 (1975); J. Jensen and J. G. Houmann, Phys. Rev. B 12, 320 (1975); J. G. Houmann, J. Jensen, and P. Touborg, Phys. Rev. B 12, 332 (1975)

44. Per-Anker Lindgard, Phys. Rev. Letters 36, 385 (1976)

45. J. D. Jackson, Classical Electrodynamics, New York: John Wiley and Sons (1962) p. 78

46. K. W. H. Stevens, Proc. Phys. Soc. A 65, 209 (1952)

47. P. L. Donoho, J. Vasconcelos, B. M. Kale, M. Torikachivili, M. Arrellano, and D. G. Pinatti, in preparation

48. W. C. Koehler, J. Appl. Phys. 36, 1078 (1965)

49. R. J. Elliott and F. A. Wedgewood, Proc. Phys. Soc. 84, 63 (1964)

50. A. del Moral and E. W. Lee, J. Phys. C 8, 3881 (1975)

51. B. R. Cooper, Phys. Rev. Letters 19, 900 (1967)

52. A. del Moral and E. W. Lee, J. Phys. F 4, 1337 (1974)

53. F. J. Darnell, Phys. Rev. 130, 1825 (1963)

54. A. R. Edmonds, Angular Momentum in Quantum Mechanics, Princeton: University Press (1957)

55. H. B. Callen and S. Shtrikman, Solid State Commun. 3, 5 (1965)

56. C. Kittel, Thermal Physics, New York: John Wiley and Sons (1969) p. 365

57. J. L. Feron, G. Huy, and R. Pauthenet, Les Elements des Terres Rares II, 17 (Colloques Inter. du C.R.N.S. No. 180, 1970)

58. J. J. Rhyne and A. E. Clark, J. Appl. Phys. 38, 1379 (1967)

59. S. Liu, D. R. Behrendt, S. Legvold, and R. H. Good Jr., Phys. Rev. 116, 1461 (1959)

59a. H. B. Huntington in Solid State Physics, F. Sietz and D. Turnbull eds., New York: Academic Press (1958) Vol. 7

60. P. Touborg and J. Hog, Phys. Rev. Letters 33, 775 (1974)

61. D. E. Eastman, Phys. Rev. 148, 530 (1966)

62. R. L. Melcher, Phys. Rev. Letters 25, 1201 (1970)

63. M. Long Jr., A. R. Wazzan, and V. R. Stern, Phys. Rev. 178, 775 (1969)

64. E. S. Fisher and D. Dever, Proceedings of the Oak Ridge Conference on Rare Earths, 1968, p. 522 (unpublished)

65. J. W. Cable and E. O. Wollan, Phys. Rev. 165, 733 (1968)

66. P. R. Bevington, Data Reduction and Error Analysis for the Physical Sciences, New York: McGraw-Hill (1969)

67. K. Levenberg, Quart. Appl. Math. 2, 164 (1944)

68. H. A. Buckmaster, Can. J. Phys. 40, 1670 (1962)

69. H. Watanabe, Operator Methods in Ligand Field Theory, Englewood Cliffs: Prentice Hall (1966)

70. C. J. Bradely and A. P. Craknell, The Mathematical Theory of Symmetry in Solids, Oxford: Clarendon Press (1972)

71. A. H. Bobeck, P. I. Bonyhard, and J. E. Geusic, Proc. IEEE 63, 1176 (1975)

72. A. E. Clark and H. S. Belson, Phys. Rev. B 5, 3642 (1972)

73. L. B. McLane, B. M. Kale, and P. L. Donoho, Proc. 1973 IEEE Ultrasonics Symposium, p. 313;
L. B. McLane, Ph.D. Thesis, Rice University; Houston, Texas (1975) unpublished

## Appendix A

### Definition of the Angular Momentum Tensor Operators

Several different definitions of the angular momentum irreducible tensor operators have appeared in the literature since their introduction by Stevens in his treatment of the crystal field interaction. Most of the definitions differ by only a constant factor, but it is necessary to take such factors into consideration when comparing results obtained by different authors. Some of the more commonly used operators are those defined by Buckmaster[68], which are denoted by the symbol $\hat{O}$. Since the operators used in this thesis are slightly different from those of Buckmaster, they are given the symbol Q to emphasize the difference. The constant factors by which the Q's differ from the operators of Buckmaster are given in Appendix C. The definition of the Q's, taken from Watanabe[69], has the advantage that, given J, the $2\ell+1$ operators of rank $\ell$ can be formed from the definition of $Q_\ell^\ell$ and one recursion relation. They can easily be calculated numerically, when necessary, by simple matrix multiplications.

Since, by definition, the irreducible operators of rank $\ell$ transform under rotations like the $2\ell+1$ spherical harmonics, they are labeled with two integer indices, $\ell (\geq 0)$ and $m (-\ell \leq m \leq \ell)$. For a given value of $\ell$, $Q_\ell^\ell(\vec{J})$ is defined:

$$Q_\ell^\ell(\vec{J}) = (-1)^\ell (J_+)^\ell$$

where $J_{\pm} = J_x \pm J_y$. The other tensor operators of rank can be calculated from the recursion relation:

$$Q_{\ell}^{m-1}(\vec{J}) = \sqrt{\ell(\ell+1) - m(m-1)}\ [J_- , Q_{\ell}^{m}(\vec{J})]$$

All five of the second rank tensor operators are used in this thesis, so they are presented explicitly here.

$$Q_2^0(\vec{J}) = \sqrt{2/3}\ (3J_z^2 - J(J+1)$$

$$Q_2^1(\vec{J}) = -J_+(2J_z + 1) \qquad Q_2^{-1}(\vec{J}) = J_-(2J_z - 1)$$

$$Q_2^2(\vec{J}) = J_+^2 \qquad Q_2^{-2}(\vec{J}) = J_-^2$$

The operators, $Q_{\ell}^{m}(\vec{J})$, are not Hermitian, except for $Q_{\ell}^{0}(\vec{J})$, so when they appear in the Hamiltonian operator, they must occur (for $m \neq 0$) in Hermitian combinations. The standard definitions for these Hermitian operators, denoted by $Q_{\ell m}^{+}(J)$, are:

$$Q_{\ell m}^{+}(\vec{J}) = \frac{1}{2}\ ((-1)^m\ Q^{m}(\vec{J}) + Q^{-m}(\vec{J}))$$

$$Q^{-}{}_{m}(\vec{J}) = \frac{1}{2i}\ ((-1)^m\ Q^{m}(\vec{J}) - Q^{-m}(\vec{J}))$$

The Hermitian operators of second rank are then $Q_2^0$ and

$$Q_{21}^{+}(\vec{J}) = J_xJ_z + J_zJ_x \qquad Q_{21}^{-}(\vec{J}) = J_yJ_z + J_zJ_y$$

$$Q_{22}^{+}(\vec{J}) = J_x^2 - J_y^2 \qquad Q_{22}^{-}(\vec{J}) = J_xJ_y + J_yJ_x$$

The other operators that appear in the calculations are:

$$Q_4^0(\vec{J}) = \sqrt{2/35}\ (35J_z^4 - 30J(J+1)J_z^2 + 25J_z^2$$

$$+ 3J^2(J+1)^2 - 6J(J+1))$$

$$Q_6^0(\vec{J}) = \sqrt{4/231}\ (231J_z^6 - 315J(J+1)J_z^4 + 735J_z^4$$

$$+ 105J^2(J+1)^2J_z^2 - 525J(J+1)J_z^2 + 294J_z^2$$

$$- 5J^3(J+1)^3 + 40J^2(J+1)^2 - 60J(J+1))$$

$$Q_{66}^+(\vec{J}) = \frac{1}{2}\ (J_+^6 + J_-^6)$$

## Appendix B

### An Expansion of the Strain Dependence of the Anisotropy Energy of a 4f Electron in a Crystalline Field of HCP Symmetry

The anisotropy energy of a 4f electron at the point $\vec{r}$ is given by equations III-13 and 14, where the nucleus of the ion with which the electron is associated is taken as the origin of the coordinate system. In the unstrained hcp lattice, all the coefficients, $B_\ell^m$, in equation III-14 are equal to zero except for $B_2^0$, $B_4^0$, $B_6^0$, and $B_6^{+6}$, so the anisotropy energy of the 4f electron in the unstrained lattice is:

$$E_a = -e(B_2^0 r^2 Y_2^0(\theta,\phi) + B_4^0 r^4 Y_4^0(\theta,\phi) + B_6^0 r^6 Y_6^0(\theta,\phi) + B_6^6 r^6 Y_6^6(\theta,\phi) + B_6^{-6} r^6 Y_6^{-6}(\theta,\phi))$$

where $B_2^0$ is nonzero since the c/a ratios of the rare earth lattices are not exactly equal to the ratio for the close-packing of spheres. The symmetry of the strained lattice is lower than hcp in general, so all the $B_\ell^m$'s for $\ell = 2$, 4, and 6 will be nonzero.

The anisotropy energy in the strained lattice can be written as a Taylor series in the strains:

$$E_a = E_a(e_{ij}=\omega_{ij}=0) + \sum_{i,j} \left(\frac{\partial E_a}{\partial e_{ij}} e_{ij} + \frac{\partial E_a}{\partial \omega_{ij}} \omega_{ij}\right) + \frac{1}{2} \sum_{\substack{i,j \\ k,l}} \left(\frac{\partial^2 E_a}{\partial e_{ij}\partial e_{kl}} e_{ij}e_{kl} + 2 \frac{\partial^2 E_a}{\partial e_{ij}\partial \omega_{kl}} e_{ij}\omega_{kl}\right.$$

$$+ \frac{\partial^2 E_a}{\partial \omega_{ij} \partial \omega_{kl}} \omega_{ij} \omega_{kl})$$

where only terms of first and second order in the strains are considered. Since the point at which the 4f electron is located is not affected by the strain, only the $B_\ell^m$'s are functions of the strain and the strain dependence of the anisotropy energy is contained in the derivatives of the $B_\ell^m$'s with respect to the strains. Analytical calculation of these derivatives is a formidable task because they involve a summation over all the ions that contribute to the crystalline electric field. The derivatives can be calculated numerically, however, from the difference in the anisotropy energy in the unstrained lattice and the energy in a lattice in which only one of the components of the strain tensor is nonzero.

Donoho[47] has done this calculation of the strain dependence of the anisotropy energy, numerically, in a model that includes 164 neighboring ions taken in complete symmetric shells. Donoho's computation showed that the contribution of the terms linear in the finite strains to the terms quadratic in the infinitesimal strains is of the same order as the contribution from terms quadratic in the finite strains. Thus, the finite strain tensor is not particularly appropriate for an expansion of the anisotropy energy. It can certainly be used if all terms

of a given order in the infinitesimal strains are kept, but it is not a natural choice.

Donoho's computation also showed that the coefficients of the spherical harmonics with m=3 are all zero in the expansion of the anisotropy energy. This is understandable from a group theoretical point of view, since the spherical harmonics with m=3 are all basis functions of the irreducible representations $B_1$ or $B_2$ of the group $D_{6h}$. Since none of the symmetry strains transform according to these representations, there is no coupling between the symmetry strains and the spherical harmonics with m=3.

Although a calculation of an arbitrary coefficient that appears in the expansion of the anisotropy energy is difficult, the coefficients of the terms that are linear in the antisymmetric part of the strain tensor can be calculated explicitly.

When the symmetric part of the strain tensor is zero, the lattice retains its full symmetry, and only suffers a rotation described by the antisymmetric part of the strain tensor. A calculation of the crystalline electric field resulting from the rotated source ions is still a formidable task, but it can be avoided since, physically, a rotation of the lattice in one sense is equivalent to a rotation of the position of the 4f electron in the opposite sense.

In the calculation, it is convenient to express the

spherical harmonics in Cartesian coordinates since the Cartesian strains are being used. Only the term, $r^2 B_2^0 Y_2^0(\theta,\phi)$, of the anisotropy energy will be considered since it is expected that, as usual, the contribution from the second-order anisotropy will dominate the higher order terms.

Since the symmetric part of the strains tensor is zero, the position of a source ion in the strained lattice, as a function of its position in the unstrained lattice is:

$$x_i' = \sum_j (\delta_{ij} + \omega_{ij}) x_j$$

Equivalently, if the ions are considered fixed, the position of the 4f electron is given by a rotation in the opposite sense:

$$y_i' = \sum_j (\delta_{ij} - \omega_{ij}) y_j$$

In the rotated system, $Y_2^0$ is:

$$r^2 Y_2^0(\theta',\phi') = \sqrt{5/4\pi}\,\frac{1}{2}(3(z')^2 - r^2)$$

and, expressed in the unrotated coordinate system, z' is:

$$z' = z - \omega_{31} x - \omega_{32} y = z + \omega_{13} x + \omega_{23} y$$

so to first order in the strains $Y_2^0$ is:

$$r^2 Y_2^0(\theta',\phi') = r^2 Y_2^0(\theta,\phi) + (3/2)(\omega_{13} xz + \omega_{23} yz)$$

$$= r^2 Y_2^0(\theta,\phi) + r^2\sqrt{6}\,(\omega_{13} Y_{21}^{+}(\theta,\phi) + \omega_{23} Y_{21}^{-}(\theta,\phi))$$

In terms of the operator equivalents, the one-ion magnetoelastic Hamiltonian, linear in the $\omega_{ij}$'s is:

$$\sqrt{6}\ P_2^0\ (\omega_{13}\ Q_{21}^+(\vec{J}) + \omega_{23}\ Q_{21}^-(\vec{J}))$$

The higher order terms in the anisotropy can be treated in the same way.

The complete one-ion magnetoelastic Hamiltonian will depend on all spherical harmonics with $\ell = 2$, 4, or 6 ($m \neq 3$), and although the spherical harmonics with $\ell = 2$ are isomorphic to the symmetry strains, the higher order spherical harmonics are not. In order to write the Hamiltonian in group theoretical notation, the higher order spherical harmonics must be classified according to the irreducible representation under which they transform. This is straightforward using the tables found in Bradley and Cracknell[70]. The complete one-ion magnetoelastic Hamiltonian (linear in the strains) is[47]:

$$\mathcal{H}_{me}^{I} = \mathcal{H}_{me}^{I,2} + \mathcal{H}_{me}^{I,4} + \mathcal{H}_{me}^{I,6}$$

$$\mathcal{H}_{me}^{I,2} = -\ [B_1^{\alpha,2} e^{\alpha,1} + B_2^{\alpha,2} e^{\alpha,2}] \sum_i Q_2^0(\vec{J}_i)$$

$$- B^{\gamma,2}[e_1^{\gamma} \sum_i Q_{22}^+(\vec{J}_i) + e_2^{\gamma} \sum_i Q_{22}^-(\vec{J}_i)]$$

$$- B^{\varepsilon,2}[e_1^{\varepsilon} \sum_i Q_{21}^-(\vec{J}_i) + e_2^{\varepsilon} \sum_i Q_{21}^+(\vec{J}_i)]$$

$$+ \sqrt{6}\ P_2^0\ [\omega_{23} \sum_i Q_{21}^-(\vec{J}_i) + \omega_{13} \sum_i Q_{21}^+(\vec{J}_i)]$$

$$\mathcal{H}^{I,4}_{me} = - [B_1^{\alpha,4} e^{\alpha,1} + B_2^{\alpha,4} e^{\alpha,2}] \sum_i Q_4^0(\vec{J}_i)$$

$$- B_1^{\gamma,4} [e_1^{\gamma} \sum_i Q_{42}^{+}(\vec{J}_i) + e_2^{\gamma} \sum_i Q_{42}^{-}(\vec{J}_i)]$$

$$- B_2^{\gamma,4} [e_1^{\gamma} \sum_i Q_{44}^{+}(\vec{J}_i) - e_2^{\gamma} \sum_i Q_{44}^{-}(\vec{J}_i)]$$

$$- B^{\varepsilon,4} [e_1^{\varepsilon} \sum_i Q_{41}^{-}(\vec{J}_i) + e_2^{\varepsilon} \sum_i Q_{41}^{+}(\vec{J}_i)]$$

$$+ \sqrt{20}\, P_4^0 [\omega_{23} \sum_i Q_{41}^{-}(\vec{J}_i) + \omega_{13} \sum_i Q_{41}^{+}(\vec{J}_i)]$$

$$\mathcal{H}^{I,6}_{me} = - [B_1^{\alpha,6} e^{\alpha,1} + B_2^{\alpha,6} e^{\alpha,2}] \sum_i Q_6^0(\vec{J}_i)$$

$$- B_1^{\gamma,6} [e_1^{\gamma} \sum_i Q_{62}^{+}(\vec{J}_i) + e_2^{\gamma} \sum_i Q_{62}^{-}(\vec{J}_i)]$$

$$- B_2^{\gamma,6} [e_1^{\gamma} \sum_i Q_{64}^{+}(\vec{J}_i) - e_2^{\gamma} \sum_i Q_{64}^{-}(\vec{J}_i)]$$

$$- B_1^{\varepsilon,6} [e_1^{\varepsilon} \sum_i Q_{61}^{-}(\vec{J}_i) + e_2^{\varepsilon} \sum_i Q_{61}^{+}(\vec{J}_i)]$$

$$- B_2^{\varepsilon,6} [e_1^{\varepsilon} \sum_i Q_{65}^{-}(\vec{J}_i) - e_2^{\varepsilon} \sum_i Q_{65}^{+}(\vec{J}_i)]$$

$$- [B_3^{\alpha,6} e^{\alpha,1} + B_4^{\alpha,6} e^{\alpha,2}] \sum_i Q_{66}^{+}(\vec{J}_i)$$

$$+ \sqrt{42}\, P_6^0 [\omega_{23} \sum_i Q_{61}^{-}(\vec{J}_i) + \omega_{13} \sum_i Q_{61}^{+}(\vec{J}_i)]$$

$$- \sqrt{12}\, P_6^6 [\omega_{23} \sum_i Q_{65}^{-}(\vec{J}_i) - \omega_{13} \sum_i Q_{65}^{+}(\vec{J}_i)]$$

$$- 12\, P_6^6\, \omega_{12} \sum_i Q_{66}^{-}(\vec{J}_i)$$

## Appendix C

### Relations of the Quantities That Appear in this Thesis to Those that Appear in the Expressions of Callen and Callen, Southern and Goodings and in the Computer Programs

The quantities that appear in this thesis, the irreducible tensor operators, the symmetry strains, the symmetry elastic constants and the one and two-ion magneto-elastic constants are defined in terms of the corresponding quantities that appear in the theories of Callen and Callen[14] and Southern and Goodings[23], and in terms of the quantities that are defined in the computer programs of Appendix D. The relations are presented in tabular form.

| Notation used in this thesis | Notation used in Callen and Callen | Notation used in Southern and Goodings | Notation used in computer programs |
|---|---|---|---|
| $Q_2^0 =$ | $2\sqrt{2}\ S^{\alpha,2}$ | $2\sqrt{2/3}\ \hat{o}_{20}$ | $\sqrt{2/3}$ J2 |
| $Q_{21}^+ =$ | $2\ S_2^{\varepsilon}$ | $2\sqrt{2/3}\ (-i\hat{o}_{21}^-)$ | J21P |
| $Q_{21}^- =$ | $2\ S_1^{\varepsilon}$ | $2\sqrt{2/3}\ (i\hat{o}_{21}^+)$ | |
| $Q_{22}^+ =$ | $2\ S_1^{\gamma}$ | $2\sqrt{2/3}\ \hat{o}_{22}^+$ | J22P |
| $Q_{22}^- =$ | $2\ S_2^{\gamma}$ | $2\sqrt{2/3}\ \hat{o}_{22}^-$ | |
| $Q_4^0 =$ | | | $\sqrt{2/35}$ J4 |
| $Q_6^0 =$ | | | $\sqrt{4/231}$ J6 |
| $e^{\alpha,1} =$ | $e^{\alpha,1}$ | $e^{\alpha,1}$ | E1A |
| $e^{\alpha,2} =$ | $2\sqrt{3}\ e^{\alpha,2}$ | $3\ e^{\alpha,2}$ | E2A |
| $e_1^{\gamma} =$ | $2\ e_1^{\gamma}$ | $2\ e_1^{\gamma}$ | E1G |
| $e_2^{\gamma} =$ | $2\ e_2^{\gamma}$ | $2\ e_2^{\gamma}$ | |
| $e_1^{\varepsilon} =$ | $2\ e_1^{\varepsilon}$ | $2\ e_1^{\varepsilon}$ | |
| $e_2^{\varepsilon} =$ | $2\ e_2^{\varepsilon}$ | $2\ e_2^{\varepsilon}$ | E2E |
| $c_1^{\alpha} =$ | $c_{11}^{\alpha}$ | | C1A |
| $c_{12}^{\alpha} =$ | $\frac{1}{2\sqrt{3}}\ c_{12}^{\alpha}$ | | |
| $c_2^{\alpha} =$ | $\frac{1}{12}\ c_{22}^{\alpha}$ | | C2A |
| $c^{\gamma} =$ | $\frac{1}{4}\ c^{\gamma}$ | $\frac{1}{4}\ c^{\gamma}$ | CG |
| $c^{\varepsilon} =$ | $\frac{1}{4}\ c^{\varepsilon}$ | $\frac{1}{4}\ c^{\varepsilon}$ | CE |

| Notation used in this thesis | Notation used in Callen and Callen | Notation used in Southern and Goodings | Notation used in computer programs |
|---|---|---|---|
| $B_1^{\alpha,2} =$ | $\frac{1}{2\sqrt{2}} B_{12}^{\alpha}$ | $\frac{1}{2}\sqrt{3/2}\ M_{20}^{\alpha,1}$ | $\sqrt{3/2}$ B1A |
| $B_2^{\alpha,2} =$ | $\frac{1}{4\sqrt{6}} B_{22}^{\alpha}$ | $\frac{1}{2\sqrt{6}} M_{20}^{\alpha,2}$ | $\sqrt{3/2}$ B2A |
| $B^{\gamma,2} =$ | $\frac{1}{4} B^{\gamma}$ | $\frac{1}{4}\sqrt{3/2}\ M_{22}^{\gamma}$ | BG |
| $B^{\varepsilon,2} =$ | $\frac{1}{4} B^{\varepsilon}$ | $\frac{1}{4}\sqrt{3/2}\ M_{22}^{\varepsilon}$ | BE |
| $D_1^{\alpha,0} =$ | $D_{11}^{\alpha}$ | $D_{11}^{\alpha}$ | |
| $D_2^{\alpha,0} =$ | $\frac{1}{2\sqrt{3}} D_{21}^{\alpha}$ | $\frac{1}{3} D_{21}^{\alpha}$ | |
| $D_1^{\alpha,2} =$ | $\frac{1}{2\sqrt{3}} D_{12}^{\alpha}$ | $\frac{\sqrt{3}}{6} D_{12}^{\alpha}$ | |
| $D_2^{\alpha,2} =$ | $\frac{1}{12} D_{22}^{\alpha}$ | $\frac{\sqrt{3}}{18} D_{22}^{\alpha}$ | |
| $D^{\gamma,2} =$ | $\frac{1}{4} D^{\gamma}$ | $\frac{1}{4} D^{\gamma}$ | |
| $D^{\varepsilon,2} =$ | $\frac{1}{4} D^{\varepsilon}$ | $\frac{1}{4} D^{\varepsilon}$ | |

# Appendix D

The FORTRAN program and subroutines that were used to fit the elastic constant data are presented. Many other programs that were used for special purposes are not given, in the interest of brevity. All the programs and subroutines that were used for special purposes were fairly straightforward modifications of the programs presented here.

```
C       MAIN02
C       MAIN PROGRAM FOR ELASTIC CONSTANT CALCULATION
C       CONVERGES TO EXPERIMENTALLY MEASURED MAGNETIZATION.
C       INCLUDES THE TEMP. DEPENDENCE OF THE ELASTIC CONSTANTS.
C       OUTPUTS THE NECESSARY DERIVATIVES TO DISK DATA FILE.
C       NOTE THAT NXZ CANNOW BE 1,2,OR 3 . IE. H PARALLEL TO A,B,OR C
      IMPLICIT REAL*8(A-H,J,O-Z)
      COMMON/MISBLK/T,J,N,N1,N2,N6/JBLK/JZ(17),J2(17),J4(17),J6(17),
     1JX(16),J21P(16),J22P(15),J66P(11)/GBLK/Q,GX,GZ/SHBLK/SX,SZ,HX,HZ,
     1AX,AZ,U,F,Z/H0BLK/H0(17),H1(16),H2(15)/CBLK/C1A,C2A,CG,CE
     1/BBLK/B1A,B2A,BG,BE/G2BLK/G1A0,G2A0,G1A2,G2A2,GG/PBLK/P2,P4,P6,
     1P66/EBLK/EE(4)/FBLK/F1(5)/HAMBLK/H(17,17)/DIABLK/E(17),EX(17),
     1A(17,17)/CRBLK/DIV(153),ET(23,17)/SUMBLK/SC(5,4),SD(18,2),
        1 SK(10,2)/DERBLK/DER(18)/NEWBLK/SIG0/B4BLK/B1A4,B2A4
        2 /DRBLK/DEP(18,25),IEC,NXZ,NH,DF(25),ECAR(3,25)
        DIMENSION D0(18),F0(5),EE0(4),EEP(4),SIGV(25),
        1 HP(25),SP(25),THP(25),CP(25),EP(4,25)
  102   FORMAT(1H1)
        CALL ERRSET(0)
        TYPE 133
  133   FORMAT(//' WANT STANDARD VALUES? 1=YES, 2=NO,
        1    NUMBER OF FIRST TEMP TO BE RUN!)
        ACCEPT 201,NDATA,IT0
  139   FORMAT(1G)
        GO TO (901,902),NDATA
  901   CALL STD
        GO TO 951
  902   CALL PNT(1)
      ACCEPT 103, J
  103   FORMAT(1G)
  104   FORMAT(/' J = ',F5.1)
  951     CALL JCALC
      DO 11I=1,4
   11   EE(I)=0
        GO TO (952,800),NDATA
  800   CALL PNT (2)
        ACCEPT 105, G,GX,GZ
  105   FORMAT(3G)
      Q=6.7187364150-2*G
  106   FORMAT(/' G-FACTOR = ',F10.5,'   EXCHANGE CONSTANTS:  GX = ',F10.5
     1,'   GZ = ',F10.5)
  801   CALL PNT(3)
        ACCEPT 107, P2,P4,P6,P66
  107   FORMAT(4G)
  952   DO 132I=1,N
        DO 132K=1,N
  132   H(I,K)=0
        DO 131 I=1,N6
  131   H(I,I+6)=P66*J66P(I)
        GO TO (805,802),NDATA
  108   FORMAT(/ ' CRYSTAL-FIELD: P2 = ',1PD12.5,'   P4 = ',D12.5,'   P6
     1 = ',D12.5,'   P66 = ',D12.5)
  802   CALL PNT(4)
        ACCEPT 107, C1A,C2A,CG,CE
  110   FORMAT(/' ELASTIC CONSTANTS: C1A = ',1PD12.5,'   C2A = ',D12.5,'
     1   CG = ',D12.5,'   CE = ',D12.5)
  803   CALL PNT(5)
        ACCEPT 107, B1A,B2A,BG,BE
  112   FORMAT(/' ONE-ION ME CONSTANTS: B1A = ',1PD12.5,'   B2A = ',D12.5,
     1'   BG = ',D12.5,'   BE = ',D12.5)
  804   CALL PNT(6)
        ACCEPT 113, G1A0,G2A0,G1A2,G2A2,GG,GE
  113   FORMAT(6G)
  114   FORMAT(/' TWO-ION ME CONSTANTS: G1A0 = ',1PD12.5,'  G2A0 = ',D12.5
     1/23X,'G1A2 = ',D12.5,'   G2A2 = ',D12.5,'   GG = ',D12.5,'   GE =
     1',D12.5)
  805   WRITE(6,102)
        CALL PNT(8)
        ACCEPT 410,IFINA,JOFINA
  410   FORMAT(A5/A6)
```

```
      CALL OFILE(2,JOFINA)
      CALL IFILE(1,IFINA)
      READ(1,105) IEC,NXZ,NT
      WRITE(2,105) NT,IEC,NXZ
      IF(NXZ.EQ.2) P66=-P66
      G=Q/6.7187364150-2
      WRITE(6,104)J
      WRITE(6,106)G,GX,GZ
      WRITE(6,108)P2,P4,P6,P66
C     WRITE(6,110)C1A,C2A,CG,CE
      WRITE(6,112)B1A,B2A,BG,BE
      WRITE(6,114)G1A0,G2A0,G1A2,G2A2,GG,GE
      CALL PNT(9)
      IF(NXZ.EQ.2) WRITE(6,115)
  115 FORMAT(///' NOTE THAT THE SIGN OF P66 HAS BEEN CHANGED
     1 BECAUSE THE FIELD IS ALONG THE B-AXIS'/' THUS EXX=EBB AND
     2 EYY=EAA')
400   ACCEPT 201,NC,TL
201   FORMAT(2G)
      DO 1001 IT=1,NT
        SX=1
        READ(1,201) T,NH,(SIGV(II),DF(II),II=1,NH)
        IF(IT.LT.IT0) GO TO 1001
        CALL ELCON(T,IEC,ELCO)
      GO TO(401,401,402),NXZ
401   CONTINUE
      SZ=0
      HZ=0
      DHZ=0
        DHX=65/NH
        HX=-DHX
        WRITE(6,1401)T,HZ,TL
1401    FORMAT('1TEMP  =  ',F6.0,'   HZ  =  ',F6.0,'   MAGTOL  =  ',
     1 1PD12.5/)
        WRITE(6,500)C1A,C2A,CG,CE,IEC,IEC,ELCO
  500   FORMAT('   C1A=',F6.0,5X,' C2A=',F6.0,5X,' CG=',F6.0,5X,' CE=',
     1 F6.0,5X,'C',I1,I1,'=',F8.0/)
        WRITE (6,1902)
      GO TO 403
402   SX=0
      SZ=0
      HX=0
      DHX=0
        DHZ=65/NH
      HZ=-DHZ
        WRITE(6,1402)T,HX,TL
1402    FORMAT('1TEMP  =  ',F6.0,'   HX  =  ',F6.0,'   MAGTOL  =  ',
     1 1PD12.5/)
        WRITE(6,500)C1A,C2A,CG,CE,IEC,IEC,ELCO
        WRITE (6,1902)
1902    FORMAT(3X,' SIGMA'7X,'THETA',10X,'I 3/2',11X,'E1A',
     1 11X,'E2A',11X,'E1G',11X,'E2E',10X,'EXX',9X,'EYY',9X,'EZZ'/)
403   DO 404 K=1,5
404   F0(K)=0
      DO 405 K=1,18
405   D0(K)=0
      DO 601 K=1,4
        EE(K)=EE0(K)
601   EE0(K)=0
      DO 1000 K=1,NH
      HZ=HZ+DHZ
      HX=HX+DHX
        SIG0=SIGV(K)
      AX=Q*HX+GX*SX
      AZ=Q*HZ+GZ*SZ
        IF(SIG0.LT.1.D-10) AX=0
        IF(SIG0.LT.1.D-10) AZ=0
        NXZP=3
        IF(NXZ.EQ.3) NXZP=2
        IF(NXZ.LT.3) NXZP=1
      CALL MAGSTR(TL,NXZP)
      CALL ENCOR(NXZP)
```

```
      CALL SUMCAL
      CALL DERCAL
        DO 406 L=1,5
      F1(L)=F1(L)-F0(L)
      IF(K.EQ.1)F0(L)=F1(L)
  406 CONTINUE
      DO 407 L = 1,18
      DER(L)=DER(L)-D0(L)
      IF(K.EQ.1)D0(L)=DER(L)
  407 CONTINUE
      DO 710 L=1,4
      EEP(L)=EE(L)-EE0(L)
      IF(K.EQ.1)EE0(L)=EE(L)
  710 CONTINUE
      SIG=DSQRT(SX*SX+SZ*SZ)
      TH=57.29577951*DATAN(SZ/SX)
        HW=HX
        IF (NXZ.EQ.3)HW=HZ
        HP(K)=HW
        SP(K)=SIG
        THP(K)=TH
        CALL IS2(SIG,CA)
        CP(K)=CA
        DO 990 L=1,4
  990   EP(L,K)=EEP(L)
        DO 991 L=1,18
  991   DEP(L,K)=DER(L)
        ECAR(1,K)=EEP(1)/3-EEP(2)/6+EEP(3)/2
        ECAR(2,K)=ECAR(1,K)-EEP(3)
        ECAR(3,K)=EEP(1)/3+EEP(2)/3
        TYPE 999,IT,K,T,HX,HZ
  999   FORMAT(2G,F8.0,F8.0,F8.0)
 1000 CONTINUE
        DO 1301 I=1,NH
 1301   WRITE(6,1302)SP(I),THP(I),CP(I),(EP(K,I),K=1,4)
        1,(ECAR(K,I),K=1,3)

 1302   FORMAT(1PD12.4,6D14.5,3D12.3)
        WRITE (6,1910)
 1910   FORMAT('  SIG ',7X,'UAA',11X,'UAB',11X,'UAD',11X,'UAP',11X,
        1 'UAQ',11X,'UBB',11X,'UBD',11X,'UBP',11X,'UBQ'/)
        DO 1303 I=1,NH
 1303   WRITE(6,1304) SP(I),(DEP(L,I),L=1,9)
 1304   FORMAT(F8.6,1P7D14.5,2D13.4)
        WRITE(6,1920)
 1920   FORMAT('  SIG ',7X,'UDD',11X,'UDP',11X,'UDQ',11X,'UPP',11X,
        1 'UPQ',11X,'UQQ',11X,'UCC',11X,'UCE',11X,'UEE'/)
        DO 1305 I=1,NH
 1305   WRITE(6,1304)SIGV(I),(DEP(L,I),L=10,18)
        CALL VEC(ELCO,T)
 1001   CONTINUE
      GO TO(400,599),NC
  599   ENDFILE 1
        ENDFILE 2
        STOP
      END



C     HOUSEHOLDER TRIDIAGONALIZATION OF SYMMETRIC MATRIX
      SUBROUTINE TRED
      IMPLICIT REAL*8(A-H,O-Z)
        COMMON /HAMBLK/A(17,17)/DIABLK/D(17),E(17),Z(17,17)
        1 /MISBLK/T,TT,N,N1,N2,N6
      DO 10 I=1,N
      DO 10 J=I,N
      Z(I,J)=A(I,J)
   10 Z(J,I)=Z(I,J)
      DO 20 II=2,N
      I=N+2-II
      L=I-2
```

```
      F=Z(I,I-1)
      G=0
      IF(L.EQ.0)GO TO 21
      DO 30 K=1,L
30    G=G+Z(I,K)**2
21    H=G+F*F
      IF(G.GT.1.32D-23)GO TO 101
      E(I)=F
      H=0
      GOTO102
101   L=L+1
      E(I)=DSQRT(H)
      IF(F.GE.0)E(I)=-E(I)
      G=E(I)
      H=H-F*G
      Z(I,I-1)=F-G
      F=0
      DO 50 J=1,L
      Z(J,I)=Z(I,J)/H
      G=0
      DO 60 K=1,J
60    G=G+Z(J,K)*Z(I,K)
      JJ=J+1
      IF(L.LT.JJ)GO TO 71
      DO 70 K=JJ,L
70    G=G+Z(K,J)*Z(I,K)
71    E(J)=G/H
50    F=F+G*Z(J,I)
      HH=F/(H+H)
      DO 80 J=1,L
      F=Z(I,J)
      E(J)=E(J)-HH*F
      G=E(J)
      DO 90 K=1,J
90    Z(J,K)=Z(J,K)-F*E(K)-G*Z(I,K)
80    CONTINUE
102   D(I)=H
20    CONTINUE
      D(1)=0
      E(1)=0
      DO 100 I=1,N
      L=I-1
      IF(D(I).EQ.0.OR.L.EQ.0)GO TO 98
      DO 120 J=1,L
      G=0
      DO 121 K=1,L
121   G=G+Z(I,K)*Z(K,J)
      DO 122 K=1,L
122   Z(K,J)=Z(K,J)-G*Z(K,I)
120   CONTINUE
98    D(I)=Z(I,I)
      Z(I,I)=1
      IF(L.EQ.0)GOTO100
      DO123 J=1,L
      Z(I,J)=0
123   Z(J,I)=0
100   CONTINUE
      RETURN
      END
```

```
C     QL ALGORITHM FOR EIGENVALUES AND EIGENVECTORS OF SYMMETRIC MATRIX
C
C
C
      SUBROUTINE TQL
      IMPLICIT REAL*8(A-H,O-Z)
        COMMON/DIABLK/D(17),E(17),Z(17,17)/MISBLK/T,U,N,N1,N2,N6
      DO 10I=2,N
10    E(I-1)=E(I)
      E(N)=0
      B=0
      F=0
      DO 20 L=1,N
      J=0
      H=1.11D-16*(DABS(D(L))+DABS(E(L)))
      IF(B.LT.H)B=H
      DO 30 M=L,N
      IF(DABS(E(M)).LE.B)GO TO 31
30    CONTINUE
31    CONTINUE
      IF(M.EQ.L)GO TO 32
40    CONTINUE
      IF(J.EQ.30)GO TO 1000
      J=1+J
      G=D(L)
      P=(D(L+1)-G)/(2*E(L))
      R=DSQRT(1+P*P)
      X=P-R
      IF(P.GT.0)X=P+R
      D(L)=E(L)/X
      H=G-D(L)
      IF(L.EQ.N)GO TO 51
      LL=L+1
      DO 50 I=LL,N
50    D(I)=D(I)-H
51    F=F+H
      P=D(M)
      C=1
      S=0
      IF((M-1).LT.L)GO TO 61
      MM=M-1
      DO 60 II=L,MM
      I=MM-II+L
      G=C*E(I)
      H=C*P
      IF(DABS(P).LT.DABS(E(I)))GO TO 100
      C=E(I)/P
      R=DSQRT(1+C*C)
      E(I+1)=S*P*R
      S=C/R
      C=1/R
      GO TO 101
100   C=P/E(I)
      R=DSQRT(1+C*C)
      E(I+1)=S*E(I)*R
      S=1/R
      C=C/R
101   P=C*D(I)-S*G
      D(I+1)=H+S*(C*G+S*D(I))
      DO 70 K=1,N
      H=Z(K,I+1)
      Z(K,I+1)=S*Z(K,I)+C*H
70    Z(K,I)=C*Z(K,I)-S*H
60    CONTINUE
61    E(L)=S*P
      D(L)=C*P
      IF(DABS(E(L)).GT.B)GOTO40
32    D(L)=D(L)+F
20    CONTINUE
      DO 200 I=1,N
      K=I
```

```
      P=D(I)
      IF(I.EQ.N)GO TO 211
      JJ=1+I
      DO 210 J=JJ,N
      IF(D(J).GE.P)GO TO 210
      K=J
      P=D(J)
  210 CONTINUE
  211   CONTINUE
        IF(K.EQ.I)GO TO 230
        D(K)=D(I)
      D(I)=P
      DO 240 J=1,N
      P=Z(J,I)
      Z(J,I)=Z(J,K)
  240 Z(J,K)=P
  230 CONTINUE
  200 CONTINUE
      RETURN
 1000 WRITE(6,1001)
 1001 FORMAT(1H1'EIGENVALUE ROUTINE FAILED')
      STOP
      END
```

```
C     CALCULATION OF J OPERATORS
C
C
C
C
C
      SUBROUTINE JCALC
      IMPLICIT REAL*8(A-H,J,O-Z)
      COMMON/JBLK/JZ(17),J2(17),J4(17),J6(17),JX(16),J21P(16),J22P(15),
     1J66P(11)/MISBLK/I,J,N,N1,N2,N6
      N=2*J+1.01
      JS=J*(J+1)
      N1=N-1
      N2=N-2
      N6=N-6
      DO 10 I=1,N
      R=J+1-I
      R2=R*R
      R4=R2*R2
      JZ(I)=R
      J2(I)=3*R2-JS
      J4(I)=35*R4-(30*JS-25)*R2+3*JS*(JS-2)
      J6(I)=R4*(231*R2-315*JS+735)+R2*(105*JS*(JS-5)+294)-5*JS*(JS*(JS-8
     1)+12)
      IF(I.NE.N)JX(I)=DSQRT(JS-R*(R-1))/2
   10 CONTINUE
      DO 20 I=1,N2
20    J22P(I)=JX(I)*JX(I+1)*2
      DO 30 I = 1, N6
30    J66P(I)=4*J22P(I)*J22P(I+2)*J22P(I+4)
      DO 43 I= 1,N1
43    J21P(I)=JX(I)*(JZ(I)+JZ(I+1))
      RETURN
      END
```

```
      SUBROUTINE PNT(N)
      GO TO (1,2,3,4,5,6,7,8,9),N
1     TYPE 10
10    FORMAT(/' ENTER J'/)
      RETURN
2     TYPE 20
20    FORMAT(/' ENTER G, GX, GZ'/)
      RETURN
3     TYPE 30
30    FORMAT(/' ENTER P2, P4, P6, P66'/)
      RETURN
4     TYPE 40
40    FORMAT(/' ENTER C1A, C2A, CG, CE'/)
      RETURN
5     TYPE 50
50    FORMAT(/' ENTER B1A, B2A, BG, BE'/)
      RETURN
6     TYPE 60
60    FORMAT(/' ENTER G1A0, G2A0, G1A2, G2A2, GG, GE'/)
      RETURN
7     TYPE 70
70    FORMAT(/' ENTER T0, DT, NT, HQ, DH, NH, NXZ, NC, TL'/)
      TYPE 80
80    FORMAT(/' ENTER INPUT FILENAME(5LETTERS) <CR>
     1  OUTPUT FILENAME(6LETTERS)')
      RETURN
      TYPE 90
90    FORMAT(/' ENTER NC,TL')
      RETURN
      END
```

```
      SUBROUTINE STD
      IMPLICIT REAL*8(A-H,J,O-Z)
      COMMON/CBLK/C1A,C2A,CG,CE/BBLK/B1A,B2A,BG,BE/GBLK/Q,GX,GZ
     1 /G2BLK/G1A0,G2A0,G1A2,G2A2,GG/MISBLK/T,J,N,N1,N2,N6
     1 /PBLK/P2,P4,P6,P66
      J=7.5
      G=4./3.
      Q=G*6.7187384150-2
      GX=57.14285714
      GZ=49.26108374
      P2=.32
      P4=-.07/60
      P6=4*1.0822510-6/7
      P66=-9.7703222D-9
      C1A=89050
      C2A=21260
      CG=58290
      CE=55000
      G1M=-7.26268
      G1P=11.4622
      G2M=4.37473
      G2P=23.1078
      G1A0=(2*G1M+G1P)/3
      G1A2=(G1P-G1M)/3
      G2A0=(2*G2M+G2P)/3
      G2A2=(G2P-G2M)/3
      GG=-14.5483
      GE=0
      B1A=-12.3053
      B2A=-6.6977
      BG=30.176
      BE=0.
      RETURN
      END
```

```
      SUBROUTINE ELCON(T,IEC,ELCO)
      DOUBLE PRECISION C1A,C2A,CG,CE,T,ELCO
      COMMON/CBLK/C1A,C2A,CG,CE
      DIMENSION C11V(17),C33V(17),C44V(17),C12V(17),C13V(17),TV(17),
     1 C66V(17)
      DATA TV/0.,25.,50.,70.,80.,85.,90.,100.,110.,150.,170.,
     1 175.,180.,185.,190.,200.,300./,
     2 C11V/7.726,7.726,7.45,6.98,6.754,6.688,6.614,7.74,
     3 7.777,7.556,7.373,7.34,7.31,7.33,7.16,7.32,7.07/,
     4 C33V/8.52,8.52,8.48,8.42,8.378,8.331,8.4,8.4,
     5 8.266,8.1,7.94,7.87,7.84,7.878,7.94,7.963,7.9/,
     6 C44V/2.702,2.7,2.689,2.65,2.64,2.633,2.633,2.678,
     7 2.675,2.625,2.59,2.565,2.565,2.56,2.555,2.546,2.47/,
     8 C66V/2.825,2.825,2.792,2.754,2.742,2.735,2.727,2.733,
     9 2.733,2.694,2.644,2.619,2.594,2.583,2.572,2.55,2.458/,
     1 C12V/2.5,2.476,2.271,1.9,1.61,1.595,1.588,2.653,
     2 2.67,2.55,2.5,2.47,2.53,2.6,2.62,2.6,2.53/,
     3 C13V/1.98,1.947,2.038,2.015,1.968,1.935,1.905,1.922,
     4 1.959,2.072,2.147,2.138,2.13,2.16,2.16,2.14,2.08/
      C=22283
      TE=SNGL(T)
      DO 100 I=1,17
      IF(TE.EQ.TV(I)) GO TO 120
      IF(TV(I).GT.TE) GO TO 140
  100 CONTINUE
      GO TO 200
  120 C11=C11V(I)
      C33=C33V(I)
      C44=C44V(I)
      C66=C66V(I)
      C12=C12V(I)
      C13=C13V(I)
      GO TO 160
  140 C11=(C11V(I)-C11V(I-1))*(TE-TV(I))/(TV(I)-TV(I-1))+C11V(I)
      C33=(C33V(I)-C33V(I-1))*(TE-TV(I))/(TV(I)-TV(I-1))+C33V(I)
      C44=(C44V(I)-C44V(I-1))*(TE-TV(I))/(TV(I)-TV(I-1))+C44V(I)
      C66=(C66V(I)-C66V(I-1))*(TE-TV(I))/(TV(I)-TV(I-1))+C66V(I)
      C12=(C12V(I)-C12V(I-1))*(TE-TV(I))/(TV(I)-TV(I-1))+C12V(I)
      C13=(C13V(I)-C13V(I-1))*(TE-TV(I))/(TV(I)-TV(I-1))+C13V(I)
  160 ELCO=C*C11
      IF(IEC.EQ.3) ELCO=C33*C
      IF(IEC.EQ.4) ELCO=C44*C
      IF(IEC.EQ.6) ELCO=C66*C
      C1A=C*DBLE(2*C11+C33+2*C12+4*C13)/9
      C2A=C*DBLE(C11+C12+2*C33-4*C13)/18
      CG=C*DBLE(C66)
      CE=C*DBLE(C44)
  155 FORMAT(7F15.4)
      RETURN
  200 TYPE 220,TE
  220 FORMAT('   DIDNT FIND TEMP=',F6.0)
      RETURN
      END



      SUBROUTINE I52(S,F)
      IMPLICIT DOUBLE PRECISION (A-H,O-Z)
      IF (S.LT.1.D-3)GO TO 20
      X0=3.*S
   10 V=DEXP(-2.D0*X0)
      C=(1.D0+V)/(1.D0-V)-1.D0/X0-S
      D=1.D0/X0**2-4.D0*V/((1.D0-V)**2)
      DEL=-C/D
      X0=X0+DEL
      IF(1.D-10.LT.(DABS(DEL)/X0))GO TO 10
      F=1.D0-3.D0*S/X0
      RETURN
   20 F=0.6D0*S**2
      RETURN
      END
```

```
C     CALCULATION OF MAGNETIZATION AND MAGNETOSTRICTION
      SUBROUTINE MAGSTR(TL,NXZ)
      IMPLICIT REAL*8(A-H,J,O-Z)
      COMMON/SHBLK/SX,SZ,HX,HZ,AX,AZ,U,F,Z/HØBLK/HØ(17),H1(16),H2(15)
     1/GBLK/Q,GX,GZ/CBLK/C1A,C2A,CG,CE/BBLK/B1A,B2A,BG,BE/G2BLK/G1AØ
     1,G2AØ,G1A2,G2A2,GG/PBLK/P2,P4,P6,PGG/MISBLK/T,J,N,N1,N2,N6/
     1JBLK/JZ(17),J2(17),J4(17),J6(17),JX(16),J21P(16),J22P(15),J66P(11)
     1/EBLK/E1A,E2A,E1G,E2E/FBLK/FA,FB,FD,FP,FQ/HAMBLK/H(17,17)
        FD=Ø
        FP=Ø
        FQ=Ø
       G1M=G1AØ-G1A2
       G2M=G2AØ-G2A2
       G1P=G1AØ+2*G1A2
       G2P=G2AØ+2*G2A2
       DEL=1.D-6
         NT=Ø
         IF(DABS(B1A).LT.1.D-6)NT=1
       GZØ=GZ
       GXØ=GX
  100  P2P=P2-B1A*E1A-B2A*E2A
       P22=-BG*E1G
       P21=-BE*E2E
       GX=GXØ+J*(G1M*E1A+G2M*E2A+GG*E1G)
       GZ=GZØ+J*(G1P*E1A+G2P*E2A)
       DO 10 I=1,N
   10  HØ(I)=P2P*J2(I)+P4*J4(I)+P6*J6(I)
       DO 11 I=1,N1
   11  H1(I)=P21*J21P(I)
       DO 12 I=1,N2
   12  H2(I)=P22*J22P(I)
       CALL CONV(NT,NXZ)
       IF(NT)14,14,15
   14  FØ=F
       DO2ØI=1,N
   20  H(I,I)=H(I,I)+DEL*J2(I)
         CALL SIGMA
       FA=(F-FØ)/DEL
         DO 21 I=1,N
   21    H(I,I)=H(I,I)-DEL*J2(I)
         IF(NXZ.EQ.1)GO TO 450
         DO 451 I=1,N
  451    H(I,I)=H(I,I)+DEL*JZ(I)
         CALL SIGMA
       FQ=J*SZ*(F-FØ)/DEL
       DO 22 I=1,N
   22  H(I,I)=H(I,I)-DEL*JZ(I)
  450    CONTINUE
         IF(NXZ.NE.3)GO TO 452
       DO 23 I=1,N1
   23  H(I,I+1)=H(I,I+1)+DEL*J21P(I)
         CALL SIGMA
       FD=(F-FØ)/DEL
         DO ØØ I=1,N1
   ØØ    H(I,I+1)=H(I,I+1)-2*DEL*J21P(I)
         CALL SIGMA
         FD=.5*(FD-(F-FØ)/DEL)
       DO 24 I=1,N1
   24  H(I,I+1)=H(I,I+1)+DEL*J21P(I)
  452    CONTINUE
         IF(NXZ.EQ.2)GO TO 453
         DO 454 I=1,N1
  454    H(I,I+1)=H(I,I+1)+DEL*JX(I)
         CALL SIGMA
       FP=J*SX*(F-FØ)/DEL
       DO 25 I=1,N1
   25  H(I,I+1)=H(I,I+1)-DEL*JX(I)
  453    DO 26 I=1,N2
   26  H(I,I+2)=H2(I)+DEL*J22P(I)
         CALL SIGMA
```

```
      FB=(F-F0)/DEL
      E1A1=(B1A*FA-G1M*FP-G1P*FQ)/C1A
      E2A1=(B2A*FA-G2M*FP-G2P*FQ)/C2A
      E1G1=(BG*FB-GG*FP)/CG
      E2E1=BE*FD/CE
      D=DMAX1(DABS(E1A1-E1A),DABS(E2A1-E2A),DABS(E1G1-E1G),DABS(E2E1-E2E
     1))
      E1A=E1A1
      E2A=E2A1
      E1G=E1G1
      E2E=E2E1
      DD=DMAX1(DABS(E1A),DABS(E2A),DABS(E1G),DABS(E2E)) + 1.E-6
      NT=1
        DDD=D/DD
      IF((D/DD).GT.TL)NT=0
      GO TO 100
15    GX=GX0
      GZ=GZ0
        IF(DABS(E1A).LT.1.D-6)E1A=0
        IF(DABS(E2A).LT.1.D-6)E2A=0
        IF(DABS(E1G).LT.1.D-6)E1G=0
        IF(DABS(E2E).LT.1.D-6)E2E=0
      RETURN
      END



C     CONVERGENCE OF FIELD VS SIGMA
      SUBROUTINE CONV(NT,NXZ)
      IMPLICIT REAL*8(A-H,J,O-Z)
      COMMON/SHBLK/SX,SZ,HX,HZ,AX,AZ,U,F,Z/H0BLK/H0(17),H1(16),H2(15)
     1 /GBLK/Q,GX,GZ/HAMBLK/H(17,17)/MISBLK/T,J,N,N1,N2,N6/JBLK/JZ
     1(17),DU(51),JX(16),DD(42)/NEWBLK/SIG0
        FQ(SX)=SIG0-SX
        FW(SZ)=SIG0-SZ
      D=1.D-6
        DO 3 I=1,N2
3       H(I,I+2)=H2(I)
      TL=1.D-5
      IF(NT.NE.0)TL=1.D-9
        GO TO (200,300,100),NXZ
100   DO 20 I=1,N
20    H(I,I)=H0(I)+AZ*JZ(I)
      DO 21 I=1,N1
21      H(I,I+1)=H1(I)+AX*JX(I)
101   CALL SIGMA
        FX=FQ(SX)
        FZ=FW(SZ)
        IF(DABS(FX).LE.TL.AND.DABS(FZ).LE.TL)RETURN
      DO 30 I=1,N
30    H(I,I)=H(I,I)+D*JZ(I)
      AZ=AZ+D
      CALL SIGMA
      FX1=FQ(SX)
      FZ1=FW(SZ)
      DO 40 I=1,N
40    H(I,I)=H(I,I)-D*JZ(I)
      AZ=AZ-D
      DO 41 I=1,N1
41      H(I,I+1)=H(I,I+1)+D*JX(I)
      AX=AX+D
      CALL SIGMA
      FX2=FQ(SX)
      FZ2=FW(SZ)
      AX=AX-D
      FXZ=(FX1-FX)/D
      FXX=(FX2-FX)/D
      FZX=(FZ2-FZ)/D
      FZZ=(FZ1-FZ)/D
```

```
      DEN=FXX*FZZ-FXZ*FZX
      D2=(FXZ*FZ-FZZ*FX)/DEN
      D1=(FZX*FX-FXX*FZ)/DEN
      AX=AX+D2
      AZ=AZ+D1
      GO TO 100
200   DO 70 I=1,N
70    H(I,I)=H0(I)
201   DO 71 I=1,N1
71    H(I,I+1)=H1(I)+AX*JX(I)
      CALL SIGMA
      FX=FQ(SX)
      IF(DABS(FX/SX).LE.TL.OR.SX.LT.1.D-10)RETURN
      DO 72 I=1,N
72    H(I,I+1)=H(I,I+1)+D*JX(I)
      AX=AX+D
      CALL SIGMA
      AX1=AX+D
      FX1=FQ(SX)
      D1=D*FX/(FX-FX1)
      AX=AX+D1-D
      GO TO 201
300   DO 80 I=1,N1
80    H(I,I+1)=H1(I)
301   DO 81 I=1,N
81    H(I,I)=H0(I)+AZ*JZ(I)
      CALL SIGMA
      FZ=FW(SZ)
      IF(DABS(FZ/SZ).LE.TL.OR.SZ.LT.1.D-10)RETURN
      AZ=AZ+D
      DO 82 I=1,N
82    H(I,I)=H(I,I)+D*JZ(I)
      CALL SIGMA
      FZ1=FW(SZ)
      D1=D*FZ/(FZ-FZ1)
      AZ=AZ+D1-D
      GO TO 301
      END
```

```
C     CALCULATION OF MAGNETIZATION AND THERMODYNAMIC FUNCTIONS
C
C
C
      SUBROUTINE SIGMA
      IMPLICIT REAL*8(A-H,J,O-Z)
      COMMON/SHBLK/SX,SZ,HX,HZ,AX,AZ,U,F,Z/DIABLK/E(17),EX(17),A(17,17)
     1/HAMBLK/H(17,17)/MISBLK/T,J,N,N1,N2,N6/JBLK/JZ(17),W(51),JX(16)
     1,DV(42)
      DIMENSION XP(17),ZP(17),G(17)
      CALL TRED
      CALL TQL
      DO 10 I=1,N
      S1=0
      S2=0
      DO20K=1,N
20    S1=S1+JZ(K)*A(K,I)**2
      ZP(I)=-S1/J
      DO 30 K=1,N1
30    S2=S2+JX(K)*A(K,I)*A(K+1,I)
10    XP(I)=-2*S2/J
      S1=0
      S2=0
      S3=0
      S4=0
      DO 40 I=1,N
      V=DEXP((E(1)-E(I))/T)
```

```
      EX(I)=V
      S1=S1+V
      S2=S2+E(I)*V
      S3=S3+ZP(I)*V
40    S4=S4+XP(I)*V
      Z=S1
      U=S2/S1
      SX=S4/S1
      SZ=S3/S1
      F=E(1)-T*DLOG(Z)
        IF(DABS(SX).LT.1.D-10)SX=0
        IF(DABS(SZ).LT.1.D-10)SZ=0
      RETURN
      END



C     CALC. OF FIRST AND SECOND ORDER ENERGY CORRECTIONS
C
C
C
      SUBROUTINE ENCOR(NXZ)
      IMPLICIT REAL*8(A-H,J,O-Z)
      COMMON/JBLK/JZ(17),J2(17),J4(17),J6(17),JX(16),J21P(16),J22P(15),
     1J66P(11)/DIABLK/E(17),EX(17),A(17,17)/CRBLK/DIV(153),ET(23,17)/MI
     1SBLK/T,J,N,N1,N2,N6/SHBLK/SX,SZ,HX,HZ,AX,AZ,U,F,Z
      DIMENSION JA(153),JB(153),JC(153),JD(153),JE(153),JP(153),JQ(153)
      DIV(1)=0
      DO 10 K=2,N
      M=(K*(K-1))/2
      L=K-1
      DIV(K+M)=0
      DO 10 I=1,L
   10 DIV(I+M)=1/(E(I)-E(K))
      DO 20 K=1,N
      M=(K*(K-1))/2
      DO 21 I=1,K
      IK=I+M
      S1=0
      S2=0
      S3=0
      S4=0
      S5=0
      S6=0
      S7=0
      DO 22 L=1,N
      P=A(L,I)*A(L,K)
      IF(NXZ.NE.1)S1=S1+P*JZ(L)
   22 S2=S2+P*J2(L)
      JA(IK)=S2
        IF(NXZ.NE.1)JQ(IK)=J*SZ*S1
        DO 23 L=1,N1
      P=A(L,I)*A(L+1,K)
      Q=A(L+1,I)*A(L,K)
      IF(NXZ.NE.2)S3=S3+JX(L)*(P+Q)
      S4=S4+J21P(L)*(P+Q)
   23 S5=S5+J21P(L)*(Q-P)
        IF(NXZ.NE.2)JP(IK)=S3*J*SX
      JD(IK)=S4
      JE(IK)=S5
      DO 24 L=1,N2
      P=A(L,I)*A(L+2,K)
      Q=A(L+2,I)*A(L,K)
      S6=S6+J22P(L)*(Q+P)
   24 S7=S7+J22P(L)*(Q-P)
      JB(IK)=S6
   21 JC(IK )=S7
```

```
      ET(1,K)=S2
      ET(2,K)=S6
      ET(3,K)=S4
        IF(NXZ.NE.2)ET(4,K)=S3*J*SX
        IF(NXZ.NE.1)ET(5,K)=S1*J*SZ
20      CONTINUE
      CALL COR1 (6,JA)
      CALL COR1 (11,JB)
      CALL COR1 (15,JD)
      CALL COR1 (21,JC)
      CALL COR1 (23,JE)
        IF(NXZ.NE.2)CALL COR1 (18,JP)
        IF(NXZ.NE.1)CALL COR1 (20,JQ)
      CALL COR2 (7,JA,JB)
      CALL COR2 (8,JA,JD)
        IF(NXZ.NE.2)CALL COR2 (9,JA,JP)
        IF(NXZ.NE.1)CALL COR2 (10,JA,JQ)
      CALL COR2 (12,JB,JD)
        IF(NXZ.NE.2)CALL COR2 (13,JB,JP)
        IF(NXZ.NE.1)CALL COR2 (14,JB,JQ)
        IF(NXZ.NE.2)CALL COR2 (16,JD,JP)
        IF(NXZ.NE.1)CALL COR2 (17,JD,JQ)
        IF(NXZ.EQ.3)CALL COR2 (19,JP,JQ)
      CALL COR2 (22,JC,JE)
      RETURN
       END


C     SECOND ORDER CORRECTIONS FOR EQUAL OPERATORS
C
C
C
      SUBROUTINE COR1(M,J)
      IMPLICIT REAL *8(A-H,J,O-Z)
      COMMON/CRBLK/DIV(153),ET(23,17)/MISBLK/T,Q,N,N1,N2,N6
      DIMENSION J(153)
      DO 10 I=1,N
      S=0
      IF(I.EQ.1)GO TO 11
      L=I-1
      DO 12 K=1,L
      MK=K+(I*(I-1))/2
   12 S=S-DIV(MK)*J(MK)**2
   11 CONTINUE
      IF(I.EQ.N)GO TO 13
      L=I+1
      DO 14 K=L,N
      MK=I+(K*(K-1))/2
   14 S=S+DIV(MK)*J(MK)**2
   13 ET(M,I)=S
   10 CONTINUE
      RETURN
      END



C     SECOND ORDER ENERGY CORRECTIONS FOR UNEQUAL OPERATORS
C
C
C
      SUBROUTINE COR2(M,J1,J2)
      IMPLICIT REAL*8(A-H,J,O-Z)
      COMMON/CRBLK/DIV(153),ET(23,17)/MISBLK/T,J,N,N1,N2,N6
      DIMENSION J1(153),J2(153)
      DO 10 I=1,N
      S=0
      IF (I.EQ.1)GO TO 11
      L=I-1
      DO 12 K=1,L
```

```
      MK=K+(I*(I-1))/2
   12 S=S-DIV(MK)*J1(MK)*J2(MK)
   11 CONTINUE
      IF(I.EQ.N)GO TO 13
      L=I+1
      DO 14 K=L,N
      MK=I+(K*(K-1))/2
   14 S=S+DIV(MK)*J1(MK)*J2(MK)
   13 ET(M,I)=2*S
   10 CONTINUE
      RETURN
      END



C     CALC. OF EQUILIBRIUM SUMS
C
C
C
      SUBROUTINE SUMCAL
      IMPLICIT REAL*8(A-H,J,Q-Z)
      COMMON/SHBLK/DA(6),U,F,Z/CRBLK/DB(153),ET(23,17)/DIABLK/E(17),
     1EX(17),DC(289)/MISBLK/T,J,N,N1,N2,N6/SUMBLK/SC(5,4),SD(18,2),
     1SE(10,2)
      DO 10 I=1,5
      S1=0
      S2=0
      S3=0
      S4=0
      DO 11 K=1,N
      X=ET(I,K)
      Y=X*X
      W=E(K)
      V=EX(K)
      S1=S1+V*X
      S2=S2+V*Y
      S3=S3+V*W*X
   11 S4=S4+V*W*Y
      SC(I,1)=S1/Z
      SC(I,2)=S2/Z
      SC(I,3)=S3/Z
   10 SC(I,4)=S4/Z
      DO 20 I=1,18
      L=I+5
      S1=0
      S2=0
      DO 21 K=1,N
      X=ET(L,K)
      V=EX(K)
      S1=S1+V*X
   21 S2=S2+V*X*E(K)
      SD(I,1)=S1/Z
   20 SD(I,2)=S2/Z
      LL=0
      DO 30 I=1,4
      M=I+1
      DO 30 K=M,5
      LL=LL+1
      S1=0
      S2=0
      DO 31 L=1,N
      V=EX(L)
      W=ET(I,L)*ET(K,L)
      S1=S1+V*W
   31 S2=S2+V*W*E(L)
      SE(LL,1)=S1/Z
   30 SE(LL,2)=S2/Z
      RETURN
      END
```

```
C     SECOND DERIVS. OF INTERNAL ENERGY
C
C
C
C
      SUBROUTINE DERCAL
      IMPLICIT REAL*8(A-H,J,O-Z)
      COMMON/SUMBLK/SC(5,4),SD(18,2),SE(10,2)/MISBLK/T,D1(3)/SHBLK/D2(6)
     1,U,F,Z/DERBLK/D(18)
      U1=1+U/T
      T2=T*T
      D(1)=F1(1,1)
      D(6)=F1(6,2)
      D(10)=F1(10,3)
      D(13)=F1(13,4)
      D(15)=F1(15,5)
      D(16)=2*(SD(16,1)*U1-SD(16,2)/T)
      D(18)=2*(SD(18,1)*U1-SD(18,2)/T)
      D(2)=F2(2,1,2,1 )
      D(3)=F2(3,1,3,2)
      D(4)=F2(4,1,4,3 )
      D(5)=F2(5,1,5,4)
      D(7)=F2(7,2,3,5)
      D(8)=F2(8,2,4,6)
      D(9)=F2(9,2,5,7)
      D(11)=F2(11,3,4,8)
      D(12)=F2(12,3,5,9)
      D(14)=F2(14,4,5,10)
      D(17)=SD(17,1)*U1-SD(17,2)/T
      RETURN
      END



      REAL*8FUNCTION F1(L,M)
      IMPLICIT REAL*8(A-H,J,O-Z)
      COMMON/SUMBLK/SC(5,4),SD(18,2),SE(10,2)/SHBLK/D(6),U,F,Z/MISBLK/
     1T,J,N1,N2,N3,N4
      U1=1+U/T
      T2=T*T
      F1      =2*(SD(L,1)*U1-SD(L,2)/T+(SC(M,1)**2*U1-SC(M,2))/T-SC(M,1)
     1*SC(M,3)/T2+(SC(M,4)-U*SC(M,2))/(2*T2))
      RETURN
      END



      REAL*8FUNCTION F2(L,M,N,K)
      IMPLICIT REAL*8(A-H,J,O-Z)
      COMMON/SUMBLK/SC(5,4),SD(18,2),SE(10,2)/SHBLK/D(6),U,F,Z/MISBLK/
     1T,J,N1,N2,N3,N4
      U1=1+U/T
      T2=T*T
      F2   =SD(L,1)*U1-SD(L,2)/T+2*(SC(M,1)*SC(N,1)*U1-SE(K,1))/T
     1-(SC(M,1)*SC(N,3)+SC(N,1)*SC(M,3))/T2+(SE(K,2)-SE(K,1)*U)/T2
      RETURN
      END
```

```
C       NOTE THAT THIS SUBROUTINE WAS WRITTEN ESPECIALLY FOR MY DY
C       SAMPLE AND MY PARTICULAR DATA SET,
C       IT MUST BE CHANGED FOR OTHER MATERIALS AND SETS OF DATA.
              SUBROUTINE VEC(ELCO,T)
        IMPLICIT DOUBLE PRECISION(A-H,O-Z)
        COMMON/DRBLK/DEP(18,25),IEC,NXZ,NH,DF(25),ECAR(3,25)
        DIMENSION V(6,25),I1X(6),I1Z(6),I3X(3),I3Z(3),DFC(25)
        DATA I1X/1,6,13,2,4,8/,I1Z/1,6,15,2,5,9/,I3X/1,13,4/,
       1 I3Z/1,15,5/
        K=1
        IF(IEC.EQ.3.OR.IEC.EQ.4) K=2
        IF((IEC-NXZ).EQ.0.AND.IEC.LT.3) K=0
        K1=MOD(K,3)+1
        K2=MOD(K+1,3)+1
        K3=MOD(K+2,3)+1
        DO 200 I=1,NH
        IF( IEC.GT.3) GO TO 100
        IF (IEC.EQ.3) GO TO 50
        DO 20 J=1,6
        IF(NXZ.NE.3) V(J,I)=DEP(I1X(J),I)
        IF(NXZ.EQ.3) V(J,I)=DEP(I1Z(J),I)
   20   CONTINUE
        GO TO 190
   50   DO 60 J=1,3
        IF(NXZ.NE.3) V(J,I)=DEP(I3X(J),I)
        IF(NXZ.EQ.3) V(J,I)=DEP(I3Z(J),I)
   60   CONTINUE
        GO TO 190
  100   IF(IEC.EQ.6) GO TO 150
        V(1,I)=DEP(10,I)
        V(2,I)=DEP(18,I)
        GO TO 190
  150   V(1,I)=DEP(16,I)
  190   DF(I)=2.*ELCO*DF(I)
        DFC(I)=DF(I)+ELCO*(ECAR(K1,I)-ECAR(K2,I)-ECAR(K3,I))
  200   CONTINUE
        IF(IEC.LT.3) GO TO 240
        IF(IEC.EQ.3) GO TO 260
        IF(IEC.EQ.4) GO TO 280
        IF(IEC.EQ.6) GO TO 300
  240   WRITE(2,250) T,NH,(DF(J),DFC(J),(V(I,J),I=1,6),J=1,NH)
  250   FORMAT(2G/(8E))
        RETURN
  260   WRITE(2,270) T,NH,(DF(J),DFC(J),(V(I,J),I=1,3),J=1,NH)
  270   FORMAT(2G/(5E))
        RETURN
  280   WRITE(2,290) T,NH,(DF(J),DFC(J),(V(I,J),I=1,2),J=1,NH)
  290   FORMAT(2G/(4E))
        RETURN
  300   WRITE(2,310) T,NH,(DF(J),DFC(J),V(1,J),J=1,NH)
  310   FORMAT(2G/(3E))
        RETURN
        END
```

## Appendix E

In this appendix, the experimental elastic wave velocities are presented as a function of the sample magnetization. The format is, more or less, self-explanatory. Each set of data begins with the frequency, polarization and direction of propagation of the elastic wave, the direction of the applied magnetic field, and the sample from which the data were obtained.

Each subset of the data begins with the temperature at which the data were taken. The data follows in two columns. The left column contains the experimentally measured magnetization, $\sigma$ $(=M/M_0)$, and the right column contains the relative change in the frequency of best overlap:

$$\frac{\Delta f}{f}(\sigma) = \frac{f(\sigma) - f(\sigma=0)}{f(\sigma=0)} .$$

DyB

$\vec{v}\,||b$ $\vec{p}\,||b$

$\vec{H}\,||a$ f=10MHz

| | |
|---|---|
| 140.0000 | 14 |
| 0.00000000E-01 | 0.00000000E-01 |
| 4.5403900E-02 | -1.5747936E-04 |
| 7.4930362E-02 | -3.4160907E-03 |
| 7.1030641E-01 | 2.0514715E-02 |
| 7.2144847E-01 | 2.2870848E-02 |
| 7.2701950E-01 | 2.3652188E-02 |
| 7.3119777E-01 | 2.4118570E-02 |
| 7.3676880E-01 | 2.4282106E-02 |
| 7.4094708E-01 | 2.4633406E-02 |
| 7.4651811E-01 | 2.4609178E-02 |
| 7.4930362E-01 | 2.4778771E-02 |
| 7.5487465E-01 | 2.4724260E-02 |
| 7.5905292E-01 | 2.4572837E-02 |
| 7.6044568E-01 | 2.4348732E-02 |
| 160.0000 | 15 |
| 0.00000000E-01 | 0.00000000E-01 |
| 4.1782730E-02 | -1.3844413E-04 |
| 8.2172702E-02 | -7.0425926E-04 |
| 1.0863510E-01 | -2.4197626E-03 |
| 6.0724234E-01 | -4.2917680E-03 |
| 6.1142062E-01 | -3.6236246E-03 |
| 6.2116992E-01 | -3.0457708E-03 |
| 6.3231198E-01 | -2.5040329E-03 |
| 6.4066853E-01 | -2.0224881E-03 |
| 6.4902507E-01 | -2.1428743E-03 |
| 6.5738162E-01 | -1.7997737E-03 |
| 6.6295265E-01 | -1.0533792E-03 |
| 6.6991644E-01 | -6.5610478E-04 |
| 6.7688023E-01 | -7.2231718E-05 |
| 6.7966574E-01 | 2.1067585E-04 |
| 170.0000 | 14 |
| 0.00000000E-01 | 0.00000000E-01 |
| 7.1030641E-02 | -4.9640409E-04 |
| 1.0863510E-01 | -1.7979514E-03 |
| 1.2534819E-01 | -3.6988159E-03 |
| 4.7632312E-01 | -7.1070537E-03 |
| 4.9582173E-01 | -4.5644962E-03 |
| 5.2367688E-01 | -1.9977238E-03 |
| 5.3760446E-01 | -8.5962660E-04 |
| 5.5431755E-01 | 1.8766496E-04 |
| 5.6824513E-01 | 7.0223018E-04 |
| 5.8217270E-01 | 1.1502046E-03 |
| 5.9331477E-01 | 1.3560307E-03 |
| 6.0445683E-01 | 1.5860716E-03 |
| 6.1699165E-01 | 1.8584885E-03 |
| 175.0000 | 15 |
| 0.00000000E-01 | 0.00000000E-01 |
| 8.0779945E-02 | -9.3754240E-04 |
| 2.6183844E-01 | -4.7493924E-04 |
| 3.7325905E-01 | -3.0531809E-03 |
| 4.2061281E-01 | -4.8850893E-03 |
| 4.5682451E-01 | -2.2513354E-03 |
| 4.8467967E-01 | -3.0840211E-04 |
| 5.0835655E-01 | 1.6221951E-03 |
| 5.2646240E-01 | 2.7016024E-03 |
| 5.4456825E-01 | 3.0963571E-03 |
| 5.4874652E-01 | 3.3122386E-03 |
| 5.5710307E-01 | 3.4911118E-03 |
| 5.6545961E-01 | 3.7069933E-03 |
| 5.7520892E-01 | 3.8982026E-03 |
| 5.8217270E-01 | 4.0647398E-03 |
| 180.0000 | 18 |
| 0.00000000E-01 | 0.00000000E-01 |
| 5.2331762E-02 | -4.8183071E-04 |
| 9.5379571E-02 | -2.8726869E-03 |
| 1.3045912E-01 | -4.7268202E-03 |
| 1.7075557E-01 | -7.5446150E-03 |
| 2.0257382E-01 | -6.6480440E-03 |
| 2.7114071E-01 | -5.1293623E-03 |
| 3.2513277E-01 | -3.3789141E-03 |
| 3.5327601E-01 | -2.2261798E-03 |
| 3.9377454E-01 | -3.7814562E-04 |
| 4.3389860E-01 | 1.5186816E-03 |
| 4.5918174E-01 | 2.8848851E-03 |
| 4.7943193E-01 | 3.8973395E-03 |
| 4.9858940E-01 | 4.9646860E-03 |
| 5.1377020E-01 | 5.6050939E-03 |
| 5.3071252E-01 | 6.1784115E-03 |
| 5.4857294E-01 | 6.5748545E-03 |
| 5.5712039E-01 | 6.7639273E-03 |
| 185.0000 | 15 |
| 0.00000000E-01 | 0.00000000E-01 |
| 8.5802196E-02 | -7.1928171E-04 |
| 1.7123383E-01 | -2.8523240E-03 |
| 2.5053959E-01 | -2.5918944E-03 |
| 2.9622074E-01 | -2.5050846E-03 |
| 3.3582393E-01 | -1.7920036E-03 |
| 3.7114208E-01 | -3.4723945E-04 |
| 4.0319253E-01 | 7.3788381E-04 |
| 4.2792987E-01 | 1.9904261E-03 |
| 4.4414748E-01 | 2.6911057E-03 |
| 4.5874699E-01 | 3.3111761E-03 |
| 4.7083245E-01 | 3.9312465E-03 |
| 4.8342360E-01 | 4.7869437E-03 |
| 4.9545594E-01 | 5.4876234E-03 |
| 5.0674736E-01 | 6.1759015E-03 |

190.0000 17

0.0000000E-01 0.0000000E-01
4.6498078E-02 -9.2997302E-05
9.6481950E-02 -7.2537896E-04
1.4398173E-01 -1.5809541E-03
1.7835980E-01 -2.0521405E-03
2.1216919E-01 -2.3931306E-03
2.2049709E-01 -2.4489290E-03
2.5213353E-01 -2.3993304E-03
2.8639094E-01 -2.0273412E-03
3.2143914E-01 -1.3763601E-03
3.5315724E-01 -5.0218544E-04
3.8040705E-01 3.5338975E-04
4.0539699E-01 1.2399640E-03
4.2675381E-01 1.9715428E-03
4.4793744E-01 2.7093214E-03
4.6755065E-01 3.1247094E-03
4.7496499E-01 3.3417031E-03

195.0000 18

0.0000000E-01 0.0000000E-01
4.0400357E-02 -1.2405486E-04
8.2380312E-02 -5.2723314E-04
1.2139435E-01 -1.0296553E-03
1.5550480E-01 -1.5134693E-03
1.8124995E-01 -1.7801872E-03
2.0020509E-01 -1.9538640E-03
2.2219928E-01 -2.0282969E-03
2.4305138E-01 -1.9848777E-03
2.6760907E-01 -1.8298091E-03
2.8538383E-01 -1.6127131E-03
3.1575948E-01 -9.9864160E-04
3.4176860E-01 -4.7140845E-04
3.6648840E-01 2.2950148E-04
3.8791290E-01 9.1180319E-04
4.0962035E-01 1.6251186E-03
4.3004946E-01 2.1523518E-03
4.3745566E-01 2.3756505E-03

200.0000 17

0.0000000E-01 0.0000000E-01
3.5317612E-02 -1.4895730E-04
7.1385509E-02 -4.3445878E-04
1.0753043E-01 -8.2547170E-04
1.3457303E-01 -1.1109732E-03
1.6132506E-01 -1.4150943E-03
1.9364228E-01 -1.5888778E-03
2.2363288E-01 -1.6385303E-03
2.3855756E-01 -1.5888778E-03
2.5109464E-01 -1.4957795E-03
2.7934148E-01 -1.1916584E-03
3.0254056E-01 -8.0685203E-04
3.2514342E-01 -4.1583913E-04
3.4769142E-01 1.6137041E-04
3.6945144E-01 8.5029791E-04
3.9018603E-01 1.4213009E-03
3.9797221E-01 1.6571499E-03

E3

210.0000 16

0.0000000E-01 0.0000000E-01
2.8976760E-02 -1.8643731E-05
7.6113411E-02 -2.6722681E-04
9.9414869E-02 -4.5987869E-04
1.3128337E-01 -7.0846176E-04
1.5371338E-01 -8.7004077E-04
1.7829674E-01 -1.0005469E-03
2.0160352E-01 -1.0751218E-03
2.2187898E-01 -9.9433231E-04
2.4655218E-01 -8.5761162E-04
2.6483873E-01 -6.8981803E-04
2.7625626E-01 -6.1524312E-04
2.8829699E-01 -3.8530376E-04
3.0764981E-01 -4.9716615E-05
3.2668353E-01 3.2315800E-04
3.3253546E-01 4.2880581E-04

220.0000 13

0.0000000E-01 0.0000000E-01
4.5399401E-02 -8.7102593E-05
9.3374744E-02 -3.1730231E-04
1.2645305E-01 -5.1017234E-04
1.4701176E-01 -6.2216139E-04
1.6694674E-01 -7.0926398E-04
1.8760084E-01 -7.5903688E-04
2.0555517E-01 -7.0926398E-04
2.2462108E-01 -7.2792882E-04
2.4198123E-01 -6.0971815E-04
2.5935107E-01 -4.6662104E-04
2.7656931E-01 -3.6085360E-04
2.8299628E-01 -2.2397810E-04

230.0000 14

0.0000000E-01 0.0000000E-01
2.9890669E-02 -3.1146050E-05
6.0997007E-02 -1.1212578E-04
9.0860172E-02 -1.9310551E-04
1.0923599E-01 -2.6785603E-04
1.2732726E-01 -3.4883576E-04
1.4434570E-01 -4.5473233E-04
1.6247142E-01 -4.4227391E-04
1.7803998E-01 -4.6096154E-04
1.9523639E-01 -4.9833680E-04
2.1014055E-01 -5.1702443E-04
2.2583795E-01 -4.0489864E-04
2.4095257E-01 -3.3637734E-04
2.4667519E-01 -2.8654366E-04

240.0000 10

| | |
|---|---|
| 0.00000000E-01 | 0.00000000E-01 |
| 3.5355122E-02 | -2.4951656E-05 |
| 7.0645750E-02 | -8.1092881E-05 |
| 9.5992051E-02 | -2.0585116E-04 |
| 1.2658979E-01 | -3.3060944E-04 |
| 1.5609369E-01 | -3.1813361E-04 |
| 1.7124285E-01 | -3.5556110E-04 |
| 1.8459444E-01 | -3.4932319E-04 |
| 1.9921176E-01 | -3.3684736E-04 |
| 2.1259524E-01 | -3.1813361E-04 |

260.0000 8

| | |
|---|---|
| 0.00000000E-01 | 0.00000000E-01 |
| 2.7920893E-02 | -4.0636403E-05 |
| 5.5951897E-02 | -7.5643787E-05 |
| 7.6184105E-02 | -1.3002916E-04 |
| 1.0072480E-01 | -1.9755300E-04 |
| 1.2463962E-01 | -2.7569993E-04 |
| 1.4752301E-01 | -3.3946293E-04 |
| 1.7025035E-01 | -3.4509196E-04 |

280.0000 8

| | |
|---|---|
| 0.00000000E-01 | 0.00000000E-01 |
| 2.2878108E-02 | 4.7629761E-05 |
| 4.3116249E-02 | -2.7578990E-05 |
| 6.2637326E-02 | 9.4010938E-06 |
| 8.3079953E-02 | -3.4470677E-05 |
| 1.0322050E-01 | -6.4559074E-05 |
| 1.2280450E-01 | -1.0905514E-04 |
| 1.4215865E-01 | -1.6671028E-04 |

300.0000 9

| | |
|---|---|
| 0.00000000E-01 | 0.00000000E-01 |
| 1.4745348E-02 | 1.3598483E-05 |
| 2.9643593E-02 | -2.1641635E-05 |
| 4.4178803E-02 | -2.9684788E-05 |
| 5.3487166E-02 | -3.5868112E-05 |
| 7.0842423E-02 | -1.2057482E-04 |
| 8.7852845E-02 | -1.0388468E-04 |
| 1.0454650E-01 | -1.5458311E-04 |
| 1.2112529E-01 | -1.7190125E-04 |

DyA

$\vec{v} \mid\mid b$ $\vec{p} \mid\mid b$

$\vec{H} \mid\mid b$ f=20MHz

195.0000 20

| | |
|---|---|
| 0.00000000E-01 | 0.00000000E-01 |
| 3.7349896E-02 | 4.8212521E-05 |
| 5.5917753E-02 | 2.2900947E-04 |
| 7.3864512E-02 | 4.0980642E-04 |
| 9.2810074E-02 | 6.0265650E-04 |
| 1.1108593E-01 | 8.7987851E-04 |
| 1.2805394E-01 | 1.1571005E-03 |
| 1.4602530E-01 | 1.5428007E-03 |
| 1.8179648E-01 | 2.4045995E-03 |
| 2.1506785E-01 | 3.2181857E-03 |
| 2.4822437E-01 | 4.4295253E-03 |
| 2.8034505E-01 | 5.7372899E-03 |
| 3.1118773E-01 | 7.0571077E-03 |
| 3.3803362E-01 | 8.3106332E-03 |
| 3.5126184E-01 | 8.8650773E-03 |
| 3.6458810E-01 | 9.5219727E-03 |
| 3.7706350E-01 | 1.0136682E-02 |
| 3.8870427E-01 | 1.0697153E-02 |
| 4.0002882E-01 | 1.1227491E-02 |
| 4.0833995E-01 | 1.1685510E-02 |

200.0000 20

| | |
|---|---|
| 0.00000000E-01 | 0.00000000E-01 |
| 3.3208500E-02 | 1.8226445E-05 |
| 5.3350878E-02 | 1.4581156E-04 |
| 6.5705935E-02 | 2.8554764E-04 |
| 8.1820071E-02 | 4.2528372E-04 |
| 9.8411349E-02 | 5.5286884E-04 |
| 1.1433487E-01 | 8.2019003E-04 |
| 1.2966457E-01 | 1.1118132E-03 |
| 1.6116771E-01 | 1.7558142E-03 |
| 1.9213026E-01 | 2.6428346E-03 |
| 2.2276683E-01 | 3.5845343E-03 |
| 2.5111216E-01 | 4.5687623E-03 |
| 2.7921270E-01 | 5.7838586E-03 |
| 3.0552885E-01 | 6.6344261E-03 |
| 3.1727546E-01 | 7.1690685E-03 |
| 3.2969869E-01 | 7.8434469E-03 |
| 3.4162751E-01 | 8.3720139E-03 |
| 3.5408690E-01 | 8.8884297E-03 |
| 3.6492061E-01 | 9.3987703E-03 |
| 3.7306641E-01 | 9.7146953E-03 |

| 210.0000 | 20 |
|---|---|
| 0.0000000E-01 | 0.0000000E-01 |
| 2.6676768E-02 | 3.6583581E-05 |
| 4.0089912E-02 | 8.5361688E-05 |
| 5.3869792E-02 | 1.4633432E-04 |
| 6.7013247E-02 | 2.4998781E-04 |
| 8.0501529E-02 | 4.3900297E-04 |
| 9.3143142E-02 | 5.5485097E-04 |
| 1.0630514E-01 | 6.2192088E-04 |
| 1.3244108E-01 | 1.1401883E-03 |
| 1.5760439E-01 | 1.5608995E-03 |
| 1.8292050E-01 | 2.1340422E-03 |
| 2.0772660E-01 | 2.8657139E-03 |
| 2.3064822E-01 | 3.6522608E-03 |
| 2.5347668E-01 | 4.5180723E-03 |
| 2.6488488E-01 | 4.8534218E-03 |
| 2.7564307E-01 | 5.3046192E-03 |
| 2.8630276E-01 | 5.7558167E-03 |
| 2.9695285E-01 | 6.1948197E-03 |
| 3.0726233E-01 | 6.6643090E-03 |
| 3.1497360E-01 | 6.9996585E-03 |

| 220.0000 | 20 |
|---|---|
| 0.0000000E-01 | 0.0000000E-01 |
| 2.3806628E-02 | 3.6305767E-05 |
| 3.3657537E-02 | 6.6560573E-05 |
| 4.5376839E-02 | 1.2707019E-04 |
| 5.6342987E-02 | 2.0573268E-04 |
| 6.8317939E-02 | 3.1464998E-04 |
| 7.8867826E-02 | 4.2961824E-04 |
| 8.8931598E-02 | 5.5668842E-04 |
| 1.1030032E-01 | 8.2898168E-04 |
| 1.3264771E-01 | 1.2101922E-03 |
| 1.5339863E-01 | 1.6579634E-03 |
| 1.7383537E-01 | 2.1480912E-03 |
| 1.9409024E-01 | 2.7108306E-03 |
| 2.1359636E-01 | 3.3401306E-03 |
| 2.2258107E-01 | 3.6487296E-03 |
| 2.3203128E-01 | 3.9996853E-03 |
| 2.4181590E-01 | 4.3627429E-03 |
| 2.5019412E-01 | 4.7318516E-03 |
| 2.5898850E-01 | 5.1070112E-03 |
| 2.6574382E-01 | 5.4035083E-03 |

| 230.0000 | 20 |
|---|---|
| 0.0000000E-01 | 0.0000000E-01 |
| 9.7781329E-03 | -1.1555216E-05 |
| 2.9514996E-02 | 1.1555216E-05 |
| 3.9032366E-02 | 4.6220866E-05 |
| 4.8392974E-02 | 9.8219341E-05 |
| 5.8605331E-02 | 1.4444021E-04 |
| 6.7980240E-02 | 2.0799390E-04 |
| 7.7861438E-02 | 2.7732519E-04 |
| 9.7160017E-02 | 4.6798627E-04 |
| 1.1581111E-01 | 7.0486820E-04 |
| 1.3459948E-01 | 9.9374862E-04 |
| 1.5307555E-01 | 1.3288499E-03 |
| 1.7177019E-01 | 1.7101720E-03 |
| 1.8973743E-01 | 2.1030494E-03 |
| 1.9867735E-01 | 2.3052657E-03 |
| 2.0786612E-01 | 2.5305924E-03 |
| 2.1640727E-01 | 2.7501415E-03 |
| 2.2536636E-01 | 2.9870235E-03 |
| 2.3398748E-01 | 3.2296830E-03 |
| 2.4063144E-01 | 3.4261217E-03 |

| 240.0000 | 15 |
|---|---|
| 0.0000000E-01 | 0.0000000E-01 |
| 1.6771495E-02 | 1.1656442E-04 |
| 3.4019717E-02 | 1.7177914E-04 |
| 5.0543618E-02 | 2.3926380E-04 |
| 6.7778638E-02 | 3.6196319E-04 |
| 8.3786665E-02 | 4.7239263E-04 |
| 1.0003845E-01 | 5.7055214E-04 |
| 1.1641779E-01 | 7.9754600E-04 |
| 1.3248938E-01 | 1.1226994E-03 |
| 1.4834936E-01 | 1.6871165E-03 |
| 1.6404881E-01 | 2.0429447E-03 |
| 1.7951909E-01 | 2.3680982E-03 |
| 1.9491739E-01 | 2.6257669E-03 |
| 2.0232777E-01 | 2.7730061E-03 |
| 2.0724658E-01 | 2.8957055E-03 |

| 250.0000 | 15 |
|---|---|
| 0.0000000E-01 | 0.0000000E-01 |
| 1.5667311E-02 | -6.1396776E-06 |
| 3.0844529E-02 | 1.8419033E-05 |
| 4.6462983E-02 | 4.9117421E-05 |
| 6.1385626E-02 | 1.2279355E-04 |
| 7.6764028E-02 | 2.0874904E-04 |
| 9.1623384E-02 | 3.7452034E-04 |
| 1.0642578E-01 | 5.2187259E-04 |
| 1.2124755E-01 | 7.9201841E-04 |
| 1.3551512E-01 | 1.0007675E-03 |
| 1.4949681E-01 | 1.2279355E-03 |
| 1.6317261E-01 | 1.4551036E-03 |
| 1.7670196E-01 | 1.6208749E-03 |
| 1.8350898E-01 | 1.7436684E-03 |
| 1.8836587E-01 | 1.8541826E-03 |

| 260.0000 | | 15 |
|---|---|---|
| 0.0000000E-01 | 0.0000000E-01 | |
| 1.4164463E-02 | 1.8447688E-05 | |
| 2.7522269E-02 | 4.9193836E-05 | |
| 4.1325402E-02 | 8.6089212E-05 | |
| 5.5144312E-02 | 1.3528305E-04 | |
| 6.8995231E-02 | 2.2752149E-04 | |
| 8.3209529E-02 | 3.9355069E-04 | |
| 9.7139295E-02 | 5.8417680E-04 | |
| 1.1129054E-01 | 9.1008596E-04 | |
| 1.2571860E-01 | 1.1806520E-03 | |
| 1.3997188E-01 | 1.5496058E-03 | |
| 1.5460783E-01 | 1.7156350E-03 | |
| 1.6946453E-01 | 1.8816642E-03 | |
| 1.7702360E-01 | 1.9308581E-03 | |
| 1.8263331E-01 | 1.9493057E-03 | |

| 270.0000 | | 15 |
|---|---|---|
| 0.0000000E-01 | 0.0000000E-01 | |
| 1.2799566E-02 | 5.5395183E-05 | |
| 2.5188694E-02 | 6.1550202E-05 | |
| 3.7852062E-02 | 1.4156547E-04 | |
| 5.0285766E-02 | 2.0927069E-04 | |
| 6.2549303E-02 | 2.7697591E-04 | |
| 7.5387118E-02 | 4.3085142E-04 | |
| 8.7549455E-02 | 5.6010685E-04 | |
| 1.0030800E-01 | 7.0167231E-04 | |
| 1.1223196E-01 | 8.6170284E-04 | |
| 1.2495900E-01 | 1.0648185E-03 | |
| 1.3746346E-01 | 1.2186940E-03 | |
| 1.4940618E-01 | 1.3848796E-03 | |
| 1.5534720E-01 | 1.4710499E-03 | |
| 1.5999467E-01 | 1.5202900E-03 | |

| 280.0000 | | 15 |
|---|---|---|
| 0.0000000E-01 | 0.0000000E-01 | |
| 1.1690373E-02 | 1.8481897E-05 | |
| 2.2982533E-02 | 5.5445691E-05 | |
| 3.4217805E-02 | 8.0088219E-05 | |
| 4.5794402E-02 | 1.1089138E-04 | |
| 5.7570107E-02 | 1.9714023E-04 | |
| 6.8407167E-02 | 2.3410403E-04 | |
| 8.0040652E-02 | 3.2651351E-04 | |
| 9.1332813E-02 | 3.8811983E-04 | |
| 1.0285252E-01 | 4.5588679E-04 | |
| 1.1388869E-01 | 5.4829627E-04 | |
| 1.2537996E-01 | 6.4686639E-04 | |
| 1.3692811E-01 | 7.8856093E-04 | |
| 1.4241775E-01 | 8.5016726E-04 | |
| 1.4657053E-01 | 8.9945232E-04 | |

| 290.0000 | | 15 |
|---|---|---|
| 0.0000000E-01 | 0.0000000E-01 | |
| 1.0606664E-02 | 3.0836787E-05 | |
| 2.1358472E-02 | 1.8502072E-05 | |
| 3.1588909E-02 | 5.5506217E-05 | |
| 4.2123996E-02 | 6.7840931E-05 | |
| 5.2559308E-02 | 1.0484507E-04 | |
| 6.2780855E-02 | 1.5418394E-04 | |
| 7.2958961E-02 | 1.9735544E-04 | |
| 8.3360128E-02 | 2.5902901E-04 | |
| 9.3462560E-02 | 3.0220051E-04 | |
| 1.0326048E-01 | 3.8237615E-04 | |
| 1.1294528E-01 | 4.8722123E-04 | |
| 1.2284404E-01 | 6.4757252E-04 | |
| 1.2775160E-01 | 7.2158081E-04 | |
| 1.3114524E-01 | 7.8942174E-04 | |

| 300.0000 | | 15 |
|---|---|---|
| 0.0000000E-01 | 0.0000000E-01 | |
| 1.1052805E-02 | 2.4694711E-05 | |
| 2.1070278E-02 | 1.2347356E-05 | |
| 3.1928534E-02 | 1.8521034E-05 | |
| 4.2254105E-02 | 6.7910456E-05 | |
| 5.2533419E-02 | 1.1112620E-04 | |
| 6.2909499E-02 | 1.7903666E-04 | |
| 7.3163270E-02 | 2.3459976E-04 | |
| 8.3461385E-02 | 3.4572596E-04 | |
| 9.3612943E-02 | 4.3215745E-04 | |
| 1.0331006E-01 | 5.1858895E-04 | |
| 1.1331254E-01 | 6.3588882E-04 | |
| 1.2284404E-01 | 7.7788341E-04 | |
| 1.2760780E-01 | 8.5814123E-04 | |
| 1.3114524E-01 | 8.9518329E-04 | |

DyB

$\vec{v} \,||\, b$ $\quad$ $\vec{p} \,||\, b$

$\vec{H} \,||\, c$ $\quad$ f=10MHz

| 160.0000 | | 12 |
|---|---|---|
| 0.0000000E-01 | 0.0000000E-01 | |
| 1.2046625E-02 | 6.1141511E-06 | |
| 2.4775188E-02 | -3.6684907E-05 | |
| 3.5225446E-02 | -9.7826418E-05 | |
| 4.7908197E-02 | -2.0176699E-04 | |
| 6.0034338E-02 | -3.3627831E-04 | |
| 7.3909823E-02 | -5.0747454E-04 | |
| 8.6990154E-02 | -7.3369814E-04 | |
| 1.0162104E-01 | -1.0394057E-03 | |
| 1.1605313E-01 | -1.3940265E-03 | |
| 1.3147918E-01 | -1.8281312E-03 | |
| 1.4511612E-01 | -2.2805784E-03 | |

```
 170.0000                                  12
0.0000000E-01   0.0000000E-01
1.3729335E-02  -1.2299745E-05
2.7239352E-02  -7.3798467E-05
3.9565049E-02  -1.5989668E-04
5.2899610E-02  -2.7674425E-04
6.7199173E-02  -4.3049107E-04
8.1367144E-02  -6.7033609E-04
9.5798299E-02  -9.7782970E-04
1.1198400E-01  -1.3652717E-03
1.2790652E-01  -1.8142124E-03
1.4488177E-01  -2.3123520E-03
1.6027792E-01  -2.8842901E-03
 175.0000                                  12
0.0000000E-01   0.0000000E-01
1.2868376E-02  -1.2340575E-05
2.5653730E-02  -4.9362300E-05
3.7567355E-02  -1.2957604E-04
5.0020622E-02  -2.5915208E-04
6.2930509E-02  -4.5660128E-04
7.6836658E-02  -7.0341278E-04
9.0825828E-02  -1.0242677E-03
1.0502255E-01  -1.4129959E-03
1.2108727E-01  -1.9498108E-03
1.3727651E-01  -2.6100316E-03
1.5151475E-01  -3.2825930E-03
 180.0000                                  12
0.0000000E-01   0.0000000E-01
1.1774092E-02  -3.0827661E-05
2.3431609E-02  -1.2947618E-04
3.5361134E-02  -3.0211108E-04
4.6668926E-02  -5.3640131E-04
5.8520734E-02  -8.8167110E-04
7.0178252E-02  -1.2084443E-03
8.5022157E-02  -8.0151917E-04
9.9322043E-02  -4.7474598E-04
1.1358307E-01  -4.1309066E-04
1.2854355E-01  -4.3775279E-04
1.4156111E-01  -4.9324257E-04
 185.0000                                  12
0.0000000E-01   0.0000000E-01
1.7608153E-02  -6.1656842E-06
2.6492267E-02  -3.6994106E-05
3.6817047E-02  -4.9325474E-05
5.1063644E-02  -1.1714800E-04
6.0187868E-02  -1.6647347E-04
7.2433539E-02  -2.4046168E-04
8.7640581E-02  -3.5760968E-04
1.0260751E-01  -4.6242632E-04
1.1701418E-01  -5.7957432E-04
1.3214119E-01  -6.7205958E-04
1.4602761E-01  -7.9537326E-04
```

```
                                           E7
 190.0000                                  11
0.0000000E-01   0.0000000E-01
2.1075174E-02  -2.4675821E-05
3.1964013E-02  -7.4027464E-05
4.2361099E-02  -1.1721015E-04
5.2687935E-02  -1.7889970E-04
6.4911536E-02  -2.6526508E-04
7.6924386E-02  -3.7013732E-04
9.0026119E-02  -4.6267165E-04
1.0242535E-01  -5.6137494E-04
1.1633496E-01  -6.8475404E-04
1.2817218E-01  -7.7111942E-04
 195.0000                                  10
0.0000000E-01   0.0000000E-01
2.0631909E-02  -3.0860768E-05
4.1881746E-02  -9.2582306E-05
6.1861398E-02  -2.1602539E-04
7.5112508E-02  -3.0243553E-04
8.7883007E-02  -3.9501783E-04
1.0010424E-01  -4.8760014E-04
1.1332102E-01  -5.9869891E-04
1.2519896E-01  -6.7893690E-04
1.3975458E-01  -7.9620783E-04
 200.0000                                   8
0.0000000E-01   0.0000000E-01
2.1198552E-02  -2.4702642E-05
4.6728986E-02  -1.1116189E-04
7.2582593E-02  -2.5320208E-04
9.6843168E-02  -4.3229623E-04
1.0965381E-01  -5.2493114E-04
1.2110374E-01  -6.4844434E-04
1.3384801E-01  -7.4107925E-04
 210.0000                                  11
0.0000000E-01   0.0000000E-01
2.9582247E-02  -1.8552197E-05
4.9857719E-02  -5.5656561E-05
6.6174792E-02  -1.2986531E-04
8.8142405E-02  -2.4736250E-04
9.9775873E-02  -3.2775530E-04
1.1038197E-01  -3.9577999E-04
1.2177370E-01  -4.6998874E-04
1.3231937E-01  -5.4419749E-04
1.4365067E-01  -6.0603811E-04
1.5425676E-01  -6.4932655E-04
 220.0000                                   7
0.0000000E-01   0.0000000E-01
4.0292900E-02  -8.6686232E-05
5.9661862E-02  -1.6718059E-04
7.9630992E-02  -2.9720994E-04
9.9490997E-02  -4.2723929E-04
1.1937829E-01  -5.7584426E-04
1.3929285E-01  -6.9348986E-04
```

DyA

$\vec{v}$ | |c  $\vec{p}$ | |c

$\vec{H}$ | |a  f=20MHz

```
 230.0000                    11
0.00000000E-01  0.00000000E-01
2.5949655E-02 -4.3385292E-05
4.2698038E-02 -1.0536428E-04
5.6551639E-02 -1.6734327E-04
7.5393570E-02 -2.6031175E-04
8.5551152E-02 -3.2229074E-04
9.4313038E-02 -3.8426973E-04
1.0421216E-01 -4.5244662E-04
1.1310328E-01 -5.0822771E-04
1.2266640E-01 -5.6400879E-04
1.3194521E-01 -6.3838358E-04
 240.0000                    4
0.00000000E-01  0.00000000E-01
5.3955217E-02 -6.7592478E-05
9.0098295E-02 -2.1506698E-04
1.2619196E-01 -4.0555487E-04
 250.0000                    8
0.00000000E-01  0.00000000E-01
2.2419052E-02  1.3422897E-04
3.6793096E-02  1.1495631E-04
4.8782609E-02  6.5245476E-05
6.5006337E-02 -1.2379164E-06
8.1341491E-02 -8.9469800E-05
9.7498361E-02 -1.9510533E-04
1.1376666E-01 -3.0571680E-04
 260.0000                    8
0.00000000E-01  0.00000000E-01
2.1310770E-02 -5.5880902E-06
3.5503743E-02 -2.6118248E-05
4.6585342E-02 -6.0327078E-05
6.2163515E-02 -1.3309373E-04
7.7805621E-02 -2.2515145E-04
9.3277239E-02 -3.3088783E-04
1.0896197E-01 -4.1609406E-04
 260.0000                    8
0.00000000E-01  0.00000000E-01
2.2759902E-02 -3.6266148E-05
3.5802093E-02 -6.3777135E-05
4.6606654E-02 -1.0940898E-04
6.2163515E-02 -1.6693418E-04
7.7720378E-02 -2.6133606E-04
9.3383794E-02 -3.6699632E-04
1.0877017E-01 -4.6077545E-04
 280.0000                    8
0.00000000E-01  0.00000000E-01
1.9515997E-02 -1.6292260E-05
3.1703928E-02 -2.0050129E-05
4.1882860E-02 -9.7765804E-05
5.5831057E-02 -1.5792843E-04
6.9760121E-02 -2.3940197E-04
8.3880519E-02 -3.4093769E-04
9.7713916E-02 -4.4935303E-04
```

```
 180.0000                    16
0.00000000E-01  0.00000000E-01
6.7700394E-02  4.2034468E-04
1.3322281E-01 -4.9714840E-03
1.9751849E-01 -1.4421455E-02
2.5520632E-01 -2.0778520E-02
2.8750241E-01 -2.2293836E-02
3.1474212E-01 -2.2667476E-02
3.3844426E-01 -2.2397625E-02
3.6655839E-01 -2.1370116E-02
4.1196742E-01 -1.9045247E-02
4.4942758E-01 -1.6398632E-02
4.8080803E-01 -1.3726070E-02
5.0204462E-01 -1.1401201E-02
5.1367752E-01 -9.2631513E-03
5.1435622E-01 -7.3793844E-03
5.0543994E-01 -6.1546764E-03
 185.0000                    16
0.00000000E-01  0.00000000E-01
5.9837111E-02 -1.8215125E-03
1.1208693E-01 -6.2170142E-03
1.6652911E-01 -1.2818051E-02
2.1726888E-01 -1.9185561E-02
2.6900833E-01 -2.4094822E-02
3.1409309E-01 -2.6497558E-02
3.4428156E-01 -2.7016507E-02
3.6139248E-01 -2.6964613E-02
3.8180592E-01 -2.6684380E-02
4.0412889E-01 -2.6046072E-02
4.2797561E-01 -2.4992605E-02
4.5444009E-01 -2.3529167E-02
4.7734463E-01 -2.1692086E-02
4.9211504E-01 -2.0067775E-02
4.9875778E-01 -1.8671801E-02
```

```
 190.0000                    19
0.00000000E-01  0.00000000E-01
4.9111150E-02 -1.0924625E-03
9.6952342E-02 -4.2049501E-03
1.4325372E-01 -8.6469438E-03
1.8934483E-01 -1.3779456E-02
2.3276420E-01 -1.8468800E-02
2.7639133E-01 -2.2374869E-02
3.1453967E-01 -2.4621631E-02
3.5090239E-01 -2.5760472E-02
3.8355724E-01 -2.5909913E-02
4.0045605E-01 -2.5734707E-02
4.1401888E-01 -2.5435825E-02
4.2699801E-01 -2.5049341E-02
4.4514471E-01 -2.4322750E-02
4.5897670E-01 -2.3560088E-02
4.7308390E-01 -2.2575841E-02
3.7486964E-01 -2.5961444E-02
3.6599596E-01 -2.5951138E-02
3.8355724E-01 -2.5940832E-02
 200.0000                    15
0.00000000E-01  0.00000000E-01
4.1311848E-02 -6.7997713E-04
7.3271709E-02 -2.1976073E-03
1.1045316E-01 -4.7943315E-03
1.4538422E-01 -7.8443738E-03
1.8026123E-01 -1.1209768E-02
2.1431149E-01 -1.4683564E-02
2.4642289E-01 -1.7615350E-02
2.8250045E-01 -2.0512644E-02
3.0639264E-01 -2.1956363E-02
3.3332913E-01 -2.3207915E-02
3.5189394E-01 -2.3799200E-02
3.6993376E-01 -2.4178607E-02
3.8536739E-01 -2.4321501E-02
3.9813332E-01 -2.4331355E-02
 210.0000                    15
0.00000000E-01  0.00000000E-01
2.9903072E-02 -3.4468665E-04
5.9554793E-02 -1.3492020E-03
8.7710696E-02 -2.7870378E-03
1.1508643E-01 -4.5794084E-03
1.4320818E-01 -6.7854029E-03
1.7239917E-01 -9.2425265E-03
1.9913063E-01 -1.1620864E-02
2.2485592E-01 -1.3861328E-02
2.4938457E-01 -1.5776801E-02
2.7453818E-01 -1.7647957E-02
2.9165548E-01 -1.8573687E-02
3.0974258E-01 -1.9563430E-02
3.2518214E-01 -2.0484235E-02
3.3857731E-01 -2.0981569E-02
 240.0000                    15
0.00000000E-01  0.00000000E-01
1.8597084E-02 -7.8680528E-05
3.6864915E-02 -3.1963964E-04
5.4304592E-02 -6.9828967E-04
7.2027210E-02 -1.2392183E-03
8.9659350E-02 -1.9670132E-03
1.0748040E-01 -2.8226639E-03
1.2411022E-01 -3.6291393E-03
1.4073102E-01 -4.6175634E-03
1.5646784E-01 -5.6010700E-03
1.7188120E-01 -6.5304838E-03
1.8294119E-01 -7.2582786E-03
1.9422526E-01 -8.0598366E-03
2.0461178E-01 -8.7925489E-03
2.1318921E-01 -9.4072405E-03
 260.0000                    15
0.00000000E-01  0.00000000E-01
1.2196143E-02 -4.9181618E-05
2.8139598E-02 -1.9180831E-04
4.1613945E-02 -4.0328926E-04
5.5786704E-02 -7.0329713E-04
6.9713280E-02 -1.0721593E-03
8.3385929E-02 -1.4951212E-03
9.7002547E-02 -2.0016918E-03
1.1062180E-01 -2.5623623E-03
1.2511074E-01 -3.2263141E-03
1.3749080E-01 -3.7820664E-03
1.4765812E-01 -4.2689643E-03
1.5700434E-01 -4.6968444E-03
1.6778045E-01 -5.2329241E-03
1.7550126E-01 -5.6263770E-03
 280.0000                    15
0.00000000E-01  0.00000000E-01
1.1699332E-02 -2.9525234E-05
2.3369706E-02 -1.1318006E-04
3.5069038E-02 -2.5096449E-04
4.6623576E-02 -4.2319502E-04
5.8264990E-02 -6.4955515E-04
7.0167033E-02 -9.2020313E-04
8.1374068E-02 -1.2203763E-03
9.2870688E-02 -1.5648374E-03
1.0462794E-01 -1.9339028E-03
1.1618248E-01 -2.3275726E-03
1.2594157E-01 -2.6818755E-03
1.3358568E-01 -2.9426817E-03
1.4221638E-01 -3.2920636E-03
1.4919544E-01 -3.5528698E-03
```

| | |
|---|---|
| 290.0000 | 15 |
| 0.00000000E-01 | 0.00000000E-01 |
| 1.0565185E-02 | -9.8452813E-06 |
| 2.0895589E-02 | -6.8916970E-05 |
| 3.1304252E-02 | -1.5752450E-04 |
| 4.1843351E-02 | -3.1504900E-04 |
| 5.2408536E-02 | -4.8241879E-04 |
| 6.2999808E-02 | -7.1378289E-04 |
| 7.3121515E-02 | -9.5991493E-04 |
| 8.3869310E-02 | -1.2405054E-03 |
| 9.4017104E-02 | -1.5604771E-03 |
| 1.0453012E-01 | -1.8706034E-03 |
| 1.0987793E-01 | -2.0675091E-03 |
| 1.2044311E-01 | -2.4367071E-03 |
| 1.2855613E-01 | -2.7271429E-03 |
| 1.3442568E-01 | -2.9388165E-03 |
| 300.0000 | 17 |
| 0.00000000E-01 | 0.00000000E-01 |
| 9.9145315E-03 | -4.9251864E-06 |
| 1.9903422E-02 | -5.4177050E-05 |
| 2.9867525E-02 | -1.5760596E-04 |
| 3.9831630E-02 | -2.5610970E-04 |
| 4.9696588E-02 | -4.0879047E-04 |
| 5.9883770E-02 | -5.8609718E-04 |
| 6.9600010E-02 | -7.9788020E-04 |
| 7.9688047E-02 | -1.0244388E-03 |
| 8.9701723E-02 | -1.2854736E-03 |
| 9.9269247E-02 | -1.5465085E-03 |
| 1.0430087E-01 | -1.6893389E-03 |
| 1.0910942E-01 | -1.8321693E-03 |
| 1.1394275E-01 | -1.9848501E-03 |
| 1.1904874E-01 | -2.1424561E-03 |
| 1.2400600E-01 | -2.2951368E-03 |
| 1.2767439E-01 | -2.4034909E-03 |

DyB

$\vec{v}\,||c$ $\vec{p}\,||c$

$\vec{H}\,||a$ f=10MHz

| | |
|---|---|
| 4.200000 | 5 |
| 0.00000000E-01 | 0.00000000E-01 |
| 5.7500000E-01 | 3.5106845E-05 |
| 9.2777777E-01 | 5.2847927E-05 |
| 9.8611111E-01 | 2.4020473E-05 |
| 9.9444444E-01 | -2.1061220E-05 |
| 20.00000 | 5 |
| 0.00000000E-01 | 0.00000000E-01 |
| 8.8972222E-01 | 6.7653757E-05 |
| 9.9055555E-01 | 4.9169913E-05 |
| 9.9222223E-01 | 2.0332228E-05 |
| 9.9805555E-01 | 2.0332228E-05 |
| 40.00000 | 7 |
| 0.00000000E-01 | 0.00000000E-01 |
| 5.8958333E-01 | 9.9961143E-06 |
| 9.5222222E-01 | 2.2590350E-04 |
| 9.7305556E-01 | 2.2108627E-04 |
| 9.7666666E-01 | 2.6293686E-04 |
| 9.7916666E-01 | 2.5997130E-04 |
| 9.8333333E-01 | 2.9700466E-04 |
| 60.00000 | 9 |
| 0.00000000E-01 | 0.00000000E-01 |
| 5.9166667E-01 | 2.4137071E-05 |
| 8.9583334E-01 | 1.9123988E-04 |
| 9.4000001E-01 | 3.9919003E-04 |
| 9.4583333E-01 | 5.2173208E-04 |
| 9.4888888E-01 | 5.9673977E-04 |
| 9.5222222E-01 | 6.7583800E-04 |
| 9.5638888E-01 | 7.5084570E-04 |
| 9.5916666E-01 | 7.4267913E-04 |
| 80.00000 | 9 |
| 0.00000000E-01 | 0.00000000E-01 |
| 5.7083333E-01 | -3.5441215E-05 |
| 8.5833333E-01 | 2.3506036E-05 |
| 8.8972222E-01 | 2.6301112E-04 |
| 8.9166667E-01 | 8.0209065E-04 |
| 8.9583334E-01 | 1.0333912E-03 |
| 8.9749999E-01 | 1.2068666E-03 |
| 8.9888889E-01 | 1.2881978E-03 |
| 9.0083333E-01 | 1.4131747E-03 |
| 90.00000 | 7 |
| 0.00000000E-01 | 0.00000000E-01 |
| 8.3541667E-01 | 1.2345494E-04 |
| 8.8750000E-01 | 9.7267529E-04 |
| 8.9166667E-01 | 1.2532547E-03 |
| 8.9583334E-01 | 1.4664951E-03 |
| 8.9972223E-01 | 1.6460659E-03 |
| 9.0305555E-01 | 1.7919672E-03 |

| 100.0000 | 9 |
|---|---|
| 0.0000000E-01 | 0.0000000E-01 |
| 2.1458333E-01 | 1.8613063E-03 |
| 6.6472222E-01 | 2.9125299E-03 |
| 8.5166666E-01 | 3.7113091E-03 |
| 8.6250000E-01 | 4.8077467E-03 |
| 8.7083333E-01 | 5.3917597E-03 |
| 8.7249999E-01 | 5.5650797E-03 |
| 8.7722222E-01 | 5.8815771E-03 |
| 8.8250000E-01 | 6.1227180E-03 |

| 120.0000 | 12 |
|---|---|
| 0.0000000E-01 | 0.0000000E-01 |
| 3.6388889E-02 | 1.9600632E-03 |
| 1.7883333E-01 | 6.2119035E-05 |
| 4.5138889E-01 | -2.1858136E-03 |
| 7.5166667E-01 | -2.7798268E-03 |
| 7.7083334E-01 | -1.7354505E-03 |
| 7.8722223E-01 | 5.4354156E-05 |
| 7.9527777E-01 | 1.2656753E-03 |
| 8.0277777E-01 | 2.1353418E-03 |
| 8.0777778E-01 | 2.8574756E-03 |
| 8.1250000E-01 | 3.4670187E-03 |
| 8.1694444E-01 | 3.9600885E-03 |

| 140.0000 | 23 |
|---|---|
| 0.0000000E-01 | 0.0000000E-01 |
| 3.2638889E-02 | 2.0541926E-04 |
| 5.2083333E-02 | -1.8639896E-04 |
| 6.4250001E-02 | -1.4645633E-03 |
| 1.3888889E-01 | -1.0522031E-02 |
| 2.0305556E-01 | -1.5980858E-02 |
| 2.6916667E-01 | -1.6106392E-02 |
| 3.6805556E-01 | -2.8789129E-02 |
| 4.2027777E-01 | -3.1775317E-02 |
| 5.2611111E-01 | -3.9820905E-02 |
| 6.3194445E-01 | -4.3628769E-02 |
| 6.5638889E-01 | -4.1053420E-02 |
| 6.9111111E-01 | -3.6705379E-02 |
| 6.9805555E-01 | -3.4807153E-02 |
| 7.0416667E-01 | -3.3780057E-02 |
| 7.1777778E-01 | -3.1261769E-02 |
| 7.2388888E-01 | -3.0223260E-02 |
| 7.2944444E-01 | -2.9317894E-02 |
| 7.3472222E-01 | -2.8500021E-02 |
| 7.3972222E-01 | -2.7925608E-02 |
| 7.4666666E-01 | -2.6856667E-02 |
| 7.5638889E-01 | -2.5943692E-02 |
| 7.5777777E-01 | -2.5791530E-02 |

| 160.0000 | 17 |
|---|---|
| 0.0000000E-01 | 0.0000000E-01 |
| 3.1944444E-02 | 2.6116881E-04 |
| 6.3888889E-02 | -3.6486818E-04 |
| 8.4722222E-02 | -1.7052787E-03 |
| 1.0138889E-01 | -4.8892337E-03 |
| 1.2916667E-01 | -9.5749092E-03 |
| 5.0555556E-01 | -1.6668715E-02 |
| 5.2916667E-01 | -1.7152645E-02 |
| 5.6111111E-01 | -1.9683678E-02 |
| 5.7083333E-01 | -1.8312542E-02 |
| 5.8194444E-01 | -2.6093836E-02 |
| 6.0138889E-01 | -1.9929484E-02 |
| 6.1666667E-01 | -1.6568856E-02 |
| 6.2777778E-01 | -1.4356603E-02 |
| 6.4722222E-01 | -1.0957568E-02 |
| 6.6111111E-01 | -8.3612425E-03 |
| 6.7500000E-01 | -6.3525471E-03 |

| 170.0000 | 16 |
|---|---|
| 0.0000000E-01 | 0.0000000E-01 |
| 3.4722222E-02 | -3.8649584E-05 |
| 7.5000000E-02 | -6.8023266E-04 |
| 1.0972222E-01 | -2.7286606E-03 |
| 4.3194444E-01 | -4.4999710E-02 |
| 4.5555555E-01 | -4.1266160E-02 |
| 4.8472222E-01 | -2.9559201E-02 |
| 5.1166667E-01 | -2.4909656E-02 |
| 5.3472222E-01 | -2.1377085E-02 |
| 5.5277777E-01 | -1.8447446E-02 |
| 5.6666667E-01 | -1.6174851E-02 |
| 5.8055556E-01 | -1.3902255E-02 |
| 5.9055556E-01 | -1.2333082E-02 |
| 6.0333334E-01 | -1.0806423E-02 |
| 6.1444445E-01 | -9.4498232E-03 |
| 6.1944444E-01 | -8.9087290E-03 |

| 175.0000 | 18 |
|---|---|
| 0.0000000E-01 | 0.0000000E-01 |
| 4.8055555E-02 | -3.4896706E-04 |
| 8.0555555E-02 | -1.0313915E-03 |
| 1.1944444E-01 | -3.3733482E-03 |
| 2.3194444E-01 | -2.8355512E-02 |
| 2.6277778E-01 | -3.1693963E-02 |
| 3.2111111E-01 | -3.8867176E-02 |
| 3.7083333E-01 | -4.1441776E-02 |
| 4.1805556E-01 | -3.0980520E-02 |
| 4.5416667E-01 | -2.6476845E-02 |
| 4.8222222E-01 | -2.2799181E-02 |
| 5.0694445E-01 | -1.9565420E-02 |
| 5.2500000E-01 | -1.6990818E-02 |
| 5.4222222E-01 | -1.4703145E-02 |
| 5.5555555E-01 | -1.2795459E-02 |
| 5.6944445E-01 | -1.1291023E-02 |
| 5.8194444E-01 | -9.8176064E-03 |
| 5.8638889E-01 | -9.2864010E-03 |

```
 180.0000                                19
0.0000000E-01  0.0000000E-01
5.4087490E-02 -4.7924928E-04
1.0615806E-01 -3.1073905E-03
1.3221302E-01 -7.6332042E-03
1.6111642E-01 -1.2031476E-02
2.0224030E-01 -1.8632748E-02
2.6014224E-01 -2.6470792E-02
3.0421332E-01 -2.8561711E-02
3.3190092E-01 -2.8279572E-02
3.5266052E-01 -2.7487265E-02
3.9209585E-01 -2.5176047E-02
4.2867017E-01 -2.2343065E-02
4.5829953E-01 -1.9158376E-02
4.7943193E-01 -1.6626858E-02
4.9632877E-01 -1.4678941E-02
5.1394036E-01 -1.2441157E-02
5.3080600E-01 -1.0385023E-02
5.4845607E-01 -8.6921905E-03
5.5712039E-01 -7.9810465E-03
 185.0000                                20
0.0000000E-01  0.0000000E-01
4.0500896E-02 -9.1482868E-04
8.5658279E-02 -4.2973885E-03
1.2613039E-01 -8.8830632E-03
1.7137256E-01 -1.5352209E-02
2.1188839E-01 -2.0733554E-02
2.5441395E-01 -2.5907333E-02
2.9656297E-01 -2.8955541E-02
3.1363589E-01 -2.9305268E-02
3.3826624E-01 -2.9451333E-02
3.5805440E-01 -2.9051576E-02
3.7123184E-01 -2.8605693E-02
3.9058575E-01 -2.7706240E-02
4.1194988E-01 -2.6303246E-02
4.2786268E-01 -2.5000192E-02
4.5132500E-01 -2.2924531E-02
4.7078067E-01 -2.1137155E-02
4.8822164E-01 -1.9484313E-02
5.0664823E-01 -1.7804565E-02
5.1373684E-01 -1.7189554E-02
 190.0000                                19
0.0000000E-01  0.0000000E-01
7.2531449E-02 -2.7860597E-03
1.0822169E-01 -6.5761739E-03
1.4409880E-01 -1.0937296E-02
1.7835980E-01 -1.5260096E-02
2.1271302E-01 -2.0284201E-02
2.5233733E-01 -2.4446045E-02
2.8979305E-01 -2.7488867E-02
3.0738603E-01 -2.8412444E-02
3.2126573E-01 -2.8826329E-02
3.4728716E-01 -2.8956626E-02
3.6546268E-01 -2.8627051E-02
3.7904947E-01 -2.8182508E-02
3.9697675E-01 -2.7335576E-02
4.1279580E-01 -2.6438826E-02
4.2651508E-01 -2.5637881E-02
4.4793744E-01 -2.4239103E-02
4.6749682E-01 -2.2867151E-02
4.7496499E-01 -2.2288478E-02
 195.0000                                16
0.0000000E-01  0.0000000E-01
6.1651084E-02 -1.8523480E-03
1.2449905E-01 -7.4974165E-03
1.8488225E-01 -1.4313598E-02
2.2182812E-01 -1.8749282E-02
2.5479173E-01 -2.2385089E-02
2.8538383E-01 -2.4612499E-02
3.1538476E-01 -2.6170156E-02
3.4038023E-01 -2.6897317E-02
3.5764683E-01 -2.7054044E-02
3.7359313E-01 -2.6950897E-02
3.8755129E-01 -2.6686823E-02
4.0257780E-01 -2.6250526E-02
4.1674799E-01 -2.5657316E-02
4.2954430E-01 -2.5059780E-02
4.3745566E-01 -2.1447434E-02
 200.0000                                16
0.0000000E-01  0.0000000E-01
5.3926793E-02 -1.2773492E-03
1.0762091E-01 -5.1667629E-03
1.6106457E-01 -1.1106054E-02
1.9372540E-01 -1.4333847E-02
2.2339613E-01 -1.7829347E-02
2.5116913E-01 -2.0758837E-02
2.7961998E-01 -2.3152911E-02
3.0234345E-01 -2.4422611E-02
3.1907355E-01 -2.5122476E-02
3.3466907E-01 -2.5577580E-02
3.4763215E-01 -2.5780273E-02
3.6251461E-01 -2.5860585E-02
3.7686935E-01 -2.5787922E-02
3.8984102E-01 -2.5589053E-02
3.9791432E-01 -2.5470496E-02
```

```
 210.0000                                16
0.00000000E-01  0.00000000E-01
4.3233981E-02 -7.6001191E-04
8.5601561E-02 -2.7001428E-03
1.2763053E-01 -4.1628793E-03
1.5378087E-01 -8.2188222E-03
1.7803385E-01 -1.0609614E-02
2.0166724E-01 -1.2958394E-02
2.2618855E-01 -1.5001642E-02
2.4655218E-01 -1.6678251E-02
2.6192461E-01 -1.7995860E-02
2.7547825E-01 -1.9007936E-02
2.8791928E-01 -1.9874885E-02
3.0170883E-01 -2.0791482E-02
3.1419797E-01 -2.1505664E-02
3.2527636E-01 -2.2051803E-02
3.3196471E-01 -2.2345878E-02
 220.0000                                16
0.00000000E-01  0.00000000E-01
3.5137572E-02 -5.1131377E-04
6.9984679E-02 -1.8773610E-03
1.0463180E-01 -3.7394589E-03
1.2645305E-01 -5.0978746E-03
1.4701176E-01 -6.7539206E-03
1.6678420E-01 -8.4900981E-03
1.8807612E-01 -1.0497195E-02
2.0534893E-01 -1.2050216E-02
2.1827460E-01 -1.3111001E-02
2.3085730E-01 -1.4110734E-02
2.4203002E-01 -1.4862441E-02
2.5434884E-01 -1.5698096E-02
2.6614596E-01 -1.6499409E-02
2.7652316E-01 -1.7178616E-02
2.8299628E-01 -1.7575457E-02
 230.0000                                16
0.00000000E-01  0.00000000E-01
3.0294992E-02 -2.9369136E-04
6.0435100E-02 -1.1823938E-03
9.0860172E-02 -2.5364254E-03
1.0952780E-01 -3.5242962E-03
1.2704024E-01 -4.5350522E-03
1.4439267E-01 -5.7250743E-03
1.6228751E-01 -7.0104508E-03
1.7785969E-01 -8.2424288E-03
1.8944506E-01 -9.1921580E-03
2.0015140E-01 -1.0107560E-02
2.1001115E-01 -1.0885651E-02
2.2079956E-01 -1.1785796E-02
2.3176246E-01 -1.2643985E-02
2.4078724E-01 -1.3322908E-02
2.4659315E-01 -1.3727210E-02
 240.0000                                16
0.00000000E-01  0.00000000E-01
2.6537092E-02 -2.2499247E-04
5.3105941E-02 -8.2370123E-04
7.9534539E-02 -1.7923129E-03
9.5992051E-02 -2.5359321E-03
1.1662281E-01 -3.3100587E-03
1.2663098E-01 -4.0841852E-03
1.4265082E-01 -4.9612746E-03
1.5605401E-01 -5.8116698E-03
1.6646883E-01 -6.5438487E-03
1.7611169E-01 -7.2493335E-03
1.8467167E-01 -7.8518558E-03
1.9429819E-01 -8.5649674E-03
2.0442686E-01 -9.2742658E-03
2.1259524E-01 -9.8462806E-03
2.1797342E-01 -1.0216183E-02
 260.0000                                15
0.00000000E-01  0.00000000E-01
2.1218875E-02 -1.6638238E-03
4.2540344E-02 -2.0102951E-03
6.2994703E-02 -2.5166763E-03
7.6184105E-02 -2.9316804E-03
8.8682389E-02 -3.3961804E-03
1.0065833E-01 -3.8873321E-03
1.1349016E-01 -4.4622460E-03
1.2467189E-01 -4.9533977E-03
1.3317649E-01 -5.3341354E-03
1.4107995E-01 -5.6806067E-03
1.4780456E-01 -6.0118486E-03
1.5551964E-01 -6.3430903E-03
1.6324422E-01 -6.7200207E-03
1.7025035E-01 -7.0817216E-03
 280.0000                                14
0.00000000E-01  0.00000000E-01
1.7325590E-02 -9.9173049E-05
3.4761804E-02 -3.0896219E-04
5.2209314E-02 -6.3318178E-04
6.2637326E-02 -8.5822830E-04
7.3286213E-02 -1.1481188E-03
8.3107719E-02 -1.4418236E-03
9.3930922E-02 -1.7698575E-03
1.0316611E-01 -2.0978914E-03
1.1050851E-01 -2.3572671E-03
1.1702193E-01 -2.5861280E-03
1.2280450E-01 -2.7997314E-03
1.3161763E-01 -3.1506515E-03
1.4221152E-01 -3.5740441E-03
```

300.0000 16

| | |
|---|---|
| 0.0000000E-01 | 0.0000000E-01 |
| 1.6319181E-02 | -5.3424715E-05 |
| 2.9471804E-02 | -1.6409019E-04 |
| 4.4373108E-02 | -3.7015695E-04 |
| 5.3487166E-02 | -5.3043109E-04 |
| 6.1198886E-02 | -6.9070524E-04 |
| 7.0842423E-02 | -8.7005964E-04 |
| 8.1717998E-02 | -1.1715277E-03 |
| 8.7806701E-02 | -1.3318018E-03 |
| 9.3856218E-02 | -1.4958920E-03 |
| 1.0048958E-01 | -1.7134069E-03 |
| 1.0452373E-01 | -1.8240724E-03 |
| 1.1021011E-01 | -2.0110589E-03 |
| 1.1593751E-01 | -2.1942293E-03 |
| 1.2112529E-01 | -2.3964800E-03 |
| 1.2431784E-01 | -2.5071455E-03 |

DyA

$\vec{v}$ ||c $\vec{p}$ ||c

$\vec{H}$ ||c f=20MHz

170.0000 21

| | |
|---|---|
| 0.0000000E-01 | 0.0000000E-01 |
| 8.8107100E-03 | -9.9549043E-06 |
| 1.6797989E-02 | -6.4706878E-05 |
| 2.5032298E-02 | -1.7421083E-04 |
| 3.3101920E-02 | -3.2353439E-04 |
| 4.1336229E-02 | -5.6245209E-04 |
| 4.9570537E-02 | -8.6607667E-04 |
| 5.8010703E-02 | -1.2045434E-03 |
| 6.6162668E-02 | -1.5231003E-03 |
| 8.2631285E-02 | -2.1154171E-03 |
| 9.9182246E-02 | -3.1357948E-03 |
| 1.1552735E-01 | -3.9321872E-03 |
| 1.3244885E-01 | -5.2810767E-03 |
| 1.4846458E-01 | -6.6548535E-03 |
| 1.6497437E-01 | -8.2327059E-03 |
| 1.7312634E-01 | -9.2033088E-03 |
| 1.8201939E-01 | -9.9947240E-03 |
| 1.8963612E-01 | -1.1209222E-02 |
| 1.9766458E-01 | -1.2120096E-02 |
| 2.0618708E-01 | -1.3419211E-02 |
| 2.1228047E-01 | -1.4150896E-02 |

E14

175.0000 21

| | |
|---|---|
| 0.0000000E-01 | 0.0000000E-01 |
| 8.7630281E-03 | 9.9945030E-06 |
| 1.7355900E-02 | -4.4975263E-05 |
| 2.5608461E-02 | -1.1993403E-04 |
| 3.4201333E-02 | -2.6985158E-04 |
| 4.2709127E-02 | -5.5969216E-04 |
| 5.1344539E-02 | -9.0949977E-04 |
| 5.9724716E-02 | -1.2093348E-03 |
| 6.8317587E-02 | -1.4342112E-03 |
| 8.5248098E-02 | -1.8889611E-03 |
| 1.0213607E-01 | -3.0533207E-03 |
| 1.1915166E-01 | -4.0477737E-03 |
| 1.3616725E-01 | -5.6019190E-03 |
| 1.5322538E-01 | -7.1960421E-03 |
| 1.7028350E-01 | -9.2049371E-03 |
| 1.7913161E-01 | -1.0269352E-02 |
| 1.8738417E-01 | -1.1298786E-02 |
| 1.9576435E-01 | -1.2593074E-02 |
| 2.0422960E-01 | -1.4032282E-02 |
| 2.1286502E-01 | -1.5401529E-02 |
| 2.1933094E-01 | -1.6655839E-02 |

180.0000 21

| | |
|---|---|
| 0.0000000E-01 | 0.0000000E-01 |
| 8.5983321E-03 | 1.0047474E-05 |
| 1.7153886E-02 | 1.0047474E-05 |
| 2.5794996E-02 | -3.5166160E-05 |
| 3.4521661E-02 | -1.3061717E-04 |
| 4.2692216E-02 | -2.4113938E-04 |
| 5.3643325E-02 | -9.6455752E-04 |
| 6.0102768E-02 | -1.2911004E-03 |
| 6.8572768E-02 | -1.4468363E-03 |
| 8.5769432E-02 | -1.6176434E-03 |
| 1.0279499E-01 | -1.8236166E-03 |
| 1.1977776E-01 | -2.7178418E-03 |
| 1.3718832E-01 | -3.4462837E-03 |
| 1.5447053E-01 | -4.3103665E-03 |
| 1.7128220E-01 | -5.7973927E-03 |
| 1.7983775E-01 | -6.8624249E-03 |
| 1.8847886E-01 | -7.5305820E-03 |
| 1.9699164E-01 | -8.4398784E-03 |
| 2.0571830E-01 | -9.3240562E-03 |
| 2.1405997E-01 | -1.0248424E-02 |
| 2.2056219E-01 | -1.1067293E-02 |

| 185.0000 | 21 |
|---|---|
| 0.00000000E-01 | 0.00000000E-01 |
| 8.5125496E-03 | -4.9657364E-05 |
| 1.6367124E-02 | -1.6883504E-04 |
| 2.4838550E-02 | -3.4760154E-04 |
| 3.2939866E-02 | -5.6609395E-04 |
| 4.1123429E-02 | -8.5907240E-04 |
| 4.9265867E-02 | -1.2066739E-03 |
| 5.7737293E-02 | -1.6188301E-03 |
| 6.6003103E-02 | -2.0309862E-03 |
| 8.2575844E-02 | -3.0439964E-03 |
| 9.8942968E-02 | -4.1811500E-03 |
| 1.1531009E-01 | -5.5616247E-03 |
| 1.3192396E-01 | -7.0761743E-03 |
| 1.4804434E-01 | -8.6503128E-03 |
| 1.6486382E-01 | -1.0437978E-02 |
| 1.7275953E-01 | -1.1306982E-02 |
| 1.8102533E-01 | -1.2245506E-02 |
| 1.8920889E-01 | -1.3154236E-02 |
| 1.9751583E-01 | -1.4102691E-02 |
| 2.0561714E-01 | -1.5051147E-02 |
| 2.1203240E-01 | -1.5810905E-02 |

| 190.0000 | 18 |
|---|---|
| 0.00000000E-01 | 0.00000000E-01 |
| 7.8845987E-03 | -3.9534286E-05 |
| 1.5615351E-02 | -1.2354464E-04 |
| 2.3346104E-02 | -2.5697286E-04 |
| 3.1230703E-02 | -1.4281761E-03 |
| 4.6153748E-02 | -1.0130661E-03 |
| 6.1769099E-02 | -1.7543339E-03 |
| 7.7115221E-02 | -2.6735061E-03 |
| 9.2422880E-02 | -3.7854078E-03 |
| 1.0799977E-01 | -5.0949811E-03 |
| 1.2319205E-01 | -6.4786811E-03 |
| 1.3846125E-01 | -7.9958092E-03 |
| 1.5399967E-01 | -9.6463657E-03 |
| 1.6938426E-01 | -1.1351282E-02 |
| 1.7707655E-01 | -1.2206211E-02 |
| 1.8492268E-01 | -1.3105616E-02 |
| 1.9226882E-01 | -1.3960545E-02 |
| 1.9830727E-01 | -1.4652395E-02 |

| 195.0000 | 21 |
|---|---|
| 0.00000000E-01 | 0.00000000E-01 |
| 1.0646795E-02 | -6.9085651E-05 |
| 1.4978939E-02 | -2.2699571E-04 |
| 2.2321556E-02 | -3.2568950E-04 |
| 2.9554034E-02 | -5.0827300E-04 |
| 3.7006790E-02 | -7.5007278E-04 |
| 4.5634366E-02 | -1.1004357E-03 |
| 5.3013696E-02 | -1.4261252E-03 |
| 5.9181494E-02 | -1.7271413E-03 |
| 7.3683162E-02 | -2.6005813E-03 |
| 8.8662102E-02 | -3.6220620E-03 |
| 1.0294349E-01 | -4.7817140E-03 |
| 1.1781229E-01 | -6.0894067E-03 |
| 1.3198354E-01 | -7.4859238E-03 |
| 1.4692577E-01 | -9.0058082E-03 |
| 1.5437853E-01 | -9.8150972E-03 |
| 1.6153758E-01 | -1.0624386E-02 |
| 1.6917390E-01 | -1.1483022E-02 |
| 1.7647980E-01 | -1.2297246E-02 |
| 1.8356543E-01 | -1.3091731E-02 |
| 1.8929267E-01 | -1.3767783E-02 |

| 200.0000 | 21 |
|---|---|
| 0.00000000E-01 | 0.00000000E-01 |
| 7.1989323E-03 | -2.9623778E-05 |
| 1.4222281E-02 | -1.0368322E-04 |
| 2.1210513E-02 | -2.2711563E-04 |
| 2.8023161E-02 | -3.9004641E-04 |
| 3.5327442E-02 | -5.7766366E-04 |
| 4.3825695E-02 | -8.7390144E-04 |
| 4.9409257E-02 | -1.1355781E-03 |
| 5.6959356E-02 | -1.5058754E-03 |
| 7.0584653E-02 | -2.2662190E-03 |
| 8.4385532E-02 | -3.1796188E-03 |
| 9.8291764E-02 | -4.2559494E-03 |
| 1.1244381E-01 | -5.4557124E-03 |
| 1.2649051E-01 | -6.7443688E-03 |
| 1.4057232E-01 | -8.1366643E-03 |
| 1.4749032E-01 | -8.8970080E-03 |
| 1.5468925E-01 | -9.6721634E-03 |
| 1.6174772E-01 | -1.0402883E-02 |
| 1.6877106E-01 | -1.1148415E-02 |
| 1.7572418E-01 | -1.1948257E-02 |
| 1.8196192E-01 | -1.2525921E-02 |

| 210.0000 | 23 |
|---|---|
| 0.00000000E-01 | 0.00000000E-01 |
| 6.7156597E-03 | -2.4656048E-05 |
| 1.3013599E-02 | -7.3968144E-05 |
| 2.1849993E-02 | -2.1204201E-04 |
| 2.6123595E-02 | -3.0573500E-04 |
| 3.2228740E-02 | -4.6846491E-04 |
| 3.9105061E-02 | -6.8050692E-04 |
| 4.5113809E-02 | -8.9254894E-04 |
| 5.1829469E-02 | -1.1785591E-03 |
| 6.4714538E-02 | -1.8245476E-03 |
| 7.7181888E-02 | -2.5642290E-03 |
| 9.0034824E-02 | -3.4222594E-03 |
| 1.0295203E-01 | -4.3937078E-03 |
| 1.0947489E-01 | -4.9164160E-03 |
| 1.1580496E-01 | -5.4687114E-03 |
| 1.2219930E-01 | -6.0407318E-03 |
| 1.2862577E-01 | -6.6324769E-03 |
| 1.3498797E-01 | -7.2390156E-03 |
| 1.4138231E-01 | -7.8356920E-03 |
| 1.4796944E-01 | -8.4915429E-03 |
| 1.5433164E-01 | -9.0980817E-03 |
| 1.6075811E-01 | -9.7588637E-03 |
| 1.6567436E-01 | -1.0276641E-02 |

| 220.0000 | 20 |
|---|---|
| 0.00000000E-01 | 0.00000000E-01 |
| 6.0501199E-03 | -1.9692405E-05 |
| 1.2070870E-02 | -9.8462023E-06 |
| 1.7944773E-02 | -1.4769303E-04 |
| 2.3759937E-02 | -2.5600126E-04 |
| 3.5507743E-02 | -5.8092593E-04 |
| 4.7284918E-02 | -1.0141588E-03 |
| 5.8533442E-02 | -1.5507769E-03 |
| 7.1132963E-02 | -2.2203186E-03 |
| 8.2528335E-02 | -2.9440145E-03 |
| 9.4305511E-02 | -3.7858647E-03 |
| 1.0570088E-01 | -4.7704850E-03 |
| 1.1160416E-01 | -5.2677182E-03 |
| 1.1744869E-01 | -5.7895669E-03 |
| 1.2344007E-01 | -6.3114156E-03 |
| 1.2916712E-01 | -6.8480337E-03 |
| 1.3524661E-01 | -7.4289596E-03 |
| 1.4109114E-01 | -7.9901931E-03 |
| 1.4702379E-01 | -8.5957345E-03 |
| 1.5142922E-01 | -9.0781986E-03 |

| 230.0000 | 20 |
|---|---|
| 0.00000000E-01 | 0.00000000E-01 |
| 6.0353864E-03 | 0.00000000E-01 |
| 1.1138031E-02 | -2.9564660E-05 |
| 1.7173417E-02 | -8.8693981E-05 |
| 2.2385797E-02 | -1.7738796E-04 |
| 3.3030023E-02 | -4.2868757E-04 |
| 4.4277789E-02 | -7.6375373E-04 |
| 5.4922015E-02 | -1.1678041E-03 |
| 6.6279516E-02 | -1.7295326E-03 |
| 7.6759141E-02 | -2.3109709E-03 |
| 8.8006905E-02 | -2.9909581E-03 |
| 9.8925467E-02 | -3.7202197E-03 |
| 1.0449448E-01 | -4.1094878E-03 |
| 1.0967943E-01 | -4.5036832E-03 |
| 1.1546792E-01 | -4.9323708E-03 |
| 1.2092719E-01 | -5.3512035E-03 |
| 1.2644134E-01 | -5.8143832E-03 |
| 1.3179089E-01 | -6.2775628E-03 |
| 1.3705814E-01 | -6.7407424E-03 |
| 1.4144751E-01 | -7.1645027E-03 |

| 240.0000 | 21 |
|---|---|
| 0.00000000E-01 | 0.00000000E-01 |
| 1.0258080E-02 | -3.4532431E-05 |
| 1.5702172E-02 | -8.8797678E-05 |
| 2.1675551E-02 | -1.6772895E-04 |
| 2.5834232E-02 | -2.4666022E-04 |
| 3.0345771E-02 | -3.3545789E-04 |
| 3.5588230E-02 | -4.6865442E-04 |
| 4.0679464E-02 | -6.4624977E-04 |
| 5.0509074E-02 | -1.0113069E-03 |
| 6.0615929E-02 | -1.3960968E-03 |
| 7.1705746E-02 | -1.9732818E-03 |
| 8.0653212E-02 | -2.4320698E-03 |
| 9.0936496E-02 | -3.0980524E-03 |
| 9.5725279E-02 | -3.3940446E-03 |
| 1.0086692E-01 | -3.7147029E-03 |
| 1.0595816E-01 | -4.1093592E-03 |
| 1.1102419E-01 | -4.4645500E-03 |
| 1.1631705E-01 | -4.8592063E-03 |
| 1.2113104E-01 | -5.2686623E-03 |
| 1.2622228E-01 | -5.6287862E-03 |
| 1.2894432E-01 | -5.9543776E-03 |

250.0000 21

| | |
|---|---|
| 0.00000000E-01 | 0.00000000E-01 |
| 9.4460878E-03 | -2.9599518E-05 |
| 1.5123163E-02 | -7.3998795E-05 |
| 1.8939288E-02 | -1.1839807E-04 |
| 2.3579885E-02 | -1.8746361E-04 |
| 2.8456045E-02 | -2.8119543E-04 |
| 3.3073085E-02 | -3.8479374E-04 |
| 3.7996359E-02 | -5.0812507E-04 |
| 4.7418890E-02 | -7.8932050E-04 |
| 5.6652970E-02 | -1.1149152E-03 |
| 6.5910607E-02 | -1.4947757E-03 |
| 7.5521589E-02 | -1.9437017E-03 |
| 8.4779225E-02 | -2.4320938E-03 |
| 8.9537605E-02 | -2.7034227E-03 |
| 9.4178203E-02 | -3.0734167E-03 |
| 9.8913024E-02 | -3.3644786E-03 |
| 1.0364785E-01 | -3.6802068E-03 |
| 1.0826489E-01 | -4.0008682E-03 |
| 1.1299971E-01 | -4.3116632E-03 |
| 1.1756964E-01 | -4.6421911E-03 |
| 1.2145643E-01 | -4.9233866E-03 |

260.0000 20

| | |
|---|---|
| 0.00000000E-01 | 0.00000000E-01 |
| 9.0285245E-03 | -2.9561164E-05 |
| 1.3301734E-02 | -5.9122328E-05 |
| 1.7596857E-02 | -1.1331780E-04 |
| 2.2286430E-02 | -1.7736699E-04 |
| 2.6493898E-02 | -2.5126990E-04 |
| 3.0898591E-02 | -3.3009967E-04 |
| 3.5281369E-02 | -4.3356374E-04 |
| 4.3959272E-02 | -6.7497991E-04 |
| 5.2702916E-02 | -9.6073794E-04 |
| 6.1358904E-02 | -1.2908375E-03 |
| 7.0124461E-02 | -1.6800595E-03 |
| 7.8890019E-02 | -2.0988426E-03 |
| 8.7699405E-02 | -2.5422602E-03 |
| 9.2126013E-02 | -2.7886032E-03 |
| 9.6486877E-02 | -3.0447999E-03 |
| 1.0091348E-01 | -3.3108504E-03 |
| 1.0527435E-01 | -3.5818278E-03 |
| 1.0967904E-01 | -3.8478783E-03 |
| 1.1298804E-01 | -4.0745139E-03 |

270.0000 17

| | |
|---|---|
| 0.00000000E-01 | 0.00000000E-01 |
| 8.3622563E-03 | -1.9683877E-05 |
| 1.6641718E-02 | -3.4446784E-05 |
| 2.0781449E-02 | -6.8893569E-05 |
| 2.9102308E-02 | -1.7223392E-04 |
| 3.3262737E-02 | -2.9033719E-04 |
| 3.7795742E-02 | -4.0844044E-04 |
| 4.1687089E-02 | -4.8717595E-04 |
| 4.9676770E-02 | -7.3322441E-04 |
| 5.7997630E-02 | -1.0186406E-03 |
| 6.6359885E-02 | -1.3286617E-03 |
| 7.4597949E-02 | -1.6878925E-03 |
| 8.2877412E-02 | -2.1406216E-03 |
| 9.1156872E-02 | -2.5982718E-03 |
| 9.7449264E-02 | -2.8836880E-03 |
| 1.0154760E-01 | -3.1346574E-03 |
| 1.0668086E-01 | -3.4200736E-03 |

280.0000 17

| | |
|---|---|
| 0.00000000E-01 | 0.00000000E-01 |
| 7.9178942E-03 | -4.9215989E-05 |
| 1.1828206E-02 | -9.8431978E-05 |
| 1.5641246E-02 | -1.3780477E-04 |
| 1.9532103E-02 | -1.8209916E-04 |
| 2.3481323E-02 | -2.2670715E-04 |
| 3.1146311E-02 | -3.0513913E-04 |
| 3.9083660E-02 | -4.7739510E-04 |
| 4.6865374E-02 | -6.9886705E-04 |
| 5.4705451E-02 | -9.3510379E-04 |
| 6.2253714E-02 | -1.2057917E-03 |
| 7.0054883E-02 | -1.5404604E-03 |
| 7.7856052E-02 | -1.8751292E-03 |
| 8.5618312E-02 | -2.2196411E-03 |
| 9.1435141E-02 | -2.5149370E-03 |
| 9.5403817E-02 | -2.7314874E-03 |
| 1.0030630E-01 | -2.9775673E-03 |

290.0000 18

| | |
|---|---|
| 0.00000000E-01 | 0.00000000E-01 |
| 7.4841485E-03 | -4.9232708E-06 |
| 1.1198640E-02 | -2.9539625E-05 |
| 1.8572457E-02 | -6.8925790E-05 |
| 2.5964663E-02 | -1.6246794E-04 |
| 2.9679155E-02 | -2.1662391E-04 |
| 3.6942640E-02 | -3.9386166E-04 |
| 4.4298068E-02 | -5.6125287E-04 |
| 5.1506388E-02 | -8.0741641E-04 |
| 5.8861817E-02 | -1.0437334E-03 |
| 6.6676960E-02 | -1.3046668E-03 |
| 7.3535897E-02 | -1.5852932E-03 |
| 7.7213611E-02 | -1.7182215E-03 |
| 8.1001657E-02 | -1.9200756E-03 |
| 8.4679372E-02 | -2.0628505E-03 |
| 8.8540970E-02 | -2.2450115E-03 |
| 9.2016412E-02 | -2.4124027E-03 |
| 9.4811475E-02 | -2.5551775E-03 |

DyB

$\vec{v}$ | |c  $\vec{p}$ | |$\hat{a}+\hat{b}$

$\vec{H}$ | |a  f=10MHz

60.0000 11

| | |
|---|---|
| 0.00000000E-01 | 0.00000000E-01 |
| 7.9387186E-01 | 3.3548260E-05 |
| 8.6072423E-01 | -3.0972277E-04 |
| 9.2807799E-01 | 6.5811048E-05 |
| 9.3871866E-01 | 2.1550535E-04 |
| 9.4428969E-01 | 2.8519802E-04 |
| 9.4846797E-01 | 3.1423453E-04 |
| 9.5264624E-01 | 3.9295069E-04 |
| 9.5487465E-01 | 4.9813242E-04 |
| 9.5766017E-01 | 6.0137334E-04 |
| 9.6100278E-01 | 7.0784055E-04 |

80.0000 12

| | |
|---|---|
| 0.00000000E-01 | 0.00000000E-01 |
| 4.3454039E-01 | -6.1581072E-05 |
| 7.6462395E-01 | 1.3185138E-03 |
| 8.3983287E-01 | 3.1680041E-03 |
| 8.8579387E-01 | 4.1375585E-03 |
| 8.9136490E-01 | 4.4317791E-03 |
| 8.9275766E-01 | 4.4078309E-03 |
| 8.9415042E-01 | 4.4523063E-03 |
| 8.9832869E-01 | 4.5946323E-03 |
| 8.9972145E-01 | 4.6733192E-03 |
| 9.0167131E-01 | 4.2860320E-03 |
| 9.0250696E-01 | 4.2114611E-03 |

100.0000 17

| | |
|---|---|
| 0.00000000E-01 | 0.00000000E-01 |
| 3.3426184E-02 | -4.1548120E-04 |
| 4.8467967E-01 | -7.9452823E-03 |
| 8.1615599E-01 | -1.1045948E-02 |
| 8.5236769E-01 | -1.0053735E-02 |
| 8.5849582E-01 | -9.7712300E-03 |
| 8.6211699E-01 | -9.5989709E-03 |
| 8.6490250E-01 | -9.4404925E-03 |
| 8.6768802E-01 | -9.3095754E-03 |
| 8.6908078E-01 | -9.1579872E-03 |
| 8.7186629E-01 | -9.0339605E-03 |
| 8.7534819E-01 | -8.9374954E-03 |
| 8.7743732E-01 | -8.8272495E-03 |
| 8.7994429E-01 | -8.7514555E-03 |
| 8.8161560E-01 | -8.6274289E-03 |
| 8.8495822E-01 | -8.5378541E-03 |
| 8.8579387E-01 | -8.4965117E-03 |

120.0000 18

| | |
|---|---|
| 0.00000000E-01 | 0.00000000E-01 |
| 8.7186629E-02 | -9.5509662E-04 |
| 5.2590529E-01 | -6.0697082E-03 |
| 6.1002786E-01 | -1.2769226E-02 |
| 7.5487465E-01 | -1.6167433E-02 |
| 7.8272980E-01 | -1.6042855E-02 |
| 7.8802229E-01 | -1.5862909E-02 |
| 7.9275765E-01 | -1.5496096E-02 |
| 7.9721449E-01 | -1.4942417E-02 |
| 8.0083565E-01 | -1.4361054E-02 |
| 8.0445682E-01 | -1.3772770E-02 |
| 8.0779944E-01 | -1.3198328E-02 |
| 8.1114206E-01 | -1.2755384E-02 |
| 8.1309193E-01 | -1.2395493E-02 |
| 8.1476323E-01 | -1.2084048E-02 |
| 8.1727020E-01 | -1.1793367E-02 |
| 8.1838440E-01 | -1.1592658E-02 |
| 8.2033426E-01 | -1.1433475E-02 |

140.0000 17

| | |
|---|---|
| 0.00000000E-01 | 0.00000000E-01 |
| 4.5403900E-02 | -1.6831003E-04 |
| 7.4930362E-02 | 7.0129178E-06 |
| 2.8969359E-01 | -6.3046130E-03 |
| 6.0584958E-01 | -1.6417240E-02 |
| 6.9359332E-01 | -1.8927865E-02 |
| 7.1030641E-01 | -1.8864749E-02 |
| 7.2033425E-01 | -1.8605271E-02 |
| 7.2674095E-01 | -1.8324754E-02 |
| 7.3147632E-01 | -1.8072289E-02 |
| 7.3676880E-01 | -1.7847876E-02 |
| 7.4150418E-01 | -1.7637488E-02 |
| 7.4596100E-01 | -1.7427101E-02 |
| 7.4874651E-01 | -1.7230739E-02 |
| 7.5376044E-01 | -1.7006325E-02 |
| 7.5793871E-01 | -1.6802951E-02 |
| 7.5988857E-01 | -1.6739835E-02 |

160.0000 16

| | |
|---|---|
| 0.00000000E-01 | 0.00000000E-01 |
| 5.2924791E-02 | -2.5442415E-04 |
| 8.7743732E-02 | -8.9755186E-04 |
| 2.7298050E-01 | -6.8058461E-03 |
| 4.6518106E-01 | -1.5074631E-02 |
| 5.2646240E-01 | -1.7053486E-02 |
| 5.7660167E-01 | -1.8926330E-02 |
| 6.0306407E-01 | -1.9039407E-02 |
| 6.2952646E-01 | -1.8544694E-02 |
| 6.4066853E-01 | -1.8226663E-02 |
| 6.4902507E-01 | -1.7936903E-02 |
| 6.5738162E-01 | -1.7640075E-02 |
| 6.6295265E-01 | -1.7399785E-02 |
| 6.7130920E-01 | -1.7145361E-02 |
| 6.7688023E-01 | -1.6905071E-02 |
| 6.7966574E-01 | -1.6813196E-02 |

```
 170.0000                          17
0.00000000E-01  0.00000000E-01
5.7103064E-02 -4.3248542E-04
6.6852367E-02 -6.1268768E-04
8.9136491E-02 -1.1316702E-03
1.1281337E-01 -1.8741035E-03
1.5041783E-01 -3.0418141E-03
2.2005571E-01 -5.1682008E-03
3.4261838E-01 -1.1511320E-02
4.1364903E-01 -1.4026944E-02
4.5682451E-01 -1.5591099E-02
4.8467967E-01 -1.6160539E-02
5.1392758E-01 -1.6268660E-02
5.3621170E-01 -1.6210995E-02
5.6824513E-01 -1.5865007E-02
5.9192201E-01 -1.5403689E-02
6.1559889E-01 -1.4942371E-02
6.2116992E-01 -1.4841458E-02
 175.0000                          17
0.00000000E-01  0.00000000E-01
3.6211699E-02 -2.7807288E-04
8.0779945E-02 -1.1051614E-03
1.3649025E-01 -3.2940941E-03
2.4512535E-01 -7.6006587E-03
3.1476323E-01 -1.0124705E-02
3.7047354E-01 -1.2477629E-02
4.2061281E-01 -1.3682612E-02
4.5543176E-01 -1.4210237E-02
4.8467967E-01 -1.4445530E-02
5.0835655E-01 -1.4481180E-02
5.2646240E-01 -1.4438400E-02
5.4317549E-01 -1.4324318E-02
5.5710307E-01 -1.4160327E-02
5.7103064E-01 -1.3967815E-02
5.8356546E-01 -1.3789563E-02
5.8774373E-01 -1.3711132E-02
 80.00000                          20
0.00000000E-01  0.00000000E-01
2.4038997E-01  3.9661817E-05
4.6796658E-01  1.0576484E-04
6.8746518E-01  6.6103028E-06
8.1058495E-01  1.2559575E-04
8.5041782E-01  6.6103027E-04
8.8384401E-01  1.7517302E-03
8.9052925E-01  2.0624145E-03
8.9220055E-01  2.2144514E-03
8.9247911E-01  2.3334369E-03
8.9415042E-01  2.3598781E-03
8.9637883E-01  2.4788635E-03
8.9749304E-01  2.5714078E-03
8.9832869E-01  2.6507314E-03
9.0000000E-01  2.7168344E-03
9.0083566E-01  2.7564963E-03
9.0139275E-01  2.8292096E-03
9.0250696E-01  2.9151435E-03
9.0334262E-01  2.9812465E-03
9.0389972E-01  2.9944672E-03
 90.00000                          20
0.00000000E-01  0.00000000E-01
1.0668524E-01 -2.6693716E-05
3.3426184E-01  6.6734290E-06
6.6434541E-01 -1.8685601E-04
8.1894150E-01 -3.6036517E-04
8.6713092E-01  2.4691687E-04
8.7966573E-01  7.0071005E-04
8.8161560E-01  8.6754578E-04
8.8551532E-01  1.0677486E-03
8.8802228E-01  1.2479312E-03
8.8997214E-01  1.3880732E-03
8.9303621E-01  1.5682558E-03
8.9554317E-01  1.6950510E-03
8.9721448E-01  1.8819070E-03
8.9832869E-01  2.0153756E-03
9.0055710E-01  2.1488441E-03
9.0250696E-01  2.2689659E-03
9.0417827E-01  2.3890876E-03
9.0668523E-01  2.5225562E-03
9.0696378E-01  2.5492499E-03
```

130.0000 25

| | |
|---|---|
| 0.0000000E-01 | 0.0000000E-01 |
| 1.3927577E-02 | 6.6276518E-06 |
| 2.6128134E-02 | -3.9765911E-05 |
| 4.0111421E-02 | -7.9531823E-05 |
| 5.4038997E-02 | -2.3859547E-04 |
| 6.7966574E-02 | -5.6997805E-04 |
| 1.0445682E-01 | -1.3387857E-03 |
| 1.6016713E-01 | -2.6046672E-03 |
| 2.1949861E-01 | -4.2814630E-03 |
| 3.1337047E-01 | -7.3368106E-03 |
| 4.2841225E-01 | -1.4328983E-02 |
| 5.4846796E-01 | 6.4432043E-01 |
| 6.4763231E-01 | -2.2162868E-02 |
| 7.0863510E-01 | -2.3852919E-02 |
| 7.3286907E-01 | -2.2872027E-02 |
| 7.4735375E-01 | -2.2547272E-02 |
| 7.4902508E-01 | -2.2003804E-02 |
| 7.6406685E-01 | -2.1175348E-02 |
| 7.6768802E-01 | -2.0625253E-02 |
| 7.7298050E-01 | -2.0154689E-02 |
| 7.7660167E-01 | -1.9644360E-02 |
| 7.7994429E-01 | -1.9240073E-02 |
| 7.8356545E-01 | -1.8789393E-02 |
| 7.8551532E-01 | -1.8378478E-02 |
| 7.9247911E-01 | -1.7583160E-02 |

180

| | |
|---|---|
| .00000000 | 0,000 |
| .10509848 | -20,127 |
| .20872255 | -46,097 |
| .30137934 | -73,366 |
| .35290687 | -86,423 |
| .39408781 | -94,792 |
| .42884176 | -100.202 |
| .45836765 | -103,376 |
| .47948721 | -104,891 |
| .49849798 | -105,107 |
| .51377020 | -104,963 |
| .53015355 | -104,098 |
| .54863146 | -103,304 |
| .55725178 | -102,366 |

E20

185

| | |
|---|---|
| .00000000 | 0,000 |
| .05620415 | -2,675 |
| .09975739 | -7,954 |
| .14502908 | -15,980 |
| .18680143 | -25,669 |
| .23310873 | -37,745 |
| .27133213 | -48,880 |
| .29792907 | -56,256 |
| .33602818 | -66,451 |
| .37141127 | -74,694 |
| .40280570 | -81,057 |
| .42819834 | -85,034 |
| .45167255 | -87,927 |
| .47114280 | -89,445 |
| .49011930 | -90,024 |
| .50689609 | -90,241 |
| .51383911 | -90,168 |

190

| | |
|---|---|
| .00000000 | 0,000 |
| .07253145 | -3,909 |
| .14363046 | -14,478 |
| .21162494 | -30,331 |
| .25213353 | -41,335 |
| .28790633 | -51,324 |
| .32117900 | -59,866 |
| .35347130 | -67,684 |
| .37897782 | -73,186 |
| .40461927 | -78,181 |
| .42645536 | -81,366 |
| .44804894 | -84,189 |
| .46744298 | -85,927 |
| .47507233 | -86,651 |

195

| | |
|---|---|
| .00000000 | 0,000 |
| .06186018 | -2,897 |
| .12408539 | -11,155 |
| .18517605 | -23,614 |
| .22182812 | -32,740 |
| .25583723 | -42,084 |
| .28595249 | -50,052 |
| .31598411 | -58,237 |
| .34397763 | -65,191 |
| .36796003 | -70,551 |
| .39731542 | -76,129 |
| .41019354 | -78,519 |
| .42948818 | -81,344 |
| .43745566 | -82,285 |

200

| | |
|---|---|
| .00000000 | 0,000 |
| .05344624 | -2,102 |
| .10762091 | -8,771 |
| .16149868 | -18,630 |
| .19422394 | -26,241 |
| .22347506 | -33,490 |
| .25116913 | -40,666 |
| .27843498 | -48,060 |
| .30247486 | -54,729 |
| .32694137 | -61,108 |
| .34792847 | -66,327 |
| .36973957 | -71,112 |
| .39001351 | -74,809 |
| .39791432 | -76,258 |

210

| | |
|---|---|
| | 0,000 |
| .00000000 | -2,018 |
| .04366179 | -5,983 |
| .08595496 | -12,542 |
| .12783756 | -17,804 |
| .15452291 | -23,210 |
| .17823102 | -28,689 |
| .20198582 | -35,032 |
| .22588175 | -40,726 |
| .24696592 | -47,070 |
| .26869582 | -52,331 |
| .28921284 | -57,449 |
| .30785470 | -62,279 |
| .32576229 | -63,793 |
| .33196471 | |

220

| | |
|---|---|
| .00000000 | 0,000 |
| .03711929 | -0,938 |
| .06975215 | -4,043 |
| .10474629 | -8,518 |
| .12667850 | -12,200 |
| .14723309 | -15,954 |
| .16678420 | -20,429 |
| .19034282 | -25,988 |
| .20668842 | -30,175 |
| .22462108 | -34,795 |
| .24203002 | -39,343 |
| .26119876 | -44,757 |
| .27656931 | -48,871 |
| .28299628 | -50,387 |

230

| | |
|---|---|
| .00000000 | 0,000 |
| .03029499 | -0,578 |
| .06053546 | -2,675 |
| .09031731 | -6,001 |
| .10952780 | -8,893 |
| .12708808 | -12,146 |
| .14443964 | -15,544 |
| .16219553 | -19,086 |
| .17803998 | -22,701 |
| .19461966 | -26,822 |
| .21018367 | -30,582 |
| .22613323 | -34,920 |
| .24099389 | -38,607 |
| .24659315 | -40,270 |

240

| | |
|---|---|
| .00000000 | 0,000 |
| .02666995 | -0,434 |
| .05341503 | -2,172 |
| .07949112 | -4,779 |
| .09594932 | -6,589 |
| .11145295 | -8,978 |
| .12658979 | -11,657 |
| .14228762 | -14,771 |
| .15601432 | -17,739 |
| .17096954 | -21,215 |
| .18451721 | -24,401 |
| .19932684 | -28,166 |
| .21305581 | -31,641 |
| .21797342 | -32,872 |

250

| | |
|---|---|
| .00000000 | 0,000 |
| .02345342 | -0,360 |
| .04723821 | -1,656 |
| .06963263 | -3,529 |
| .08480495 | -5,401 |
| .09868081 | -7,201 |
| .11188716 | -9,506 |
| .12567347 | -11,954 |
| .13819681 | -14,402 |
| .15269066 | -17,355 |
| .16346040 | -19,659 |
| .17646734 | -22,612 |
| .18928484 | -25,636 |
| .19408309 | -26,789 |

260

| | |
|---|---|
| .00000000 | 0,000 |
| .02076240 | -0,252 |
| .04229624 | -1,514 |
| .06306357 | -3,281 |
| .07615003 | -4,709 |
| .08878338 | -6,295 |
| .10082449 | -7,954 |
| .11352289 | -10,190 |
| .12473643 | -12,353 |
| .13788439 | -15,021 |
| .14792966 | -17,329 |
| .15971542 | -20,069 |
| .17061403 | -22,809 |
| .17448212 | -23,819 |

280

| | |
|---|---|
| .00000000 | 0,000 |
| .03306529 | -0,955 |
| .05072564 | -1,968 |
| .06275053 | -3,090 |
| .08319101 | -5,768 |
| .09379364 | -7,215 |
| .10327488 | -8,879 |
| .11026551 | -10,254 |
| .12309826 | -12,643 |
| .13408519 | -15,103 |
| .14374439 | -17,274 |
| .14588437 | -17,781 |

300

| | |
|---|---|
| .00000000 | 0,000 |
| .02952089 | -0,792 |
| .05363150 | -2,571 |
| .07088952 | -4,772 |
| .08799127 | -7,786 |
| .10447819 | -11,286 |
| .12121642 | -15,230 |
| .12434067 | -15,956 |

$\vec{v}$ ||b  $\vec{p}$ ||a  DyB

$\vec{H}$ ||a  f=10MHz

| | |
|---|---|
| 170.0000 | 9 |
| 4.8607242E-01 | 0.0000000E-01 |
| 5.1253482E-01 | 4.6865347E-04 |
| 5.3621170E-01 | 9.0002768E-04 |
| 5.5571031E-01 | 1.3527043E-03 |
| 5.7103064E-01 | 1.8639627E-03 |
| 5.8217270E-01 | 2.1568711E-03 |
| 5.9192201E-01 | 2.4178259E-03 |
| 6.0584958E-01 | 2.6894318E-03 |
| 6.1559889E-01 | 2.9716891E-03 |
| 175.0000 | 7 |
| 4.2061281E-01 | 0.0000000E-01 |
| 4.5543176E-01 | 1.7108545E-04 |
| 4.8467967E-01 | 4.1943530E-04 |
| 5.0835655E-01 | 8.0023841E-04 |
| 5.2646240E-01 | 1.0817016E-03 |
| 5.4317549E-01 | 1.4293914E-03 |
| 5.5626741E-01 | 1.7274112E-03 |
| 180.0000 | 17 |
| 0.0000000E-01 | 0.0000000E-01 |
| 5.2507281E-02 | -4.9416338E-04 |
| 1.0492186E-01 | -2.0535233E-03 |
| 1.5783170E-01 | -2.8881104E-03 |
| 2.0872255E-01 | -4.0246862E-03 |
| 2.5704977E-01 | -4.9031988E-03 |
| 3.0095264E-01 | -5.6060090E-03 |
| 3.5192024E-01 | -6.1440980E-03 |
| 3.9419212E-01 | -6.2978377E-03 |
| 4.2875599E-01 | -6.2539121E-03 |
| 4.5823137E-01 | -6.1166445E-03 |
| 4.7954246E-01 | -5.8695628E-03 |
| 4.9840649E-01 | -5.6005183E-03 |
| 5.1372766E-01 | -5.2820574E-03 |
| 5.2996793E-01 | -4.9690873E-03 |
| 5.4845607E-01 | -4.7933848E-03 |
| 5.5718607E-01 | -4.6561171E-03 |
| 185.0000 | 13 |
| 0.0000000E-01 | 0.0000000E-01 |
| 4.2066109E-02 | -1.5502881E-04 |
| 8.4938706E-02 | -4.7577808E-04 |
| 1.2855554E-01 | -9.0344377E-04 |
| 1.7040111E-01 | -1.5235590E-03 |
| 2.1135664E-01 | -2.1704034E-03 |
| 2.5041417E-01 | -2.8493227E-03 |
| 2.9633485E-01 | -3.5817001E-03 |
| 3.3592607E-01 | -4.1964696E-03 |
| 3.7096244E-01 | -4.4263399E-03 |
| 4.2806416E-01 | -4.4530690E-03 |
| 4.7072889E-01 | -4.2071612E-03 |
| 5.1378796E-01 | -3.7206915E-03 |
| 190.0000 | 17 |
| 0.0000000E-01 | 0.0000000E-01 |
| 3.5802291E-02 | -6.4207175E-05 |
| 7.2652011E-02 | -2.9428288E-04 |
| 1.0798262E-01 | -6.3672115E-04 |
| 1.4398173E-01 | -1.0861714E-03 |
| 1.7779226E-01 | -1.5463228E-03 |
| 2.1184269E-01 | -2.0920838E-03 |
| 2.5223543E-01 | -2.8037133E-03 |
| 2.8847323E-01 | -3.4083308E-03 |
| 3.2109224E-01 | -3.8577811E-03 |
| 3.5331431E-01 | -4.1948688E-03 |
| 3.7883448E-01 | -4.3286337E-03 |
| 4.0461927E-01 | -4.3767891E-03 |
| 4.2651508E-01 | -4.3393349E-03 |
| 4.4799320E-01 | -4.2590760E-03 |
| 4.6755065E-01 | -4.1413628E-03 |
| 4.7507233E-01 | -4.0985580E-03 |
| 195.0000 | 17 |
| 0.0000000E-01 | 0.0000000E-01 |
| 3.1404780E-02 | -1.6065031E-05 |
| 6.1546541E-02 | -1.6600532E-04 |
| 9.3163262E-02 | -4.3375584E-04 |
| 1.2501600E-01 | -7.5505646E-04 |
| 1.5510038E-01 | -1.1299072E-03 |
| 1.8507812E-01 | -1.5957931E-03 |
| 2.2164246E-01 | -2.1312941E-03 |
| 2.5479173E-01 | -2.7471203E-03 |
| 2.8562764E-01 | -3.2772663E-03 |
| 3.1553470E-01 | -3.7217322E-03 |
| 3.4044979E-01 | -3.9680626E-03 |
| 3.6578222E-01 | -4.1661980E-03 |
| 3.8749098E-01 | -4.3375584E-03 |
| 4.0956300E-01 | -4.2786532E-03 |
| 4.2960044E-01 | -4.2143931E-03 |
| 4.3751181E-01 | -4.1983281E-03 |
| 200.0000 | 14 |
| 0.0000000E-01 | 0.0000000E-01 |
| 5.3175436E-02 | -1.0519118E-04 |
| 1.0753043E-01 | -5.4699416E-04 |
| 1.6097772E-01 | -1.2570346E-03 |
| 1.9414088E-01 | -1.7303950E-03 |
| 2.2410605E-01 | -2.1301215E-03 |
| 2.5109464E-01 | -2.5298480E-03 |
| 2.7968959E-01 | -2.9137958E-03 |
| 3.0273756E-01 | -3.1662546E-03 |
| 3.2663190E-01 | -3.4239730E-03 |
| 3.4792847E-01 | -3.5765003E-03 |
| 3.6991242E-01 | -3.7342870E-03 |
| 3.9035854E-01 | -3.7868826E-03 |
| 3.9814589E-01 | -3.7921422E-03 |

```
 210.0000                                14
0.0000000E+01  0.0000000E+01
4.2877473E+02 -7.9001838E-05
8.4753197E+02 -3.1600735E-04
1.2735444E+01 -7.3735049E-04
1.5364589E+01 -1.0428243E-03
1.7823102E+01 -1.3904323E-03
2.0198582E+01 -1.7538408E-03
2.2618855E+01 -2.0751150E-03
2.4655218E+01 -2.3700551E-03
2.6841333E+01 -2.7071297E-03
2.8781129E+01 -2.9704691E-03
3.0764981E+01 -3.1916742E-03
3.2537361E+01 -3.3970790E-03
3.3215507E+01 -3.4444801E-03
 220.0000                                14
0.0000000E+01  0.0000000E+01
3.4729633E+02 -5.2730379E-05
6.9752146E+02 -2.5837885E-04
1.0463180E+01 -5.1148467E-04
1.2650942E+01 -7.6986352E-04
1.4701176E+01 -1.0809728E-03
1.6689256E+01 -1.3551707E-03
1.8723098E+01 -1.6610069E-03
2.0555517E+01 -1.9668431E-03
2.2487168E+01 -2.2937715E-03
2.4251770E+01 -2.5837885E-03
2.6025191E+01 -2.8738056E-03
2.7689223E+01 -3.1374575E-03
2.8317894E+01 -3.2112800E-03
 230.0000                                14
0.0000000E+01  0.0000000E+01
3.0345531E+02 -6.8637441E-05
6.0736155E+02 -2.0591232E-04
9.0564090E+02 -4.2766406E-04
1.0943054E+01 -6.0189755E-04
1.2718376E+01 -8.0780988E-04
1.4434570E+01 -9.9260299E-04
1.6214954E+01 -1.2671528E-03
1.7799491E+01 -1.5258631E-03
1.9466373E+01 -1.7740139E-03
2.1014055E+01 -2.0274444E-03
2.2609105E+01 -2.3231134E-03
2.4082858E+01 -2.5765439E-03
2.4671620E+01 -2.6451813E-03
 240.0000                                14
0.0000000E+01  0.0000000E+01
2.6404240E+02 -1.0574961E-05
5.3061783E+02 -9.5174644E-05
7.9404288E+02 -2.3264913E-04
9.6120228E+02 -3.7012362E-04
1.1136899E+01 -5.0231063E-04
1.2658979E+01 -6.5036007E-04
1.4212614E+01 -8.4599685E-04
1.5605401E+01 -1.0310587E-03
1.7093049E+01 -1.2319829E-03
1.8467167E+01 -1.4381946E-03
1.9890485E+01 -1.6444064E-03
2.1251849E+01 -1.8664806E-03
2.1808881E+01 -1.9880926E-03
 250.0000                                14
0.0000000E+01  0.0000000E+01
2.3453421E+02  5.2956284E-06
4.6848843E+02 -7.4138798E-05
7.0167796E+02 -2.0123388E-04
8.4842566E+02 -3.0185082E-04
9.8421870E+02 -4.2365028E-04
1.1174160E+01 -5.4544972E-04
1.2574508E+01 -7.1490984E-04
1.3794921E+01 -8.7377869E-04
1.5128913E+01 -1.0485344E-03
1.6360013E+01 -1.2074033E-03
1.7660752E+01 -1.3556809E-03
1.8914312E+01 -1.5780973E-03
1.9415442E+01 -1.6522361E-03
 260.0000                                14
0.0000000E+01  0.0000000E+01
2.1113537E-02 -4.7721560E-05
4.2086981E+02 -1.2195510E-04
6.3063575E+02 -2.4391020E-04
7.6184105E+02 -3.4995811E-04
8.8547721E+02 -4.5070362E-04
1.0069157E+01 -5.7796112E-04
1.1345742E+01 -7.5294017E-04
1.2467189E+01 -8.5898809E-04
1.3671023E+01 -1.0498743E-03
1.4777328E+01 -1.2089462E-03
1.5937697E+01 -1.3733205E-03
1.7028066E+01 -1.5217875E-03
1.7454240E+01 -1.5854163E-03
```

```
 280.0000                    14
0.0000000E+01  0.0000000E+01
1.7296837E+02 -2.1266867E-05
3.4445557E+02 -6.9117318E-05
5.1952624E+02 -1.5418479E-04
6.2609023E+02 -2.4456897E-04
7.3061900E+02 -3.2431972E-04
8.3052187E+02 -4.5192093E-04
9.3738717E+02 -5.5293855E-04
1.0313892E+01 -6.7522303E-04
1.1336628E+01 -8.3472453E-04
1.2277779E+01 -9.6764245E-04
1.3273241E+01 -1.1218273E-03
1.4213221E+01 -1.2653786E-03
1.4591079E+01 -1.3185458E-03
 300.0000                    14
0.0000000E+01  0.0000000E+01
1.4942050E+02 -1.5992835E-05
2.9619053E+02 -6.9302285E-05
4.4518815E+02 -1.2794268E-04
5.3414988E+02 -1.9724497E-04
6.2247101E+02 -2.3989253E-04
7.1242662E+02 -3.1985670E-04
7.9694323E+02 -3.6783521E-04
8.7898987E+02 -4.7445411E-04
9.6513690E+02 -5.8107301E-04
1.0466034E+01 -6.6636813E-04
1.1321003E+01 -7.7831798E-04
1.2112529E+01 -8.9026782E-04
1.2436350E+01 -9.2758444E-04
```